Title
Engineering Macrophages for Cell-Based Therapies

Author
Lee, Simon

Publication Date
2017

Peer reviewed|Thesis/dissertation

Engineering Macrophages for Cell-based Therapies

by

Simon Lee

DISSERTATION

Submitted in partial satisfaction of the requirements for the degree of

DOCTOR OF PHILOSOPHY

in

Bioengineering

in the

GRADUATE DIVISION

of the

UNIVERSITY OF CALIFORNIA, SAN FRANCISCO

Acknowledgements

I would like to first thank my research mentor, Dr. Francis Szoka, who has guided me through the ups and downs of my research. I am thankful for his constant encouragement and support in the face of difficulties. His zeal for discovery, science and teaching has been inspiring to observe, and I, along with the others he has touched, are lucky to have experienced it. Lastly and most importantly, I thank Frank for teaching me to stay simultaneously critical and optimistic, a trait I hope to continue as I move beyond the walls of UCSF.

I would also like to thank my other research mentors through my time at UCSF who have been instrumental in my progress by providing valuable feedback and support. These include Dr. John Dueber and Dr. Michael McManus for serving on my dissertation committee and Dr. Tejal Desai and Dr. Tamara Alliston for serving on my qualifying exam committee. I also appreciate the administrative help from Steve Ha and SarahJane Taylor. Additionally, I would like to thank Dr. Steve Connolly and Kristin Olson for all their help during my time at UC-Berkeley. I wish to also thank my past research mentors, including Dr. Edgar Acosta, Dr. A. Wilhelm Neumann and Zdenka Policova at the University of Toronto, Dr. Masaru Kuno and Dr. Yanghai Yu at the University of Notre Dame, Bruce Farrand and Isadora van Riemsdijk at ArcelorMittal-Dofasco, Dr. Juewen Liu at the University of Waterloo and Dr. Naveen Chopra at the Xerox Research Center of Canada.

I thank my family, especially my parents, Mary and Roger Lee, for teaching me the value of hard work, encouraging me to pursue my studies and supporting me throughout my entire life. I must also thank my brother, Edward Lee and his wife, Nancy Ho Woo,

who have always provided perspective and levity. I wish to also thank my grandma, Yin Liang, who helped raise me as a child and continually puts me to shame with her athleticism. While I now live far away from home, my family will remain a source of support and pride no matter where I am. My parents are my inspiration to pursue work that aids in human health and I hope to emulate the compassion they have shown through their work to continue helping others.

Words cannot express how grateful I am for my better half, Joseph Testa. He has been my number one cheerleader and I cannot imagine how the last 5 years would have been without his support. Thank you for continually inspiring me and sharing in the struggles and triumphs without complaint. I will always be indebted to him and can only hope to repay him with the same care and patience he has shown me.

My work would have been impossible without the support from the members of the Szoka Lab I have worked with. Especially Dr. Saul Kivimäe who mentored me throughout my time in the Szoka lab and guided me on innumerable experiments and protocols. I will never forget how his bright Estonian disposition would fill the lab with optimism. I am also grateful for Aaron Dolor, who has patiently listened to my ranting and raving for the last several years. I would also like to thank the other members of the Szoka lab, including Dr. Jonathan Sockolosky, Dr. Matt Tiffany, Dr. Aditya Kohli, Dr. Paul Kierstad and Dr. Vincent Venditto for their help.

Lastly, I would like to thank my funding sources that have made my graduate education possible, including support from the UC-Berkeley/UCSF Bioengineering Graduate Program, NIH R21CA182703 and the Natural Sciences and Engineering Research Council of Canada.

Engineering Macrophages for Cell-Based Therapies

Simon Lee

Abstract

In the last decade, the promise of cell-based therapy has come closer to fruition. Although macrophages (MΦ) play important roles in immunity, development and homeostatic tissue maintenance, they have not yet been incorporated into this cell therapy revolution. This reality may change due to a better understanding of MΦ development, plasticity and diverse phenotypical behaviors. As such, there is now the information needed to devise and develop MΦ cell-based therapies.

In this dissertation, I describe the engineering approaches I employed to improve and develop MΦ for cell-based therapies. I first focused on developing a means of generating large numbers of functional MΦ in vitro by the reversible expression of the Hoxb8 transcription factor. I next investigated the biodistribution and survival of transplanted Hoxb8 dependent progenitors (HDP) and macrophages arising from them (HDP-MΦ) in immunocompetent BALB/c and immunodeficient NCG mice. This was enabled by incorporating a number of genetic modifications into the HDP including: constitutively active GMCSFR, luciferase and an inducible IRF8, and by pretreating animals with liposomal clodronate. This combination of factors led to improving the post-transplantation survival of HDP from <1 day to 7 days in BALB/c mice. In addition, I engineered HDP to overexpress iduronidase (IDUA) as a potential cell vector to deliver therapeutic doses of IDUA in the mouse for the treatment of Hurlers Syndrome. These techniques and results described here can guide new approaches for developing novel MΦ-based therapeutics.

Table of Contents

1 Chapter 1: Introduction to MΦ and cell based therapeutics 1
1.1 Overview of MΦ 1
1.1.1 Origins of tissue MΦ 1
1.1.2 Sources of MΦ for cell-based therapies 4
1.1.3 Functional polarization of MΦ 7
1.2 Cell Based Therapeutics 9
1.2.1 Stem cell therapeutics 12
1.2.2 T-cell therapeutics 16
1.2.3 MΦ-based therapeutics 22
1.2.3.1 Human Clinical Trials: *ex vivo* educated or generated cells 22
1.2.3.2 Recent animal trials: *ex vivo* modified MΦ 29
1.2.3.2.1 MΦ without extensive modifications 29
1.2.3.2.2 MΦ as delivery vehicles 32
1.2.3.2.3 Genetically Engineered MΦ 37
1.2.3.3 *In vivo* survival: pharmacokinetics and biodistribution of administered MΦ in animals 44
1.3 Research motivation, potential pitfalls and opportunities 47
2 Chapter 2: Generation and characterization of *ex vivo* MΦ and MΦ progenitors 55
2.1 Novel methods of collecting MΦ 55
2.2 Generation of MΦ from Hoxb8 driven myeloid progenitors (HDP) 57
2.3 Modification and Validation of HDP 61
2.4 Characterization of HDP and MΦ 65
2.4.1 Growth kinetics of HDP 65
2.4.2 Polarization potential of *ex vivo* generated MΦ 68
2.4.3 Phagocytosis of bacteria and liposomes by *ex vivo* generated MΦ 70
2.4.4 Chemotaxis towards tumor secretions 71
2.5 Conclusions 73
2.6 Methods 74
2.6.1 Cell Culture 74
2.6.2 Limited Dilution Cloning 74
2.6.3 Luciferase activity 75

2.6.4 Colony PCR to identify presence of genetic constructs 75
2.6.5 Supplemental GMCSF Media 76
2.6.6 Lentivirus and Retrovirus Production 76
2.6.7 Lentivirus and Retrovirus Transduction 77
2.6.8 Lin^- bone marrow culture and infection 77
2.6.9 Determining proliferation rate 77
2.6.10 MΦ polarization assay 78
2.6.11 Quantitative real time PCR 78
2.6.12 Flow Cytometry 78
2.6.13 Plasmid Construction 79
2.6.14 Liposome and Bacterial Uptake 79
2.6.15 Transwell studies 80
3 Chapter 3: Exploratory engraftment studies of *ex vivo* derived MΦ and HDP 82
3.1 Injection and cell transplantation parameters 83
3.2 Identification of a method for tracking cells post injection 85
3.3 Identifying an appropriate route of administration 89
3.3.1 IV Studies 89
3.3.1.1 Reducing the entrapment of IV injected cells in the lung 89
3.3.1.2 Evading the reticuloendothelial system 92
3.3.1.3 Reducing a foreign immune rejection response 96
3.3.1.4 Reducing the thrombin response 97
3.3.1.5 Reducing the complement response 98
3.3.1.6 Summary 100
3.3.2 Lung instillation 102
3.3.3 Intraperitoneal and subcutaneous injection 104
3.3.3.1 Characterization of cells in *in vitro* matrigel cultures 105
3.3.3.1.1 Matrigel does not substitute serum or GMCSF 105
3.3.3.1.2 Long term *in vitro* cultures of HDP 108
3.3.3.2 Matrigel as a physical support in tumored and healthy animals 113
3.3.3.2.1 Cytokine stimulated cells 115
3.3.3.2.2 CCR2 overexpression 120

3.3.3.2.3 Effect of other physical supports 122
3.4 Conclusion 124
3.5 Methods 127
3.5.1 Animals 127
3.5.2 Transplanting cells into mice 127
3.5.3 Labelling cells with PEG (PEGylation) 129
3.5.4 Serum exchange 130
3.5.5 Biodistribution 130
3.5.6 Cytokine stimulation 132
3.5.7 4T1 tumoring of mice 132
3.5.8 *In vitro* matrigel cultures 132
3.5.9 Transwell studies 133
3.5.10 Statistics and modeling 133
4 Chapter 4: Clodronate pretreatment improves acute survival of transplanted Hoxb8 myeloid progenitor cells expressing constitutively active GMCSFR in immunocompetent mice 134
4.1 Introduction 135
4.2 Hoxb8: a method for unlimited myeloid progenitors and MΦ 138
4.3 Constitutively active GMCSFR Hoxb8-dependent myeloid progenitors (HDP) differentiate into MΦ 140
4.4 HDP-on-MΦ retain M1/M2 polarization responses and remain highly phagocytic 143
4.5 HDP-on and MΦ survive at least 7 days in immunodeficient mice 146
4.6 Clodronate pretreatment improves survival of HDP-on in immunocompetent mice 149
4.7 Liposomal clodronate pretreatment does not enhance post-transplantation cell survival in immunocompetent mice beyond 7 days 155
4.8 Conclusions 158
4.9 Materials and Methods 167
4.9.1 Cell culture 167
4.9.2 Plasmid Construction 168
4.9.3 Lin^- bone marrow culture and generating Hoxb8 dependent progenitors 169

4.9.4 Lentivirus and retrovirus production 169
4.9.5 Lentiviral and retroviral transduction 170
4.9.6 MΦ M1/M2 polarization 170
4.9.7 qPCR 170
4.9.8 Flow cytometry 171
4.9.9 MΦ phagocytosis 171
4.9.10 Animals 173
4.9.11 Cell transplantation 173
4.9.12 Biodistribution 174
4.9.13 Statistics 175
5 Chapter 5: MΦ gene therapy for Hurlers Syndrome 176
5.1 Hurlers Syndrome 176
5.2 *In vitro* expression of IDUA in Cos-7 cells 177
5.3 IDUA expression in HDP and HDP-MΦ 179
5.4 Pharmacokinetic considerations 180
5.5 Conclusion 184
5.6 Methods 185
5.6.1 Transfection 185
5.6.2 IDUA Activity 185
5.6.3 Western blot 186
6 Chapter 6: Summary, conclusions and future work 187
6.1 Summary of Findings 187
6.2 Future work 190
6.3 Conclusions and Outlook 193
7 References 196
8 Appendix 237
8.1.1 Lentivirus and Retrovirus Production 237
8.1.2 Lentivirus and Retrovirus Transduction 238
8.1.3 Lin^- bone marrow culture and infection 239
8.1.4 qPCR 242
8.1.5 Flow Cytometry 244

8.1.6 Plasmid Construction 245
8.1.7 IDUA Activity 246
8.1.8 Western blot 246

List of Figures

Figure 1-1: Tissue-resident MΦ can be found throughout the body in virtually all tissues and organs. 4

Figure 1-2: General scheme of cell based therapies. 10

Figure 1-3: Overview of the development of T-cell therapeutics. 19

Figure 1-4: Therapeutic MΦ collected from human blood via leukapheresis and elutriation. 23

Figure 1-5: Modeling of MΦ uptake of drug particles. 33

Figure 2-1: Overview of modified HDP and MΦ system. 58

Figure 2-2: Differentiation of HDP into MΦ. 59

Figure 2-3: Retroviral transduction of Hoxb8 MΦ progenitors. 63

Figure 2-4: Validation of insertion of AutoGMCSFR and IRF8-ERT genetic constructs. 65

Figure 2-5: Growth potentials of HDP 67

Figure 2-6: Quantitative PCR of M1 and M2 MΦ markers of *ex vivo* MΦ. 69

Figure 2-7: *Ex vivo* derived MΦ maintain *in vitro* phagocytic potential. 71

Figure 2-8: *Ex vivo* MΦ preferentially migrate towards 4T1 conditioned media 72

Figure 3-1: Schematic of biodistribution experiments. 85

Figure 3-2: Comparing DiD and luciferase reporter activity as methods for quantifying the number of cells in animal organs. 87

Figure 3-3: The detection limits of a luminescence based assay for HDP expressing luciferase. 88

Figure 3-4: Injection fluids modify the lung entrapment of 4DDP injected IV. 91

List of Figures (continued)

Figure 3-5: Composition of injection fluid influences the number of cells at in the lung or spleen 24 h post injection. 92

Figure 3-6: PEG-labeled cells to improve the *in vivo* biocompatibility of cells. 94

Figure 3-7: *In vivo* biodistribution of HDP treated with DSPE-PEG 2 h post IV injection. 95

Figure 3-8: *In vivo* biodistribution of HDP cultured in BALB/c serum for 7 days 2h post injection. 97

Figure 3-9: *In vivo* biodistribution 2 h post transplantation of HDP IV injected into mice pretreated with thrombin inhibitors. 98

Figure 3-10: Genetic constructs and flow cytometry for Auto-Crry cells. 99

Figure 3-11: *In vivo* biodistribution of genetically modified HDP IV injected into thrombin inhibited mice 2 h post transplantation. 100

Figure 3-12: Biodistribution of HDP IV injected into mice 2 h and 24 h post injection. 102

Figure 3-13: *In vivo* biodistribution of HDP transplanted by lung instillation at 1 day and 7 days post instillation. 104

Figure 3-14: Representative micrographs of HDP cultured in high molecular weight matrigel for 19 days. 107

Figure 3-15: Survival of HDP cells growing in matrigel over time in transwell cultures. 109

Figure 3-16: Evaluation of M1/M2 and monocyte/MΦ gene expression in long term matrigel cultures of HDP. 111

List of Figures (continued)

Figure 3-17: *In vivo* biodistribution of 4DDP injected IP or subcutaneously with matrigel (MG). 114

Figure 3-18: 4DDP preferentially migrate towards 4T1 conditioned media. 116

Figure 3-19: *In vivo* biodistribution of 4DDP treated with cytokines injected IP with matrigel in animals with 2-3 week old orthotropic 4T1 tumors. 117

Figure 3-20: 4DDP injected IP with matrigel can be detected in selected sections of 4T1 tumors from selected animals. 120

Figure 3-21: Genetic construct for CCR2+ cells. 121

Figure 3-22: *In vivo* biodistribution of CCR2+ 4DDP injected IP with matrigel in animals with 2-3 week old orthotropic 4T1 tumors..... 122

Figure 3-23: *In vivo* biodistribution of 4DDP injected IP with varying injection medias in healthy animals. 123

Figure 4-1: Generation of Hoxb8-dependent myeloid progenitors (HDP) and MΦ (HDP-MΦ). 139

Figure 4-2: Characterization of HDP-on and HDP-on-MΦ. 142

Figure 4-3: Gene expression of HDP-on treated with M1 and M2 inducers. 144

Figure 4-4: Relative gene expression of MΦ and M1/M2 markers of M1/M2 polarized HDP-on MΦ treated with opposing M1/M2 inducers. 145

Figure 4-5: Functional analysis of HDP-on-MΦ for MΦ behaviors. 146

Figure 4-6: Biodistribution of HDP, HDP-on, HDP MΦs and HDP-on MΦs in immunodeficient NCG mice 7 days post injection. 148

List of Figures (continued)

Figure 4-7: Biodistribution of HDP, HDP-on, HDP-MΦ and HDP-on-MΦ in immunodeficient NCG mice 7 days post injection. 149

Figure 4-8: Biodistribution of HDP and HDP-on in mice pretreated with liposomal clodronate. 150

Figure 4-9: Biodistribution of HDP and HDP-on in mice pretreated with liposomal clodronate 1 day post-transplantation. 151

Figure 4-10: Biodistribution of HDP and HDP-on in mice pretreated with liposomal clodronate 7 days post-transplantation..... 152

Figure 4-11: Biodistribution of macrophages derived from HDP and HDP-on in mice pretreated with liposomal clodronate 1 and 7 days post-transplantation. 154

Figure 4-12: Biodistribution of HDP-on in clodronate-pretreated BALB/c mice at 1, 3, 7 and 14 days post-transplantation. 156

Figure 4-13: Pharmacokinetics of HDP-on in NCG mice and liposomal clodronate treated BALB/c mice..... 157

Figure 4-14: Biodistribution of HDP-on in immunodeficient NCG mice 14 days post-transplantation..... 158

Figure 4-15: Biodistribution of HDP-on in clodronate-pretreated BALB/c mice which received a second injection of HDP-on. 165

Figure 4-16: Model of two-stage immune rejection of HDP. 167

Figure 5-1: Overview of autologous genetically engineered MΦ expressing IDUA (IDUA-MΦ) to treat a mouse model of Hurlers syndrome. 177

Figure 5-2: IDUA expression constructs. 178

List of Figures (continued)

Figure 5-3: Activity and expression of modified IDUA in Cos-7 cells. 179

Figure 5-4: Transduction of HDP with IDUA retrovirus. 180

List of Tables

Table 1-1: Human Clinical Studies using MΦ 27

Table 1-2: Minimally modified therapeutic MΦ in animal models 31

Table 1-3: MΦ as drug delivery vehicles in animal models 36

Table 1-4: Gene modified MΦ therapies in animal models 43

Table 2-1: Modifications made to HDP 64

Table 2-2: Summary of MΦ polarization responses. 68

Table 3-1: Summary of modifications made to improve post transplantation cell survival 83

Table 3-2: Reference chart for various cell types injected in this section 84

Table 6-1: Other immunodeficient animal models 191

1 Chapter 1: Introduction to MΦ and cell based therapeutics

1.1 Overview of MΦ

1.1.1 Origins of tissue MΦ

Macrophages (MΦ) are distributed in all organs where they serve critical functions in maintaining homeostasis in adult tissues [1]. Tissue specific MΦ are involved in phagocytosis of dead and infected cells, maintain T cell tolerance in healthy tissues and initiate immune responses upon bacterial infection [2-4]. MΦ can be best viewed as tissue auxiliary cells that carry out surveillance for tissue integrity, maintain tissue turnover and recruit the immune system to overcome larger tissue damage. In cancer, tumors promote normal MΦ functions of tissue repair preferentially over inflammatory responses for the benefit of tumor growth [5].

For 40 years the dominant theory stated that all MΦ originate from bone marrow derived monocytes based on classic studies by Zanvil Cohn's laboratory at Rockefeller University in the 1960/70s [6]. This view has been dramatically changed in the light of high resolution fate mapping studies that demonstrate the mixed origins of tissue resident MΦ with minimal contribution of bone marrow derived cells during homeostasis [7]. Tissue resident MΦ are deposited during embryonic development originating from yolk sac cells as early as embryonic day 8.5 (microglia progenitors, subset of heart and liver MΦ progenitors) and from fetal liver after gastrulation (Langerhans cells in skin, spleen, heart, lung, peritoneum, kidney MΦ) [8-12]. In homeostatic conditions in most adult tissues, MΦ populations are maintained by self-renewal [13]. Monocyte-independent replenishing of steady state MΦ numbers is regulated in tissues by MafB dependent repression of MΦ specific enhancers which control self-renewal genes common to embryonic stem cells [14].

However, the signals which regulate MafB dependent repression remain unknown. Self-renewal of MΦ can also be induced in disease conditions exemplified by IL-4 dependent signaling in helminth infection models where the immune response is primarily regulated by local expansion of tissue MΦ [15].

The exceptions to the observation that most tissue MΦ are replaced by tissue resident precursors occurs in MΦ located in high antigenicity environments, such as dermal and intestinal MΦ as well as in most heart MΦ. These sites are replenished at steady state, by bone marrow derived monocytes that undergo differentiation into tissue specific MΦ upon entry into the tissues [16-18].

Inflammatory signals during infection or in a tumor microenvironment cause an influx of $Ly6C^{high}$ $Ccr2^{+}$ monocytes to disease sites. This increases local MΦ concentration leading to a mixture of locally derived and bone marrow generated cells [19]. Embryonically derived MΦ can be partially replaced by bone marrow derived monocytes in conditions that deplete resident tissue MΦ [20]. Monocyte-derived MΦ can thus establish a new population of cells that closely resemble the tissue specific MΦ phenotype that was acquired from the initial embryonically derived cells. In MΦ-depletion studies in heart, liver and spleen, depleted embryonic MΦ are replaced by bone marrow monocyte-derived MΦ. These results highlight the complex interplay between bone marrow derived cells and locally renewing tissue MΦ [20].

Therapeutically, the plasticity of monocyte-derived cells, to adopt local specific MΦ functionality, is critical for potential cell therapy applications that aim to replace local MΦ populations with engineered cells. In animal models of pulmonary alveolar proteinosis, in which there is a defect in alveolar MΦ production, adoptively transferred wild type alveolar

MΦ assume lung specific function and have demonstrated very long persistence (up to one year duration of the experiment) [21, 22].

Gene expression programs of the known tissue-specific MΦ populations are highly diverse, and mirror specific functions required in a given organ as well as functions required in distinct compartments of the same organ (Figure 1). However, transcription factors and the signals that establish tissue-specific gene expression programs in MΦ, are largely unknown. The few exceptions include: heme responsive Bach1 in red pulp MΦ, lipids sensing PPARγ in alveolar MΦ or retinoic acid induced Gata6 in peritoneal MΦ [23-25]. Recent discoveries indicate that tissue environment derived signals induce expression of master transcription factors; that in combination with MΦ lineage determining transcription factors PU.1and C/EBP, lead to specific transcriptional programs and cellular phenotypes [26]). Such a combinatorial model can explain the tissue environment dependent diversification of monocyte-derived MΦ populations. The model also rationalizes MΦ tissue transplantation experiments. For instance, placing peritoneal MΦ into an alveolar environment leads to a remarkable 70% genome-wide gene expression reprogramming to reflect the newly acquired alveolar MΦ phenotype [27].

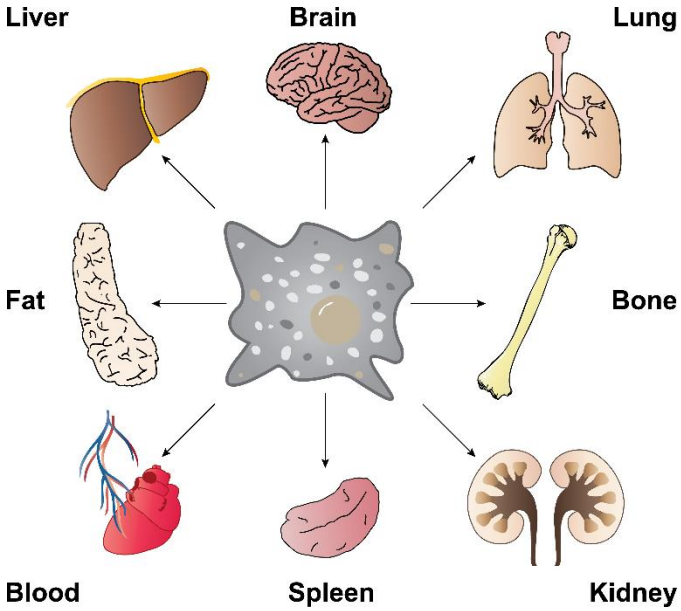

Figure 1-1: Tissue-resident MΦ can be found throughout the body in virtually all tissues and organs. These MΦ perform a variety of tasks including phagocytosis of dead cells and debris, modulating innate immune responses, maintaining homeostatic growth, repair and metabolism. MΦ from different tissues have distinct gene expression profiles, but in some cases, due to phenotypic plasticity, MΦ from one tissue can be transplanted to another and adopt the new tissue-resident profile [27].

This exceptional plasticity of tissue MΦ phenotypes, combined with the centrality of a variety of subtypes of MΦ in control of tissue homeostasis and activation of immune responses to outside and internal insults, make MΦ ideal building blocks for a variety of future tissue replacement therapies [28].

1.1.2 Sources of MΦ for cell-based therapies

Excluding transformed MΦ-like cell lines, two principal sources of MΦ have been utilized to produce *ex vivo* MΦ that can be modified for therapeutic purposes. The first set of techniques is based on differentiating a collection of monocytes from blood or from extracted bone marrow into MΦ in MCSF1 containing media. The second source is by

isolation of pre-existing MΦ from body cavity lavages (alveolar, peritoneal) of resident or elicited (e.g. thioglycollate, peptone) MΦ [29]. Once in cell culture, MΦ can be further incubated with immune stimulators (e.g. LPS, cytokines) to induce different polarizations that mimic *in vivo* phenotypes [30].

The classical MΦ collection methods, such as those used to prepare bone marrow derived MΦ from lavages, have a large body of literature and are well characterized but can only be used to produce relatively small numbers of a particular type of MΦ. Other MΦ elicitation techniques (polyacrylamide beads, proteose peptone) are often poorly characterized which leads to *in vivo* studies that can be difficult to compare and interpret both within and across laboratories. These wide ranging collection methods also produce MΦ with different phenotypes. Regardless of the collection method employed, monocytes or MΦ are produced in relatively low numbers. Plus, these MΦ typically fail to proliferate as they differentiate *in vitro* and are difficult to genetically modify, making cell line generation and genetic engineering infeasible.

For the purpose of autologous therapies, each batch of MΦ requires returning to the donor. The reason is that *in vitro*, monocytes exit cell cycle after 7-10 days of proliferation and differentiation and do not divide; moreover, monocytes have a short life span as they differentiate further into MΦ [31, 32]. To address this need for generating large numbers of MΦ, an alternative strategy that has emerged over the last 10 years is production of MΦ from proliferative, conditional developmentally-arrested, primary MΦ progenitors. Non-transformed self-renewing progenitor cells are established by overexpression of a transcription factor, Hoxb8, in bone marrow progenitors, in media supplemented with GMCSF or Flt3L [33, 34]. Hoxb8 activity leads to the blockade of

progenitor differentiation. This results in rapidly proliferating, clonable cells. Removal of Hoxb8 activity allows progenitors to resume differentiation and produce differentiated MΦ. Hoxb8-GMCSF progenitors differentiate by default into MΦ when Hoxb8 activity is removed [34]. Hoxb8-Flt3L cells are more primitive progenitors that can be differentiated into MΦ in MCSF1 containing media after Hoxb8 removal [33].

Conditional progenitor-derived MΦ production has several major advantages over classical MΦ production methods. First, large numbers of progenitors can be accumulated prior to initiating differentiation. This theoretically enables unlimited cell numbers to be produced. Second, conditionally immortalized progenitors are rapidly dividing cells which enables genetic engineering far more readily than using non-dividing MΦ. Unlike classical monocyte or MΦ isolation techniques, a single cell isolation from the donor is sufficient to generate conditional progenitor lines that can be stored frozen for use in an unlimited number of cell transfer experiments. These attributes dramatically reduce cell production costs while providing a well characterized clonal line for future experiments. The current disadvantage is that conditional progenitor cell based-MΦ have not yet been extensively characterized, hence investigators are unfamiliar with their properties in comparison to directly isolated MΦ populations with their decades of use in research. Fortunately, technological advances in MΦ molecular phenotype characterization *in vivo* have delineated a very large collection of markers that describe MΦ functional states [35]. This knowledge base can be used to categorize the conditional progenitor-derived MΦ that have been differentiated *in vitro.*

1.1.3 Functional polarization of MΦ

MΦ carry out tissue-specific homeostatic functions by regulating gene expression programs in response to the local tissue environment. Such reversible transcriptional programming is termed as MΦ polarization, to distinguish it from permanent tissue-specific MΦ differentiation. Cell-cell contacts and soluble signaling molecules like cytokines, growth factors and extracellular polymers dictate functional polarization of MΦ through intracellular and transmembrane sensors. Historically, MΦ polarization was depicted as a bipolar system of classically (interferon gamma, IFNγ) activated pro-inflammatory MΦ designated as the M1 state and alternatively (IL-4) activated anti-inflammatory MΦ as the M2 state of polarization; to be analogous to Th1 and Th2 type of responses of T cells [5, 36].

It is apparent now that MΦ polarization is a continuum of overlapping functional states that involve a plethora of signals and corresponding dynamic gene expression programs. Given the diversity of MΦ gene expression responses to environmental stimuli, it is critical to describe in detail, the workflow of *ex vivo* MΦ manipulations and to characterize the molecular and cellular properties of the resulting therapeutic cell lines to meaningfully interpret, reproduce or predict outcomes in MΦ based therapies [37]. Understandably this has not been the case in early MΦ adoptive transfer experiments because of the lack of knowledge of MΦ phenotypes.

Changes in MΦ phenotype in response to soluble ligands (e.g. IL-4 and IFNγ) are primarily mediated by NFκB, Signal Transducer and Activator of Transcription (STAT) and Interferon Response Factor (IRF) transcription factor families [38]. *Ex vivo* produced MΦ can be polarized with a variety of defined stimuli, resulting intransient acquisition of

specific gene expression programs and functionality. Historically, LPS and IFNγ have been used to induce pro-inflammatory cytokine expression (IL-12, IL-6, and TNFα) and nitric oxide production [38, 39]. These transcriptional responses are mediated by JAK-STAT (STAT1/2) and TLR4 signaling that activate NFκB and Irf5/Irf8 transcription factors.

A distinct gene expression program is induced by IL-4 that upregulates MΦ mannose receptor expression and arginase production along with a distinct set of anti-inflammatory cytokines (e.g. IL10, CCL17). IL-4 signaling is mediated by STAT6 and Irf4 transcription factors [40]. At the enhancer level the distinct transcriptional responses are exclusive, suppressing the alternative gene expression program. Irf5 recruits transcriptional activators on IFNγ target genes in response to TLR4 signaling while also binding to IL-4 target gene promoters but acting as a transcriptional repressor of these genes [41]. Similarly STAT1 downstream IFNγ receptor directs transcriptional programs that induce pro-inflammatory polarization while suppressing STAT6 dependent activation of anti-inflammatory genes. Different polarization programs are independent modules that can be silenced without negatively affecting competing transcriptional programs. STAT6 knockout cells are unable to mount the IL-4 dependent transcriptional program but are still competent to induce gene expression in response to IFNγ [42]. It is thus possible to engineer MΦ with exquisitely selective sensitivity to tissue environment signals. After cell transfer, this tactic could reduce side effects of cell therapies while retaining the intended *ex vivo* induced functional polarization *in vivo*. Detailed knowledge of the transcriptional circuitry of reversible MΦ polarization may thus enable genetic engineering to “lock” ex vivo-produced MΦ polarizations into permanent functional states for therapeutic use.

In conclusion, the last decade of research on the molecular underpinnings of MΦ differentiation, functional diversity and cell signaling in tissues and *in vitro* environments should enable much better informed strategies to harness this cell type for therapeutic use. This can now be accomplished through genome engineering to customize responses in disease microenvironments or to small molecule effectors that can be administered to regulate MΦ.

1.2 Cell Based Therapeutics

Over the last decade, cell based therapeutics have been developed to exploit endogenous or engineered behaviors of various cell types for therapeutic purposes. In general, cells are collected from a patient, propagated and re-engineered for a specific application, before reinfusion back into the patient (Figure 1-2). These cells renter the body and perform designed functions (i.e. killing tumor cells) and may or may not survive in the host for a long period of time. Modifications to cells for these purposes are usually performed via genetic engineering techniques using lentivirus or retrovirus, but may also include just simple culture to increase the number of cells to be reinfused. Regardless of the modifications, most cell based therapies rely on the endogenous function of the targeted cell type and its role in the disease to be treated. Modifications are made to imbue complementary, synergistic or amplifying characteristics to these endogenous traits that can enhance the therapeutic benefit of the modified cell. Furthermore, increased understanding of the specific biology of disease and the interaction with the body, combined with advances in synthetic biology and genetic engineering has led to the ability to better design cells with specific behaviors and attributes that can be therapeutically beneficial.

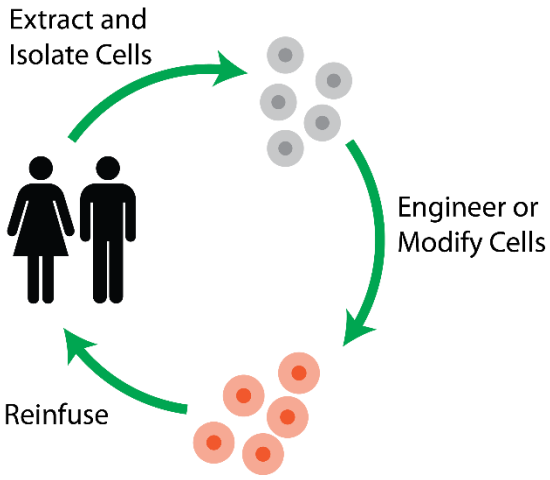

Figure 1-2: General scheme of cell based therapies. Cells are collected from the patient, modified (proliferated, genetically engineered, purified, etc.), and reinfused back into the patient for a therapeutic benefit.

Excluding cord blood products, there are currently only four cell based products approved by the FDA as of January 2017. These include: Gintuit (allogeneic cultured keratinocytes and fibroblasts in bovine collagen) for gum grafting and recovery in oral surgery, Carticel (autologous cultured chondrocytes) for implantation and repair of cartilage damage in the femoral condyle, Laviv (autologous fibroblasts) for improvement of the appearance of nasolabial wrinkles and Provenge (autologous dendritic cells) for the treatment of asymptomatic metastatic and castrate resistant prostate cancer. Two generalized criteria can be used to describe these products. The first is based upon the sourcing of the cells, and as expected, most of the approved products are autologous, allowing the problem of transplantation rejection to be bypassed. However, this creates additional problems because of the need to make an individualized product for each patient. This could impact drug efficacy and dosage, while substantially increasing the cost due to higher manufacturing and quality assurance expenses. The second is based on the application and degree of manipulation of the cells prior to use in patients. Gintuit,

Carticel and Laviv are minimally modified, essentially relying on well-established cell culture techniques to grow and expand the desired cells to a therapeutic dose. This fits well with their approved indications which center around healing, repairing or replacing damaged or missing tissue. However, Provenge is unique as it was developed as a cancer vaccine and manipulated much more than other approved products. In this case, dendritic cells are harvested from a patient and pulsed with a prostate cancer antigen, prostatic acid phosphatase (PAP), fused with a survival factor, GMCSF. After expansion to a minimum of $50x10^6$ cells, the cells are reinfused back into the patient, whereupon the cells activate the patient's immune system to recognize and destroy the prostate cancer cells expressing PAP. However, due to the high cost for Provenge ($100,000 per treatment course) and only modest positive results (increased overall survival of 4 months), sales were far below expectations and Dendreon, the manufacturer of the treatment, declared bankruptcy in 2015 and the rights to Provenge have passed through multiple companies and are now owned by the Sanpower Group as of January 2017. It remains unclear what the future outlook for Provenge may be. Nonetheless, the type of therapy it provided was revolutionary and is valuable in regards of evaluating the scientific innovations and possible marketability of future cell based therapies. Furthermore, the technologies and logistics developed to manufacture and deliver a personalized therapy for each treatment will surely be built upon by the next generation of cell based therapies. From a scientific standpoint, future cell based therapies already in clinical trial testing have built upon the model of modified autologous cells for even further therapeutic benefits, and product approvals are expected later this year for CAR-T cell therapies which will be discussed in the following section. Looking beyond currently approved cell

based therapy products, there has been much excitement in the development of stem cells and T-cells for therapeutic purposes. The following sections will briefly describe their progress.

1.2.1 Stem cell therapeutics

Due to their potential to differentiate into any cell type, stem cells have been studied for use in mostly tissue engineering applications and conditions where certain cell types or tissue are damaged and need replacement. The discovery of the Yamanaka factors allowed for the reprogramming of human fibroblasts into induced pluripotent stem cells (iPSCs) which could be differentiated into a wide variety of cell types and subsequently accelerated the study of stem cell therapeutics. In the last decade, the conditions to differentiate a wide variety of cells from iPSCs have been described, creating a large interest in their application as replacement cells for diseased tissue. In addition, genetic modifications can also be performed in iPSCs to further endow the final differentiated cells with additional properties useful for research (i.e. Fluorescence) or therapy (i.e. Correction of a mutated disease gene). The recent development of CRISPR/Cas9 genetic engineering techniques will no doubt accelerate this process. However, due to the perceived risk of inadvertent oncogenic mutations using viral vectors to introduce the Yamanaka factors to generate iPSCs, stem cells from a different source have also been used. Mesenchymal stem cells (MSCs), found in virtually all tissues are usually collected from the bone marrow, are capable of differentiation into bone, adipose and cartilage, have been of particular interest [43]. MSCs also secrete proangiogenic, antiapoptotic and immunomodulatory factors and have been studied extensively for their therapeutic potential in a wide variety of clinical applications. The earliest clinical trials

used MSCs in the treatment of children with bone defects caused by osteogenesis imperfecta [44], or metachromatic leukodystrophy and Hurler syndrome [45]. These first studies demonstrated the potential of MSCs in treating these genetic diseases by supplying allogenic MSCs capable of producing healthy bone. In the case of the first osteogenesis imperfecta trial, new dense bone growth was detected and bone growth increased by 21 to 29 grams compared to an expected complete lack of bone growth [44]. Updated trials have since demonstrated that while MSCs do not engraft substantially into the bone post transplantation, MSCs secrete a currently unknown mediator which stimulates chondrocyte proliferation and bone growth [46]. This is in contrast to bone marrow transplantation techniques, whereby transplanted cells engraft and directly product collagen and new bone growth [46, 47]. Despite the benefit observed in osteogenesis imperfecta, initial trials for metachromatic leukodystrophy and Hurler syndrome were less successful, with poor engraftment of transplanted MSCs and only slowed bone degeneration [45]. Furthermore, these conditions manifest with a multitude of other major cardiac and neurological defects, which were unchanged. Currently, lysosomal storage diseases such as these are treated with bone marrow transplants due to the greater therapeutic benefit [48]. MSCs have seen success in applications for cartilage replacement and repair in patients with chronic knee osteoarthritis. In a pilot study, 11 of 12 patients treated with an intra-articular injection of $40x10^6$ autologous of bone marrow derived MSCs showed a decrease of poor cartilage areas and an overall increase in high quality cartilage up to one year post treatment [49]. In a similar trial in patients with degenerative disc disease, 9 of 10 patients treated with an injection of $25x10^6$ autologous bone marrow derived MSCs into the nucleus pulposus area reported a significant decrease in pain and

an increased disc space water content one year post treatment [50]. In general, it seems that MSCs have had marked success in treatment of bone and cartilage repair. In other conditions, the results have been mixed. Another area of particular interest for MSCs is for treatment of cardiovascular damage due to the inability of the heart to regenerate tissue following a myocardial infarction and subsequent tissue damage [51]. The applications of MSC therapy rely on four proposed mechanisms for regeneration of cardiovascular tissue post injury or during aging: (1) paracrine factors are released by cardiac progenitor cells to trigger proliferation of existing cardiomyocytes, (2) cardiac progenitor cells differentiate into proliferating cardiomyocytes, (3) mature cardiomyocytes dedifferentiate and re-enter the cell cycle as proliferating cardiomyocytes or (4) injury results in epicardium activation, development of new blood vessels and cardiomyocyte proliferation [52]. While the simplest approach would be a belief that transplanted MSCs may engraft and differentiate into new cardiomyocytes, it is likely any therapeutic benefit will arise from a mixture of the described mechanisms. Animal trails have demonstrated some success in the use of MSCs to repair damaged myocardial tissue [52], subsequent studies have shown that transplanted MSCs are rarely observed in the heart and the benefit of MSC administration is likely not due to newly transplanted MSCs differentiating into myocardial tissue, but rather an unexpected effect due to secretion of anti-inflammatory factors when transplanted MSCs embolized in the lungs [53]. Despite this, a meta-analysis of 33 randomized controlled studies using bone marrow derived MSCs to improve cardiac function after a myocardial infarction showed a statistically significant improvement in left ventricular ejection fraction (LVEF), but no improvement in mortality and morbidity [54]. The applications of MSCs is not only limited to bone and cardiac

conditions, as clinical trials are being conducted in across a wide spectrum of indications, ranging from gastrointestinal, diabetes, immune/autoimmune and neurological indications [55].

As seen in the osteogenesis imperfecta and myocardial repair studies, the success of these therapies may not be a direct consequence of survival and engraftment of the transplanted MSCs. However, it appears that in some cases where transplanted MSCs are able to differentiate and engraft into the tissue (i.e. Osteoarthritis), enhanced survival of transplanted MSCs may further improve the clinical outcomes of these treatments. It remains unclear as to what benefits enhanced post-transplantation survival may have in other therapeutic applications, but it represents a significant unexplored area that may have important consequences on the efficacy of MSC therapies. While these unintended consequences have yielded some positive therapeutic effects, the exact mechanisms of these positive effects are not fully understood. A greater understanding of the molecular mechanisms for these therapeutic benefits will allow researchers to better design and engineer MSCs, identify the best patients and develop optimal transplantation methods that are necessary in order to further advance the use of MSCs in the clinic [56]. Despite this, clinical trials across a wide variety of indications are currently in progress. A search of “stem cell therapy” or “mesenchymal stem cell therapy” in January 2017 on clinicaltrials.gov shows 1496 and 238 open studies, respectively. With this many trials ongoing, it is obvious there is a continuous appetite to push stem cell therapies further into the clinic. Hopefully these trials will reveal more important insights which can be used to develop the next generation of stem cell therapies.

1.2.2 T-cell therapeutics

Unlike the stem cell therapeutics which are mostly used for regenerative applications, T-cell therapeutics are universally used as an anti-cancer therapeutic. This is based upon the ability of T-cells to recognize specific antigens on tumor cells and target them for destruction using innate T-cell mechanisms. The development of these therapies are the results of an increasing understanding of T-cell biology, genetic engineering and cancer immunology, and have resulted in very impressive clinical results [57, 58]. T-cell therapeutics have evolved over the last three decades, beginning with the less engineered tumor-infiltrating lymphocyte (TIL) method to the highly designed chimeric antigen receptor T-cell (CAR-T). Though both methods are quite different, they can be complementary and insights in one area have been used to inform the development of the other [59].

TILs are endogenous T-cells targeted towards a tumor antigen that is naturally found in tumors, and the presence of high levels of TILs is typically correlated with better overall survival [60, 61]. However, the tumor microenvironment inhibits the activity of immune cells and limits the ability of natural levels of TILs to prevent the tumor from spreading. In 1986, Rosenberg et al. [62] described a method to extract and expand TILs from a murine tumor *ex vivo* using IL-2 stimulation. In combination with a cyclophosphamide treatment to suppress the immune system, transplantation of large numbers of TILs into mice bearing hepatic and pulmonary metastatic tumors resulted in elimination of the metastases in >50% of animals [62]. These studies quickly moved to human trials using a similar methodology. In humans, autologous TILs were generated by collecting TILs from a patient's tumor tissue and culturing the TILs in IL-2 until a suitable dose was achieved

(approximately 10^{11} cells per patient) [63]. A cyclophosphamide pretreatment and large dose of IL-2 was also co-administered with the TILs. These initial trials demonstrated especially strong performance in metastatic melanoma, with objective responses observed in about one third of patients [63]. Over the last two decades, multiple clinical trials have been conducted using TILs to treat metastatic melanoma, while varying multiple aspects of the treatment (i.e. Young vs old TILs, IL-2 dosing, type and dose of pre-treatment chemotherapeutic) [64]. For a deeper review of TIL clinical trials, see [64-68]. A critical development was the realization of the need for lymphodepleting preconditioning to increase the efficacy of TIL treatment. Lymphodepletion increased the engraftment and expansion potential of infused TILs by reducing other T-cells from competing for antigen-presenting cell interactions, decreasing immunosuppressive Tregs and removing NK cells which compete for the cytokines IL-7 and IL-15 that are important for maintaining TIL activity [69, 70]. Despite the positive results that have come from TIL therapies, interest has waned due to high costs, significant patient-to-patient variability and the development of CAR-T therapies.

Over the last decade, CAR-T therapies have taken the banner of T-cell therapies due to the hope that by applying a deeper understanding of T-cell biology and protein/genetic engineering techniques, an engineered and controlled T-cell response could be generated towards any chosen antigen. CAR-T therapies still rely upon the same basic principles of TIL therapies, where a T-cell is used to attack tumor cells based on detection of an antigen. However, TILs are directed toward an antigen that develops endogenously, whereas CAR-T are directed towards a specific antigen that has been specifically chosen and engineered into the CAR-T. This is done in CAR-T by the

Chimeric Antigen Receptor, a recombinant fusion protein comprised of a ligand recognition domain from a monoclonal antibody joined with a membrane bound intracellular signaling domain that triggers a cytotoxic T-cell response when the ligand/antigen is bound (Figure 1-3). One advantage of this method over a transgenic TCR is that MHC matching does not need to occur and a single CAR design can be used for all patients. Another is the use of antibody recognition domains significantly enhances the specificity when compared to TILs. In CAR-T therapy, a patient's T-cells are collected and the CAR is introduced into a patient's T-cells by retroviral insertion. Following ex vivo proliferation, lymphodepletion is performed on the patient and the cells are reinfused with a bolus of IL-2 to promote CAR-T survival and *in vivo* proliferation. Due to the similarities between CAR-T and TIL therapies, the knowledge developed with lymphodepletion methods developed from TIL therapy is directly applicable to CAR-T and has been used extensively to identify pre-conditioning regimens for CAR-T therapies. The development of CAR-T has moved through multiple generations, mostly by incorporating an increasing number of signaling domains in the cytoplasmic portion, as reviewed in [71]. Each subsequent generation has demonstrated increasingly more efficacy in clinical trials and current trials are trying to identify the optimal combination of signaling domains [72].

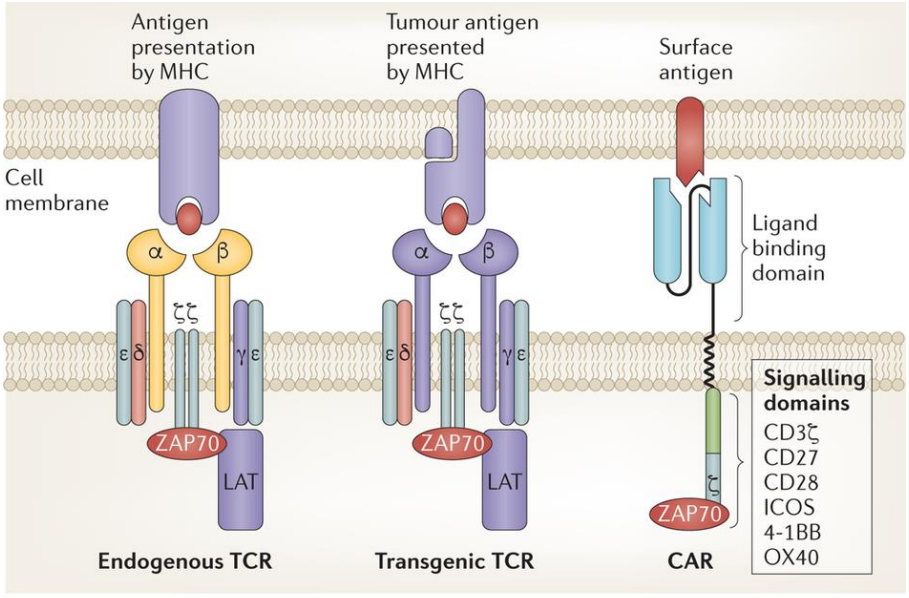

Figure 1-3: Overview of the development of T-cell therapeutics. T-cell therapeutics have evolved over multiple forms from endogenous TCRs to fully designed chimeric antigen receptors (CARs), which enable finer control over which antigens will trigger a T-cell response, but also the downstream signaling events that occur when an antigen is detected. Adapted from: [71]

In the clinic, CAR-T has proven especially effective against B-cell malignancies, particularly B-cell acute lymphoblastic leukemia (B-ALL). B-cell malignancies have been excellent targets for multiple reasons: B-cells express multiple well conserved and specific cell surface markers, minimizing off-target effects; B-cell tumors circulate in the blood, reducing the added difficulty for CAR-T to migrate into a solid a tumor space; and induced B-cell aplasia (due to CAR-T removing *all* B-cells, including healthy B-cells) is a non-lethal condition that can be readily treated [71]. There have been multiple clinical trials using CAR-T targeted towards CD19 that have been successful, with high overall response rates for B-ALL patients (80%) [73-75] and Non-Hodgkin's lymphoma (50-72%) [76]

refractory lymphoma (50-80%) [77]. Despite such high response rates, the treatments have been tempered due to multiple cases of resistance reported, where CD19 has been downregulated or mutated. Relapse rates have ranged from 18-36%, with the vast majority of relapses caused by the development of a $CD19^-$ tumor. Serious side effects have been observed, including cytokine release syndrome, B-cell aplasia and neurological toxicity, though concurrent efforts have minimized the severity and duration of these effects [78]. CAR-T have been developed against other B-cell targets, including CD20, CD22 ROR1, and IgK, and it is hoped that simultaneous targeting of multiple targets can reduce relapse rates [71, 72]. In combination with follow-on studies of the earliest CAR-T trials which have demonstrated detection of transplanted CAR-T at least 11 years post infusion, CAR-T may represent a long-lasting treatment for B-ALL and other B-cell malignancies [79]. Treatments of other hematological diseases, including Hodgkin Lymphoma, multiple myeloma and acute myeloid leukemia are also currently undergoing development and clinical trials [72]. In encouraging developments, as of late 2016, Novartis and Kite Pharma have each announced intentions for filing for FDA approval for their own CD-19 targeted CAR-T therapies for B-ALL by the end of 2017 [80].

Much progress has been made in CAR-T therapies in the treatment of hematological conditions, but progress in treatment of solid tumors has been much more challenging. Nonetheless, progress, albeit slower, has been made in CAR-T therapies for solid tumors. Clinical trials are currently underway for a variety of CAR-T against other targets, including prostate-specific membrane antigen (prostate cancer), mesothelin and fibroblast activation protein (malignant pleural mesothelioma), EGFR (glioma), carcinoembryonic antigen (liver adenocarcinoma), CD171/L1-CAM (neuroblastoma),

HER2 (glioblastoma, metastatic breast/colon/ovarian cancer) and many more [72]. The reasons for why solid tumors have been much harder to treat when compared to hematological tumors are multifaceted. One reason for this is that solid tumors are much harder to access – liquid tumors are directly accessible by cells infused intravenously, while accessing a solid tumor requires proper recruiting/targeting of cells to the tumor and the need to cross significant physical barriers like the extracellular matrix to reach tumor cells [81]. It has been found following *ex vivo* modification and proliferation, CAR-T have a reduced ability to degrade extracellular matrix, and genetic modification CAR-T to overexpress heparanase improved matrix degradation, tumor infiltration and anti-tumor activity in a murine model of neuroblastoma or melanoma [82]. Studies have also shown a rapid die-off of infused CAR-T, with only a small percentage surviving a short time post-infusion [81]. While CAR-T are able to proliferate *in vivo* and still provide a therapeutic response, this rapid decrease indicates overall numbers of CAR-T are exceptionally low at the start, further reducing the likelihood of CAR-T successfully trafficking towards a solid tumor site. Not only does successful treatment require effective trafficking and proliferation/accumulation of CAR-T in solid tumors, the CAR-T must maintain anti-tumor activity in a relatively more immunosuppressive tumor microenvironment that encourages T-cell exhaustion [83]. Newer generations of CAR-T, which are capable of self-stimulation, are less susceptible to immunosuppression, and have been shown to accumulate in higher numbers in solid tumors and correlate with greater clinical benefit [84]. Other techniques include combination therapy with checkpoint blockade to reduce T-cell immunosuppression [85], “armored” CARs which secrete pro-inflammatory IL-12 to also counter immunosuppression [86], preventing immune recognition and removal of foreign

CARs and improving persistence by simultaneously removing B cells [87], and increasing solid tumor targeting by targeting tumor-vasculature targets such as VEGFR-2 [88]. It remains unclear if these techniques will bring CAR-T treatments against solid tumors up to the standard set in hematological conditions, but it demonstrates that the problem is in fact multifaceted and will require consideration of the effects of survival, trafficking, proliferation and immunosuppression on developing CAR-T for solid tumor therapies.

1.2.3 MΦ-based therapeutics

The following sections will extensively review the state of MΦ based therapeutics, starting with examining human trials from the last 30 years then looking at more recent animal trials.

1.2.3.1 Human Clinical Trials: *ex vivo* educated or generated cells

The use of *ex vivo* educated cells has the longest history in MΦ-based therapies. The concept is supported by the discovery of high levels of monocyte and MΦ recruitment towards tumors *in vivo* and animal experiments demonstrating the cytotoxic potential of IFNγ-treated primary MΦ [89-91]. Multiple groups attempted to develop a therapy that would collect blood monocytes, proliferate and differentiate these monocytes into MΦ, "educate" MΦ into a cytotoxic phenotype *ex vivo*, and inject these MΦ into patients, whereupon they would hijack existent MΦ recruiting signals from the tumor or the metastatic sites to traffic to and destroy the tumor [92]. A host of secondary technologies were developed in order to bring these ideas to reality, most notably the abilities to harvest and purify monocytes from human blood using leukapheresis and elutriation [93, 94] and then culture these cells in sterile conditions to produce up to 10^9 cells on a weekly basis per patient (Figure 1-4).

Substantial efforts were made to utilize these cells as an anti-cancer therapeutic, with the earliest human clinical trials occurring in the mid-1980s against multiple cancer types [92].

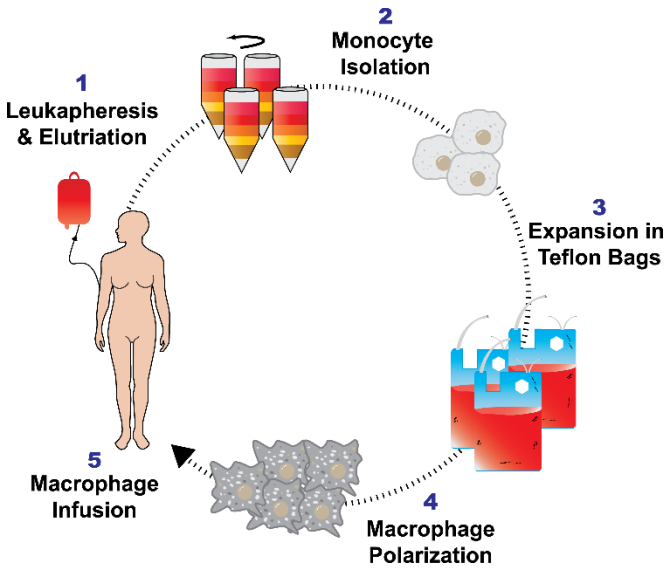

Figure 1-4: Therapeutic MΦ collected from human blood via leukapheresis and elutriation. Monocytes are purified from blood via leukapheresis and elutriation, followed by culture in Teflon bags. Monocytes proliferate and differentiate in media with cytokines (IFNγ and GMCSF) over a period of 7-10 days, generating up to 10^7-10^9 cells per patient.Despite the persistent attempts to use this methodology against multiple cancers, regardless of the dose, schedule and methods of administration, most of the clinical trials were unsuccessful in even slowing the progression of cancer [92]. A review of these trials in the context of the current understanding of MΦ biology and cell-based therapeutics, reveals several important considerations for the future development of MΦ-based cell therapies ([92], Table 1-1).

First, dose-escalation studies in humans demonstrated the relative safety of administering large numbers and frequent doses of autologous MΦ. In the 11 human clinical trials in Table 1-1, the majority of reported side effects were slight fevers and chills,

with no serious side effects at the highest doses (which are limited to ~10^9 as that is the largest number of MΦ that can be extracted and cultured from a patient in one leukapheresis) or frequencies (up to one dose every 24 hours for 3 days). In these autologous studies, immune rejection events were not observed. However, when coupled with the fact that none of these trials succeeded in their therapeutic goals, this safety result should be viewed with caution since perhaps a therapeutic dose of MΦ needs to be orders of magnitude larger than was administered in these trials or the viability of infused cells needs to be improved. If we draw a parallel to CAR T-cell therapies, dangerous and deadly occurrences of tumor lysis syndrome and cytokine release syndrome ("cytokine storms") have been observed in cases of successful tumor destruction by the cell therapy [95]. It is evident that researchers must consider the safety concerns that may arise if conditions can be engineered to enhance the cytotoxicity of MΦ against tumor cells; this could lead to a dangerous milieu of cytokines, dying cells and inflammation.

Second, it is clear from the evolution of clinical trial design and the associated pharmacokinetic/biodistribution studies, that the trafficking potential of the MΦ into tumors was overly optimistic. Early trials injected cells intravenously, hoping to rely on an innate recruiting signal from the tumor to attract the injected cells either directly out of circulation, or from an initial engraftment site (i.e. the lung, liver or spleen) to the tumor. Follow-on studies using Indium-111 labelled cells showed radioactive signals primarily concentrated in the lung immediately post injection, followed by relocation of the signal to the liver and spleen [96, 97]. Distribution of the signal into the tumor was rarely observed and appeared spurious and inconsistent ([92], Table 1). The signal would eventually dissipate from the

lung, liver and spleen but trafficking into the tumor did not seem to occur. This pattern of distribution suggests that the MΦ were being primarily trapped in the lungs soon after injection, a result mimicked in the intravenous injection of mesenchymal stem cells (MSCs) [53, 98, 99].

Based on the biodistribution results indicating residence of signal in the lung and liver, investigators began targeting lung [100] and liver [101] cancers. Other trials infused the MΦ directly into the tumor location including intraperitoneal injections in patients with metastatic lesions in the peritoneum [94, 102] and intravesically into the bladder of bladder cancer patients [103, 104]. Initial trial results in treatment of bladder cancer were positive enough to warrant further comparative trials against standard therapies [103]. However, MΦ instillations were not nearly as effective as the standard therapy in the bladder [104]. Since the completion of this trial in 2010, there are few human clinical trials for anticancer MΦ cell therapy listed in clinicaltrials.gov. There is a Russian clinical trial assessing the Safety of Autologous M2 MΦ in Treatment of Non-Acute Stroke Patients listed on ClinicalTrials.gov (Identifier NCT01845350) although the status of this trial has not been updated since 2013.

Third, it is interesting to note the homogenous methods employed to collect, isolate, culture and prepare the human MΦ for injection. Cells were almost always collected from the blood and isolated using a combination of leukapheresis and elutriation (Figure 1-4). The monocytes collected from this procedure were then cultured, propagated and differentiated in Teflon bags with GMCSF for ~6 days, and then "educated" into a cytotoxic phenotype using 100-1000 U/mL IFNγ for 18 hours prior to injection [96]. This became known as the "MΦ Activated Killer" (MAK) protocol, and was

used with minimal modifications for the published human anticancer clinical trials. While it can be appreciated that the MAK protocol generated high numbers of cells which behaved as expected *in vitro* [105], the trial data clearly indicates that these cells did not mediate a pronounced antitumor response in patients. As described earlier, significant advances in the understanding of MΦ biology were made concurrently with these trials. The newer discoveries illustrate the importance of cell origin, polarization method and perhaps most importantly, the contextual nature of MΦ, which modify their behavior based on the integration of many signals in the environment [106]. The latter feature is especially important because the tumor microenvironment is capable of providing signals to polarize MΦ towards a M2 tissue repair phenotype, further increasing the malignancy of the tumor [107-109]. It is now apparent that in order to harness the cytotoxic and immunomodulatory nature of MΦ, a nuanced understanding of their development, behavior and disease interaction is required.

A more recent application using MΦ as a cell therapy can be seen in Vericel's (formerly Aastrom) Ixmyelocel-T [110], an autologous multicellular therapy that is currently undergoing clinical trials for dilated cardiomyopathy and critical limb ischemia. Bone marrow aspirates are collected and differentiated using a proprietary process that yields a mixture of cells enriched for regenerative MΦ and mesenchymal stromal cells, while reducing the overall proportion of other granulocytes. In current clinical trials, 30-300x10^6 cells are injected once into multiple locations into the affected heart or limb tissue. Vericel has reported that the combination of cells in ixmyelocel-T is able to aid in tissue remodeling and immunomodulation through the secretion of extracellular matrix proteins, anti-inflammatory cytokines, chemokines and growth factors [110-112]. Analysis of the MΦ

component of the multicellular product revealed high expression of M2 markers (CD206 and CD163), indicative of a regenerative phenotype [111]. However, it is not clear what synergistic effects arise from the other cell types. In a recent clinical trial, Vericel showed Ixmyelocel-T improved symptoms and reduced major adverse cardiovascular events (14% of Ixmyelocel-T treated patients compared to 56% of conventionally treated patients experienced events) in ischemic dilated cardiomyopathy [112]. In a trial for critical limb ischemia, time to first occurrence of treatment failure (amputation, doubling of wound area, *de novo* gangrene, mortality) increased significantly and a reduction, but not statistically significant, in total events was achieved [113]. The results from Vericel represent an important accomplishment in the development of MΦ-based cell therapies and underscores the importance of MΦ phenotype on potential disease targets for MΦ therapies.

Table 1-1: Human Clinical Studies using MΦ

Cell Type + Activation Method	Route+ Dose	Disease	Effect	PK/BD	Ref
Leukapheresis and elutriation, cultured 7 days, 18h in 1000U/mL IFNγ	*i.p.,* $3.5x10^7$ cells/dose, weekly for 8 weeks	Colorectal cancer with peritoneal metastasis	N/A	In-111 label, signal stayed within the peritoneum for 5 days, blood peaked at 9% at 48h, no transfer to other organs	[96]
Leukapheresis and elutriation, cultured 7 days, 18h in 200U/mL IFNγ	*i.v.* or *i.p.,* 1-$4x10^8$ cells/dose, escalating every 2 weeks (*i.v.*) or weekly (*i.p.*)	Systemic metastasis (*i.v.*), Peritoneal metastasis (*i.p.*)	Only therapeutic effect: 2/7 disappearance of peritoneal ascites	N/A	[94]

Cell Type + Activation Method	Route+ Dose	Disease	Effect	PK/BD	Ref
MAK, Activated with mifamurtide	*i.p.,* Escalating weekly dose from 10^7-10^9/dose	Peritoneal carcinomatosis (ovarian, pancreatic, gastric, appendicieal)	No therapeutic response. Increase of IL-1, IL-6 and TNFα in peritoneal cavity	In-111 label, signal stayed in abdominal cavity for up to 7 days, no signal in lungs, liver or spleen, 0.5% in blood	[102]
MAK, patients dosed with 50 μg/m^2 IFNγ prior to cell collection	*i.v.* via hepatic artery, 1-10x10^8 cells/day, 3 sequential days, depending on cell recovery from patient	Colorectal or stomach cancer with liver metastasis	No therapeutic response	In-111, 1h: 18% lung, 56% liver, 7d: 12% lung, 43% liver	[101]
MAK	*i.v.,* 1x10^9 cells/dose weekly for 6 weeks	Colorectal cancer	No therapeutic response. 11/14 showed progression, 3/14 stabilized	N/A	[114]
MAK, activated with 1ng/ml LPS for 30 mins. Patients dosed with 2-4 ng/kg LPS prior to cell collection	*i.v.,* 3x10^6-4x10^8 cells/dose, escalating weekly for 7 weeks	Cancer (Colorectal, renal, pancreatic, melanoma or NSC lung)	Increase in TNFα and IL6 by 40x, 1/9 patients with stable disease (<25% growth), 8/9 showed progression	N/A	[115]
MAK	*i.v.,* 3x10^9/dose, 3 doses over 2 weeks	Metastatic renal cell carcinoma	Transitory stabilization (n = 8) or partial regression (n = 1) in 9 of 15 patients	In-111 label, at 72h, lung (6%), liver (24%), spleen (11%), blood (3%)	[116]

Cell Type + Activation Method	Route+ Dose	Disease	Effect	PK/BD	Ref
MAK	Intravesically, $2x10^8$/dose, weekly for 6 weeks	Superficial Bladder Cancer	Recurrence occurred significantly less frequent with standard treatment than with cells (12% vs. 38%; $p < 0.001$)	N/A	[104, 117]
Ixmyelocel-T – bone marrow aspirate enriched for regenerative MΦ and mesenchymal stromal cells by a proprietary process	Local injection to multiple sites in affected heart or limb, 30-$300x10^6$/dose	Dilated cardiomyopathy or critical limb ischemia	Reduced major adverse cardiovascular events (14% treated, 56% control), reduced time to first occurrence of treatment failure	N/A	[112, 113]

1.2.3.2 Recent animal trials: *ex vivo* modified MΦ

The recent studies using ex vivo educated MΦ to treat diseases in various animal models are described in the following sections (Tables 2-4).

1.2.3.2.1 MΦ without extensive modifications

In an Adriamycin-induced nephropathy, both M1 and M2 ex vivo polarized spleen- or bone marrow-derived MΦ injected ($1x10^6$ cells 5 days post nephropathy induction) via the tail vein were capable of trafficking to the kidney [118, 119]. Unfortunately, this trafficking was not quantified, though injected MΦ were detected in the kidney up to 23 days post-injection by histology. However, only M2 polarized spleen-derived MΦ provided any therapeutic benefit, though it is unclear how long the MΦ maintained a M1 or M2 phenotype. While the enhanced therapeutic benefit of M2 MΦ over M1 MΦ was fully

expected, the effect of cell origin was surprising. The authors of the studies suggested that this was because the bone marrow-derived MΦ maintained a certain degree of proliferation, resulting in the eventual loss of M2 polarization and adoption of an M1 phenotype. Maintenance of a M1 phenotype may be possible by overloading MΦ with iron, which has been shown to hold MΦ in a proinflammatory state in human chronic venous ulcers that impairs wound healing [120].

In another study, $1x10^6$ autologous microglia (brain-resident MΦ) derived from the bone marrow of young (3 mo) and aged (17 mo) male mice were transplanted intranasally or intravenously into healthy female mice and their presence in various organs detected using Y-chromosome specific qRT-PCR [121]. Twenty-eight days post transplantation, only microglia derived from young mice were found in the brains of aged mice, and aged microglia could not be found in either young or aged mice, regardless of route of administration (no data was provided regarding the number of microglia which reached the brain). The authors hypothesize that this surprising result may be due to the changes in brain signaling during aging; most notably an increase in MΦ-attractive chemokines (MIP-1α, MIP-1β and CCL5) and survival signals (CD40LR). The results in the kidney and brain illustrate the importance of the origin of the MΦ and their target destination in determining the behaviors of transfused MΦ in disease models. Proinflammatory MΦ have also been shown to impair *staphylococcus aureus* biofilm formation and bacterial burden in a catheter-associated bacterial biofilm mouse model when 10^6 MΦ are locally injected in catheter-adjacent tissue. Importantly, when compared to neutrophils or naïve MΦ, proinflammatory MΦ were able to overcome and reprogram the local environment to

a proinflammatory milieu as shown by enhanced expression of proinflammatory proteins (CXCL9, CCL5, IFNγ, IL-10, IL-17, CXCL2 and IL-6) in the local tissue [122].

Table 1-2: Minimally modified therapeutic MΦ in animal models

Cell Type + Activation Method	Route + Dose	Disease	Effect	PK/BD	Ref
CD11b+ cells isolated from spleens, polarized to M1 (2.5 µg/ml LPS for 2h), M2 IL-4/13 (10ng/ml for 48h) or M0 (untreated)	*i.v.,* $1x10^6$ cells injected 5 days post induced nephropathy	Adriamycin-induced nephropathy in SCID mice	M1/M2 localized to kidneys, M2 protected against structural and function damage	DiI label, combined with F4/80-FITC costain, non-quantitative. Detection in kidney, spleen and liver 24h post injection, accumulation in kidney up to day 21	[119]
$CD11b^+$ cells isolated from bone marrow, 10 ng/ml MCSF for 6 days. M2 polarization: IL-4/13 (10ng/ml for 48h)	*i.v.,* $1x10^6$ cells injected 5 days post induced nephropathy	Adriamycin-induced nephropathy in SCID mice	Bone marrow derived M2 MΦ did not prevent renal injury due to MCSF induced proliferation causing phenotype instability	CFSE label, non-quantitative. Detection in spleen at d2, increasing at d23	[118]
Autologous Microglia derived from bone marrow of young (3 mo) or aged (17 mo) mice	Intranasal or *i.v.,* 10^6 single cell dose	Healthy C57BL/6	Only microglia from young mice migrate to brain in both young or aged mice	Y-Chromosome specific qPCR for detection in lung, blood kidney and liver, brain, non-quantitative	[121]

Cell Type + Activation Method	Route+ Dose	Disease	Effect	PK/BD	Ref
BMDM in MCSF supplemental media from L929 cells for 7-10 days. M1: 10 ng/ml IFNγ	Locally to four sites surrounding catheter, 10^6 single cell dose	*Staphylococcus aureus* (MRSA) biofilm infection in catheter implanted in flank tissue	M1-polarized MΦ significantly impair biofilm formation and bacterial burden in catheter and nearby tissue	N/A	[122]

1.2.3.2.2 **MΦ as delivery vehicles**

The defining attribute of MΦ is their ability to phagocytose material via a variety of mechanisms; hence loading appropriately modified micro and nanomaterials such as: drug crystals, bacteria, gold particles, inert emulsions or liposomes can result in an appreciable level of drug per MΦ. A substantial amount of literature has been published with respect to drug delivery to the reticuloendothelial system [123-128], the effects of varying size and shape of materials for targeted drug delivery [129-133], and trafficking of drugs at the intra- and extracellular level [134-136]. From a purely theoretical basis the highest level of drug loading in MΦ occurs when sparingly soluble drug crystals are loaded. The amount of drug which can be loaded into a MΦ will vary based upon the number of drug particles taken up per cell, drug particle size, drug density and packing factor (percentage of particle that is drug) (Figure 1-5). Assuming realistic values for these variables, one can reasonably expect an approximate range of 10-100 µg/1x10^6 cells. Additionally, the drug cannot kill the MΦ before it reaches the target and it must be able to leave the MΦ once it reaches the target. The prodigious phagocytic ability, when combined with the

trafficking of MΦ to disease sites, especially highly inflammatory sites, has inspired multiple other groups to explore using MΦ as drug delivery vehicles, reviewed in [137].

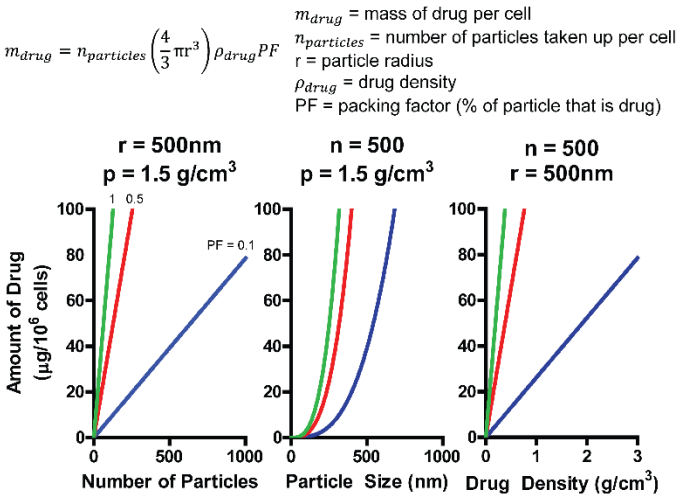

Figure 1-5: Modeling of MΦ uptake of drug particles. Based on the equation described in the figure, a theoretical uptake of 10-100 µg per 10^6 cells is possible. Drug uptake is a function of number of particles phagocytosed ($n_{particles}$), drug particle radius (r), drug density (ρ_{drug}) and packing factor (PF -percentage of particle that is drug). Based on the equation, theoretical drug loading is presented as a function of $n_{particles}$, r and ρ_{drug} at PF values of 0.1 (blue), 0.5 (red) and 1 (green).The potential advantage of using MΦ for drug delivery is multi-faceted. Material contained inside MΦ can enjoy an extended half-life as the encased drug is not rapidly eliminated via renal excretion or liver metabolism, protected from immediate immune recognition, and from clearance by the endogenous RES system. In addition to an extended circulation half-life, MΦ can enable slow release of drug, as seen in the studies from the Gendelman and Batrakova laboratories [138-144]. HIV antiretroviral drugs were delivered via MΦ in a humanized mouse model to HIV infected cells implanted in the CNS and a sustained release of drug at a concentration capable of inhibiting HIV replication was observed over 10 days with no reported side

effects [141, 142, 145]. In a mouse model of Parkinson's disease, RAW264 MΦ injected intravenously were found to migrate into the space surrounding the insult that induced the Parkinson's phenotype and delivered plasmid DNA expressing GDNF to nearby cells. The authors speculate that the DNA was delivered from the MΦ into the surrounding cells via exosomes [138]. While ensuring the MΦ will carry the drug is easy, delivery of the drug once the MΦ reaches its target site remains a challenge. To date, most publications have exploited the passive release of the drug through cell death, slow release of a drug capable of crossing the cell membrane, or through an exosome mechanism (Table 1-3). One tactic to ensure the potentially toxic drug cargo does not kill the MΦ prior to delivery is to package the drug into a liposome as described for doxorubicin instead of using the free drug [146]. This approach seems to rely on the death of the MΦ when it reaches the target. This tactic could be difficult to control if MΦ fail to localize in large enough numbers to deliver an effective dose at the target site. Selecting a sparingly soluble drug that is relatively non-toxic to the MΦ and can be released as it becomes soluble is one effective innovative method. HIV antiretroviral therapy drugs were milled and combined with block co-polymers to form drug crystals known as NanoART [141, 142, 145] that were readily phagocytosed by MΦ, up to 45 μg/1x10^6 cells, and solubilized slowly in the cell, enabling slow release. The time scale for this release was such that MΦ could be injected, migrate to various tissues, and still contain the vast majority of the drug. The drug crystal slowly dissolved, and since the drugs can permeate cell membranes, the drug was slowly released out of the cell. A similar mechanism was used to deliver Nanozymes in a Parkinson's disease model [139, 140]. Nanozymes are a combination of the therapeutic enzyme, catalase, with block co-polymers. Bone marrow derived MΦ readily

phagocytosed Nanozyme, and increased the circulation half-life and tissue AUC of catalase when compared to injection of the free protein [139, 140]. These methods could in theory also be applied to deliver drugs to other conditions with inflammatory pathologies that recruit MΦ, such as, bacterial infections, cancer and chronic inflammatory diseases.

An alternative release mechanism proposed by Batrakova and co-workers is that the MΦ can package and release certain cargos in exosomes [138, 147]. Exosomes are small vesicles released by all cells which can contain protein, DNA and/or RNA. The relevance is that exosomes have been shown to act as an intercellular signaling transport system [148] and could potentially provide delivery over short distances to adjacent cells after the MΦ has migrated to the disease site [138, 147]. The contents of an exosome is unique to the cell from which they originate, and often contains markers from the cell of origin [148]. Exosomes isolated from MΦ which have been transfected with plasmid DNA have been found to carry the protein produced by the transfected plasmid DNA, the mRNA for the protein and the transfected plasmid DNA [138, 147]. Batrakova's group has demonstrated exosomes isolated from *in vitro* MΦ cultures can act as delivery vehicles for protein, plasmid DNA or mRNA [149]. In effect, the exosomes act as horizontal gene transfer vehicles for plasmid DNA or mRNA to adjacent cells.

An interesting approach to achieve a therapeutic effect is to bypass the need for drug to leave the MΦ by using agents that act via physical mechanisms irrespective of whether or not they are inside of the cell. The Gendelman group has loaded MΦ with super paramagnetic iron oxide nanoparticles for imaging purposes [144], whereas the Baek and Hirschberg groups have loaded gold nanoshells into MΦ for photothermal therapies [150, 151]. Both of these applications take advantage of the trafficking aspect of MΦ to

disease sites, but their effects are triggered by external sources, so they do not have to be released from the MΦ.

Table 1-3: MΦ as drug delivery vehicles in animal models

Cell Type + Modification	Dose	Disease	Effect	PK/BD	Ref
BMDM in 1000U/ml MCSF + catalase mixed with PEI-PEG block copolymer (Nanozyme)	*i.v.,* 25ug nanozyme per $1x10^6$ cells, $5x10^6$ cells/dose	Parkinson's Disease in wildtype Balb/c mice (MPTP induced)	Reduced microgliosis, increased dopaminergic neuronal survival	I-125 labeled catalase, 24h post injection: spleen (0.6%), liver (1.2%), lung (0.6%), kidney (1%), brain (0.5%), improved clearance, half-life, AUC, MRT and Vd in BMDM/nanozyme	139, 140, 143
Murine BMDM (10d in 2mg/ml MCSF) + Indinavir (IDV) or Super paramagnetic iron oxide (SPIO)	*i.v.,* $2x10^7$ cells/dose, incubated with $5x10^{-4}$ M IDV for 12 h. Injected prior to viral challenge	Hu-PBL-NOD/SCID mice, reconstituted with human PBLs, *i.p.* injected with HIV-1 ADA	51% reduction in HIV-1 p24 antigen at day 14. Enhanced CD4+ T-cell survival	Sustained response over 10 days, 4-50 fold of clinical effective plasma levels in multiple organs (liver, spleen, lung, lymph nodes)	144
Peritoneal MΦ from Thioglycollate treated mice + liposomal doxorubicin, iron oxide	*i.v.,* Doxorubicin: $5x10^6$ cells/wk, 5 weeks, 30 µg dox	Xenograft A549 subcutaneous and metastatic tumor in nude mouse	Reduced tumor volume when compared to equal amount of free doxorubicin	IO labeled cells detected by Prussian blue staining in s.c. tumor. Not quantitative	146

Cell Type + Activation Method	Route+ Dose	Disease	Effect	PK/BD	Ref
$CD14^+$ monocytes from human blood buffy coat + Gold nanoshells	*i.v.,* 10^7 cells 4 wks post tumoring	Human MDA-MB-231 BR brain metastatic xenograft in nude mice	N/A (photothermal therapy not performed)	Tracking by anti-human CD68 and fluorescent microspheres show trafficking of monocytes from lungs to liver, spleen and brain metastasis	[152]

1.2.3.2.3 Genetically Engineered MΦ

Perhaps the most exciting potential application of MΦ is the use of genetic engineering to augment existing MΦ behaviors or endow new functionalities [153]. Since MΦ are heavily implicated in inflammation, healing and general homeostatic maintenance in virtually all tissues [106], they are a logical cell type for the development of new genetically engineered therapeutics.

The failure of early trials which used *ex vivo* educated anti-tumor MΦ, might have been due to lack of MΦ trafficking into the tumor or to the plasticity of MΦ which would likely result in a rapid loss of the anti-tumor phenotype due to re-education from the tumor microenvironment [107-109]. Genetic engineering methods that can be used to enforce specific therapeutic behaviors are listed in Table 1-4. For instance, IFNβ is implicated in inhibiting angiogenesis in tumors by repressing pro-angiogenic (VEGF and MMP9) and homing receptor (CXCR4) genes in neutrophils [154]. IFNβ-deficient MΦ treated with exogenous IFNβ, upregulate genes (iNOS and IL-12b) associated with cytotoxic phenotypes [155]. Thus, sustained expression of IFNβ may enhance the cytotoxic activity of MΦ while also modulating the tumor microenvironment.

MΦ generated from an iPSC-derived myeloid line transfected to constitutively express IFNβ, were injected three times weekly, for three weeks ($2x10^7$ cells/dose) into the peritoneum of a SCID mouse with an intraperitoneal disseminated NUGC-4 human gastric tumor. This protocol significantly inhibit tumor growth, with an untreated tumor growing 5x over 14 days, whereas in the group treated with MΦ-IFNβ the tumor only doubled in size [156]. Importantly, treatment with unmodified iPSC-derived MΦ resulted in *enhanced* tumor growth of 10x over 14 days, indicating the unmodified cells are either pro-tumorigenic or the tumor is able to repurpose these MΦ into a pro-tumorigenic phenotype. A cytotoxic effect was also observed *in vitro* and IFNβ-expressing MΦ mediated more cytotoxicity than MΦ expressing IFNγ or TNFα, even though IFNγ or TNFα are generally regarded as more potent cytotoxic mediators. The authors indicated this outcome may reflect the reduced levels of expression of IFNγ or TNFα in the transduced MΦ due to the toxicity of high levels of IFNγ and TNFα.

Escobar et al. performed autologous hematopoietic stem cell transplants with selective expression of IFNα in $TIE2^+$ tumor-associated MΦ in MMTV-PyMT, a spontaneous breast cancer mouse model, at 5.5 weeks [157]. Administration of IFNα has proven effective in solid and hematologic cancers though is limited due to high toxicity [158, 159]. However, the highly localized $TIE2^+$-MΦ-mediated delivery of IFNα reduced lung metastatic areas 5-fold and primary tumor size 3-fold without apparent toxic effects [157].

Rather than attempting to change endogenous MΦ behavior, a number of investigators have modified MΦ to express therapeutic proteins [21, 22, 138, 147, 160-162]. For instance, P450 reductase, an enzyme that catalyzes the conversion of the prodrug cyclophosphamide (CPA) into toxic metabolites, was inserted into CD14+ human

monocytes using an adenovirus [160]. To further increase the specificity of P450 reductase expression in the hypoxic tumor, the expression was placed under the control of a synthetic hypoxia responsive promoter, OBHRE. A single intraperitoneal injection of $2x10^6$ modified MΦ, followed by weekly intraperitoneal injections of CPA, in two different human ovarian carcinoma xenograft peritoneal models resulted in a doubling of median survival time (HU: 49 to 21 days, TOV21G: 106 to 56 days) when compared to mice treated with unmodified MΦ and CPA. A similar study was performed where intraperitoneally injected RAW264 cells stably transfected with intracellular rabbit carboxylesterase, a prodrug convertor for irinotecan to SN38, in a peritoneal Pan02 pancreatic tumor, was able to minimally increase mouse survival time by approximately 10% [162].

In an interesting application of MΦ or MΦ-like cell lines as bioreactors, RAW264 cells were transfected with plasmid DNA encoding glial cell-line derived neurotrophic factor (GDNF) [138, 147], catalase or luciferase [138]. The modified cells ($5x10^6$ cells in a single dose) were intravenously injected via tail vein into a Parkinson's disease mouse model. In this mouse model, Parkinson's-like pathology is induced by an intracranial injection of 6-hydroxydopamine (6-OHDA), resulting in strong inflammation of the brain. Transfected RAW264 cells were found in the brain hemisphere injected with 6-OHDA up to 21 days post administration, and the respective protein transfected into RAW264 cells was found to be expressed. In the case of GDNF and catalase, neuron degeneration was reduced and neuroprotective behavioral effects were observed as quantified using rotarod and aphomorphine toxicity rotation tests [138, 147] when compared to unmodified RAW264 cells. Live animal imaging 30 days post transplantation with luciferase-expressing RAW264

cells revealed luciferase expression only in the brain, though it is not clear if this is arising from the transplanted RAW264 or other neuronal cells transfected by secreted exosomes from MΦ containing luciferase plasmid. Confocal microscopy on organ slices collected 1 and 5 days post transplantation revealed GFP-expressing RAW264 cells could be found in the lesioned hemisphere, spleen, lymph node and liver, with the number of GFP+ cells increasing in the lesioned hemisphere from day 1 to day 5 and decreasing in the other organs. Additionally, polarizing RAW264 cells towards an M2 phenotype using IL-4 further enhanced the neuroprotective effects, though it is not clear if this was due specifically to the M2 phenotype, an enhancement in cell survival or a change in MΦ trafficking to the brain.

GMCSF, a growth factor for monocytes and MΦ, or components of its cognate receptor, has also been transduced into MΦ for two different applications. In the first, autologous or allogenic monocytes were purified from rabbit blood, transduced with adenovirus to express GMCSF and differentiated into MΦ [161]. Transplantation of $3x10^7$ autologous GMCSF-MΦ or allogenic unmodified MΦ via an ear vein injection upstream of a post arterial ligation model in rabbits revealed augmented blood vessel growth. The authors found in the allogenic, but not the autologous, transplant of unmodified MΦ, inflammation was induced, leading to recruitment and heavy infiltration of endogenous monocytes into the affected areas which aided in arteriogenesis. While the autologous MΦ appeared to infiltrate, this was insufficient for therapeutic benefit. Autologous MΦ infected with GMCSF adenovirus were able to mimic the effect observed using allogenic unmodified MΦ. The addition of GMCSF was chosen to improve monocyte lifespan and because local injections of GMCSF improve arteriogenesis [163].

The most exciting application of a MΦ-based therapy were reports of a treatment of pulmonary alveolar proteinosis [21, 22]. This condition occurs in mice due to the loss of the beta subunit of the GMCSF receptor (*Csf2rb*). Loss of *Csf2rb* results in poor MΦ survival in the lungs, progressive accumulation of lung surfactant and eventual respiratory failure. Two groups, Happle and coworkers [21] and Suzuki and colleagues [22] demonstrated wildtype or *Csf2rb*-corrected MΦ instilled into the lung engrafted in the lungs, survived for at least 9 months and highly significantly, improved the survival of the *Csf2rb*$^{-/-}$ mice. This was suggested to be due to the survival advantage granted to the wildtype or gene-corrected MΦ by a functional GMCSF receptor and an unoccupied MΦ niche due to the lack of other MΦ within the lung capable of competing for local GMCSF. At one year post transplantation, Suzuki et al. show gene-corrected MΦ transplanted into *Csf2rb*$^{-/-}$ mice were able to self-renew to levels found in wildtype mice. Importantly, using histology and flow cytometry, *Csf2rb*$^{-/-}$ mice transplanted with GFP-labeled MΦ showed complete integration of transplanted MΦ throughout the intra-alveolar and interstitial spaces. Microarray analysis confirmed gene expression profiles of the alveolar MΦ in the transplanted and untreated wildtype mice were virtually indistinguishable. This is especially surprising because prior to transplantation, the gene-corrected MΦ isolated from bone marrow, are distinct from alveolar MΦ. The ability for transplanted MΦ to dynamically alter their phenotype to match the local tissue-resident MΦ lends further credence to the concept that local tissue microenvironments provide instructive signals which can shape the behavior of MΦ [106].

Genetically engineered MΦ have great potential and further modifications of MΦ to augment their behavior could form the basis of new therapies. For example, increasing

GMCSF or GMCSF receptor expression may increase survival of transplanted MΦ in tissues beyond the lung [21, 22] or blood vessels [160]. As the development, identity and behavior of the many tissue resident MΦ are better understood, it may be possible to engineer MΦ *ex vivo* that migrate into and survive in specific organs after administration by activation of specific transcription factors [164, 165]. Phenotype plasticity may also be altered. For example, knocking out proteins in the NFκB pathway may lock polarization of MΦ in a cytotoxic M1 phenotype, as shown with IKKβ knock out MΦ adoptively transferred into an ID8 tumored mouse, where a M1 cytokine profile (IL-10, IL-12p70, TNFα) and differential expression of M1/M2 genes (IL-12p40 and arginase-1) were observed up to 14 days post transfer in tumor ascites and tumor associated MΦ, respectively [166, 167]. However, it should be noted that the tumor associated MΦ profiled for M1 genes may not necessarily be the cells adoptively transferred, as these could not be distinguished from the endogenous population. Overexpression of miR-222 in RAW264 cells co-injected with 4T1 breast tumor cells inhibited tumor growth by limiting MΦ chemotaxis and suppressing tumor growth by inhibiting the CXCL12-CXCR4 axis [168]. Inhibition of STAT3 by overexpression of STAT3β in tumor associated MΦ also suppressed tumor growth [169]. Proliferative capacities can be programmed into MΦ in a variety of means; Hoxb8 overexpression at the monocyte progenitor level results in a self-renewing capacity, whereupon loss of Hoxb8 results in MΦ differentiation [34]. It was recently discovered that transiently reduced expression of the MafB transcription factor activates a self-renewal program in tissue-resident MΦ [14, 170, 171]. This observation opens the door to controlled proliferation of MΦ *in vivo*, which may be necessary to induce high

levels of engraftment. This could increase the potency of the treatment. With the advent of techniques like CRISPR-Cas9, engineered cell behaviors are closer to reality.

Table 1-4: Gene modified MΦ therapies in animal models

Cell Type + Modification	Dose	Disease	Effect	PK/BD	Ref
Autologous or allogenic blood monocytes + GMCSF	*i.v.* (ear vein), $3x10^7$ cells single dose	Arteriogenesis post arterial ligation in rabbits	Allogenic, but not autologous, GMCSF expressing monocytes resulted in augmented vessel growth	β-Gal expression, non-quantitative. Infiltration in ligation site at 24h (no data on other sites)	161
CD14+ human monocytes + P450 reductase for prodrug cyclophosphamide (CPA)	*i.p.,* $2x10^6$ cell single dose, 1mg CPA weekly	HU or TOV21G tumor xenograft in nude mice	HU: Median survival increase from 21 to 49 days, TOV21G: From 56 to 106 days	N/A	160
iPSC-derived myeloid line + IFNβ	*i.p.,* $2x10^7$ cells/dose, 3 doses/week for 3 weeks	NUGC-4, MIAPaCa-2 in SCID mice	IFNβ modified cells inhibited tumor growth; NUGC-4: 5x (untreated) vs 2x, MIAPaCa-2: 2x vs 0.1x	N/A	156
RAW264 + GDNF, catalase or luciferase, Polarization: M1 (IL-4 (20ng/ml) 48h)	*i.v.,* $5x10^6$ cells, (single dose)	Parkinson's Disease in wildtype Balb/c mice (6-OHDA induced)	Reduced neuroinflammation, improved performance on rotarod behavioral tests	Luciferase transfected cells injected, significant difference between diseased and healthy mice in signal visualized in brain	138, 147

Cell Type + Activation Method	Route+ Dose	Disease	Effect	PK/BD	Ref
Wildtype mouse BMDM or Human MΦ differentiated from CD34+ cord blood in GMCSF	Endotracheal instillation, $2x10^6$ cells (single dose)	Pulmonary alveolar proteinosis (*Csf2rb*$^{-/-}$)	Prevention of mortality and normalized disease-related biomarkers	Persistence of at least nine months in lungs	[21]
RAW264 + doxycycline inducted - intracellular rabbit carboxylesterase (converter of prodrug irinotecan to SN38)	*i.p.*, $2x10^6$ cells/dose (day 5, 9, 13 post tumoring), doxycycline (day 7, 11, 15)	*i.p.* Pan02 pancreatic tumor	Increased average survival of 2.5 days (10%) compared to doxycycline control	Tracking of PKH26 fluorescent label on RAW264 cells injected *i.p.* found label only in tumor	[162]
IFNα restricted to tumor-associated $TIE2^+$ MΦ	Hematopoietic stem cell transplantation	MMTV-PyMT primary and metastatic breast tumor	5x reduction of total lung metastatic area, 3x reduction of primary tumor size	N/A	[157]

1.2.3.3 ***In vivo* survival: pharmacokinetics and biodistribution of administered MΦ in animals**

An important rationale for MΦ based cell therapy is that injected MΦ can migrate to the site of innate recruiting signals generated by inflammatory conditions. In this respect there is a paucity of studies that examine the fate of administered MΦ in a systematic and quantitative manner. In publications where MΦ are used as drug delivery vehicles and BD/PK of the drug is measured, there are slightly enhanced pharmacokinetics when drugs are packaged within MΦ. For example, the plasma half-life

of catalase is increased from 2.5h to 3.3h following its delivery in a MΦ. Despite the small increase in PK, tissue AUC increased significantly by 2-3x depending on the organ [139]. This would be indicative of either drug release from MΦ or drug remaining in MΦ which have left the circulation and entered the tissue [139]. In the HIV anti-retroviral MΦ delivery study the biodistribution of indinavir, a small molecule HIV antiretroviral, showed significantly higher levels of drug within the: spleen, lung, liver and lymph nodes. Remarkably, the levels were stable over 10 days, further supporting the “drug depot” model, although it was not evident if the drug was in the original loaded MΦ or rather if the MΦ had been destroyed and the drug crystal had distributed to these organs after release from the MΦ [144].

The Choi and Baek groups have attempted to trace the trafficking of the MΦ by tracking the loaded material through histology. Iron oxide particles were loaded into MΦ prior to intravenous injection into a nude mouse bearing a xenograft human tumor, and iron oxide particles were detected in the tumor using Prussian blue staining 5 days post injection [146]. However, no other organs were evaluated, so it is unclear whether this was a specific trafficking effect. Moreover they did not demonstrate the iron oxide was in the original MΦ that were loaded with the iron. Loading of liposomal doxorubicin into MΦ showed a modest effect on reducing tumor growth, when compared to a similar dose of free liposomal doxorubicin [146] however here again, it was not clear if the liposomes were delivered by MΦ which had migrated into the tumor.

In another study, MΦ loaded with gold nanoshell particles were injected directly into the tumor. Histological analysis of the tumor for the gold nanoshells post photothermal therapy revealed the vast majority of gold remained immediately adjacent

to the injection site as large aggregates, indicating minimal migration of the MΦ away from the injection site into the tumor [150]. Human monocytes loaded with gold nanoshells intravenously injected into nude mice with human MDA-MB-231 BR brain metastases were able to cross the blood brain barrier and co-localized with metastatic sites 24 hours post injection. To confirm the identity of human monocytes by histology, anti-human CD68 in conjunction with monocytes loaded with fluorescent microspheres were used [152]. In another qualitative study, intravenously injected luciferase transfected RAW264 MΦ followed by live animal imaging in a mouse model of Parkinson's disease have demonstrated trafficking of MΦ towards sites of inflammation [138], but it remains unclear how much of the initial MΦ successfully survives the injection process, migrates towards the brain and what (if any) off-target migration occurs.

In more quantitative studies demonstrating the use of gene corrected ($CD131^+$) MΦ transplanted into the lungs of Csf2rb ($CD131^-$)-deficient mice, engraftment and survival kinetics were evaluated by tracking the percentage of $CD131^+$ cells in bronchoalveolar lavage as determined by flow cytometry. Over a period of 12 months, $CD131^+$ cells rose from zero to 69% of bronchoalveolar lavage cells due to proliferation of the transplanted MΦ. Transgene specific PCR conducted at 1 year after transplantation showed transplant-derived cells present only in the lung, but not in blood, bone marrow or spleen [22]. In general, the reliance on histology for MΦ markers and/or tracking loaded materials to show presence of MΦ in various tissues has not resulted in a quantitative understanding of the effect of the route of administration on the time dependent persistence of injected MΦ in the blood or other tissues.

1.3 Research motivation, potential pitfalls and opportunities

The field of MΦ-based therapies is emerging but several gaps in understanding need to be addressed for the field to progress as a cell based therapy. Specifically there are needs for: 1) quantitative methods to evaluate the biodistribution, kinetics and survival after administration of live MΦ in an animal, 2) the use of explicitly defined primary MΦ rather than transformed cell lines in animal studies, 3) the extension of tactics developed in stem cell delivery fields to administer MΦ so that a high portion of injected cells survive the initial administration and 4) the use of niche generating methods to enhance MΦ engraftment.

First, over the last ten years, a series of groups have published results attempting to map the trafficking of transplanted cells. The vast majority of these studies label the MΦ with a fluorescent dye, radioactive marker or imaging particle that is tracked post transplantation. The results are often similar; the signal is first confined to the lung, then is observed to move to the liver and spleen, much like the results observed in the initial human trials and in studies using MSCs [53, 98, 172-174]. A significant concern is that these methods do not indicate the viability of the cell. All of these tracking materials can be transferred to other cells if the transplanted MΦ dies (especially highly phagocytic endogenous MΦ). Since the signal is not coupled with cell viability, one cannot be sure if living cells are tracked. If the MΦ die, signals that are observed would represent the trafficking of other cells or the normal metabolism of the marker.

In order to trace the efficacy of a cell-based therapy, it is critical to be able to accurately determine the trafficking and position of the viable transplanted cells. This can be accomplished using more techniques which track live cells [98, 172]. For example,

luciferase or fluorescent protein activity is rapidly lost when not within a cell, so detection of these proteins can be used as a method to determine the viability of transplanted cells [175-177]. Due to the lack of PK/BD data on systems where signal is coupled directly to cell viability, the efficiency (percentage of administered cells that lodge in the target site and their survival time) and extent of engraftment has not been determined [118, 119, 121, 139, 140, 143, 144, 146, 150, 156, 160].

A related concern is the lack of quantitative analysis that is applied to the biodistribution of transplanted MΦ into other sites. Few studies report the percentage of dose or absolute number of cells that are observed in various organs, making it difficult to evaluate the engraftment efficiency in non-target sites. While it is understandable that certain techniques do not easily lend themselves to quantitation, the application of quantitative histological assessment using donor MΦ specific antibodies is required to indicate the presence of transplanted MΦ in the tissue of interest (i.e. Anti-human CD68 staining for human monocytes in a mouse background [152]). The number of stained MΦ profiles in multiple sections not only in the target organ but also in organs such as the spleen, liver and lung would improve the current understanding of where the injected cells go and how long they remain. Quantitation of cell biodistribution and survival provides essential information in determining paths forward for the development of MΦ therapies. For example, if therapeutic efficacy is observed, despite a very low number of engrafted cells, it may indicate the effect is not due to the engrafted cells but to a molecule secreted from the injected MΦ elsewhere in the body. An example of this behavior is reported in a myocardial infarction mouse model with intravenously injected MSCs that are mostly entrapped in the lungs. Entrapped MSCs in the lung secrete TSG-6, an anti-inflammatory

protein that decreased the systemic inflammatory response, reduced infarct size and improved cardiac function [53]. As with other cell-based therapeutics, immune rejection is a possible concern. To our knowledge, these events have not occurred partly due to the use of autologous material, but may also be due to the lack of engraftment data or a robust means of tracking cell survival post injection.

Quantitative biodistribution studies coupled with gene expression profiling of the transplanted MΦ may provide guidance on why those cells were able to engraft, while the majority of the population was not. This information could direct the development of genetically modified lines with improved engraftment towards specific organs. Due to the lack of such data in the literature, these questions cannot yet be answered.

Second, the MΦ used in the reviewed publications are generated from a variety of sources using a number of different protocols. Ranging from cell lines (RAW264, THP-1), collection from blood, isolation from bone marrow, or spleen, the behaviors and phenotypes can vary widely. MΦ cell lines, while possessing many of the same characteristics, are nonetheless significantly different from primary MΦ. Compared to primary cells, cell line MΦ are exceptionally robust, requiring no extra growth factors for survival. This likely affects their trafficking and ability to engraft into other organs in ways that may be difficult to mimic using primary cells. While cell lines provide proof of concept information, the genetic differences between cell lines and primary cells may lead to misconceptions concerning survival and engraftment efficiency. Due to their replication potential, cell lines have a potential tumorigenicity or virus shedding that make them poor candidates for translation into the clinic.

Investigators should be very explicit in the methods section in their publications concerning the collection and differentiation protocols, including the animal strain, any pretreatments, age, anatomic source of precursor cells/monocytes/MΦ, culture conditions and cytokine treatment [37]. As mentioned earlier, changing the source of MΦ from spleen to bone marrow resulted in significant different results in a model of nephropathy [118, 119]. Specification of MΦ subtypes has also become incredibly complex over the last decade, and the M1/M2 paradigm is fading in favor of a more dynamic classification based upon describing the MΦ based on the full context of its' origin and differentiation pathway, growth medium conditioning and gene expression profile [37, 109]. As a corollary, the behavior of MΦ *post* transplantation need also be studied. Suzuki et al. performed an outstanding characterization of the infused MΦ post transplantation, to establish that bone marrow derived MΦ are capable of adopting a lung-resident MΦ profile [22].

It is interesting to note that many studies utilized immunocompromised mice. Due to the lack of comparable data with immunocompetent mice, it is not clear what the effects using immunocompromised mice would have had on the outcome. Systematic studies that examine the multifaceted interactions between endogenous immune cells and transplanted MΦ in autologous models using a variety of immunocompromised mice should provide instructive and interesting results that may be applicable for developing effective therapies in humans using transplanted MΦ.

Third, the field of mesenchymal stem cell (MSC) transplantation can provide guidance towards determining or increasing the trafficking, survival and tracking of transplanted MΦ [178, 179]. While in depth tracking studies of intravenously injected MΦ have yet to be performed, the results in MSC transplantation mimic some aspects of the

results observed in the human clinical trials of MΦ cell therapy. Intravenous injection of $5x10^5$ fluorescent DsRed-expressing MSCs radiolabeled with Cr-51 demonstrated a distinct separation of detectable viable fluorescent protein and radiolabel in the blood, lungs, liver, spleen, kidneys and bone marrow. The majority of Cr-51 signal was detected in the lungs one hour after administration, followed by migration of the signal to the liver at 24h. The presence of live MSCs was determined by culturing cell suspensions generated from organs collected at 5 min, 1, 24, or 72h for up to 7 days and identification of $DsRed^+$ MSCs by fluorescence microscopy and flow cytometry for CD44, a MSC-specific marker. In contrast to the radiolabel measurements, live MSCs were detected only up to 24h in the lungs, and were not found in other organs examined at any other time points [98]. This differential observed between live cell and radioactivity signals was hypothesized to be radioactive cell debris undergoing liver clearance. Repeating similar experiments in immunodeficient mice lacking NK, T and B cells or an ischemia-reperfusion liver injury model did not alter these results, indicating an adaptive immune response was not responsible for loss of HSCs nor did a strong inflammatory signal recruit HSCs to the liver [98]. This study showed MSCs injected intravenously are short-lived and viable MSCs cannot be detected beyond the lungs 24h post injection. Similar experiments tracking transplanted MSCs have also shown the majority of MSCs to be trapped in the lungs [172-174, 180].

MSC entrapment in the lungs may be due to the size of cultured MSCs (~20 μm diameter), which exceed the diameter of pulmonary capillaries [172]. Ge and coworkers by fractionating MSCs into small (~18 μm) and large (~30 μm) cells, showed that when injected into intra-internal carotid artery considerably higher rates of infarct in the brain

when larger MSCs were injected [181]. Whereas 3D cultured HSCs were uniformly smaller (~13 μm) and did not induce infarcts in the brain. MΦ are approximately 20-30 μm in diameter, placing them within the range for lung entrapment. Culturing MΦ in 3D cultures or pretreatment with osmotic agents to temporarily shrink MΦ [182-185] prior to injection may reduce overall cell size and prevent entrapment in the lung. Reduced rates of injection (0.2 mL/min compared to >1mL/min) of MSCs into the carotid artery of rats have also reduced the risk of stroke [186]. The Heilshorn lab has shown that packaging multiple cell types in a hydrogel or protein engineered scaffold with growth factors may also protect from injection stress induced cell death [187, 188] and increase long term survival, as seen with dorsal subcutaneous transplantation of adipose-derived stem cells in nude mice [189] and intramuscular transplantation of stem cell derived endothelial cells in an ischemic hind limb mouse model [190].

Pretreatment of transplanted cells has been employed in attempts to reduce lung entrapment and/or increase cell survival [99, 178, 179]. Fischer and colleagues blocked adhesion of MSCs to endothelial cells by inactivation of the VCAM-1 counter-ligand (CD49d) on MSCs and administered the MSCs in two boluses. This modestly improved the passage of MSC through the lung from ~0.15% to 0.3% [173]. Cardiomyocytes derived from embryonic stem cells treated using a combinations of methods (including heat shock, matrigel co-injection, ZVAD-fmk2 (caspase inhibitor), IGF-1 (Akt pathway activator), Bcl-XL (blocks cell death), cyclosporine A (attenuates mitochondrial death) and pinacidil (mimics ischemic preconditioning)) lead to better engraftment post-injection in an ischemic heart [191]. These types of pretreatments may help to identify potential druggable targets that may increase overall survival of injected MΦ [192]. However, in

viewing the totality of the data, it appears that the diameter and deformability of the transplanted cells may be the most important parameters that impact transit beyond the lung and survival after injection.

Finally, preparation of the host for transplantation can also be performed to enhance engraftment and survival of transplanted cells. Vasodilation using sodium nitroprusside reduces lung entrapment in HSC transplantation [193]. Tissue MΦ also occupy specific niches, and removal of endogenous MΦ from these niches may open them for newly transplanted MΦ. As mentioned previously, gene-corrected MΦ were able to engraft and adopt lung-specific MΦ markers in lungs lacking alveolar MΦ [21, 22]. Liposomal clodronate can specifically deplete MΦ subsets in various organs depending on route of administration [194] and potentially creates tissue MΦ niches available for newly transplanted MΦ.

The work described in this dissertation will follow the extensive work done by others to develop MΦ for therapeutic applications by applying engineering principles to measure and study the behavior of MΦ in the context of transplantation. While there have been many studies in both animal models and humans, the kinetics and biodistribution of cells post transplantation is poorly studied and understood. Better understanding of these areas would enable not only further development of MΦ-based cell therapies, but the basic principles could be used to better understand and improve the outcomes of stem cell and T-cell therapeutics. The following chapters will describe the methods and results of the strategies we have used to: 1) Efficiently generate large numbers of primary-like cells for engraftment studies, 2) Enable quantitative measurement of cell survival post

transplantation and 3) Enhance cell survival and engraftment of transplanted MΦ and MΦ progenitor cells.

2 Chapter 2: Generation and characterization of *ex vivo* MΦ and MΦ progenitors

2.1 Novel methods of collecting MΦ

There are two classical methods of collecting primary MΦ: differentiating cells from the bone marrow in MCSF or collecting MΦ from the peritoneal cavity following an intraperitoneal thioglycollate injection. While these methods are able to generate MΦ for small scale studies, it is impractical to scale these methods for developing a cell based therapy which requires hundreds of millions of cells.

An alternative approach would be to use transformed MΦ or monocyte cell lines, such as RAW264, RAW309 or THP-1. However the genetic alterations in these cell lines have been so far transformed, their ability to recapitulate primary MΦ behavior is questionable. For example, these cell lines are able to survive without the need for GMCSF or MCSF, a critical cytokine that extensively impacts MΦ survival and behavior. However, recent discoveries in MΦ and monocyte biology enable large scale *in vitro* MΦ cultures that are able to generate the numbers of cells required for cell therapy studies in an economical and efficient manner.

The Sieweke group has described a method to generate self-renewing MΦ by knocking out two transcription factors, MafB and c-Maf, also known as Maf-double knockout (MafDKO) MΦ [170]. Removal of these factors results in an adherent cell line that maintains, phagocytosis, migration, adhesion, surface marker expression and polarization potential, key MΦ behaviors. One significant difference is that MafDKO require high levels (100 ng/mL) of MCSF to be supplemented in the media. This is in comparison to a conventional protocol to generate bone marrow derived MΦ, which requires culturing bone marrow aspirates, which contain myeloid progenitor cells, in 10

ng/mL of MCSF. We were able to acquire a vial of these MafDKO cells from the Sieweke group, and while the cells were able to replicate as described in the original paper, the proliferative capacity was not maintained beyond 10 passages (about one month) despite our best efforts. We attempted numerous methods to maintain the cells, including changing serum sources and becoming hypervigilant for potential contamination. Furthermore, the cells were strongly adherent to tissue culture plastic and were incredibly difficult to remove from the plastic in order to be passaged. While these cells demonstrate a self-renewal/proliferative capacity and maintained MΦ characteristics, we were unable to generate the numbers of MΦ required for our studies.

We turned to the method described by Wang et al [34], which relies on an overexpression of Hoxb8 in myeloid progenitor cells to regulate their differentiation potential. Hoxb8 is a transcription factor that is normally downregulated as myeloid progenitor cells differentiate into a terminally differentiated cell (i.e. MΦ, dendritic cell). Continual overexpression of Hoxb8 results in a sustained myeloid progenitor state, which is characterized by a non-adherent suspension culture and cells with a rapid proliferation rate. In Wang et al [34], Hoxb8 activity is controlled by transducing purified myeloid progenitor cells with a lentiviral expression construct that contains Hoxb8 fused with the estrogen receptor (Hoxb8-ERT). The estrogen receptor restricts Hoxb8 from entering the nucleus, thus preventing transcriptional regulation. Addition of 4-hydroxytamoxifen (4-OHT) allows Hoxb8-ERT to enter the nucleus and act to maintain the myeloid progenitor cell in its current state. Maintenance of 4-OHT in the culture media retains the cells in a highly proliferative state. Removal of 4-OHT from the culture media restricts Hoxb8-ERT from entering the nucleus, returning the cell to an unmodified state, and differentiation to

a terminal state to occur as dictated in conventional protocols. As described in the following section, we modified this methodology by constitutively expressing Hoxb8 to generate large numbers of MΦ and MΦ progenitors (Figure 2-1).

2.2 Generation of MΦ from Hoxb8 driven myeloid progenitors (HDP)

Typically, myeloid progenitors rapidly differentiate into terminal cells when cultured *in vitro*, so to generate large numbers of myeloid progenitor cells, we adapted the method described by Wang et al to generate a line of Hoxb8 driven myeloid progenitor cells (HDP) which overexpress Hoxb8 and remain as progenitor cells [34]. For full experimental methods, please refer to the methods section. In short, *lin*$^-$ cells are isolated from mouse bone marrow and transduced with lentiviral and retroviral constructs (Figure 2-1a). *Lin*$^-$ cells lack all known lineage myeloid markers (CD5$^-$, CD45R$^-$ (B220), CD11b$^-$, Gr-1$^-$ (Ly-6G/C)$^-$, 7-4$^-$, and Ter-119$^-$) for differentiated cells and are thus considered naïve and the most "stem-like", making these cells the most versatile to generate large numbers of not just MΦ, but other fully differentiated myeloid cells, including dendritic cells and neutrophils [34, 195]. The first construct, flox-Hoxb8-ZsGreen, is transduced using a lentivirus into *lin*$^-$ cells and endows the cells with continuous self-renewal and proliferative capacities due to overexpression of Hoxb8. This construct also contains puromycin as a selectable marker. Over the course of a week, cells which contain Hoxb8 will continue to proliferate in suspension culture, while those that do not will differentiate and adhere to the tissue culture plastic. Cells positive for the Hoxb8 construct, as indicated by both sustained proliferation and expression of ZsGreen are transduced with a retrovirus, containing the second construct ind-Cre-ERT-RFP, which contains a 4-OHT inducible Cre recombinase. Upon activation of the Cre recombinase by addition of 4-OHT to the media,

the regions between the loxP sites on the Hoxb8 construct are excised, effectively returning Hoxb8 expression back to endogenous levels. The HDP cell can then proceed to differentiate into a MΦ if supplied with GMCSF or MCSF. As shown in Figure 2-2, addition of 4-OHT for 7 days converts HDP from rapidly proliferating suspension cells into a non-proliferating adhesive cell with a similar morphology as bone marrow derived MΦ. The protocol as described is relatively flexible, and in the Szoka lab, we have generated HDP cells from both BALB/c and C57BL/6 mouse strains.

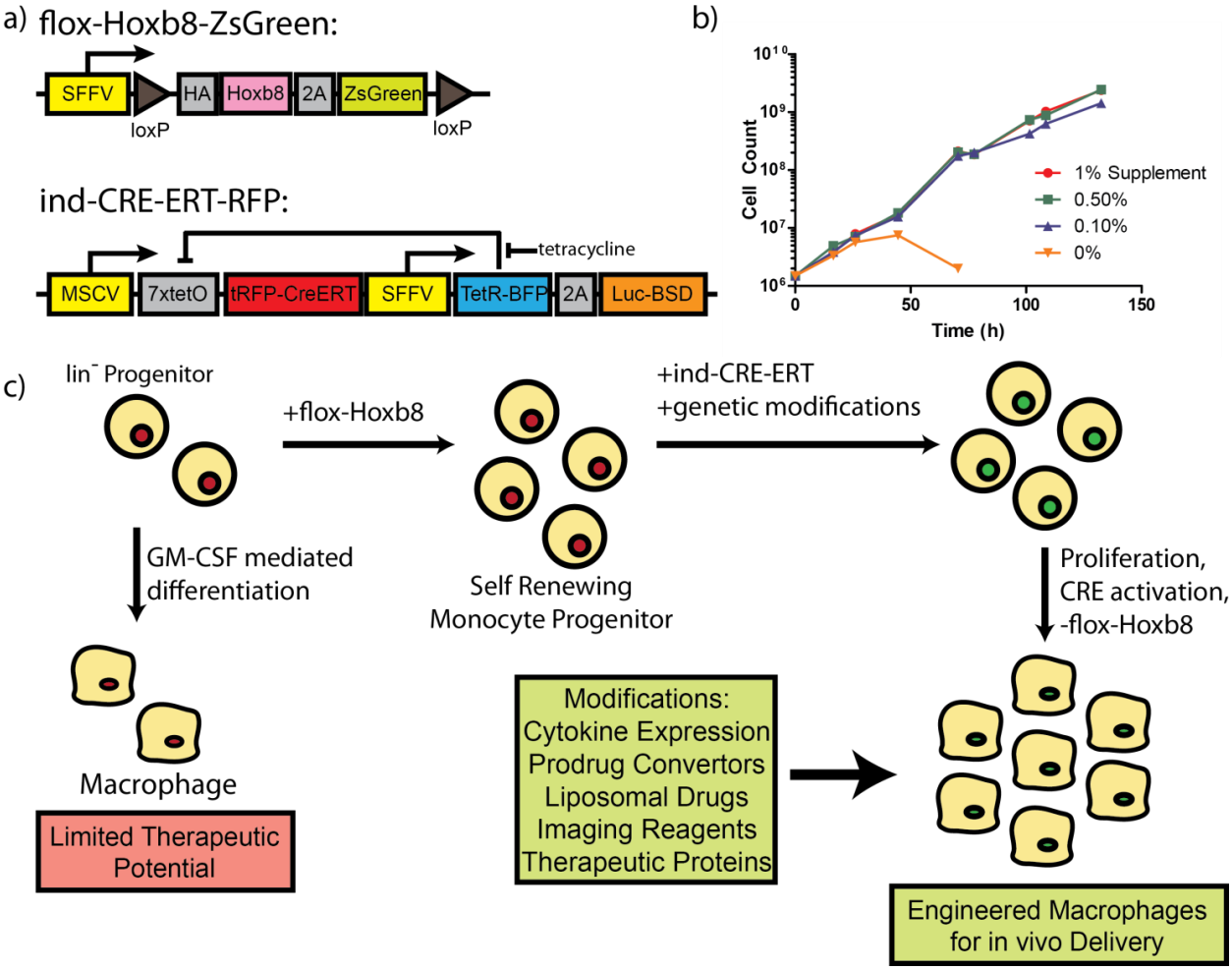

Figure 2-1: Overview of modified HDP and MΦ system. A) Genetic constructs used to transiently immortalize monocyte progenitors using a loxP-flanked Hoxb8 transcription

factor expression cassette. An inducible Cre-ERT system allows for removal of Hoxb8 and continuation of MΦ differentiation. B) Growth curves of HDP cells in GMCSF-L929 conditioned media reveals rapid proliferation, with doubling times of approximately 12 hours. C) Flow diagram illustrating the steps to produce MΦ from bone marrow. The progenitor state is highly proliferative and can be genetically modified using a retroviral construct to express a wide array of cytokines, therapeutic and imaging proteins. MΦ can also be loaded with liposomal drugs.

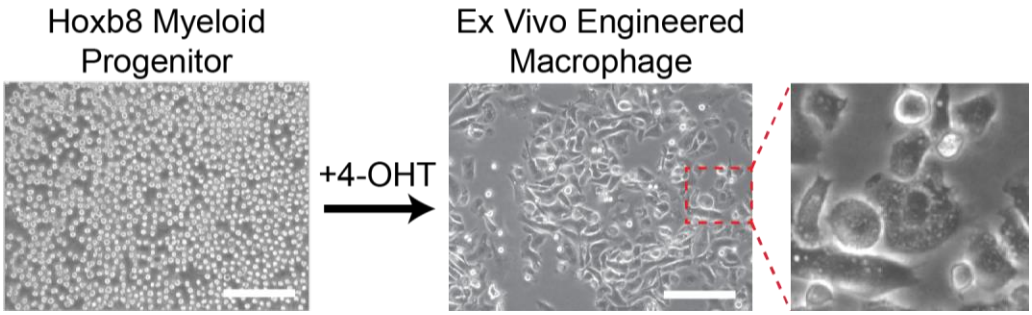

Figure 2-2: Differentiation of HDP into MΦ. Brightfield images of HDP that have differentiated into MΦ after 7 days of exposure to 200 nM 4-OHT. Note the flat and extended morphology of the treated cells and transition from suspension to adherent culture. Scale bar = 150 µm

Differentiating MΦ in the process described above proceeds in multiple stages over the 7-10 day process. As the 4-OHT works to activate the Cre recombinase to excise the constitutively expressed Hoxb8 construct and the excess Hoxb8 protein is degraded from the cell, the HDP cease to proliferate within the first 5 days and begin to return to their regular cellular programming to differentiate. By providing GMCSF in the cell culture media during this process, signaling is provided to instruct these cells to differentiate into MΦ. Morphologically, cells transition from small and rounded cells in suspension to a larger size that is more irregular and generally more adherent. This occurs over the first

3-5 days, and while the cells transition, they also take on a more granular appearance and lose their shiny appearance. The cells also become more morphologically distinct from one another, with blebs and tendrils reaching out from the center of the cell. While the easiest to observe cells are adherent, approximately 10-20% of the cells remain in suspension. This appears to be a temporary state dependent on the cell density of the culture, as these “suspension MΦ” will also adhere strongly to tissue culture plastic if transferred into a new tissue culture plate. By the 7-10 day mark, the vast majority of cells have taken on the larger and granular morphology which we identify as a MΦ. In comparison to bone-marrow derived MΦ, the time frame from beginning differentiation to acquiring a fully differentiated MΦ is approximately the same (~7 days), placing these *ex vivo* MΦ on a similar differentiation time scale as bone-marrow derived MΦ. However, we felt that due to the fact that HDP are already predisposed towards a MΦ fate, the time required to differentiate these cells could be reduced further. To study this, we attempted to differentiate the cells using similar conditions, but with different environments, including, tissue culture plates coated in poly-L-lysine or gelatin and in lower oxygen environments. Poly-L-lysine or gelatin coated plates caused the cells to rapidly die, while low oxygen environments did not have any observable effect on the time scale to achieve similar morphological changes.

Once fully differentiated, the cells are very adherent to the tissue culture plastic, but can be removed by first rinsing the cells with D-PBS and using HyQTase (HyClone), a gentler alternative to trypsin. We also used tissue culture plates coated with temperature sensitive poly(N-isopropylacrylamide) (PNIPAAm) to release the cells from the plate by cooling the plates for 10-15 minutes. This was also a successful and gentle way to remove

cells from the plate, but produced similar results to HyQTase with much higher cost. Thus, the HyQTase method was used for all subsequent studies that required removing differentiated MΦ from tissue culture plastic.

2.3 Modification and Validation of HDP

Generation and modification of HDP requires both retroviral and lentiviral transduction methods. A second generation lentiviral system was used to transduce *lin*$^-$ cells with the flox-Hoxb8-ZsGreen construct. While the infectivity was not quantitatively measured, due to the survival advantage conferred by Hoxb8 overexpression, Hoxb8-positive cells rapidly expanded and formed ≈100% of the culture while all other cells died or differentiated and stopped proliferating. For unknown reasons, lentivirus was unable to successfully transduce any other constructs into the Hoxb8-positive cells. To move the project forward, we attempted to use non-viral methods. These methods included electroporation, which resulted in a significant acute cell death and very limited success with most plasmids (a plasmid encoding only RFP was able to transfect <1% of cells in the best case scenario), and a myriad of transfection reagents advertised as strong performers for hard-to-transfect cells (Promega: Viafect, Fugene6; Roche: XtremeGene9; Gemini: Continuum; Invitrogen: Lipofectamine 2000, Lipofectamine 3000; Mirus: TransIT-LT1, TransIT-X2, TransIT-2020; Qiagen: Effectene and Promokine: Promofectin), which were universally unsuccessful.

Due to the failure of the other options, we employed retrovirus to transduce HDP. The exact protocol is described in the methods section, and by using a murine stem cell virus (MSCV) retrovirus, we successfully transduced a sufficient percentage of cells that could be purified using antibiotic selection, as shown in Figure 2-3. Using this method, we

have modified HDP with a variety of constructs, endowing the cells with numerous characteristics (as illustrated Figure 2-1C and listed in Table 2-1). The applications of these various modifications will be explained in later sections, but include therapeutic enzymes, fluorescent tags, luminescent enzymes and functional transcriptional factors. The main restraint in using retrovirus is the size limitation of the construct that can be added. The size of the MSCV genome is about 8.5kb, meaning the construct to be inserted cannot exceed that size (for a HIV-1 based lentivirus, this is about 10kb). Larger constructs are also packaged into viral particles less efficiently, reducing the overall titer. It is thus clear that the success of the transduction process depended upon both the construct as well as the selection marker used. In particular, puromycin was a much more robust selection agent, while hygromycin was unable to remove all uninfected cells. Retroviral transduction was the most efficient method for genetic modification in our hands and was used exclusively in the studies described in this dissertation.

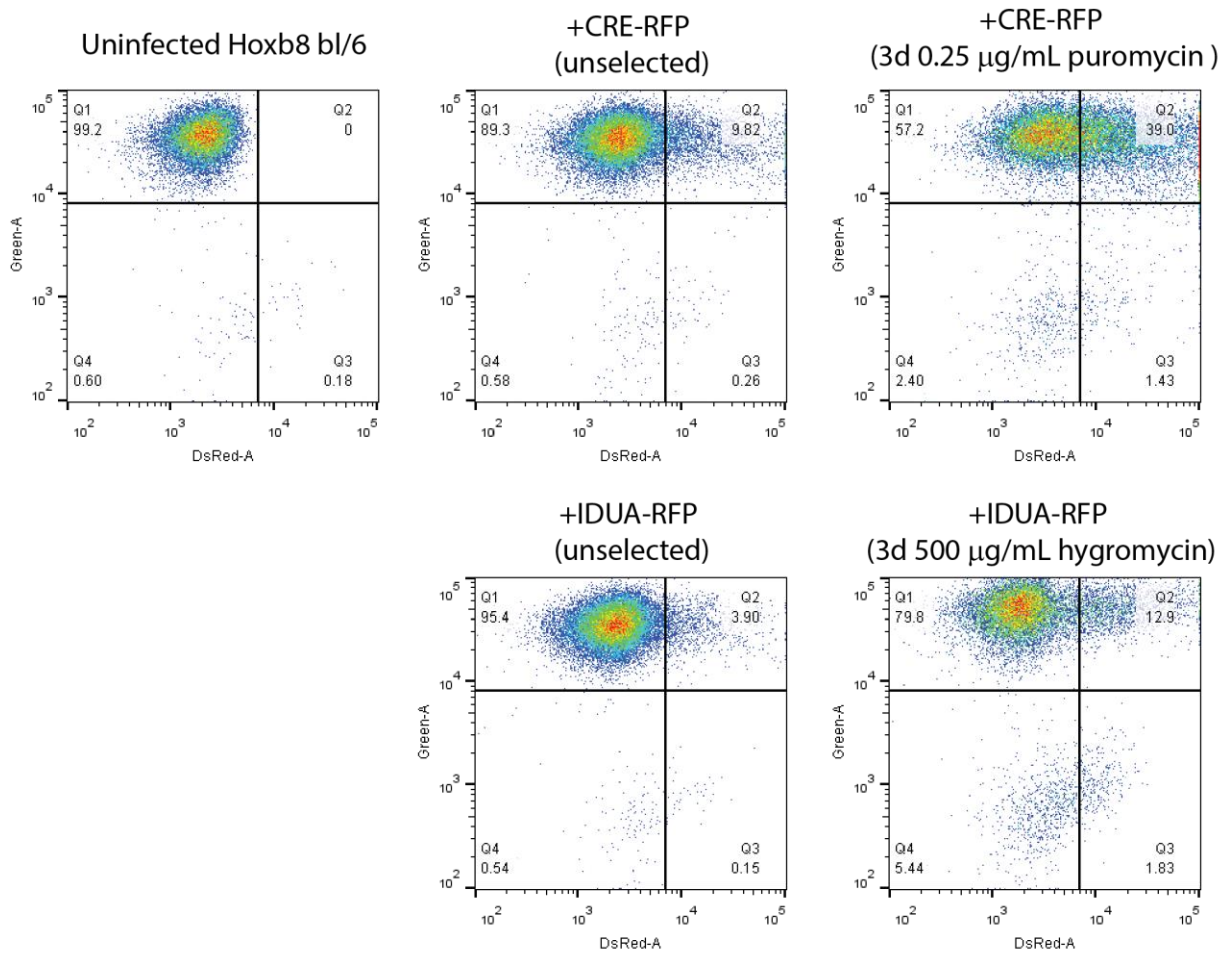

Figure 2-3: Retroviral transduction of Hoxb8 MΦ progenitors. Hoxb8 MΦ progenitors generated from C57BL/6 mice were retrovirally transduced with retrovirus for Cre-RFP or IDUA-RFP. FACS was conducted on uninfected cells, infected cells (3 days post infection) and selected cells following 3 days of selection using the antibiotic indicated. Successful infection is dependent upon the construct used, and is further improved with antibiotic selection.

Table 2-1: Modifications made to HDP

Modification	Description	Purpose
Cre-ERT	Cre recombinase fusion with estrogen receptor	Inducible Cre recombinase activity to induce Hoxb8 excision
Luc	Luciferase enzyme (luminescence)	Luciferase expression to detect live cells in biodistribution experiments
L452E GMCSFR (AutoGMCSFR)	Constitutively active MCSF receptor	Cell proliferation and survival without MCSF supplement
IRF8-ERT	Irf8 transcription factor fusion with estrogen receptor	Inducible Irf8 activity to further enhance MΦ differentiation
IDUA	Therapeutic protein expression - Iduronidase	To systematically deliver a therapeutic protein over a long period of time

To further purify the cells positive for the added constructs, FACS was used to isolate and collect cells positive for a fluorescent marker included on the construct. For constructs which lacked fluorescent tags, monoclonal cell lines were generated by limited dilution cloning on a semi-solid MethoCult media and the presence of the construct was identified using colony PCR, as shown in Figure 2-4.

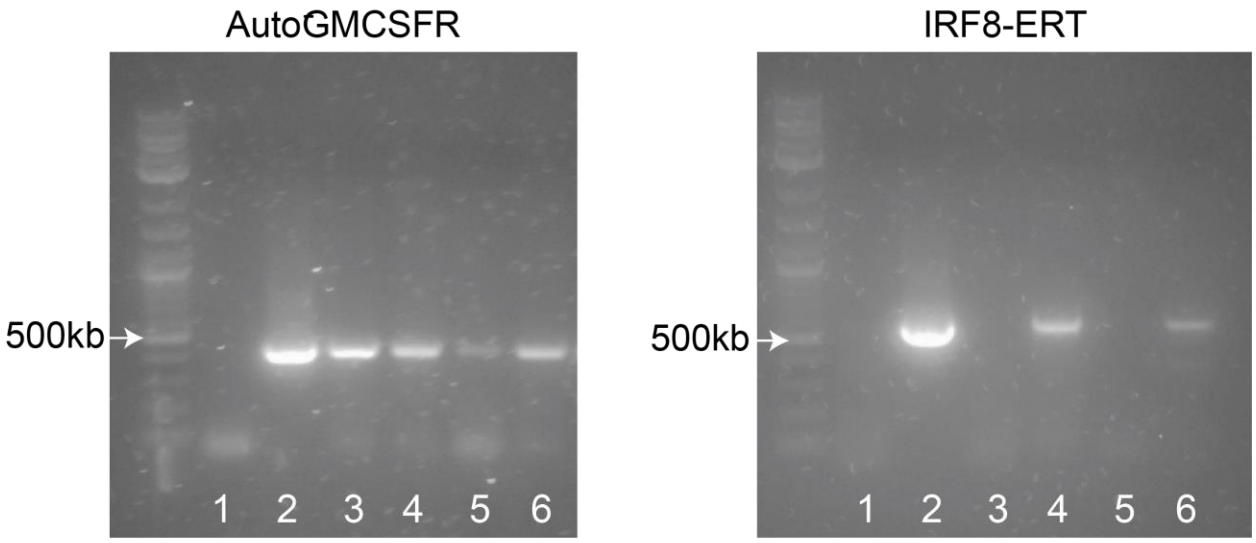

1) Negative control (unmodified cells)
2) Positive control (corresponding plasmid)
3) C57BL/6-IDUA-CRE + AutoGMCSFR
4) C57BL/6-IDUA-CRE-AutoGMCSFR + IRF8
5) C57BL/6 + AutoGMCSFR
6) BALB/c-RFP+AutoGMCSFR-IRF8

Figure 2-4: Validation of insertion of AutoGMCSFR and IRF8-ERT genetic constructs. Colony PCR was performed using construct specific primers and genomic DNA as a template. PCR products were visualized on a 1.5% Et-Br stained agarose gel and compared against a positive control. Positive controls for both AutoGMCSFR and IRF8-ERT confirmatory tests were 20 ng of the respective plasmid spiked into genomic DNA of an unmodified HDP line.

2.4 Characterization of HDP and MΦ

The following sections will describe the characterization of HDP and MΦ. The methods used are discussed in the methods section of this chapter.

2.4.1 Growth kinetics of HDP

Myeloid progenitor cells must replicate at rapid rates to provide a high number of myeloid cells for homeostasis. This can be observed when bone marrow derived MΦ are

generated from bone marrow aspirates. Initially, the large differentiated or differentiating cells quickly settle or die due to the lack of the specific cytokine required for their differentiation. Within 24 hours, there is a rapid expansion of very small non-adherent cells that saturates the culture dish; these are myeloid progenitor cells that will differentiate into various myeloid subtypes depending on the cytokine supplied. This behavior is retained in HDP. Overexpression of Hoxb8 locks progenitor cells at a stage that undergoes constant self-renewal, while also preventing typical differentiation mechanisms from taking place. As shown in Figure 2-5A, when grown in media containing conditioned media from a L929 cell line lentivirally transduced with a GMCSF construct (5-10 µg/mL GMCSF in supplement, 50-100 ng/mL GMCSF in a 1% supplement media), HDP proliferate at an incredibly rapid pace. This doubling rate of ~12 hours is maintained even with very low levels of GMCSF supplement (5-10 ng/mL), as shown by a titration of the L929 supplement down to 0.10% of total media volume. The 12 hour doubling rate was calculated by fitting the growth curve to an exponential growth equation. However, the supplement is absolutely necessary, as beyond 48 hours, the cells will begin to die without any supplement (Figure 2-5A). It is also important to note that if using only recombinant GMCSF, higher amounts of GMCSF is required to maintain this proliferative capacity. This is presumably due to the L929 supplement containing other unidentified cytokines and survival factors normally secreted by L929 cells which act synergistically to augment GMCSF activity. Combined with the overall expense of using recombinant GMCSF, HDP were maintained in 1% GMCSF supplement media unless otherwise noted.

We were also interested in determining the proliferative kinetics in low oxygen environments due to the hypoxic environment that could be experienced by HDP and MΦ when transplanted. As shown in Figure 2-5B, proliferative capacity was maintained down to 2.5% levels (for reference, regular atmosphere at sea-level is 18-20% and the summit of Mt. Everest is approximately 6.5% O_2). While at first glance this may seem like a surprising result, direct localized measurements of oxygen levels in the bone marrow of healthy live animals have shown heterogeneity in oxygen tension, with levels as low as 1.3% O_2 (9.9 mmHg) [196]. Thus, it is reasonable that myeloid progenitor cells in the bone marrow may be exposed low oxygen environments *in vivo* and thus be capable of proliferating as low as 2.5% O_2 *in vitro*.

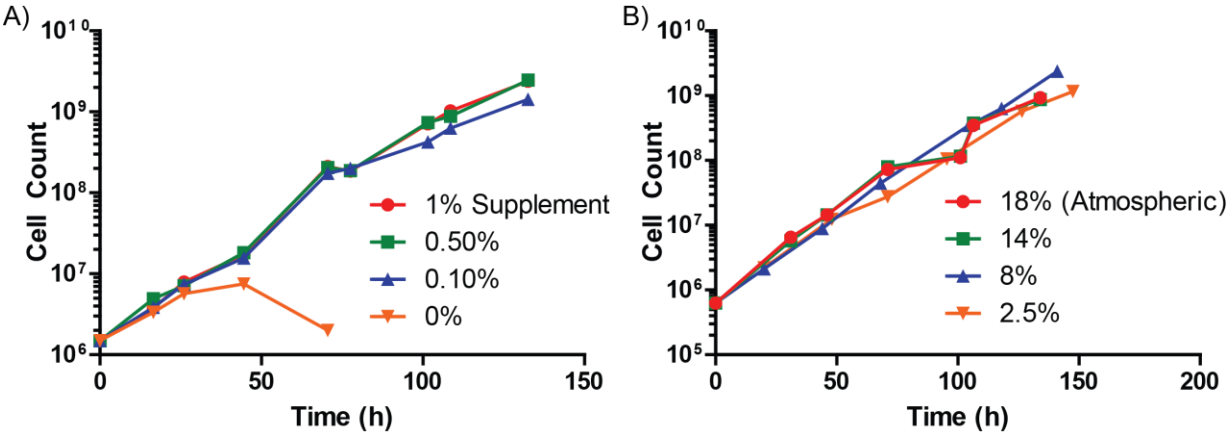

Figure 2-5: Growth potentials of HDP. A) Growth curves of HDP grown in media containing supplement made from conditioned media from GMCSF expressing L929 cells. B) Growth curve of HDP grown in 1% supplement at different oxygen tension levels. Even at low levels of supplement or oxygen concentration, proliferation remains rapid at a doubling rate of approximately 12 hours.

2.4.2 Polarization potential of *ex vivo* generated MΦ

While HDP can proliferate at rapid rates, it is also important to characterize the functional behaviors of MΦ. A key property of MΦ is their polarization potential. In classical descriptions of MΦ behavior, MΦ polarization has been split into two groups: M1, the inflammatory subtype, and M2, the regenerative subtype [37, 197, 198]. As described in the introduction, these classifications describe generalized behaviors of the MΦ. M1 MΦ are implicated in inflammatory environments where a MΦ's cell killing properties are required during bacterial infection or other immune responses. In contrast, M2 MΦ arise in healing and regenerative environments, such as removing cell debris, reducing immune responses to return to homeostasis and tissue regeneration. The most important property is that MΦ respond and polarize based on signals from the environment which guide the MΦ towards inflammatory or regenerative behaviors. While current descriptions of MΦ polarization have become increasingly nuanced whereupon MΦ exist on a spectrum of behaviors, there are still canonical methods which will polarize naïve (M0) MΦ into the classical M1 and M2 phenotypes (Table 2-2).

Table 2-2: Summary of MΦ polarization responses.

	Inducing Agents	Gene Products Upregulated
M1 – inflammatory MΦ	LPS, CpG	iNOS, IL12b, TNF
M2 – healing MΦ	IL4	Arg1, CD206, CCL17

To determine if the MΦ generated from HDP maintain the same polarization potentials, *ex vivo* generated MΦ were exposed to cytokines and other agents that are known to induce M1 and M2 transitions. As shown in Figure 2-6, qPCR of *ex vivo* MΦ treated with known M1 and M2-inducing agents resulted in the upregulation of genes

associated with the M1 and M2 states. For example, LPS and CpG are components of bacterial cell membrane and should illicit a vigorous inflammatory MΦ response [198]. This is exemplified in a 1000-fold increase in iNOS expression, a key component of the MΦ anti-bacterial response. Other canonical M1 markers, such as Il12b and Tnf are also increased, 800- and 5-fold, respectively. Conversely, IL-4, a known cytokine for triggering M2 polarization, results in the upregulation of M2 genes, Arg1 (12x), Cd206 (4x) and Ccl17 (40x), in the *ex vivo* MΦ. Based on these results, we can conclude that *ex vivo* MΦ respond to M1 and M2 stimulants in similar ways.

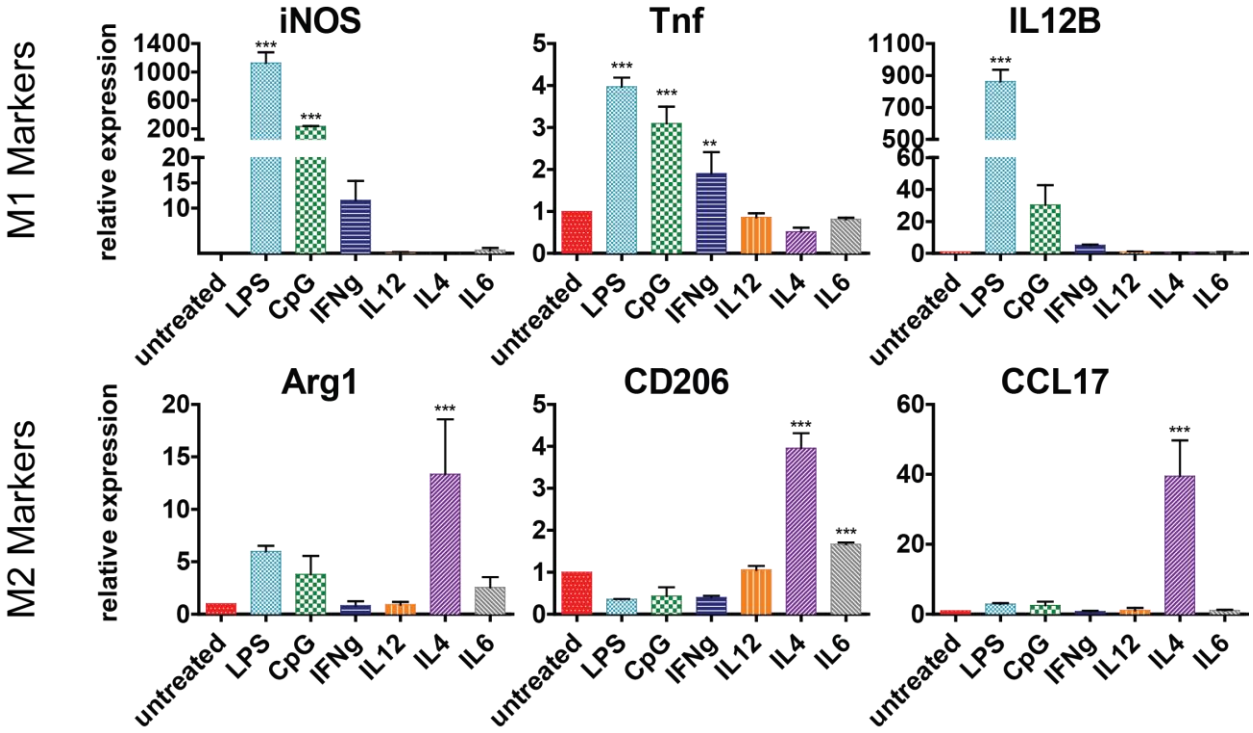

Figure 2-6: Quantitative PCR of M1 and M2 MΦ markers of *ex vivo* MΦ. MΦ were differentiated for 7 days in 200 nM 4-OHT and then treated overnight with a variety of agents: 10 ng/mL LPS, 2uM CpG, 50 ng/mL IFNγ, 50 ng/mL IL-12, 50 ng/mL IL-4 or 50 ng/mL IL-6. Relative expression is calculated by comparing expression levels between treated and untreated MΦ.

2.4.3 Phagocytosis of bacteria and liposomes by *ex vivo* generated MΦ

MΦ are professional phagocytes, and for this reason, it is important to characterize the ability of *ex vivo* derived Hoxb8 MΦ to phagocytose bacteria and other materials. This trait is particularly important for applications that may involve using MΦ as drug delivery vehicles, as has been done using RAW MΦ loaded with a sparingly soluble antiretroviral drug for HIV therapy to deliver drug to the brain [141, 142, 145]. The ability to recognize and phagocytose bacteria is also a key indicator of endogenous MΦ behavior. As shown in Figure 2-7, *ex vivo* generated MΦ are highly phagocytic for both fluorescently labelled liposomes and live *E.coli*. The strong uptake of both bacteria and liposomes indicates *ex vivo* MΦ maintain strong phagocytic capabilities.

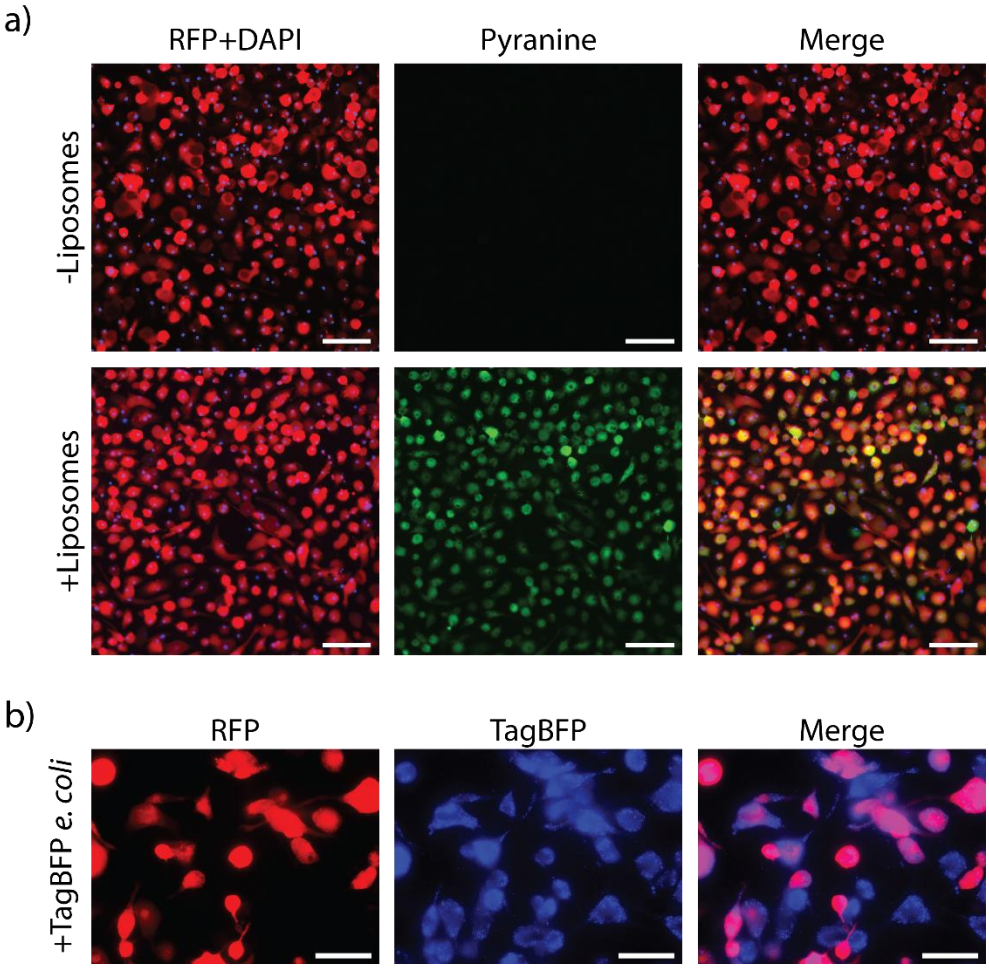

Figure 2-7: *Ex vivo* derived MΦ maintain *in vitro* phagocytic potential. A) RFP-MΦ were incubated with 500 nM pyranine labelled liposomes for 3h, fixed, and stained. Pyranine can be observed throughout the cytosol of all cells. Scale bar = 100 μm. B) RFP- MΦ treated with live TagBFP expressing *E. coli* for 30 min. Scale bar = 50 μm

2.4.4 Chemotaxis towards tumor secretions

MΦ are recruited to sites of inflammation, including tumor sites by secreted factors. In particular, tumors rely upon recruitment and reprogramming of MΦ from an inflammatory (M1) to regenerative (M2) phenotype to aid in the growth and spread of the tumor site [199-201]. As a part of our study in developing *ex vivo* MΦ for anti-tumor therapeutics, we were interested in determining if these cells would also be directly

recruited by tumor signals. To accomplish this, a transwell study was performed to determine the ability of *ex vivo* MΦ to migrate towards conditioned media from a 4T1 breast cancer cell line. As shown in Figure 2-8, *ex vivo* MΦ migrate more strongly towards 4T1 conditioned media when compared to regular growth media. This data suggests *ex vivo* MΦ are capable of responding to tumor secreted signals and may be strongly recruited by tumors *in vivo*, a critical requirement for developing *ex vivo* MΦ for cancer therapeutics.

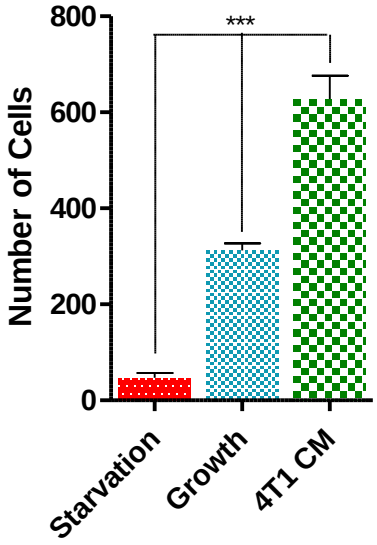

Figure 2-8: *Ex vivo* MΦ preferentially migrate towards 4T1 conditioned media. $5x10^4$ MΦ were plated in a 24 well size, 8 µm transwell insert (Corning) overnight in full growth media prior to switching to migration conditions for 24 hours (top level containing 0.5% serum media with no supplements, bottom level containing experimental medias). Following migration, membranes were washed, fixed with 70% ethanol, stained with 1% Crystal Violet and the number of cells on the bottom side of each membrane was counted using an inverted microscope. 4T1 conditioned media (CM): 50% CM generated over 3 days of a growing 4T1 culture, 50% RPMI with 10% serum; Growth media: RPMI with 10% serum

and 1% GMCSF-L929 conditioned media; Starvation media: RPMI with 0.5% serum. Statistics: *** = $p < 0.001$, N = 3 transwells per condition.

2.5 Conclusions

We were able to adapt the method developed by *Wang et al* to isolate primary *lin*$^-$ murine myeloid cells to generate Hoxb8-dependent myeloid progenitor (HDP) which do not differentiate and are capable of self-renewal, with a doubling time of approximately 12 hours. The ability to generate large number of cells enabled further development of HDP to be used for a MΦ based therapy. The Hoxb8 expression cassette is flanked by loxP sites and thus can be excised with a Cre recombinase. By using retrovirus to further modify the HDP, we were able to add a Cre recombinase fused to an estrogen receptor, allowing for inducible Cre activity under the control of 4-hydroxytamoxifen (4-OHT). Excision of Hoxb8 by 4-OHT treatment resulted in cells with behaviors similar to those of primary MΦ. These *ex vivo* generated MΦ respond to M1 and M2 polarization signals by upregulating established genes for M1 and M2 polarization, as shown by qPCR. Furthermore, a phagocytic phenotype is maintained as exhibited by strong uptake of bacteria and liposomes. *Ex vivo* MΦ also exhibit an expected chemotactic response to conditioned media from a 4T1 breast tumor cell line culture. Additionally, HDP can be modified and genetically engineered further by retroviral transduction. For the reasons outlined above, *ex vivo* MΦ derived from HDP represent a logical template for developing MΦ based therapies.

2.6 Methods

2.6.1 Cell Culture

Reagents were acquired from the UCSF Cell Culture Facility (UCSF CCF) unless otherwise indicated. HDP were cultured in RPMI-1640 (50 mM HEPES, 1% PenStrep/Amphotericin B antibiotic/antimycotic, 1% Glutamax (Gibco), 10% heat inactivated fetal calf serum (Hyclone), 0.55 mM 2-mercaptoethanol (Life Technologies), 1% GMCSF supplement (see Methods)), using flasks from GrenierBioOne or plates from Corning. Cells were cultured in a humidified incubator maintained at 37°C and 5% CO_2. *Ex vivo* MΦ were differentiated by culturing cells in 200 nM 4-hydroxytamoxifen (4-OHT) (Enzo) for 10 days. Differentiation was started with a cell density of 2-4x10^5 cells/mL and passaged as necessary.

To determine the effect of oxygen tension on proliferation rate, cells were grown in an incubator with an O_2 sensor that displaced excess O_2 by addition of N_2. L929 cells were cultured in DMEM (50 mM HEPES, 1% PenStrep/Amphotericin B antibiotic/antimycotic, 1% Glutamax (Gibco), 10% heat inactivated fetal calf serum (Hyclone)).

2.6.2 Limited Dilution Cloning

Limited dilution cloning was performed to generate monoclonal cell lines from the polyclonal population that resulted from retroviral transduction. In a 10 cm round tissue culture dish, 1x10^4 cells were grown in a semi-solid MethoCult M3234 media (Stem Cell Technologies) supplemented with 10% GMCSF supplement and the appropriate antibiotic (6 µg/mL blasticidin, 0.2 µg/mL puromycin, 30 µg/mL zeocin, 500 µg/mL hygromycin or 1 mg/mL neomycin). After 5-7 days, single colonies can be visually

observed growing in the culture dish. Individual colonies were carefully picked using a 100 µL pipette tip and transferred to a 24 well plate containing 500 µL of growth media. Following 3-4 days of culture, individual lines were assayed by colony PCR to validate presence of the desired insertion. Alternatively, a functional assay (i.e. Fluorescence or luciferase activity) was performed.

2.6.3 Luciferase activity

Luciferase activity was determined using SteadyGLO (Promega) as per manufacturer protocols. In short, 100 µL of cell suspension was mixed with 100 µL SteadyGLO in a glass tube. The contents were mixed and total luminescence was measured using a luminometer (MGM Instruments) over a 10 second period.

2.6.4 Colony PCR to identify presence of genetic constructs

Following generation of monoclonal cell lines, genomic DNA was extracted by pelleting approximately $5x10^5$ cells and heating the pellet in 100 µL 25 mM NaOH at 95°C for 15 min. The mixture was cooled on ice for 10 min before addition of 100 µL 40 mM Tris (pH = 7.4). Following centrifugation to remove any debris remaining, the supernatant was used without further purification as genomic DNA to be tested by colony PCR. The colony PCR reaction was assembled; 10 µL of GoTaq Green (Promega), 0.5 µL 10 µM forward primer, 0.5 µL 10 µM reverse primer (see below), 4 µL 4M betaine, 4 µL water and 1 µL genomic DNA. The PCR reaction performed as per Promega protocols. The products were then visualized on a 1.5% Et-Br agarose gel.

Validation Primers

Construct	Forward Primer	Reverse Primer	Size (bp)
AutoGMCSFR	GTCCCCTACATCGTGAC CTGGG	CTCTAGCTGGTGATAGAG GGTCATGTTG	436
IRF8-ERT	GTCCCCTACATCGTGAC CTGGG	CTTTATATGGCTCAGAAA TGTC	562

2.6.5 Supplemental GMCSF Media

A GMCSF expressing L929 cell line was generated by transducing L929 cells with a lentiviral construct (pLVX-GMCSF-IRES-tdTomato). Positively transduced cells were isolated by FACS and used to generate the supplemental media. GMCSF L929 cells were grown to confluency, whereupon the media was switched to a low serum formulation (DMEM, 50 mM HEPES, 1% PenStrep/Amphotericin B antibiotic/antimycotic, 1% Glutamax (Gibco), 0.5% heat inactivated fetal calf serum (Hyclone)). This reduces the proliferation capacity of the cells but maintains survival. After 3 days, the media was collected, centrifuged, filtered and frozen for future use. GMCSF levels were measured following the protocols from a GMCSF ELISA kit from Boster.

2.6.6 Lentivirus and Retrovirus Production

A second generation lentivirus was used, requiring three plasmids: pCMV-dR8.91 (Delta 8.9) (containing gag, pol and rev genes), VSV-G (envelope) and expression construct (pLOX-insert). For murine stem cell retrovirus, two plasmids are required, the packaging vector (pCL-Eco) and expression construct (pMSCV). All base constructs were acquired from Clontech. For specific step-by-step instructions, please refer to the appendix. In general, for both retrovirus and lentivirus, HEK293T cells were transfected with the required plasmid and the media was collected and replaced for three days. The virus containing media was concentrated by mixing it with Lenti-X or Retro-X concentrator

(Clontech) and centrifugation. The concentrated virus was resuspended in a small volume and was used without further purification for viral transduction.

2.6.7 Lentivirus and Retrovirus Transduction

Cells were transduced with retrovirus or lentivirus using the spinfection method. Briefly, $2x10^4$ cells were added to a retronectin treated 48 well plate along with 50 µL of retrovirus or lentivirus. The plate was centrifuged for 90 min at 4000 rpm then allowed to recover overnight in a humidified 5% CO_2 32°C incubator. The following day, the culture was returned to a humidified 5% CO_2 37°C incubator. After 3-5 days, the culture was expanded and tested for successful integration of the desired modifications. For full experimental methods, please refer to the appendix.

2.6.8 Lin^- bone marrow culture and infection

Lin^- cells were collected from the bone marrow of healthy female BALB/c and C57BL/6 mice by purifying the cells using a magnetic bead mixture and associated column. Following collection, the lin^- cells were grown in tissue culture plates overnight before they were transduced by lentivirus encoding the Hoxb8 construct. For step-by-step instructions, please refer to the appendix.

2.6.9 Determining proliferation rate

The number of cells was counted using a hemocytometer. Cells were stained with Trypan blue to exclude dead cells from the count. Cells were passaged 1:20 every two days. An appropriate correction factor incorporating the number of passages was applied to calculate the number of cells to have grown since the start of the culture.

2.6.10 MΦ polarization assay

MΦ were generated by culturing $4x10^5$ cells/mL HDP in growth media with 200 nM 4-OHT (Enzo) for 7 days. On day 7, cells were moved to 6 well plates by treating tissue culture flasks with 1x D-PBS wash, followed by Hyqtase (Hyclone) treatment for ~10 min until cells can be dislodged by tapping the flask. Cells were counted and $2x10^5$ cells were plated per well in a 12 well plate in growth media. The next day, the media was changed for the appropriate polarization media: 10 ng/mL LPS (Sigma), 2uM CpG (Invivogen), 50 ng/mL IFNγ, 50 ng/mL IL-12, 50 ng/mL IL-4 or 50 ng/mL IL-6 (Peprotech). Following an overnight treatment, cells were washed with PBS and RNA was collected using the RNeasy Mini Kit (Qiagen) following the manufacturer protocols. The expression of M1/M2 genes was then measured by qPCR.

2.6.11 Quantitative real time PCR

DNA for quantitative real time PCR (qPCR) was generated by collecting RNA from cell samples and performing reverse transcription. qPCR was performed using standard techniques using a BioRad CFX96 thermocycler. Each readout was normalized against an internal mouse actin value and then compared appropriately to other samples to determine fold change. For each sample and each gene, three replicates were performed and averaged to yield a single value for each sample. To generate multiple values for statistical analysis, multiple experimental samples were subjected to the described method. For step-by-step instructions, please refer to the appendix.

2.6.12 Flow Cytometry

Flow cytometry was conducted at the UCSF Flow Cytometry core on a BD Fortessa instrument. Cells were labelled with antibodies according to manufacturer instructions and

the data was analyzed using FlowJo. Cell sorting was conducted on a BD FACSAria instrument. Please refer to the appendix for a step-by-step protocol for flow cytometry.

2.6.13 Plasmid Construction

Plasmids for lentivirus and retrovirus production were cloned using standard techniques, including restriction cloning and Gibson assembly (appendix), depending on the applicability of each technique to the desired product. For production of plasmids containing Hoxb8, GMCSFR and IRF8, murine cDNAs were acquired from GE Dharmacon. To engineer the constitutive activity of GMCSFR, a Quikchange Lightning Kit (Agilent) was used to modify the leucine in position 452 to glutamic acid (L452E). Vectors for plasmid construction were obtained from Addgene or commercially available from Clontech. Constructs were sequence verified and sequence maps are available digitally.

2.6.14 Liposome and Bacterial Uptake

Fluorescent liposomes were made with a 3:1:2 ratio of HSPC:DSPG:Cholesterol, (HSPC: L-α-phosphatidylcholine, hydrogenated (Soy), DSPG: 1,2-distearoyl-sn-glycero-3-phospho-(1'-rac-glycerol) (Avanti)) with 1% 8-Hydroxypyrene-1,3,6-Trisulfonic Acid (HPTS). A lipid film of the formulation was produced by placing it under a rotary evaporator and high vacuum overnight. The film was reconstituted with HBS (140 mM NaCl, 10 mM HEPES) and sonicated at room temperature for 40 min to form liposomes. The liposomes were then dialyzed for 24 h in 2 L of HBS in a 10000 MW dialysis cassette (ThermoScientific) to remove unencapsulated HPTS and filtered through a 0.45 µm filter. Lipid films were prepared as described and sonicated with D-PBS under argon at 45°C for 20 mins. DiD-labelled liposomes were extruded through 100 nm filters before sterile

filtering. The size and charge of the liposomes was determined using a Zetasizer (diameter 76 nm, PDI 0.76, charge -57 mV). Fluorescent bacteria was generated by transforming a BL21 *E. coli* strain with a pGEX-TagBFP plasmid.

Uptake experiments were performed on MΦ differentiated from HDP treated with 200 nM 4-OHT for 10 days. $1x10^5$ MΦ were plated overnight in a 12 well plate prior to incubation with liposomes or bacteria. For fluorescent imaging, MΦ were incubated with a 500 µM HPTS-liposome solution or 10% live TagBFP-E. coli culture in serum free media for 3 h or 30 min, respectively, in a humidified 5% CO2 37°C incubator. Following the incubations, wells were rinsed with D-PBS. Cultures treated with liposomes were DAPI stained prior to imaging on a fluorescent microscope, while cultures treated with bacteria were imaged directly.

2.6.15 Transwell studies

MΦ were differentiated for 7 days by treating HDP with 200 nM 4-OHT before $5x10^4$ MΦ were plated in a 24 well size, 8 µm transwell insert (Corning) overnight in full growth media prior to switching to migration conditions for 24 hours (top level containing 0.5% serum media with no supplements, bottom level containing experimental medias). Three different medias were tested: 4T1 conditioned media (50% conditioned media generated over 3 days of a growing 4T1 culture, 50% RPMI with 10% serum), growth media (RPMI with 10% serum and 1% GMCSF-L929 conditioned media) and starvation media (RPMI with 0.5% serum). Before use, 4T1 conditioned media was centrifuged and filtered to remove any cell debris. Following migration, a cotton swab was used to remove the cells from the top layer of the membrane which was then fixed with 70% ethanol and

stained with 1% Crystal Violet. The number of cells on the bottom side (touching the bottom level) of each membrane was counted using an inverted microscope.

3 Chapter 3: Exploratory engraftment studies of *ex vivo* derived MΦ and HDP

Cell-based therapies require transplanted cells to survive and perform a desired function *in vivo*. The application dictates if survival needs to be relatively short, such as for acute bacterial infection, or as in the case for gene therapies, to be prolonged. Overall cell survival is affected by numerous variables including: route of administration, disease state, cell type, genetic modifications, co-injected materials and immunological state of the host. In this chapter, we developed well tolerated injection protocols and a method to quantify live cells in organ lysates using a sensitive luciferase-based assay. Using these techniques we determined the biodistribution of transplanted HDP, 4-day differentiating progenitors (4DDP) and MΦ in healthy, and 4T1 tumored syngeneic BALB/c mice. Furthermore, we studied the biodistribution, overall engraftment and survival potential of HDP, 4DDP and MΦ from genetic modifications to the cells, altered injection route/conditions and various cell/animal pretreatments (a complete list can be seen in Table 3-1). We found intraperitoneal co-injections of matrigel with 4DDP resulted in the best overall survival at 7 days post-injection and was limited to the peritoneal cavity. The findings described here were used to guide follow-on experiments to enhance the survival of HDP and MΦ.

Table 3-1: Summary of modifications made to improve post transplantation cell survival

Route	Modification	Target	Reference
IV	1 M mannitol injection fluid	Reduce cell size to bypass lung entrapment	202, 203
IV	Labeling cells with high molecular weight PEG	Evading the reticuloendothelial system	204-207
IV	Syngeneic serum exchange	Reduce foreign immune response from bovine serum	
IV	Pretreatment of mouse with aspirin, argatroban, sucrose octasulfate or dextran sulfate	Reduce thrombosis	208-214
IV	Retroviral transduction of Crry-expressing construct	Reduce complement activity	215
IP	Co-injection with matrigel or hyaluronic acid	Encapsulate cells and provide a niche for survival	191, 216
IP	M1/M2 prestimulation	Alter cell phenotype and behavior	1
IP	Retroviral transduction of CCR2-expressing construct	Induce chemoattraction to 4T1 tumor	217

3.1 Injection and cell transplantation parameters

We first determined the maximum tolerated dose for both intravenous (IV) and intraperitoneal (IP) routes before embarking on *in vivo* biodistribution studies. MΦ were differentiated over 10 days in 200 nM 4-OHT and concentrated by centrifugation into an injectable volume of 100 µL for IV and 500 µL for IP injections. Healthy wildtype 6-8-week old female BALB/c mice received a single dose ranging from $1x10^6$ to $5x10^6$ cells. IV injections were performed in the tail vein and IP injections in the lower right quadrant of the abdomen. For IV injections, the maximal tolerated dose that did not result in observable distress or death within 30 minutes was $2x10^6$ cells. For IP injections, there did not appear to be adverse effects at the maximum dose of $5x10^6$ cells. Unless otherwise noted, these became the standard doses for all *in vivo* experiments discussed in this dissertation. With either injection route at these doses, there were no short or long term adverse effects observed.

Throughout this chapter, cell transplantation experiments were done with a variety of cell types (Table 3-2). Progenitor cells are defined as HDP which have not been treated with 4-OHT to induce excision of Hoxb8 and begin the differentiation process. Progenitors are highly proliferative, grow in suspension culture and appear to be small and round cells under the microscope. MΦ are defined as HDP which have undergone 4-OHT treatment for at least 10 days to complete the differentiation process. MΦ are non-proliferative, grow in adherent culture and appear as large granular cells with an irregular ruffled edge under the microscope. A third cell type, the 4-day differentiating progenitor (4DDP) was also used. 4DDP were used because we hypothesized that since progenitor cells were proliferative, this state was better equipped to survive the initial shock of injection in comparison to a fully differentiated MΦ which lacks proliferative capacity. By differentiating progenitor cells for only 4 days out of the 10 required for full differentiation, we speculated these cells would retain a high enough level of Hoxb8 protein to provide progenitor-like behaviors, including limited proliferation and potentially enhanced acute survival. We also though that Hoxb8 excision to be complete within 4 days, and therefore these differentiating progenitors would fully differentiate into MΦ *in vivo* post-injection.

Table 3-2: Reference chart for various cell types injected in this section

Nomenclature	Tamoxifen treatment	Proliferative Status	Suspension or Adherent	Morphology
Progenitor (HDP)	None	Rapid ($t_{1/2}$ < 12 h)	Suspension	Round, shiny and smooth appearance
4 Day Differentiating Progenitor (4DDP)	200 nM for 4 days	Mixed. ~25% still proliferating slowly. Remainder have stopped.	Mixed	Mostly like MΦ, suspension cells are larger and slightly granular
MΦ (MΦ)	200 nM for 10 days	None	Adherent	Granular, flat, irregular

3.2 Identification of a method for tracking cells post injection

We evaluated two methods for tracking cells post injection in order to quantitatively determine the biodistribution of injected cells. In the first method, cells were labelled with DiD, a lipid dye that inserts into the cell membrane, immediately before injection. In the second method, luciferase activity was used. The cells were transduced with luciferase under the same construct as the Cre recombinase (CMV-RFP-Cre-ERT-2A-Luc-Bsd). To directly compare the two methods, luciferase expressing 4DDP were labelled with DiD and injected IV into healthy animals (Figure 3-1). Three days after cell injection, animals were euthanized and the liver, spleen and lungs were collected. Organ lysates were made using a Wheaton dounce tissue grinder with radioimmunoprecipitation assay (RIPA) lysis buffer containing protease inhibitors.

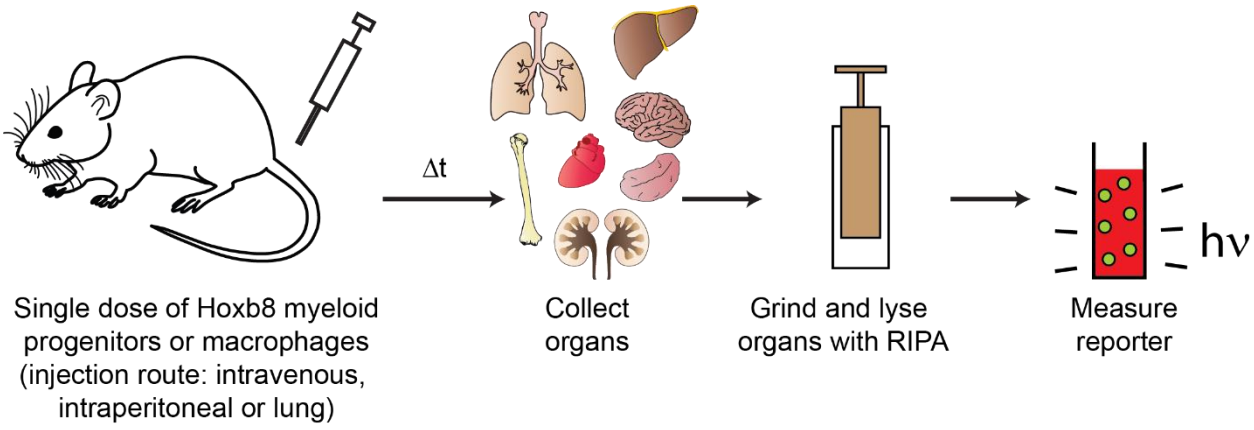

Figure 3-1: Schematic of biodistribution experiments. Mice were injected IV or IP with a single dose of cells and euthanized after a defined period. Organs were collected and lysed in RIPA before analysis for luciferase activity or DiD fluorescence.

The total DiD was determined by measuring the fluorescence in the organ lysate and comparing to a standard curve generated using known amounts of DiD in RIPA. Luciferase activity was determined by measuring total luminescence in 100 µL of organ

lysate using a SteadyGlo kit and comparing the luminescence to a standard curve generated using a known number of luciferase-expressing cells in RIPA. The presence of organ lysate reduced total luciferase signal by approximately 10% when compared to the same number of cells measured in RIPA buffer. In both cases, the total signal was scaled appropriately based on total volume of organ lysate. There was a significant differential between DiD labeling and luciferase activity, with DiD reporting significantly higher values (20-40% for DiD vs <0.0005% for luciferase activity in the liver) for identical samples (Figure 3-2). We think the reason for this discrepancy is because the DiD label was transferred from the injected cells that had died to resident cells in the organs, whereas luciferase activity is quickly inactivated in dead cells, and therefore cannot provide a signal if the dead cells are phagocytosed. DiD is not supposed to be easily transferred from one live cell to another, but if a DiD labelled cell dies, the membranes in cellular debris retain the DiD label and can be phagocytosed by other cells. The strong signal found in the liver is likely explained by this process due to the high number of phagocytic cells in the liver.

Luciferase activity is only observed in a live cell because when the cell dies, luciferase is released and the serum stability of luciferase is low with a circulatory half-life of approximately 20 min [218]. Given the short half-life of luciferase and the time durations used for biodistribution studies (ranging from 20 min to 18 days in this chapter), any luciferase activity observed will in live cells and not luciferase from dead cells or debris. To summarize, the signal observed from DiD is due to DiD from dead cell debris and does not represent the number of live cells. Thus, we used luciferase activity to determine the biodistribution of injected cells for the following studies in this dissertation.

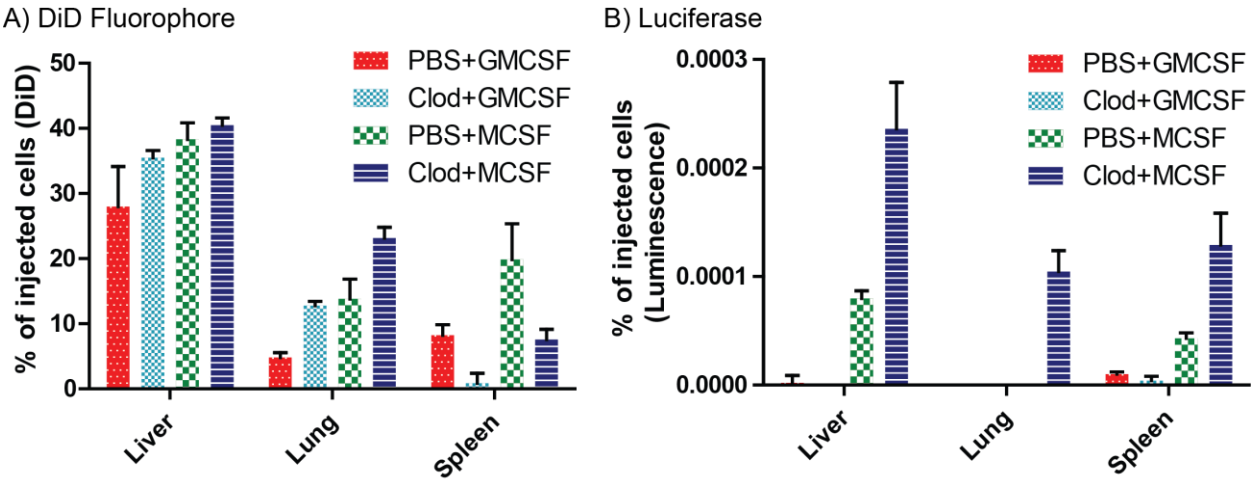

Figure 3-2: Comparing DiD and luciferase reporter activity as methods for quantifying the number of cells in animal organs. Luciferase expressing 4DDP were labelled with DiD prior to IV injection. Animals were sacrificed after 3 days. Organs were lysed in RIPA buffer and protease inhibitor and the total DiD and luciferase activity was measured. A) Biodistribution according to DiD detection shows DiD strong signal in liver, lungs and spleen. B) Biodistribution according to luciferase activity in the same samples as A. Experimental conditions: Healthy female BALB/c mice were injected IV with 100 µL liposomal clodronate (5 mg/mL) 2 days prior to cell injection. RFP-Cre-ERT-2A-Luc Hoxb8 4DDP, treated overnight with 10 ng/mL MCSF or GMCSF for 12 h prior to injection. $1x10^6$ cells were injected IV in 100 µL 1M mannitol. N = 3 animals per condition.

The detection limits of luciferase-expressing cells was established by measuring the luminescence of an increasing number of cells in RPMI (Figure 3-3A). There is a linear detection range from several hundred cells up to ~$2x10^5$ cells in a 100 µL sample. Beyond the linear range, the luminometer approaches a saturation of ~$6.5x10^6$ RLUs (relative light units). Thus, we diluted samples appropriately to stay within the detection range of the luminometer. We then apply appropriate correction factors to determine the total

number of luciferase-expressing cells in the organ. Another consideration is the impact of cells which do not express luciferase to interfere with the assay. This is critical to consider as the biodistribution studies requires detection of luciferase activity in organ lysate samples, which may interfere with the luciferase assay. A serial dilution of luciferase-expressing cells was mixed with either liver lysate in RIPA or RIPA alone and luciferase activity was measured (Figure 3-3B). Luminescence between the two conditions remained similar, demonstrating the assay did not experience interference from liver lysate. Based on these results, luciferase activity is a robust and sensitive method of determining the biodistribution of live cells in tissue homogenates.

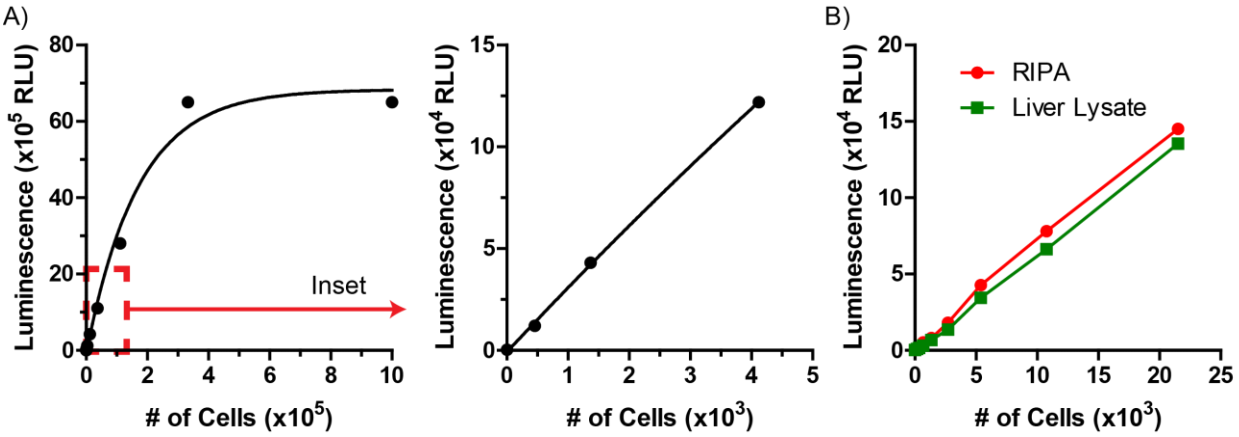

Figure 3-3: The detection limits of a luminescence based assay for HDP expressing luciferase. A) Serial dilution of HDP into RPMI shows a linear relationship between total luminescence and the number of cells up to approximately $2x10^5$ cells within a 100 µL test sample. Inset: linear relationship is maintained down to a few hundred cells. The data was fit using a one-phase decay model. B) Comparison of luciferase activity in liver lysate and RIPA. (N = 1 per condition)

3.3 Identifying an appropriate route of administration

We transplanted HDP, 4DDP and *ex vivo* derived MΦ into syngeneic BALB/c mice by intravenous (IV) tail vein injection, lung instillation and intraperitoneal (IP) injection. In the following sections we discuss our findings using these three routes of administration and the overall survival of HDP and MΦ.

3.3.1 IV Studies

3.3.1.1 Reducing the entrapment of IV injected cells in the lung

In initial studies where MΦ were injected by the IV route, we observed high doses of cells (≥2.5x10^6 cells) caused respiratory distress in the mice. Reduction of the dose to 2x10^6 cells prevented this from occurring, but based on these results, we hypothesized cells were occluding the lung and causing the respiratory distress. When injecting 2x10^6 4DDP by IV tail vein injection in a 100 U heparin solution, approximately 50% of the cells are found in the lungs at 20 min post injection (Figure 3-4A). The high number of 4DDP entrapped in the lungs at this time point was problematic as it caused irritation or death (at a dose ≥2.5x10^6 cells) in the mice. Moreover, we thought it would prevent circulation of the cells and thus reduce engraftment in other organs. To address this, we reduced the size of the cells by injecting the cells in hyperosmolar mannitol solutions of varying concentration. Mannitol has been safely used as an osmotic agent to reduce brain swelling in traumatic brain injury and thus a small dose of mannitol co-injected with the cells should have a minimal impact on the health of the animal [203]. More importantly, mannitol solutions at the concentration used here are hypertonic and cell diameter in mannitol solutions decrease in a reversible manner.

We varied the concentration of mannitol in the injection solution and IV injected 4DDP into mice and measured the total percentage of injected cells present by luciferase activity in the lungs 20 min post injection. Increasing the mannitol concentration significantly reduces the percentage of injected 4DDP retained in the lungs (Figure 3-4A), with 1 M and 0.75 M mannitol treatments resulted in 10-15% retention compared to ~50 % retention using 100 U/mL heparin ($p < 0.001$). Going forward, 1 M mannitol was used as the preferred injection fluid for all IV experiments unless otherwise indicated. Furthermore, the shrinking effects are fully reversible. As shown in Figure 3-4B, 4DDP were incubated in 1 M mannitol and then passed through a 28 gauge needle into a larger volume of unmodified RPMI do not appear morphologically different from cells in RPMI that were passed through the needle.

Since the initial experiments showed a large percentage of the injected cells were trapped in the lung, we performed a single animal per group biodistribution experiment to learn if any of the pretreatments resulted in significant cell numbers in the spleen or liver at 20 min or 24 h. While 1 M mannitol allowed for 4DDP to bypass the lungs, this did not enable the cells to engraft or survive in the spleen or lung beyond 20 min. Two hours post injection, the total percentage of injected cells found in the lung and spleen among the mannitol treated cells and the non-treated cells were similar, and at 24 h, no luciferase signal was detected in either organ (Figure 3-5). Based on these results, we continued developing other methods to increase the survival of IV injected cells.

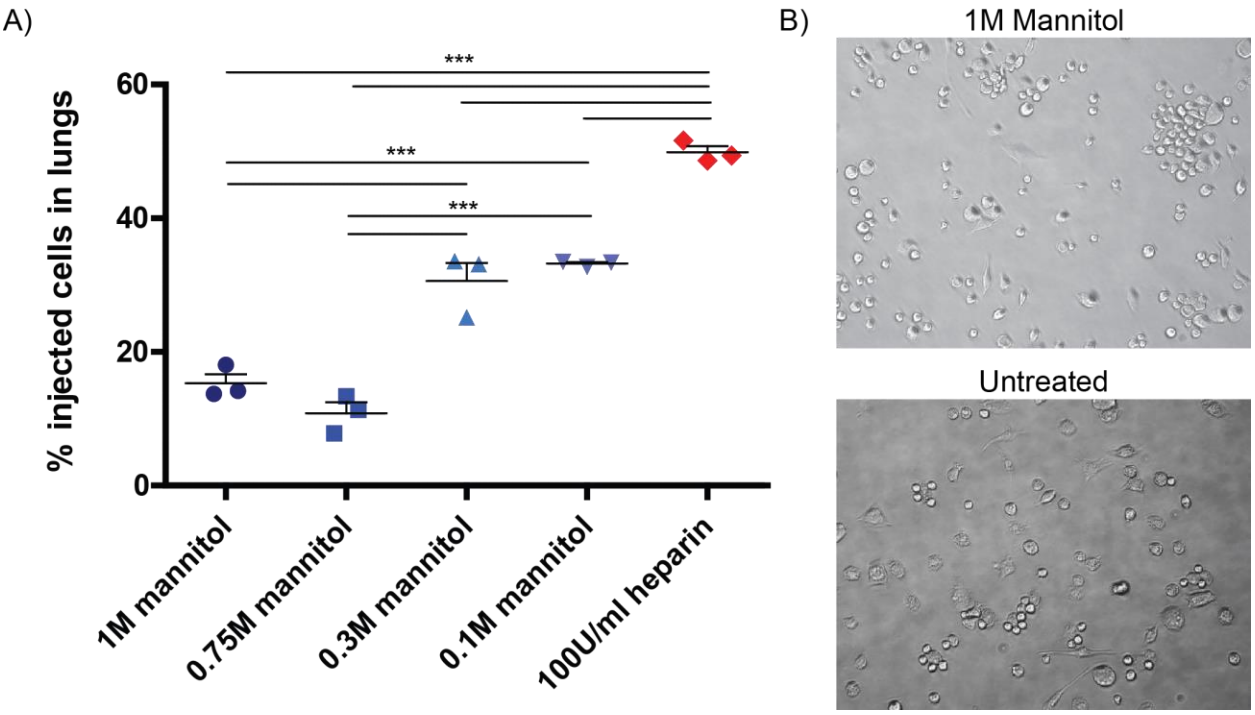

Figure 3-4: Injection fluids modify the lung entrapment of 4DDP injected IV. A) Total percentage of injected cells found in the lungs 20 min post IV injection. $2x10^6$ 4DDP were resuspended in 100 µL of the injection fluids indicated in RPMI and injected by tail vein injection into healthy syngeneic BALB/c mice. Mice were euthanized after 2 h and the lungs were collected and total percentage of injected cells in the lung was determined by luciferase activity. Cells: RFP-Cre-ERT-2A-LucBsd Hoxb8 4DDP. Statistics: $p < 0.001$, N = 3 animals per condition. B) Images of cells resuspended in 100 µL 1M mannitol or plain RPMI (untreated) and injected through a 28 gauge insulin syringe into RPMI.

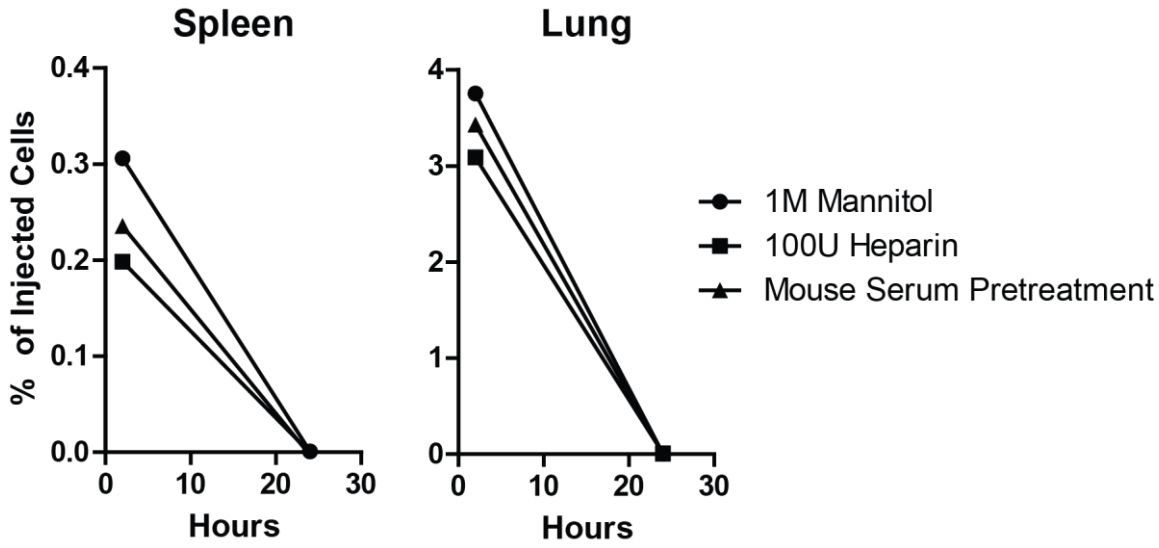

Figure 3-5: Composition of injection fluid influences the number of cells at in the lung or spleen 24 h post injection.Experimental conditions: Cells: BALB/c RFP-Cre-ERT-2A-LucBsd Hoxb8 4DDP; Animals: healthy 8 week BALB/c female mice. N = 1 animal per condition.

3.3.1.2 Evading the reticuloendothelial system

While we are able to reduce the percentage of cells retained in the lung at 20 mins by modifying the injection fluids, the signal from live cells was greatly diminished within 2 h post injection. Live cells were undetectable at the 24 h sampling time. Based upon the distribution of DiD signal as shown in (Figure 3-2), we hypothesized the cells or their fragments were being removed from circulation by the reticuloendothelial system (RES), which is mostly comprised of tissue MΦ found in the liver, spleen and bone marrow.

In the field of drug delivery, a classical method to evade the RES and improve circulation half-life of nanoparticles is through the use of high molecular weight polyethylene glycol (PEG) [219]. Coating the surface of a particle with high molecular weight PEG creates a hydrophilic barrier around the particle, which impedes serum proteins or other cellular components from binding to the particle and reduces the adhesion energy

between the PEG-coated particle and other cells. Blocking these interactions thus prevents the recognition of the PEG-coated particle by the RES, endowing a “stealth” status to the particle and increasing the circulation half-life. This technique has been employed heavily in the Szoka lab to improve the circulation half-life of liposomes [220-223]. We adapted this method to coat HDP with 2000 or 5000 MW PEG by incubating the cells with 100 μM DSPE-PEG2K or DSPE-PEG5K in serum-free conditions. DSPE-PEG is composed of PEG attached to a phospholipid that allows for the insertion of the lipid portion (DSPE) into the cell membrane with the PEG portion extending outward, creating a hydrophilic barrier around the cell membrane to protect the cell (Figure 3-6). We used two protocols to coat HDP with DSPE-PEG. The first protocol labelled the cells in Teflon jars which reduced cell adhesion to the jar surface during the labeling procedure. The second protocol labelled the cells in standard tissue culture-treated plastic. Labelling in standard tissue culture plastic resulted in cells adhering to the plate. These adherent cells were not used to form the injected dose.

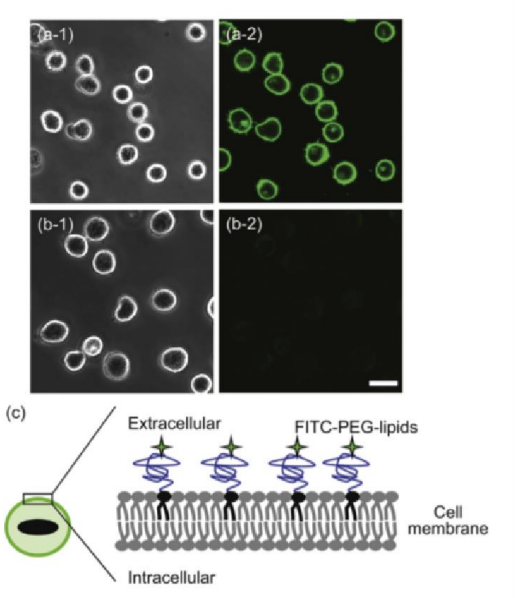

Figure 3-6: PEG-labeled cells to improve the *in vivo* biocompatibility of cells. HEK293 cells incubated with A) FITC-PEG-DSPE or B) FITC-PEG for 30 mins. (L: Phase contrast, R: confocal fluorescence imaging). Scale bar = 20 µm. C) Schematic of FITC-PEG-DSPE inserting into the cell membrane to form a PEG layer surrounding the cell. Adapted from [206]

PEG labelling was modestly able to enhance the overall survival of HDP 2 h post transplantation (Figure 3-7). Labelling with DSPE-PEG2K in tissue culture plastic increased the percentage of injected cells detected in the spleen to ~8.5% ($1.7x10^5$ cells, $p < 0.001$) and had modest increases in the liver and blood of <0.5% ($1x10^4$ cells, $p < 0.001$), while the signal in the lung remained similar to unlabeled controls. The untreated cells prepared in TC plastic had a higher cell number in the liver ($1.5x10^4$ cells, $p < 0.05$), but in no other tissues. It is unclear why this may have occurred. There was no difference between DSPE-PEG2K and DSPE-PEG5K labelled progenitors when labelling was performed in Teflon jars. Interestingly, the increased cell numbers in the spleen and blood observed in labeling cells with DSPE-PEG2K in tissue culture plastic was not seen when

the labeling was performed in Teflon, which performed similarly to the control using 1 M mannitol with no labeling procedure. We hypothesized this may be due to the tissue culture plastic selectively removing cells that are highly adherent, as only the suspension cells post-labelling were used for injections. This might result in the suspended cells being less adherent, and perhaps less likely to interact with the RES system, further enhancing the “stealth” characteristic the PEG labelling conferred. Combined survival in the liver and spleen was below 10% 2 h post-injection. This did not appear to be a large enough organ biodistribution to justify continued development of the PEG-coating technique. It did suggest that conditions could be identified to promote cell biodistribution and survival.

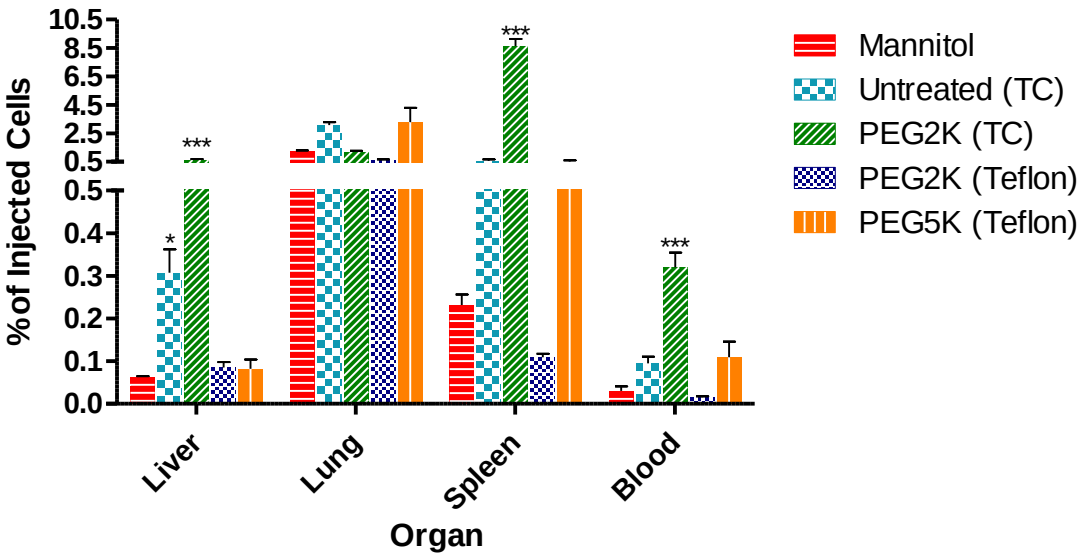

Figure 3-7: *In vivo* biodistribution of HDP treated with DSPE-PEG 2 h post IV injection. To add large PEG chains to HDP, cells were labelled in serum free media containing 100 µM of DSPE-PEG2K/5K in either tissue culture plates (TC) or Teflon jars. Untreated label indicates cells were subjected to the same labelling procedure as other conditions, but without the addition of DSPE-PEG. Mannitol label indicates no labelling procedure was used prior to injection. Experimental conditions: Dose: $2x10^6$ cells in 100 µL 1 M mannitol

in RPMI; Cells: BALB/c RFP-Cre-ERT-2A-LucBsd HDP cells; Animals: healthy 8 week BALB/c female mice; Statistics: * = $p< 0.05$, *** = $p < 0.001$, compared to mannitol control in same organ, N = 3 animals per condition.

3.3.1.3 Reducing a foreign immune rejection response

All HDP and MΦ are cultured and propagated in a media which contains fetal calf serum. As a result, these cells will process bovine proteins for MHC I presentation. While the cells are derived from a BALB/c mouse and are injected into a syngeneic BALB/c mouse, these bovine proteins may trigger a foreign immune rejection response to target the injected cells as non-self for elimination. To mitigate this possibility, we cultured HDP for 7 days prior to injection in media which used BALB/c serum rather than fetal calf serum. The cells were washed and replated with fresh BALB/c-containing media on days 2, 4 and 6. HDP continued to proliferate during this procedure, but for an unknown reason, a precipitate would form in the culture approximately 24 h after transfer to BALB/c serum. The precipitate was not bacterial or fungal contamination, and could be removed by centrifugation at low speeds to isolate cells from the precipitate. However, the precipitate would return by the next day. To remove the precipitate, the media was changed every 2 days. On day 7, the HDP were injected IV and the animals were euthanized 2 h post injection. The cells cultured in BALB/c serum had marginally more cells in the evaluated organs, with the cells in the lung increasing from ~0.5% to 3% ($6x10^5$ cells, $p < 0.01$) and the liver from 0.05% to 0.3% ($6x10^4$ cells, $p < 0.001$) (Figure 3-8). We decided the improvement was not substantial enough to further study.

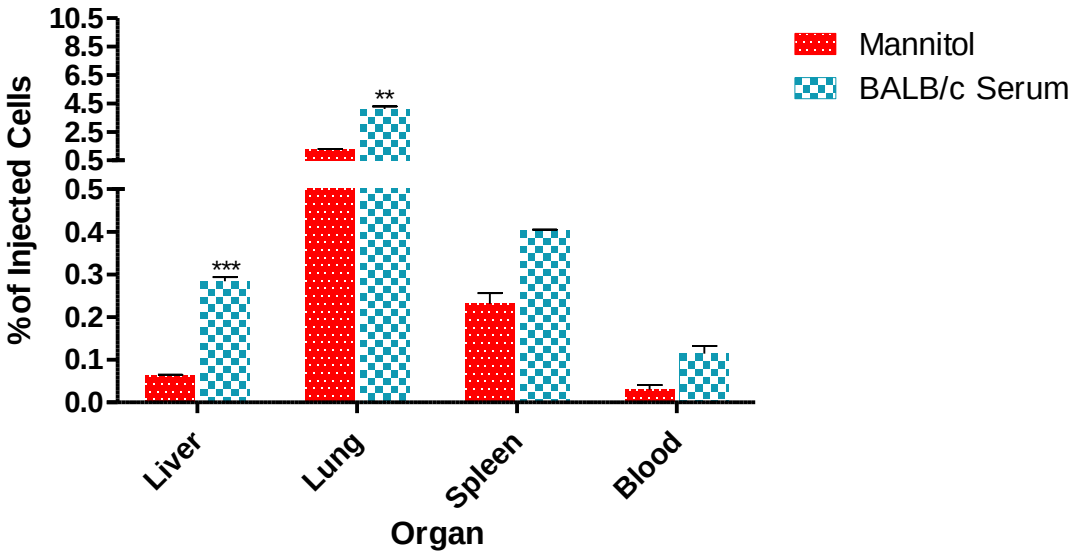

Figure 3-8: *In vivo* biodistribution of HDP cultured in BALB/c serum for 7 days 2h post injection. HDP were cultured in growth media with 10% BALB/c serum for 7 days prior to injection. Experimental conditions: Dose: $2x10^6$ cells in 100 µL 1 M mannitol in RPMI; Cells: BALB/c RFP-Cre-ERT-2A-LucBsd HDP cells; Animals: healthy 8 week BALB/c female mice; Statistics: ** = $p < 0.01$, *** = $p < 0.001$, compared to mannitol control in same organ, N = 3 animals per condition.

3.3.1.4 Reducing the thrombin response

We hypothesized cells may have been trapped elsewhere in the body due to thrombosis, preventing cells from circulating and also trapping them in place for destruction by the instant blood-mediated inflammatory response (IBMIR) [224]. To reduce thrombosis, animals were treated with known thrombin inhibitors, including aspirin [211, 212], dextran sulfate [209, 213], argatroban [208, 214] and sucrose octasulfate [210]. Animals were given two doses of each inhibitor by IP injection 24 h and 2 h prior to cell transplantation. Two hours post transplantation, the impact of each of the thrombin inhibitors on the survival of the injected cells was modest (Figure 3-9). While there was some improvement in the

lung for animals treated with dextran sulfate and sucrose octosulfate (~6.5% or $3.25x10^5$ cells, $p < 0.01$), the overall enhancement across the other organs, while statistically significant, did not result in survival improvement large enough to justify continue with these inhibitors.

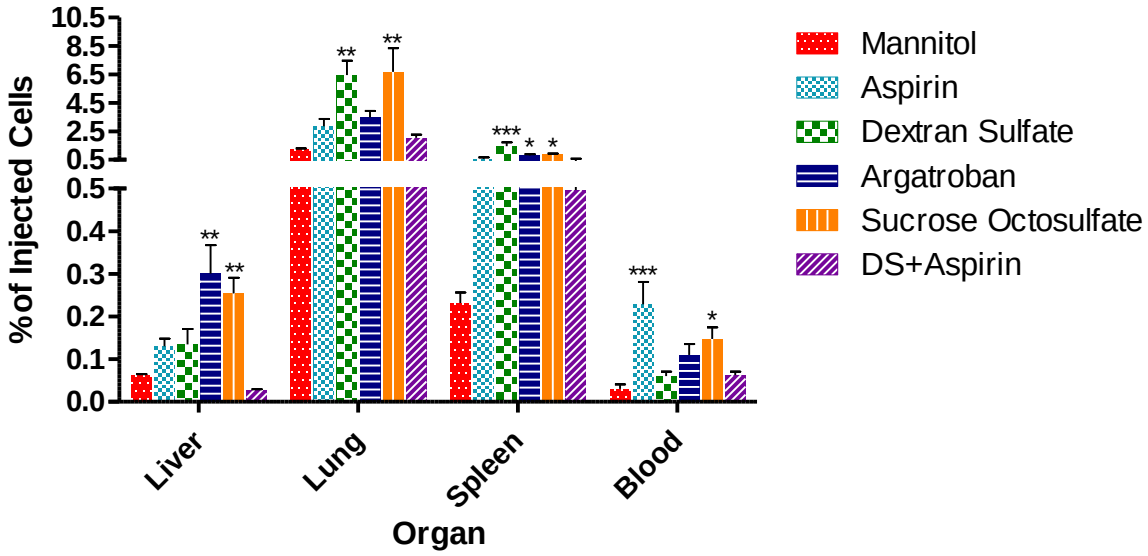

Figure 3-9: *In vivo* biodistribution 2 h post transplantation of HDP IV injected into mice pretreated with thrombin inhibitors. Mice were injected IP 24 h and 2 h prior to cell injection with thrombin inhibitors: Dextran sulfate (1 mg), sucrose octasulfate (1 mg), argatroban (200 µmol), or aspirin (2 mg). Experimental conditions: Dose: $2x10^6$ cells in 100 µL 1 M mannitol in RPMI; Cells: BALB/c RFP-Cre-ERT-2A-LucBsd HDP cells; Animals: healthy 8 week BALB/c female mice; Statistics: * = $p < 0.05$, ** = $p < 0.01$*** = $p < 0.001$, compared to mannitol control in same organ, N = 3 animals per condition.

3.3.1.5 Reducing the complement response

The complement system in the blood, which recognizes and destroys foreign cells, bacteria and is activated by certain materials represented a barrier that may have impact the acute survival post IV injection. We generated a Hoxb8 cell line which overexpressed

Crry (Auto-Crry), a complement inhibitor, at the cell surface (Figure 3-10) [215]. While there was improvement in the lung (1.2% in unmodified control vs 3.5% or 4.5% for Auto-crry HDP injected with or without dextran sulfate pretreatment, respectively, $p < 0.05$), spleen (0.2% vs 1%, $p < 0.01$) and blood (0.03% vs 0.2% for no dextran sulfate pretreatment, $p < 0.01$). Here again, we did not consider the improvement in the number of cells detected in the organs at 2 h post transplantation substantial enough to warrant further study (Figure 3-11).

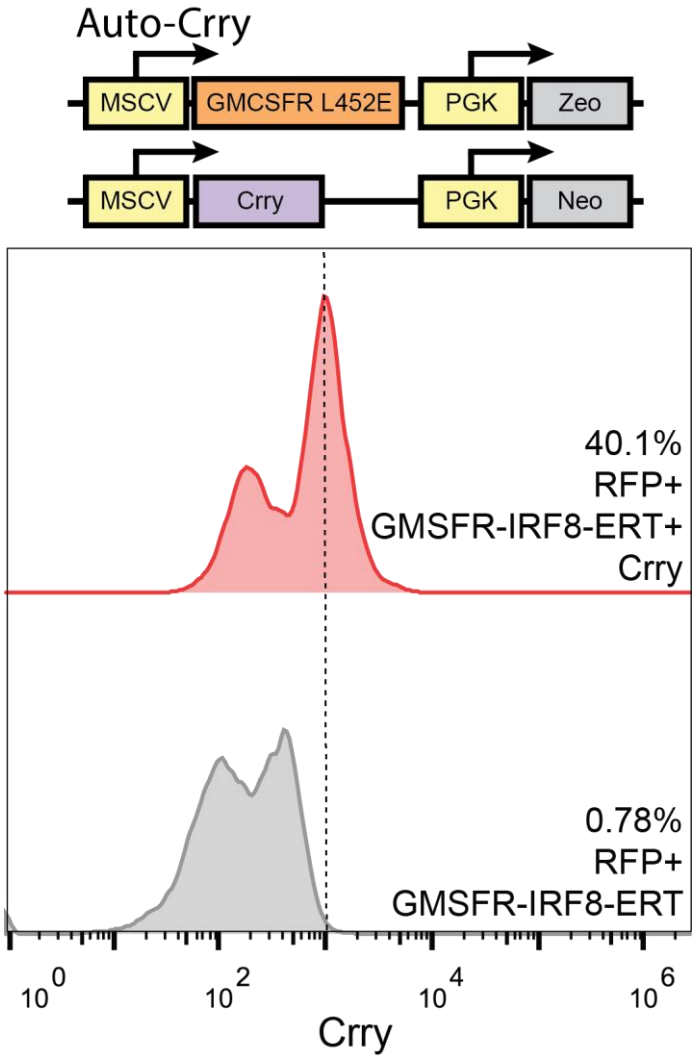

Figure 3-10: Genetic constructs and flow cytometry for Auto-Crry cells. These genetic constructs were transduced using retrovirus into BALB/c RFP-Cre-ERT-2A-LucBsd HDP

cells. Flow cytometry demonstrates elevated Crry expression of transduced cells (methods as described in Chapter 2, using APC-labelled rat anti-mouse Crry/p65 (BD-Pharmigen, Clone 1F2)).

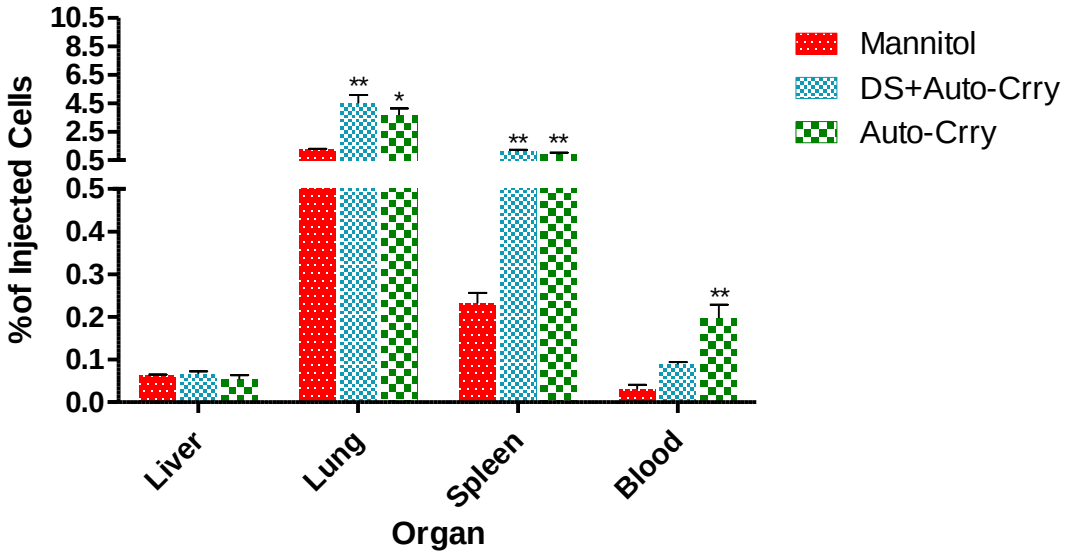

Figure 3-11: *In vivo* biodistribution of genetically modified HDP IV injected into thrombin inhibited mice 2 h post transplantation. Auto-Crry cells express both a constitutively active GMCSFR (See Chapter 4) and Crry, a complement inhibitor. DS = animals were IP injected with 1 mg dextran sulfate 24 h and 2 h prior to cell injection. Experimental conditions: Dose: $2x10^6$ cells in 100 µL 1 M mannitol in RPMI; Cells: BALB/c RFP-Cre-ERT-2A-LucBsd HDP cells; Animals: healthy 8 week BALB/c female mice; Statistics: * = $p< 0.05$, ** = $p < 0.01$*** = $p < 0.001$, compared to mannitol control in same organ, N = 3 animals per condition.

3.3.1.6 Summary

Using the IV route of injection for 4DDP, we developed an injection solution of 1 M mannitol which reduced the percentage of injected cells trapped in the lungs from ~50% to <20% 20 min post injection. Avoidance of the lung resulted in a low percentage (<5%)

of the injected 4DDP in the lungs, liver and spleen 2 h post injection. We hypothesized that tactics that modified the cell surface or interfered with intrinsic systems associated with foreign material response would increase cell survival. We employed a number of methods to modify responses in the blood that may have reduced the survival of 4DDP and HDP. These included PEGylation of the cells to evade the RES, culturing cells in syngeneic BALB/c serum to prevent a foreign immune rejection response, dosing animals with thrombin inhibitors to reduce thrombosis and modifying cells to express a complement inhibitor to reduce complement activation. None of the treatments improved survival beyond 10% of the injected number of cells across all measured tissues (liver, spleen, lung, brain, heart, kidney and blood) at 2 h post cell injection. There were small improvements (<~5%) from these treatments on survival at the 2 h point. However, we did not use combinations of treatments because no cells were detectable in the various organs at 24 h post cell injection (a selection from each of the strategies is presented at Figure 3-12). This motivated us to examine other routes of injection: lung instillation or intraperitoneal administration.

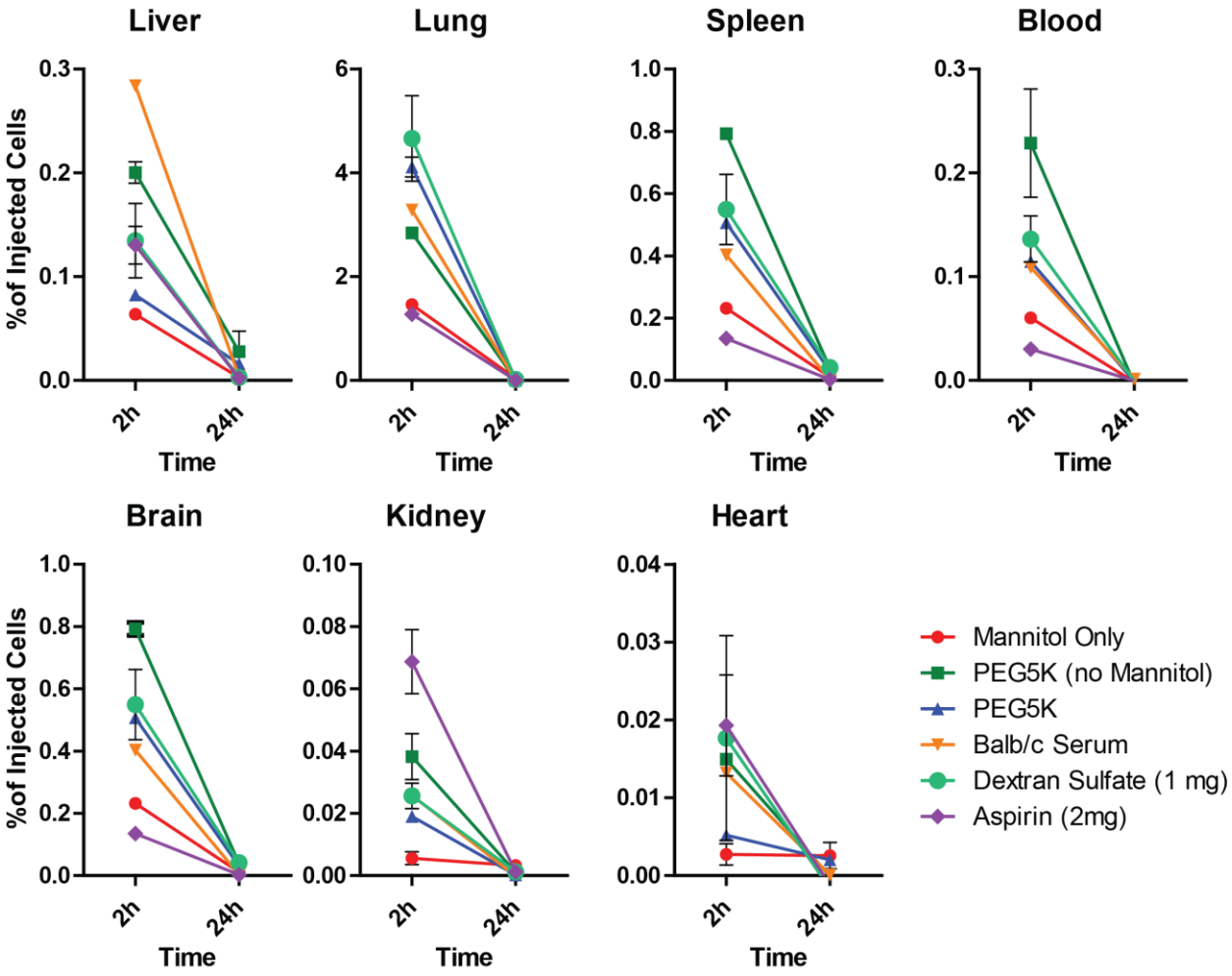

Figure 3-12: Biodistribution of HDP IV injected into mice 2 h and 24 h post injection. Cells were either labelled with DSPE-PEG5K or mice were injected IP 24 h and 2 h prior to cell injection with thrombin inhibitors: Dextran sulfate (1 mg), sucrose octosulfate (1 mg), argatroban (200 µmol), or aspirin (2 mg). Experimental conditions: Dose: $2x10^6$ cells in 100 µL 1 M mannitol in RPMI; Cells: BALB/c RFP-Cre-ERT-2A-LucBsd HDP cells; Animals: healthy 8 week BALB/c female mice. Statistics: * = p< 0.05, ** = p < 0.01*** = p < 0.001, compared to mannitol control in same organ, N = 3 animals per condition.

3.3.2 Lung instillation

A number of groups demonstrated successful transplantation of MΦ by directly instilling the cells into the lungs. Happle and Suzuki transplanted $2x10^6$ wildtype MΦ into

Csf2rb deficient mice and detected the transplanted cells at least 9 months post transplantation using flow cytometry [21, 22]. *Csf2rb* deficient mice have a severe lack of alveolar MΦ, leading to accumulation of lung surfactant in the lungs and are a model for pulmonary alveolar proteinosis. At 3 months post-instillation, Happle demonstrated 2.7% of cells in the lung were the transplanted MΦ [21]. In a separate study, Suzuki showed 40% of cells in the bronchoalveolar lavage were transplanted MΦ [22]. Suzuki also demonstrated by measuring Ki67 expression, a marker of proliferation, that wildtype MΦ engrafted in the lung and were able to proliferate. The engraftment and survival in the reports was aided by the significantly reduced number of endogenous lung MΦ in the *Csf2rb*$^{-/-}$ mice. They suggested that the absence of MΦ provided empty niches for the transplanted MΦ to occupy. *Csf2rb* encodes for the GMCSF receptor, and in the presence of GMCSF, provides survival and proliferation signals to MΦ. Thus the wildtype MΦ had a survival and proliferative advantage over the small number of endogenous *Csf2rb*$^{-/-}$ MΦ. Over time, wildtype MΦ were able to outcompete the endogenous MΦ for the remaining niches.

The long term engraftment of wildtype MΦ in these mice encouraged us to use the route to deliver 4DDP (BALB/c RFP-Cre-ERT-2A-LucBsd Hoxb8) directly into the lung. Only 0.1% of the injected HDP ($2x10^4$ cells) were detected in the lung 1 day post injection. The number of cells were undetectable at 7 days post injection (Figure 3-13). In the spleen, no HDP were detected at 1 or 7 days post injection. Comparing our experiments with Happle and Suzuki, we instilled HDP into healthy wildtype BALB/c mice what had few empty niches in the lungs and the transplanted HDP did not have a functional advantage that was absent when compared to endogenous MΦ. We hypothesize that the transplanted HDP were unable to engraft or survive. This result demonstrated to us the

importance of generating a niche or providing an environment for transplanted cells in which they could survive. Based on our experience in the IV route we decided to proceed with the IP/SC injection route.

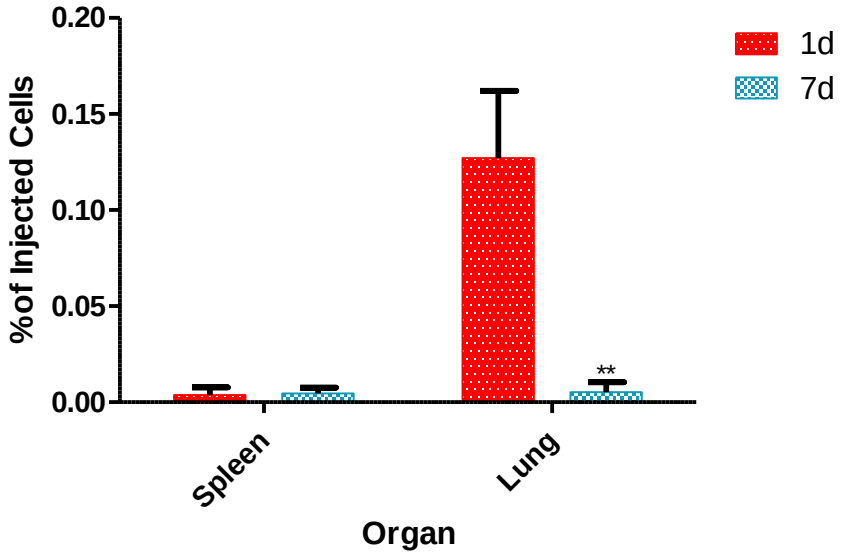

Figure 3-13: *In vivo* biodistribution of HDP transplanted by lung instillation at 1 day and 7 days post instillation.. Experimental conditions: Dose: $2x10^6$ cells in 200 µL RPMI; Cells: BALB/c RFP-Cre-ERT-2A-LucBsd HDP cells; Animals: healthy 8 week BALB/c female mice. Statistics: ** = $p < 0.01$, N = 5 animals per condition.

3.3.3 Intraperitoneal and subcutaneous injection

We next examined intraperitoneal (IP) or subcutaneous routes of administration. These routes do not immediately expose cells to the hydrodynamic stress of blood flow, complement, thrombosis or to removal by the RES (liver, bone marrow and spleen). Thus, we thought these routes of administration would be more favorable to the survival of the transplanted cells in comparison to the IV and lung routes. In addition, we could inject the cells in a protective matrix that has afforded prolonged survival of transplanted cells in the subcutaneous and peritoneal locations [225-227].

Matrigel (MG) is a commercially available product that is composed of a protein mixture that resemble the components of the extracellular matrix. It is secreted by Engelbreth-Holm-Swarm (EHS) mouse sarcoma cells. A unique property of MG is that it adopts a liquid state at 4°C, and forms a stable gel at 37°C. By adding cells to cold MG, the cell-MG mixture can be loaded into a syringe and injected into an animal, whereupon the mixture forms a solid gel containing cells in the injection space. This method has been used by many groups to successfully transplant a wide variety of cell types, including human neural precursor cells [225], pancreatic islets [226] and ovarian cells [227]. We hypothesized the HDP and MΦ could benefit from the protective and survival benefits of MG when injected into the peritoneal cavity. To guide our *in vivo* experiments, we studied the impact of MG on *in vitro* cultures of HDP by culturing HDP for up to 49 days in matrigel and measuring the viability, luciferase activity and gene expression profiles.

3.3.3.1 Characterization of cells in *in vitro* matrigel cultures

MΦ and myeloid cells have highly plastic phenotypes that can be polarized from one phenotype to another depending on environmental signals. MG represents a substitute for the extracellular matrix, and have been shown to modify the behaviors of cells which are exposed to the MG [228, 229]. Before embarking on *in vivo* biodistribution studies using MG, we characterized the interactions between HDP and MG. We examined the survival benefits of MG on HDP cells and the effects of long term MG cultures on overall HDP cell survival, M1/M2 polarization and MΦ differentiation.

3.3.3.1.1 Matrigel does not substitute serum or GMCSF

We determined if MG alone can support the survival and growth of HDP *in vitro*. Since MG is a biological product formed from the secretion of cells in culture, it is possible

MG could supplement or replace the need for growth factors or cytokines required to support cell survival. *In vitro* cultures of HDP in MG containing both fetal calf serum and GMCSF supplement were able to support sustained growth and proliferation of HDP cells for up to 19 days (Figure 3-14). Cultures containing only serum or GMCSF supplement were unable to sustain long term growth, as determined by visual observation of cultures. While there appears to be smaller clusters of cells evident in the culture containing serum with no GMCSF supplement, these clusters are remnants of small cell cultures which stopped expanding after several days. Cell clusters in cultures containing both serum and GMCSF supplement continued to grow and expand. Thus, MG alone is unable to replace the growth and survival benefits conferred from fetal calf serum and GMCSF supplement.

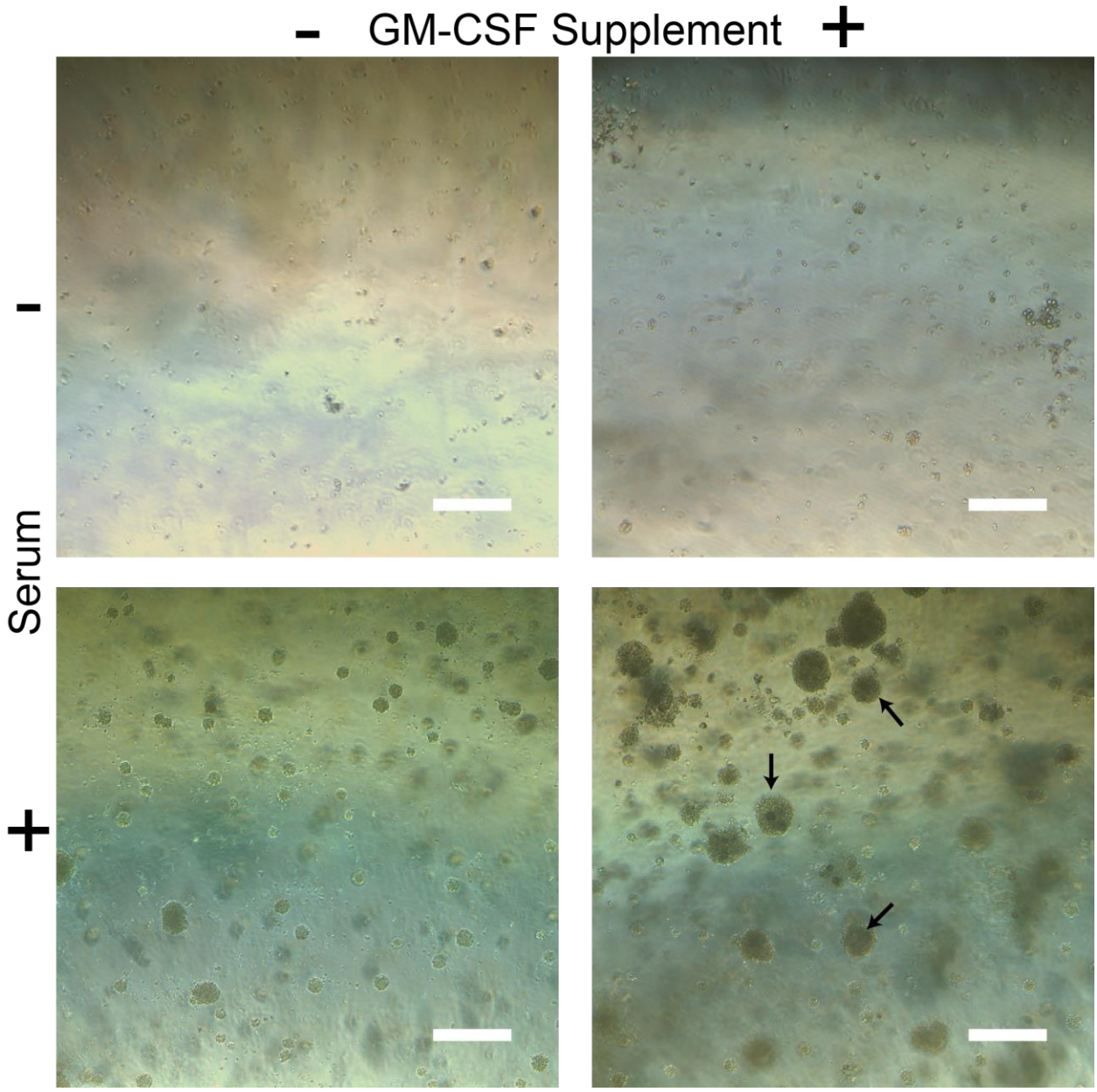

Figure 3-14: Representative micrographs of HDP cultured in high molecular weight matrigel for 19 days. HDP were seeded in a 1:1 (v/v) mixture of matrigel and RPMI containing (+) or not containing (-) fetal calf serum or GMCSF supplement. Clusters of cells (arrows) can be observed growing in cultures containing both serum and GMCSF supplement. Scale bar = 500 µm. Images were taken from a representative section of the culture (N = 1 culture per condition)

3.3.3.1.2 Long term *in vitro* cultures of HDP

In the appropriate conditions, HDP formed cell clusters in MG within several days that persist for at least 19 days. The solid-gel of the MG prevents the free movement of cells so we assumed each cluster arose from a single cell. We hypothesized as the clusters enlarged, the centers of these clusters became diffusion limited and received reduced nutrients (and could not remove toxic materials) from their surroundings. This would lead to growth stasis or death. When cells were extracted from long term (7, 14 and 49 d) MG cultures and stained using Trypan Blue, a live/dead cell stain, the percentage of live cells decreased in older cultures. The percentage of live cells declined significantly between 7 d and 21 d cultures ($p < 0.05$). However, there was no significant difference between the 21 d and 49 d cultures (Figure 3-15A). While the total percentage of live cells dropped from 60% to 40% between 7 d and 21 d, the total number of live cells were statistically similar at these times (Figure 3-15B). This data suggests that between these two time points, the number of live cells stayed constant but a large number of cells died over this time period. By 49 d, total live cells and the live percentage were similar to that observed in the 21 d cultures. This implies a steady state had been reached. This experiment demonstrates that HDP are capable of surviving up to 49 days in an *in vitro* MG culture. As the cultures aged, the MG slowly degraded and the total volume of solid gel remaining in the culture decreased. MG cultures with no cells which underwent the same media change schedule as MG cultures with cells did not lose the solid gel,

indicating that the processes of cell growth, proliferation and death was likely responsible for the breakdown of the MG.

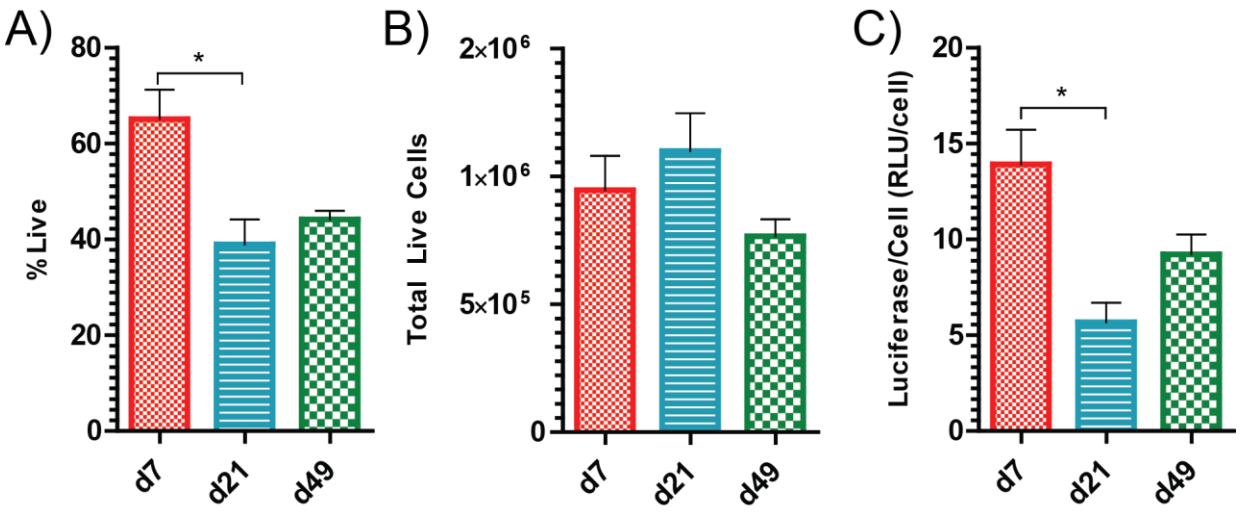

Figure 3-15: Survival of HDP cells growing in matrigel over time in transwell cultures. HDP cultured in matrigel were evaluated for: A) Percent live cells by trypan blue staining, B) total live cells retrieved from culture and C) luciferase activity. Statistics: * = $p< 0.05$, N = 3 separate cultures per time point.

It should be noted that luciferase activity per cell varied at each time point (Figure 3-15C). Myeloid cells are highly responsive to the environment [1, 37], so we hypothesized extended culture in MG may have altered the overall gene expression. Due to the reduction in luciferase activity in the oldest cultures, we suspected expression of other genes may have also changed. However, as a caveat for all qPCR analysis, the results presented in this section represents an average measurement from a bulk number of cells. It is important to consider that HDP grew in distinct clusters within the MG, and thus the cells on the outer and inner layers of the cluster likely experienced different environments (i.e. Cell debris, waste materials, and contact with MG) (see Figure 3-14). Therefore the gene expression profiles of the cells from the outer and inner layers may

be different. Due to the averaging effect of bulk qPCR, the gene expression changes discussed in this section may not accurately represent the diversity of individual cell responses to long term MG culture.

In extended MG culture there is an altered expression of genes related to M1/M2 polarization and MΦ differentiation. There was significant ($p < 0.01$) elevation of *iNOS* (M1) and *Arg1* (M2) expression as the age of the culture increased (Figure 3-16A). We also measured gene expression of the cells from extended MG cultures for MΦ and HDP markers (Figure 3-16B). There is a 10-fold enhancement of the MΦ gene, *Emr1* (F4/80) and ~10-fold reduction of the HDP markers, *Elane*, *Prtn3*, *Ms4a3* and *Plac8*. In comparison, MΦ differentiated from HDP typically have a 100-fold enhancement of *Emr1* and at least 100-fold reduction of the HDP markers.

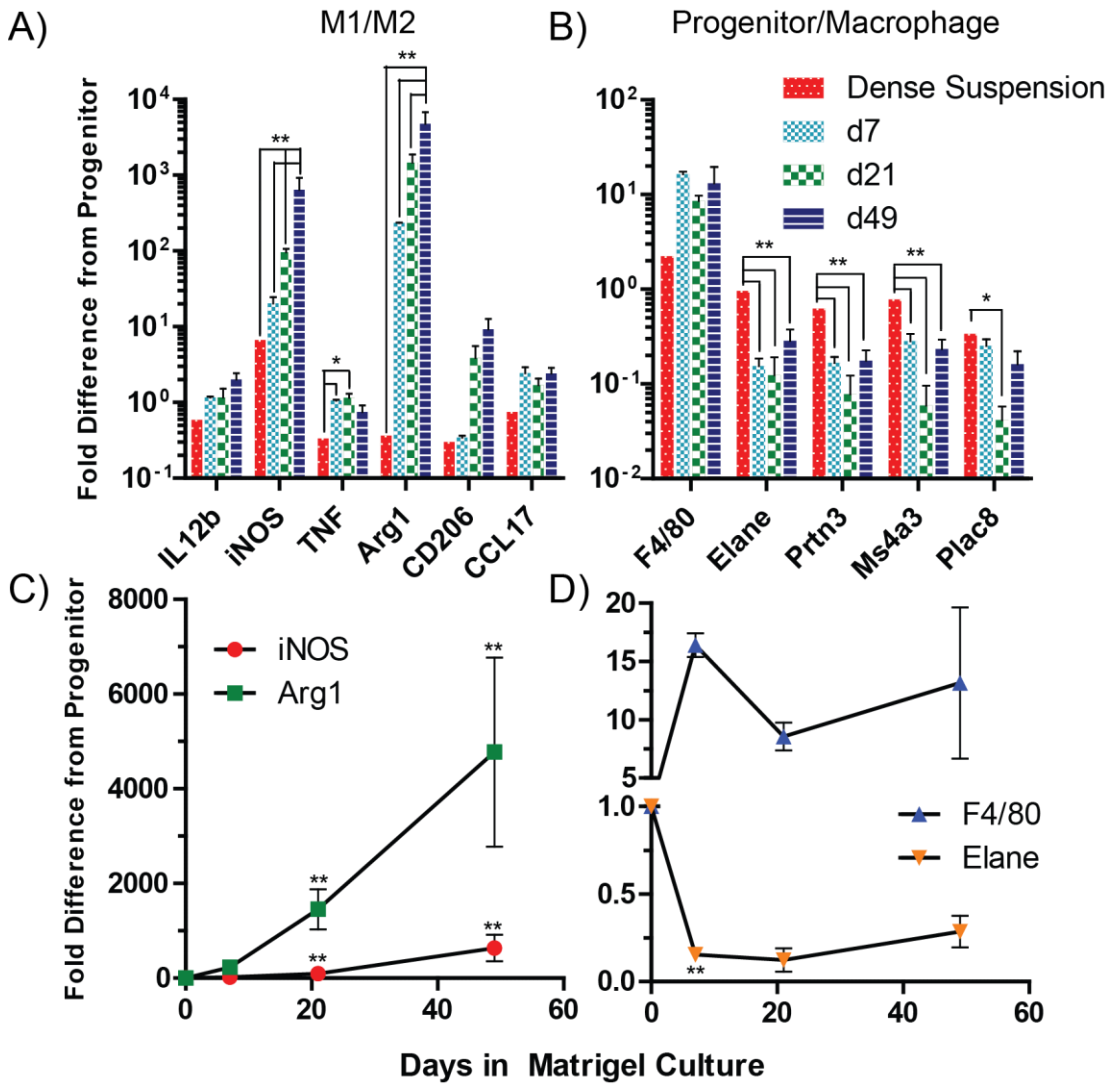

Figure 3-16: Evaluation of M1/M2 and monocyte/MΦ gene expression in long term matrigel cultures of HDP.A) Cells isolated from long term *in vitro* matrigel cultures were analyzed for gene expression of known M1/M2 and HDP/MΦ genes to determine the effects of long term cultures. Fold difference was expressed as a difference from a healthy suspension culture of HDP. A dense suspension culture was included as a comparison to isolate the effects of an unhealthy/dense culture containing cell debris and dying cells from a dense matrigel culture. Statistics: * = $p< 0.05$, ** = $p < 0.01$, N = 3 separate cultures per time point for matrigel cultures, N = 1 for dense suspension. B) Expression of selected

M1/M2 and HDP/MΦ genes presented over time in MG culture. Statistics: ** = $p < 0.01$ for comparison against previous time point.

The consistent increase in *iNOS* and *Arg1* with time (Figure 3-16C) may be due to a stress response from the constant exposure to dead and dying cells, triggering a sterile inflammation response. Sterile inflammation is an inflammatory response caused by non-microbial mechanisms, including physical trauma, ischaemia-repurfusion injury or chemically induced injuries [230]. IL-1α and IL-1β are released from hypoxic dying cells, and when supernatants of dying cells were mixed with MG and injected into mice, endogenous MΦ infiltrate into the MG [231]. Recruitment of MΦ is an indication of inflammation [230], thus clearly demonstrating the inflammatory nature of dead and dying cells in MG. Due to the solid-gel nature of the culture, cell debris could not be removed and the live cells would be constantly exposed to cell debris, resulting in a persistent sterile inflammatory environment. Myeloid derived suppressor cells (MDSCs), which include MΦ, recruited to inflamed prostates have increased *iNOS* and *Arg1* expression [232]. A possible explanation for this behavior is that MDSCs are upregulating these genes as an anti-inflammatory behavior to reduce local inflammation [232], and this may also be occurring with the HDP cells in long term MG culture.

This would be unique behavior in HDP which should not exhibit M1/M2 polarization behaviors, especially due to the lack of intentionally added M1 (LPS/IFNγ) or M2 (IL-4) inducers in the extended MG cultures. While best efforts were made to prevent accidental exposure of cultures to LPS or other inducers, the results we observe may be due to an unintentional addition of other materials to the culture.

There was no change in macrophage/progenitor gene expression between 7 d and 49 d MG cultures (Figure 3-16D), indicating the change is consistent and did not mimic the changes in fully differentiated MΦ. Therefore, the cells recovered from long term MG cultures were not MΦ, but expressed genes at a level between HDP cells and fully differentiated MΦ. This may explain the MΦ-like behavior of *iNOS/Arg1* upregulation observed in these long term cultures. Additionally, this effect in MΦ and HDP-specific genes is observed within 7 days and is held constant, demonstrating this may be an effect of the MG itself, rather than a result of the effects of a long term culture (Figure 3-16D). It is well established that cells cultured in ECM substitutes, including MG, alter effector function and gene expression of human hepatocytes [229], colorectal cancer cell lines [229] and lung cancer cell lines [228].

3.3.3.2 Matrigel as a physical support in tumored and healthy animals

In vitro MG cultures of HDP cells demonstrated HDP cells are able to survive and proliferate for up to 49 days when cultured with media containing fetal calf serum and GMCSF supplement. These extended MG cultures demonstrated a reduction in luciferase activity, and in terms of gene expression, an increase in a subset of M1/M2 genes (*iNOS*/*Arg1*), an increase in the MΦ gene (*Emr1*) and a decrease in HDP genes (*Elane*, *Prtn3*, *Ms4a3* and *Plac8*). However, the changes in the MΦ and HDP gene expression were 10 to 100-fold less than what is expected from fully differentiated MΦ. Due to the long term *in vitro* survival of HDP cells in MG, we determined if co-injecting 4DDP with MG would improve the *in vivo* survival of HDP cells.

Co-injecting 4DDP with MG resulted in a significant improvement ($p < 0.001$) in the survival and recovery of HDP, with upwards of ~60% recovery ($3x10^6$ cells) 72 h after IP

injection, compared to <0.5% recovery ($2.5x10^4$) when 4DDP were injected only with RPMI (Figure 3-17). In these animals, solid pieces of MG could be recovered from the injection site. Injecting the MG/cell mixture in the SC space also resulted in significant survival, with ~50% ($2.5x10^6$ cells) of the injected cells recovered at 168 h. It should be noted that the recovery for both 72 h and 168 h time points for SC injections is probably underestimated due to the difficulty in performing a flush in the SC space to recover all of the MG fragments. In all cases, the more MG that could be recovered, the higher the number of 4DDP that were detected by luciferase activity. No significant percentage of injected 4DDP (<0.01%) were detected in other tissues. This suggests either the HDP remained in the MG exclusively, or any 4DDP which migrated out of the MG were removed by various mechanisms. The following sections will describe our attempts to enhance cell migration beyond the MG to other tissues.

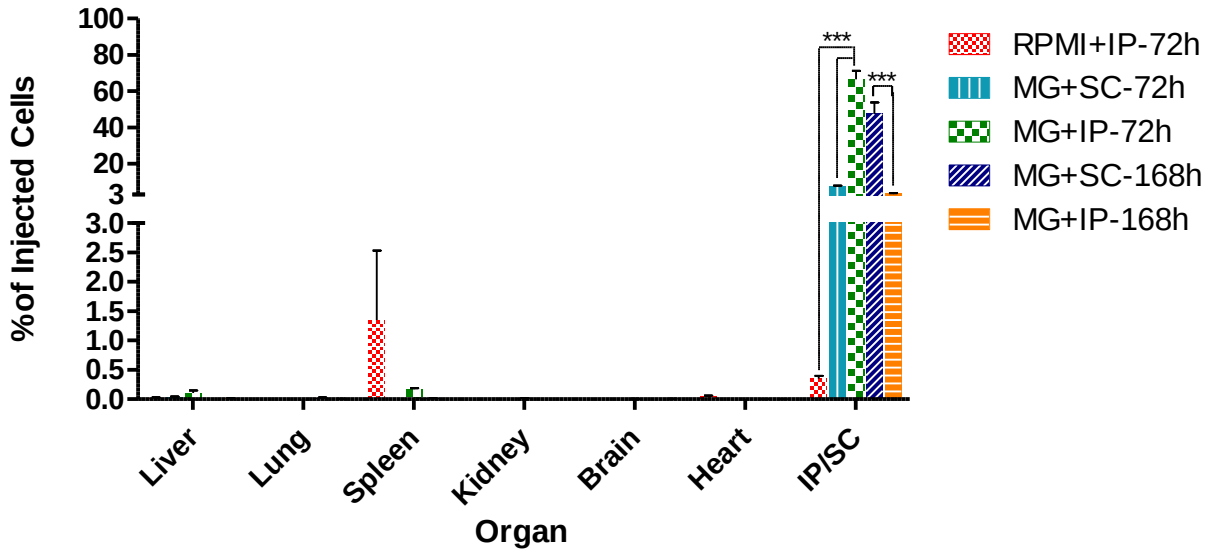

Figure 3-17: *In vivo* biodistribution of 4DDP injected IP or subcutaneously with matrigel (MG). Animals were sacrificed 72h or 168h after cell transplantation, as indicated. The

respective injection site (IP or subcutaneous (SC) space) was flushed with 5 mL of RPMI to collect contents, including MG fragments to determine total percentage of injected cells in the peritoneal or subcutaneous spaces. Experimental conditions: Dose: $5x10^6$ cells in 500 µL 1:1 (v/v) mix of MG and RPMI; Cells: BALB/c RFP-Cre-ERT-2A-LucBsd Hoxb8 4DDP; Animals: healthy 8 week BALB/c female mice. Statistics: *** = $p < 0.001$, compared to other conditions at the same time point in the same organ, N = 3 animals per condition.

3.3.3.2.1 Cytokine stimulated cells

4DDP co-injected with MG were retained in the MG but were not be detected in other tissues (liver, lung, spleen, kidney, brain or heart). This may be due to no signal to enhance the migration of 4DDP out of the matrigel. MΦ and myeloid cells are actively recruited to tumors [107, 108, 197], and we reasoned that a tumor model could recruit 4DDP out of the matrigel and into the tumor and perhaps into other tissues. As demonstrated in Section 2.4.4, MΦ derived from HDP migrated in a transwell assay in significantly higher numbers towards conditioned media from a 4T1 murine breast tumor cell line in comparison to unmodified growth media. A similar experiment conducted using 4DDP produced similar results (Figure 3-18).

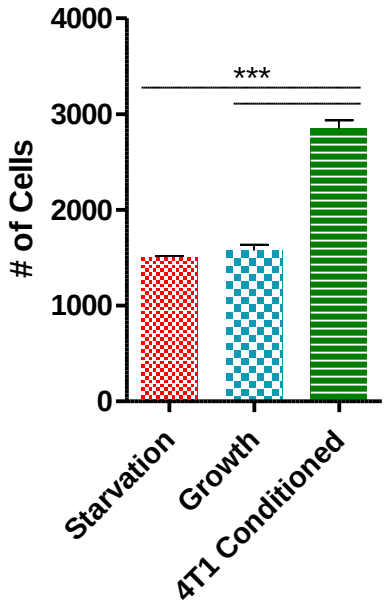

Figure 3-18: 4DDP preferentially migrate towards 4T1 conditioned media. $5x10^4$ 4DDP were plated in a 24 well size, 8 µm transwell insert (Corning) in migration conditions for 24 hours (top level containing 0.5% serum media with no supplements, bottom level containing experimental medias). The number of cells which migrated to the bottom level were determined by measuring total luciferase activity and comparing to a standard measuring the luciferase activity of a known number of 4DDP. 4T1 conditioned media (CM): 50% CM generated over 3 days of a growing 4T1 culture, 50% RPMI with 10% serum; Growth media: RPMI with 10% serum and 1% GMCSF-L929 conditioned media; Starvation media: RPMI with 0.5% serum. Statistics: *** = $p < 0.001$, N = 3 transwells per condition.

Metastatic breast tumors were established in female BALB/c mice with an orthotopic injection of $3x10^5$ 4T1 cells into the mammary fat pad. 4T1 cells quickly form a large primary tumor and metastasize to multiple tissues, include the lung, liver and brain [233]. 2-3 weeks after tumoring, the animals were injected IP with matrigel and 4DDP. We

also tested the effect of M1/M2 pre-polarization on the overall biodistribution of the IP injected 4DDP.

The biodistribution of injected 4DDP in tumored animals with naïve, unpolarized 4DDP were similar to those from healthy animals; the vast majority of the signal retained in the IP, particularly in the recovered MG pellets. Importantly, the total percentage of injected cells exceeded 100% for animals injected with unpolarized differentiating HDP 7 days post injection (Figure 3-19), indicating that the cells were actively proliferating within the IP space. This is important because it indicates that in 4T1 tumored animals, the endogenous milieu of cytokines and growth factors in the peritoneal cavity is sufficient to sustain the growth and survival of at least $5x10^6$ 4DDP.

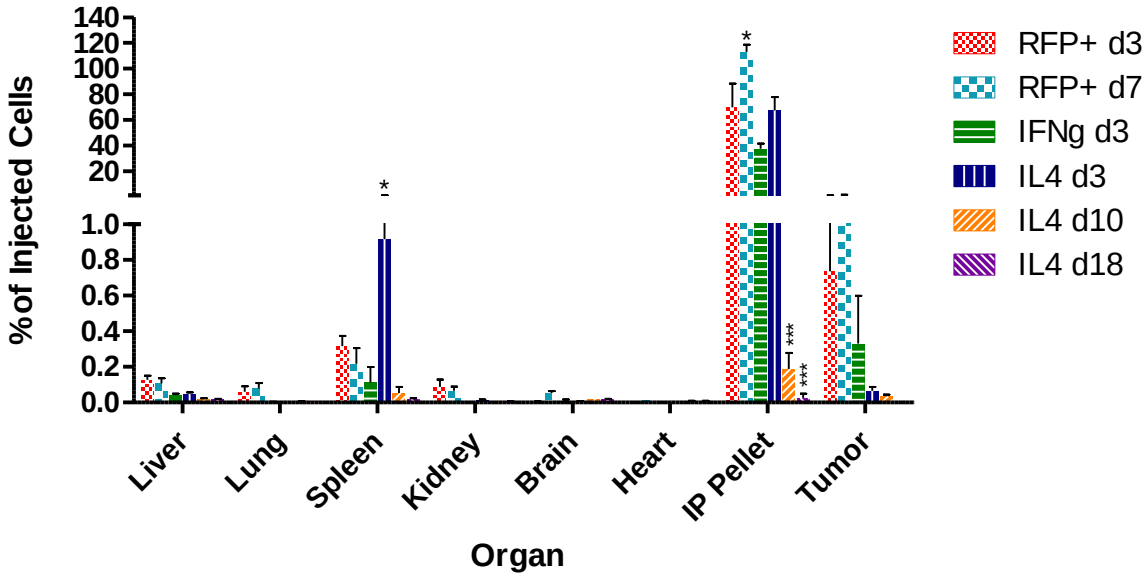

Figure 3-19: *In vivo* biodistribution of 4DDP treated with cytokines injected IP with matrigel in animals with 2-3 week old orthotropic 4T1 tumors. Prior to injection, cells were partially differentiated with 4 days of 200 nM 4-OHT (4DDP) and stimulated with cytokines for 3 days (40 ng/mL IL-4 or 40 ng/mL IFNγ). Animals were sacrificed at the times indicated.

The peritoneal cavity was flushed with 5 mL of RPMI to collect contents, including matrigel fragments to determine total percentage of injected cells in the IP. Experimental conditions: Dose: $5x10^6$ cells in 500 µL 1:1 (v/v) mix of matrigel (MG) and RPMI; Cells: 4DDP from BALB/c RFP-Cre-ERT-2A-LucBsd HDP cells; Animals: 10-12 weeks old BALB/c female mice at time of cell injections with 2-3 week old 4T1 tumors; Statistics: * = $p < 0.05$, *** = $p < 0.001$, compared to the control RFP+ d3 in the same organ, N = 3 animals per condition.

Three day post-injection studies using IFNγ (M1) and IL-4 (M2) treated 4DDP showed that compared to M2 polarized 4DDP, M1 polarized 4DDP had better survival in the IP than M2 polarized 4DDP (~80% versus ~40%), and ~1% ($5x10^4$ cells) of the injected cells was found in the spleen. However, there was minimal signal in the tumor for 4DDP polarized with either cytokine.

Due to the 1% of injected cells in the spleen for M1 polarized 4DDP, we pursued additional experiments at 10 and 18 days post cell injection. In these animals injected with M1 polarized 4DDP, not only did the signal in the spleen become undetectable, the detectable percentage of injected cells in the IP fell significantly between 3 days and 10/18 days ($p < 0.001$).

Importantly, at 10 days post 4DDP injection, it has been 24 days since the mouse was tumored and the tumors metastasized. When the peritoneal cavity of these animals were flushed, the recovered solution was dense and cloudy with undefined cells and no matrigel pellets could be found. Since the MG gels were not fully degraded after 49 d *in vitro*, this suggests that endogenous components (i.e. Cells and enzymes) *in vivo* are primarily responsible for the observed MG degradation. It is possible the matrigel was

complete degraded by the cells which infiltrated the IP. This would have resulted in the loss of the survival-enhancing scaffold for the 4DDP and lead to the elimination of the injected 4DDP. Large 4T1 tumors (>3 weeks) are capable of invading the peritoneal cavity [233]. We suspect that these invading tumor cells, which are naturally predisposed to be more adept at degrading extracellular matrix [234], are responsible for the degradation of the MG. Invading 4T1 cells in the peritoneal cavity may have also reduced the ability of the primary tumor to recruit 4DDP due to a stronger chemoattractant gradient present in the peritoneal cavity. However, we did not investigate if the cells found in the IP flushes were 4T1 cells and instead focused on other modifications.

While there was no statistically significant difference between the various tested conditions on the percentage of injected cells detected in the tumor, histology of tumors in selected animals with higher luciferase activity revealed the presence of the injected cells in selected sections (Figure 3-20). However, this observation was not universal between animals in the same experimental cohort, or even within a single tumor. Due to this, our confidence in using this M1/M2 repolarization as a method to enhance the migration of injected cells into 4T1 tumors was limited.

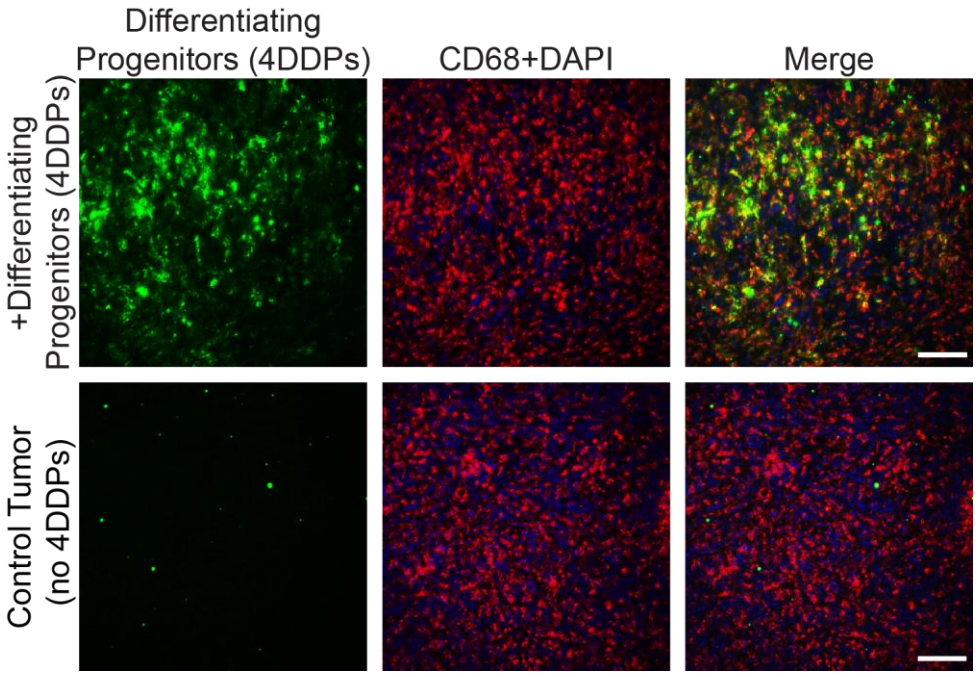

Figure 3-20: 4DDP injected IP with matrigel can be detected in selected sections of 4T1 tumors from selected animals. Co-localized staining of 4DDP (green, Anti-RFP) and the MΦ-specific marker, CD68 (red, Anti-CD68) demonstrates tumor contains both endogenous MΦ and 4DDP. Scale bar = 100 μm

3.3.3.2.2 <u>CCR2 overexpression</u>

An alternative approach to enhance the migration of 4DDP out of the MG, a CCR2 overexpressing HDP line was generated. CCR2 is the corresponding receptor to CCL2, a chemoattractant ligand that is known to be secreted by 4T1 tumors [217]. By combining a CCR2 overexpressing HDP line with a tumor model which secreted CCL2, we hypothesized that the tumor would cause the CCR2+ cells to migrate out of the MG and towards the tumor.

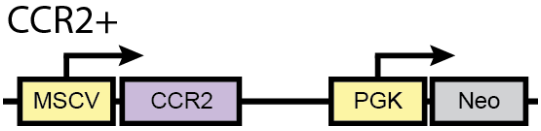

Figure 3-21: Genetic construct for CCR2+ cells. This genetic construct was transduced using retrovirus into BALB/c RFP-Cre-ERT-2A-LucBsd HDP cells.

The biodistribution of CCR2+ cells is similar to the unmodified cells, demonstrating there was no discernable impact on tumor localization of 4DDP with the CCR2 modification (Figure 3-22). Perhaps the chemoattraction via CCL2 is not strong enough signal to attract cells from the MG, which offered a relatively safe environment for cells to survive and proliferate. Alternatively, it is also possible cells did migrate beyond the MG, but were removed before or after reaching another tissue by mechanisms like a lack of survival cytokines or targeting by the immune system. Another explanation is that the chemoattraction of 4DDP to the primary tumor may be reduced due to the much closer proximity of local 4T1 cells secreting cytokine which interrupt the cytokine gradient from the primary tumor.

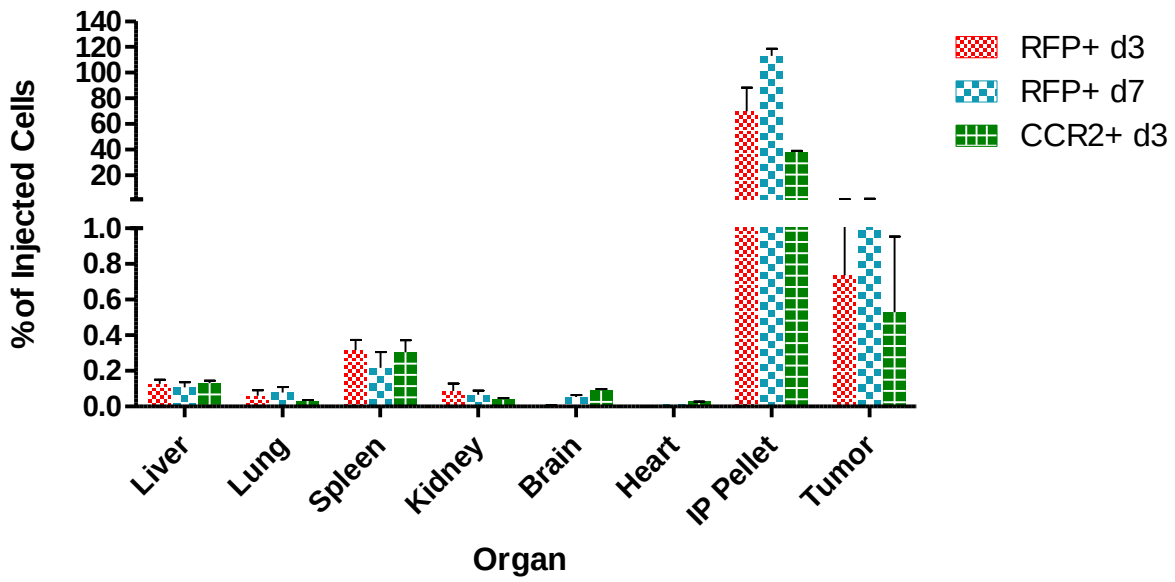

Figure 3-22: *In vivo* biodistribution of CCR2+ 4DDP injected IP with matrigel in animals with 2-3 week old orthotropic 4T1 tumors. Animals were sacrificed at the times indicated. The peritoneal cavity was flushed with 5 mL of RPMI to collect contents, including matrigel fragments to determine total percentage of injected cells in the IP. Experimental conditions: Dose: $2x10^6$ cells in 500 µL 1:1 (v/v) mix of matrigel (MG) and RPMI; Cells: BALB/c RFP-Cre-ERT-2A-LucBsd HDP cells treated for 4 d with 200 nM 4-OHT; Animals: 10-12 weeks old BALB/c female mice at time cell injections with 2-3 week old 4T1 tumors. Statistics: no significance identified in this data set when compared to the control RFP+ d3 in the same organ, N = 3 animals per condition.

3.3.3.2.3 <u>Effect of other physical supports</u>

In addition to MG, we were interested if another material would perform as a co-injected matrix to aid the post-transplantation survival of HDP and MΦ. MG is composed of high molecular weight proteins, which together form a solid-gel matrix that resembles the extracellular matrix. Hyaluronic acid (HA, MW: 10000k) has been used in the past to

transplant cells *in vivo* [235, 236] and is a component of the extracellular matrix. Co-injecting 4DDP with high molecular weight HA did not improve cell survival in the peritoneal cavity (Figure 3-23). Nor did it increase cell migration into the spleen. In comparison, MG co-injection was superior in the percentage of injected cells detected, albeit the cells are confined to the MG in the peritoneal space.

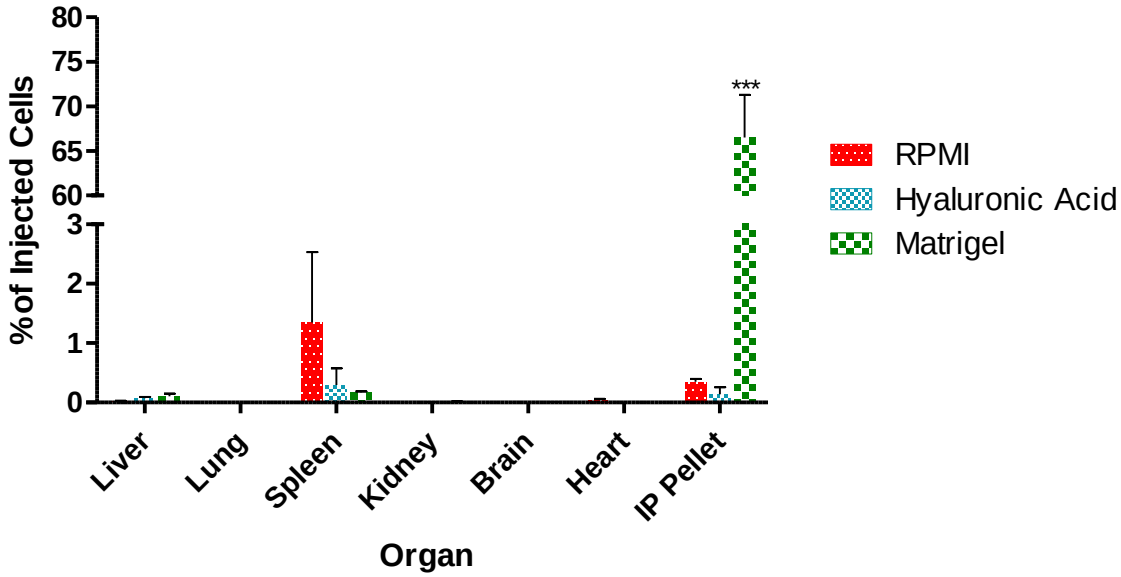

Figure 3-23: *In vivo* biodistribution of 4DDP injected IP with varying injection medias in healthy animals. Animals were sacrificed 72 h post injection. The IP was flushed with 5 mL of RPMI to collect contents, including matrigel fragments to determine percentage of injected cells in the IP. RPMI and MG injection data sets are the same as those in Figure 3-17. Experimental conditions: Dose: $2x10^6$ cells in 500 µL 1:1 (v/v) mix of RPMI and matrigel or hyaluronic acid (MW: 10000k); Cells: BALB/c RFP-Cre-ERT-2A-LucBsd HDP cells treated for 4 d with 200 nM 4-OHT; Animals: healthy 8 week BALB/c female mice; Statistics: *** = $p < 0.001$, compared to RPMI media only in same organ, N = 3 animals per condition.

3.4 Conclusion

Our goal in this phase of the thesis was to transplant HDP, MΦ and 4 day differentiated progenitors (4DDP) by various routes of administration (intravenous, lung instillation, subcutaneous and intraperitoneal) into mice and quantify their survival and biodistribution. We quantified live cells from organ lysates using a luciferase-based assay. IV injections of MΦ in RPMI lead to entrapment the lung, and the use of 1 M mannitol as an injection solution reduced the percentage of injected cells entrapped in the lungs from 50% to 20% at 20 min post-injection. Avoiding the lung did not result in detectable luciferase activity in the other organs tested (liver, spleen, and lung) 24 h post-injection. We hypothesized the cells were being targeted or killed in the blood, and used techniques described in the literature to reduce the impact of the RES [204-207], the innate immune system, thrombosis [208-214] and complement [215] on killing of the injected 4DDP into animals. We attempted a number of tactics to improve cell survival post-transplantation in the IV route, including: evading the RES by PEGylation of the cell surface, reducing the immune response to foreign serum proteins by culturing cells in syngeneic BALB/c serum, reducing the thrombin/complement response by pretreating mice with small molecular inhibitors or overexpressing the complement inhibitor, Crry, on the cell surface to inhibit complement activation. However, these techniques did not improve overall biodistribution or survival of the injected cells, with <0.1% of the injected cells detected by luciferase activity 24 h post-injection.

We were motivated to transplant HDP via lung instillation by Happle and Suzuki, who were able to transplant wildtype MΦ into *Csfr2b*-deficient mice by lung instillation and demonstrate survival in the lung up to 9 months post-transplantation [21, 22]. Our

attempts to transplant HDP into the lung of healthy wildtype BALB/c mice was unsuccessful, resulting in <0.1% of injected cells in the lungs at 1 d and 7 d post-injection. However, closer analysis of the differences between our attempt and the success from the two groups demonstrated to us two primary concepts. Firstly, *Csfr2b*-deficient mice are severely deficient in the number of tissue MΦ, and thus there are numerous empty niches for transplanted MΦ to occupy without competition for cytokines or other survival signals. Suzuki demonstrated tissue-levels of GMCSF decreased significantly post-transplantation, presumably because transplanted cells were utilizing the endogenous GMCSF that *Csfr2b*-deficient MΦ are unable to process [22]. Alternatively, we hypothesize GMCSF production by other cells may have been reduced as a feedback response due to the presence of functional MΦ. In support, dysfunctional tumor associated MΦ demonstrate the opposing behavior, where a paracrine feedback loop exists between GMCSF-secreting endothelial cells and EGF-secreting MΦ, which promotes proliferation and tumor metastasis [237]. Secondly, *Csfr2b*-deficient MΦ are also functionally deficient, particularly with respect to proliferative capacity [22]. The wildtype MΦ were able to proliferate in the lung post-transplantation and thus able to outcompete *Csfr2b*-deficient MΦ and eventually successfully engraft in the lung [21, 22]. To increase the survival and engraftment potential of transplanted MΦ, the lesson from these studies is to consider the availability of a specific niche and to provide a proliferative or survival advantage for the transplanted cells in the niche.

We shifted focus to the IP injection route, which provided the opportunity to co-inject cells with a solid-gel biomaterial, matrigel (MG), which is similar to the extracellular matrix. Using *in vitro* cultures, we demonstrated MG does not supplant the requirement

for serum components and GMCSF supplement for HDP to survive and proliferate. However, if these are provided, HDP can survive at least 49 days in MG. Additionally, by qPCR analysis, HDP cultured in MG upregulated some M1 and M2 genes (*iNOS* and *Arg1*) and expressed HDP/MΦ-specific genes at levels between naïve HDP and fully differentiated MΦ. Initial *in vivo* experiments co-injecting 4DDP with MG demonstrated a significant improvement in the number of 4DDP recovered, with ~60% ($3x10^6$ cells) of the injected cells found in the IP cavity. However, 4DDP were only found in the solid matrigel fragments in the peritoneal cavity, and few 4DDP (<0.1% of injected cells per tissue) were detected in the other tissues assayed (liver, spleen, lung, kidney, heart, lungs and blood). We hypothesized the 4DDP were isolated to the MG and did not migrate to other tissues.

To enhance cell migration beyond the MG, we tumored animals with 4T1 cells to provide an endogenous chemoattractant signal that is known to recruit endogenous MΦ. In these tumored animals, we also injected 4DDP which were polarized with IFNγ (M1) or IL-4 (M2) *in vitro* before injection because we hypothesized polarization may affect the migratory behavior of the 4DDP in the context of a tumor. Lastly, we used retrovirus to transduce the cells with CCR2, the cognate receptor to CCL2, a chemoattractant ligand that is secreted by 4T1 tumors [217]. These techniques did not enhance the trafficking of transplanted cells out of the MG to other tissues. However, when unmodified 4DDP were injected IP with MG into a 4T1 tumored mouse and biodistribution was measured, we were able to detect greater than 100% of the original injected cells in the peritoneal cavity. This demonstrates that in 4T1 tumored animals, there are sufficient growth factors and cytokines to support the survival and proliferation of injected 4DDP. In selected animals and tumor sections, 4DDP were also found in the tumor (Figure 3-20).

The lessons learned in the chapter demonstrated that the IP cavity was the best route of administration. While the benefits of MG on cell survival only lasted until the MG degraded *in vivo*, it proved that 4DDP co-injected with MG are capable of surviving and proliferating *in vivo* for up to 7 days. The lesson learned from the successful studies of Happle and Suzuki informed us of the importance of generating a niche for transplanted MΦ and myeloid cells. In addition, these groups showed that transplanted cells may be aided by possessing a survival and proliferative advantage over endogenous cells. In the next chapter, we apply the lessons learned in these experiments to develop a methodology to enhance the survival and engraftment potential of HDP and MΦ *in vivo*.

3.5 Methods

3.5.1 Animals

All mice used in this study were purchased from Charles River Laboratories (Wilmington, MA) and maintained under pathogen-free conditions at the University of California, San Francisco (UCSF). All mouse procedures were approved by the UCSF Institutional Animal Care and Use Committee (IACUC). The strain used in this study was BALB/c (strain #028). All mice used were female.

3.5.2 Transplanting cells into mice

Tail vein injection

Mice were placed under a heat lamp prior to injection to dilate tail veins for better visualization of the tail vein. After 10 min under the heat lamp, mice were placed into a restraint to isolate the tail. The tail was turned slightly to better visualize the vein, the needle was inserted and the contents slowly injected. Tail vein injections were limited to 100 µL using a 28 gauge insulin syringe. If 1 M mannitol solution (Sigma) was used to

suspend the cells, the mannitol was prepared in RPMI and sterile filtered before use. After injection, mice were returned to the cage and observed for 10 min to ensure there were no adverse effects. Adverse effects were not observed using a dose of $2x10^6$ cells per injection.

Lung instillation

Mice were sedated using isoflurane and restrained vertically. A 100 µL solution containing the cells was prepared and slowly administered in drops using a pipettor applied to the airway at the back of the throat. Care was taken to administer the solution slowly to ensure minimal obstruction of the airway and coughing by the mouse. After the solution was administered, the restraints were removed and the mouse was returned to the cage for observation for 10 min to ensure there were no adverse effects. No adverse effects were observed.

Intraperitoneal injection

Mice were scruffed and the ventral side was exposed. The head was tilted down slightly and the bottom right quadrant of the abdomen was wiped with an alcohol wipe. A 28 gauge insulin syringe containing up to 500 µL of solution was inserted bevel side up and slowly injected. For matrigel studies, the cell dose was resuspended in 250 µL RPMI and mixed with 250 µL matrigel (StemCell Technologies) on ice to form a 1:1 (v/v) mixture. The mixture was drawn into syringes and kept cold immediately prior to injection to prevent the matrigel mixture from solidifying in the syringe. For high molecular weight 10000k hyaluronic acid (HA-10000k), a 1 mg/mL HA-10000k (Lifecore) solution was made in D-PBS and sterile filtered prior to mixing with a RPMI cell solution to form a 500 µL 1:1 (v/v) mixture. For thrombin and complement inhibition studies the following

solutions were made in D-PBS and sterile filtered: 4 mg/mL aspirin (Bayer) [211, 212], 2 mg/mL dextran sulfate (Sigma) [209, 213], 400 µM argatroban (Sigma) [208, 214] and 2 mg/mL sucrose octosulfate (Sigma) [210]. After the injection, the mouse was placed in a cage and observed for 10 min to ensure no adverse effects. No adverse effects were observed.

Preparing cells for injections

Adherent MΦ and 4DDP were removed from tissue culture flasks using Hyqtase (GE) and gentle tapping of the flask. After removal from the flask, the cells were treated identically to suspension cells. Suspension HDP cells were washed twice with plain RPMI, counted and the required dose was resuspended in 100 µL for IV injection or 500 µL for IP injection. For matrigel co-injections, the matrigel and cells were mixed on ice and kept cold until injection to prevent solidification in the syringe. For each round of injections, the DiD signal or luciferase activity per cell was determined to enable the determination of the percentage of injected cells in each organ. To ensure an appropriate standard value was generated for luciferase activity, the luminometer readout was held below $3x10^6$ RLUs to be within the linear range of detection. This was accomplished by testing the luciferase activity of $1\text{-}2x10^5$ cells and adjusted accordingly to ensure results were within the linear range of detection.

3.5.3 Labelling cells with PEG (PEGylation)

Cells were labelled with PEG using a protocol adapted from the Iwata lab. [204-206] Cells were labeled by first washing the cells twice with serum-free RPMI before incubating the cells in 100 µM 1,2-distearoyl-sn-glycero-3-phosphoethanolamine-N-[(polyethylene glycol)-2000/5000] (ammonium salt) (DSPE-PEG2K/5K) (Avanti) in serum-free RPMI for 4 h at 37°C in a tissue culture-treated flask or sterilized, endotoxin-free Teflon jar. Teflon

jars were rendered by endotoxin free by overnight treatment in a 180°C oven. After 4 h, the suspension cells were collected and washed twice with serum-free RPMI before IV injection.

3.5.4 Serum exchange

Cells were washed twice with serum-free RPMI before transfer into the standard media formulation with the fetal calf serum replaced with BALB/c serum (Innovative Research). The cells were cultured and split as necessary in the BALB/c serum media for 7 days prior to injection.

3.5.5 Biodistribution

Processing organs for luciferase and DiD measurement

Animals were euthanized by an IP injection of sodium pentobarbital (200 mg/kg) and cervical dislocation, as approved by UCSF IACUC. Organs were collected and placed on ice. Organs were weighed and lysed by using a Wheaton dounce grinder and radio immunoprecipitation assay (RIPA) buffer (150 mM NaCl (Sigma), 1% Triton -100 (Sigma), 10% Glycerol (molecular grade, Roche) and 50 mM Tris (Fisher)) containing 1x protease inhibitor (BioTool). The organ lysates were centrifuged at 3000 rpm for 5 min and the supernatant was used for further analysis. Blood samples (~50-200 µL) were collected into a tube containing 10 µL 1 mg/mL heparin in D-PBS (Alfa Aeser) and were not processed further. Flushes of the peritoneal cavity were collected by injecting 5 mL of plain RPMI into the peritoneal cavity of a euthanized mouse. The mouse was massaged slightly to ensure proper mixing in the peritoneal cavity before a cut was made into the abdomen to drain the fluid into a collection dish. This solution was collected and stored on ice until ready for measurement. Due to cell settling, before measurement of samples

from the peritoneal cavity, the solution was mixed thoroughly by inverting the tube several times prior to measurement.

Determining total percentage of injected cells per organ

Prior to injection, cells were labelled with fluorescent DiD (Molecular Probes, ThermoFisher) following manufacturer protocols. Cells were resuspended in serum-free RPMI at a concentration of 10^6/mL and 5 µL of DiD solution was added per mL of cell suspension. After a 20 min incubation at 37°C, the cells were centrifuged and washed three times with serum-free RPMI. To determine DiD levels in organ lysates, 100 µL of clarified organ lysate was diluted into 400 µL of RIPA buffer and total fluorescence was measured using a fluorometer (Fluorlog, Horiba) (excitation 644, emission 665). Luciferase activity was determined using SteadyGLO (Promega) as per manufacturer protocols; 100 µL of organ lysate was mixed with 100 µL SteadyGLO in a glass tube. The contents were mixed and total luminescence was measured using a luminometer (MGM Instruments) over a 10 second period. For both cases, total percentage of injected cells in each organ was calculated by taking the raw values measured in the respective methods and applying an appropriate correction for dilutions and total volume of organ lysate. These values were then compared to a standard value generated for each round of injections by measuring the luminescence value of a known number of cells using the same methods described above. To ensure an appropriate standard value was generated, the luminometer readout was held below $3x10^6$ RLUs to be within the linear range of detection. This was usually accomplished by testing the luciferase activity of 1-$2x10^5$ cells.

3.5.6 Cytokine stimulation

HDP and MΦ were prepared as described in prior sections (2.6.1). To polarize cells, the media was changed for the appropriate polarization media: for M1, 40 ng/mL IFNγ (Peprotech), or for M2, 40 ng/mL IL-4 (Peprotech). Following an overnight treatment, cells were washed with D-PBS and processed for injection.

3.5.7 4T1 tumoring of mice

Metastatic breast tumors were established in female BALB/c mice with an orthotopic injection with $3x10^5$ 4T1 murine breast tumor cells into the mammary fat pad. Tumors were allowed to progress for 2-3 weeks before use in biodistribution studies. Animals were monitored and treated according to UCSF IACUC regulations.

3.5.8 *In vitro* matrigel cultures

Matrigel and HDP mixtures were prepared by suspending $5x10^4$ cells in 200 µL RPMI and mixing 1:1 (v/v) with matrigel on ice. The mixture was pipetted into the top of a 12-well transwell insert and placed in a humidified 5% CO_2 37°C incubator for 10 minutes to form a solid gel plug. The respective media (with or without fetal calf serum or GMCSF supplement) was added to the bottom and top of the transwell and the culture was returned to the incubator. The media on both sides of the transwell was carefully replaced every 2-3 days until the end of the experiment. To remove cells from the matrigel, Cultrex organoid harvesting solution (Trevigen) was used according to manufacturer's instructions. After cells were isolated from the matrigel, trypan blue staining and a hemocytometer was used to determine the total number of live and dead cells. RNA was collected using the RNeasy Mini Kit (Qiagen) following the manufacturer protocols and qPCR was performed as described in Chapter 2 (2.6.11).

3.5.9 Transwell studies

4DDP were differentiated from HDP (RFP-Cre-ERT-2A-LucBsd) treated for 4 days with 200 nM 4-OHT. $5x10^4$ 4DDP were plated in a 24 well size, 8 µm transwell insert and placed in migration conditions for 24 hours (top level containing 0.5% serum media with no supplements, bottom level containing experimental medias). Three different medias were tested: 4T1 conditioned media (50% conditioned media generated over 3 days of a growing 4T1 culture, 50% RPMI with 10% serum), growth media (RPMI with 10% serum and 1% GMCSF-L929 conditioned media) and starvation media (RPMI with 0.5% serum). Before use, 4T1 conditioned media was centrifuged and filtered to remove any cell debris. Following migration, the cells from the bottom level were collected by centrifugation. The pellet was resuspended in 100 µL RPMI and mixed with 100 µL SteadyGLO to determine the total luciferase activity. The total number of cells in each well was calculated using a luciferase activity standard determined by measuring the activity of a known number of cells. The transwells were also stained and fixed as per 2.6.15 to determine the number of cells which were adherent to the underside of the transwell membrane, but no adherent cells were counted.

3.5.10 Statistics and modeling

Statistics and modeling was performed using GraphPad Prism 5. To determine significance between data sets, one way ANOVA was performed, followed by a multiple comparison Bonferroni posttest. Significance was reported as follows: * = $p < 0.05$, ** = $p < 0.01$ or *** $p < 0.001$. Lines of best fit where generated using the one phase decay or linear fit model depending on the data set, as indicated in the experimental description.

4 Chapter 4: Clodronate pretreatment improves acute survival of transplanted Hoxb8 myeloid progenitor cells expressing constitutively active GMCSFR in immunocompetent mice

New methods to produce large numbers of macrophages (MΦ) *in vitro* have reinvigorated interest in MΦ based therapies. Myeloid progenitor cells, precursors to MΦ, can be cultured indefinitely when Hoxb8 activity is maintained [34]. We generated Hoxb8-dependent progenitors (HDP) by transducing lineage negative bone marrow cells with a construct containing a constitutively expressed Hoxb8 flanked by loxP sites. HDP can be cultured indefinitely and differentiate into functional MΦ when Hoxb8 is removed using a tamoxifen-inducible Cre recombinase. We genetically modified HDP with constitutively active GMCSFR and tamoxifen-induced IRF8 for use as a transplantable cell for developing MΦ-based therapies, which we have termed HDP-on. HDP-on are able to proliferate in the absence of GMCSF and differentiate rapidly into functional MΦ with the addition of tamoxifen and ruxolitinib. Five million HDP transplanted via intraperitoneal injection into immunodeficient NCG mice survive in the peritoneal cavity for 14 days and migrate into the liver, spleen, kidney, bone marrow, brain, lung, heart and blood. In immunocompetent BALB/c mice, HDP cannot be detected 1 day post-transplantation in any tissues, while HDP-on are detected 1 day post-transplantation almost exclusively in the peritoneal cavity. Neither HDP nor HDP-on were detected 7 days post-transplantation. Pretreatment of BALB/c mice with liposomal clodronate improves the survival of HDP at 1 day, and also significantly enhances survival 7 days for HDP and HDP-on in the peritoneal cavity, spleen and liver. In BALB/c mice pretreated with liposomal clodronate, the numbers of cells found in the liver, spleen, kidney and bone marrow steadily increase

for the first week, while peritoneal cavity levels decrease slightly. At 14 days post-transplantation, no cells were detected in any tissue analyzed. Acute (<7 days) post-transplantation survival of HDP can be improved in immunocompetent mice by two means: using HDP-on and liposomal clodronate pretreatment. The modifications to HDP and liposomal clodronate pretreatment described here can guide new approaches for MΦ-based therapeutics.

4.1 Introduction

Macrophages (MΦ) straddle the innate and adaptive immune systems, playing important roles in homeostatic tissue maintenance and in the immunopathology of many diseases, including cancer, bacterial infections, trauma and arthritis [106, 238-240]. To mediate these functions, MΦ are highly plastic, responding to changes in the environment by taking on inflammatory (M1) or regenerative (M2) phenotypes [1, 37, 241]. Furthermore, specialized MΦ perform critical functions and in virtually all tissues, ranging from recycling heme in the kidney [23], to maintaining proper neuronal development in the brain [242]. Genetically engineering MΦ can augment their homeostatic roles, phenotypic plasticity and diverse tissue niches to resolve dysregulated tissue functions. These applications may utilize gene therapy to produce therapeutic proteins [139, 147, 157, 160, 243], or deliver poorly soluble drugs [137, 142, 146]. As MΦ biology is more extensively explicated, the broad range of behaviors that MΦ possess provide an opportunity for engineering novel MΦ-based therapies.

The history of MΦ-based therapies began over 40 years ago but progress to date has been limited due to the difficulty to generate the 10^7-10^8 MΦ required for human studies [244]. This barrier is partially because primary MΦ do not usually proliferate *in vitro*,

unlike T-cells and MSCs, which facilely proliferate *in vitro* [55, 81, 245]. The earliest clinical trials for MΦ-based cell therapies for cancer treatment occurred over 30 years ago, where large numbers of autologous MΦ (10^8-10^9) were collected from patient blood, conditioned with granulocyte MΦ colony stimulating factor (GMCSF) and IFNγ *in vitro* and reinfused [94, 244, 246]. At best, two or three doses of MΦ could be collected and infused. While there were minimal side effects, the efficacy was modest and mixed (for a review of MΦ-based cell therapies, see [244]). In more recent reports, tumor-derived MΦ-cell lines such as RAW264 or RAW309 have been used in animal studies [138, 147]. These lines are problematic for therapeutic development due to their tumorigenicity. Studies which employ bone marrow derived MΦ, lack a practical means to generate the MΦ numbers required for a therapy [244].

There have been a few reports of altering the expression of transcription factors to induce self-renewal in MΦ and myeloid progenitors, which can differentiate into MΦ. These include MafB and c-Maf double knockout (Maf-DKO) MΦ [171] and Hoxb8-dependent myeloid progenitors (HDP) which are held in a self-renewing state [33, 34]. Maf-DKO MΦ and MΦ derived from HDP are functionally similar to endogenous MΦ from other sources [171, 247] and are a good starting point for the development of MΦ-based therapeutics.

To perform further studies which required large numbers of MΦ, we were interested in simplifying and accelerating the process of generating large numbers of MΦ. The self-renewal capabilities of HDP described by Wang and collaborators were dependent upon a tamoxifen dependent Hoxb8-ERT and required culturing in 1 µM 4-hydroxytamoxifen (4-OHT). Removal of 4-OHT would stop Hoxb8 activity and the HDP would differentiate into a MΦ. We asked if a modified HDP with constitutively expressed

Hoxb8 flanked by loxP sites and a 4-OHT induced Cre recombinase could produce a self-renewing HDP that could undergo 4-OHT inducible MΦ differentiation. HDP also require GMCSF to survive and proliferate. GMCSF signals through GMCSFR, and a single point mutation of GMCSFR (L452E) renders GMCSFR constitutively active and ablates the requirement for external GMCSF in myeloid cells [248]. We reasoned that addition of constitutively active GMCSFR to HDP would remove the need for GMCSF to survive and proliferate.

To increase the rate of differentiation, we identified IRF8 as a transcription factor which is upregulated during MΦ differentiation [249]. By expressing 4-OHT induced IRF8-ERT, we hypothesized we could bypass the time required for IRF8 to be endogenously expressed and increase the differentiation rate of HDP. By using a combination of lentivirus and retrovirus, we generated a modified HDP with constitutively active Hoxb8 and GMCSFR, and 4-OHT inducible Cre and IRF8. We demonstrate in this report that this new form of HDP, known as HDP-on, maintains the same growth and differentiation characteristics of HDP, with cytokine and 4-OHT free self-renewal and 4-OHT inducible rapid differentiation into MΦ.

Maf-DKO MΦ are nontumorigenic when injected into an immunodeficient mouse [171]. Yet it is unclear if Maf-DKO survive and engraft in this model. To our knowledge, there have been no reports of the *in vivo* survival of HDP and HDP-derived MΦ. We sought to quantitatively determine the survival potential of HDP-on and HDP-on MΦ in immunodeficient NCG (lacking B, T and NK cells) and immunocompetent BALB/c mice.

In this manuscript, we describe two advances for the development of MΦ-based therapies: a modified *ex vivo* method using Hoxb8, constitutively active GMCSFR, inducible Cre and IRF8 (HDP-on) to facilely and rapidly generate large numbers of functional MΦ, as well as quantitatively validating the ability of clodronate-loaded liposome pretreatment to improve acute post-transplantation survival of HDP in immunocompetent BALB/c mice.

4.2 Hoxb8: a method for unlimited myeloid progenitors and MΦ

Primary MΦ are terminally differentiated cells and cannot be expanded *in vitro*. Recent reports described methods to circumvent this developmental block. One method, as described by Wang et al. used a tamoxifen-induced Hoxb8 to hold a myeloid progenitor cell in a self-renewing state. This cell would differentiate into a MΦ when Hoxb8 expression is reduced by removal of 4-hydroxytamoxifen (4-OHT) from the media [34]. We modified this method by using a lentivirus to transduce primary lin^- bone marrow cells with a construct containing a constitutively expressed Hoxb8 flanked by loxP sites. Serial transduction with a Cre recombinase fused with an estrogen receptor (Cre-ERT) endowed the cell with inducible Cre activity that could excise the Hoxb8 cassette with addition of 4-OHT. This enables the differentiation of the progenitor cell towards a MΦ state that can be specified by the presence of GMCSF in the growth media (Figure 4-1). The construct containing Cre-ERT also contained luciferase, a traceable marker to allow the detection of live HDP. Cells that die do not contribute to luciferase activity as the enzyme has poor serum stability and has a very short circulatory half-life of under 20 minutes [218]. This reporter enables biodistribution studies by allowing for the total number of live cells to be determined from organ lysates. This cell, the Hoxb8-dependent myeloid progenitor

(HDP), formed the basis of our studies. HDP require GMCSF to proliferate and survive, which was provided by using a GMCSF supplement generated from the conditioned media of GMCSF expressing L929 cells. Furthermore, HDP can be cultured indefinitely in suspension culture to high densities (1-2x10^6/mL) and then differentiated into adherent MΦ by adding 4-OHT to the media for 10 days. This model allows for the generation of the high number of HDP and HDP-derived MΦ (HDP-MΦ) required for the development of a MΦ-based therapy.

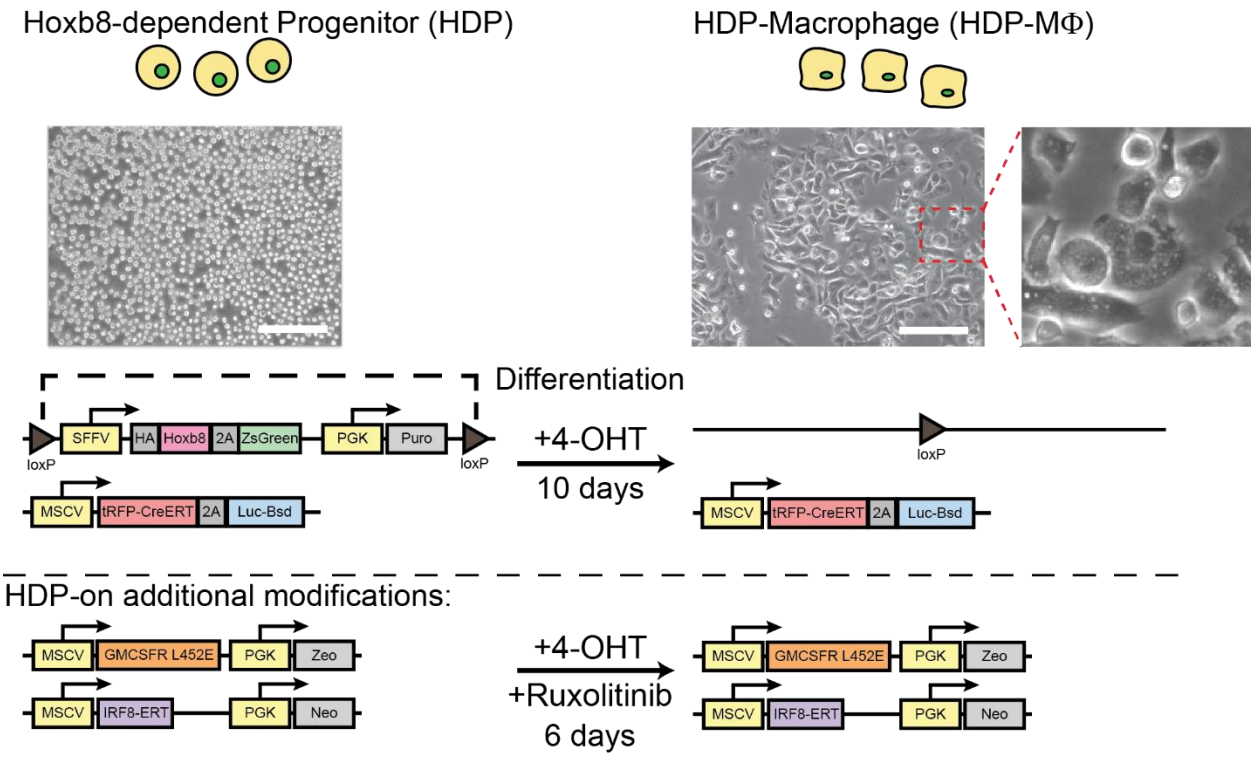

Figure 4-1: Generation of Hoxb8-dependent myeloid progenitors (HDP) and MΦ (HDP-MΦ). Lin$^-$ cells were isolated from bone marrow and transduced using a lentivirus with a Hoxb8 construct flanked by loxP sites. Subsequent transduction with retrovirus inserted a Cre-ERT recombinase with a luciferase reporter, which respectively served to induce the excision of Hoxb8 in the presence of 4-hydroxytamoxifen (4-OHT) and provided a

reporter to be quantified for biodistribution studies. Excision of Hoxb8 lead to differentiation of HDP into HDP-MΦ in 10 days. Modified HDP, known as HDP-on, were serially transduced with retroviruses encoding a constitutively active GMCSFR and IRF8-ERT. HDP-on differentiate into HDP-on-MΦ in 6 days when treated with 4-OHT and ruxolitinib. Scale bar = 150 μm.

4.3 Constitutively active GMCSFR Hoxb8-dependent myeloid progenitors (HDP) differentiate into MΦ

To further enhance the performance of HDP, two additional genetic modifications were made: a constitutively active GMCSFR and IRF8-ERT, forming HDP-on (Figure 4-1). Constitutively active GMCSFR results from a single point mutation (L452E) [248] and in myeloid cells and MΦ, results in survival and proliferation without the need for GMCSF. We hypothesize this modification could potentially increase the overall *in vivo* survival potential due to a limited pool of GMCSF *in vivo* [22]. Additionally, reducing the need for cytokine (either recombinant or from conditioned media) reduces the cost of materials to maintain these cells. HDP-on in media without GMCSF supplement proliferate as rapidly as HDP with GMCSF supplement, with a doubling rate of ~12 h (Figure 4-2A). This proliferation rate enables rapid generation of high number of cells for differentiation into MΦ. To further enhance the ability to rapidly generate MΦ, IRF8-ERT was also added to HDP. IRF8 is a transcription factor that is upregulated during MΦ differentiation [249], and constitutive expression of 4-OHT inducible IRF8 results in a faster differentiation process by reducing the time for endogenous IRF8 to be expressed and migrate to the nucleus. In comparison to HDP which lack IRF8-ERT, addition of IRF8-ERT reduces the time required for differentiation from 10 to 6 days, further simplifying the amount of processing

required to generate MΦ. While HDP require only 4-OHT to differentiate, HDP-on also require ruxolitinib, a Jak2 inhibitor which inhibits GMCSFR activity. Gene expression analysis of HDP-on differentiated for 6 days in 40 nM 4-OHT and 1 μM ruxolitinib by quantitative PCR for MΦ- and HDP-specific genes [33, 34] reveals upregulation of the MΦ marker, F4/80 (*Emr1*) and significant downregulation of HDP genes *Elane*, *Prtn3*, *Ms4a3* and *Plac8* (Figure 4-2B). Flow cytometric analysis of differentiating HDP-on over 6 days also demonstrates increased surface F4/80 expression (Figure 4-2C), a hallmark of MΦ differentiation. Ruxolitinib alone does not affect F4/80 expression, while 4-OHT alone increases F4/80 expression to a smaller degree. Combination treatment results in significantly more F4/80 expression by day 6, demonstrating the synergistic effects of ruxolitinib and 4-OHT on rapidly differentiating HDP-on into MΦ. Based upon the gene expression and flow cytometry of differentiated HDP-on, we believe HDP-on efficiently differentiate into MΦ and could serve as a model for generating MΦ for further studies.

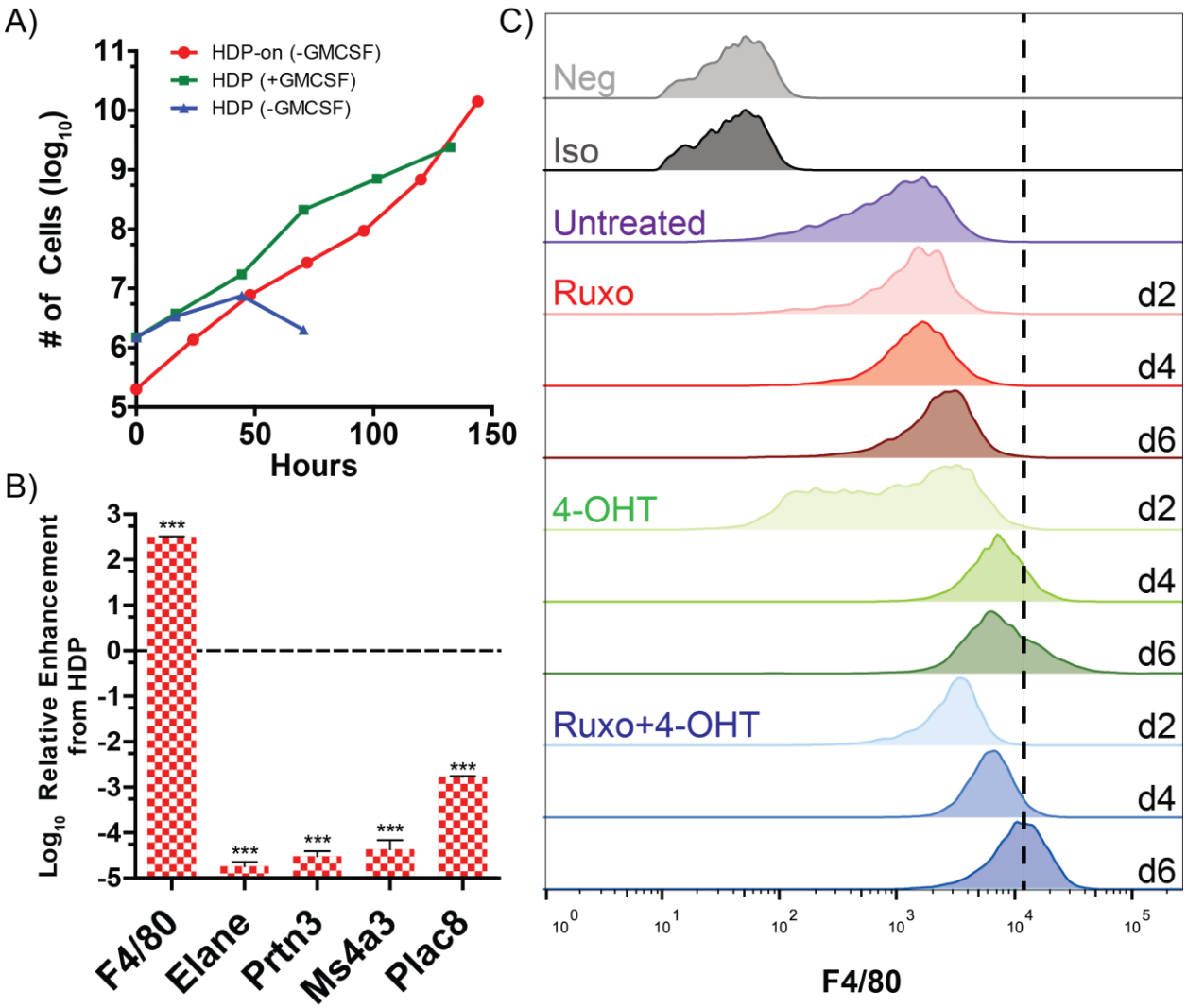

Figure 4-2: Characterization of HDP-on and HDP-on-MΦ. A) Proliferation curves of HDP-on and HDP with and without GMCSF supplement. B) Gene expression analysis by qPCR of known MΦ and HDP genes confirm MΦ status of HDP-on treated in 40 nM 4-OHT and 1 μM ruxolitinib for 6 days. Expression is presented as fold enhancement from untreated HDP-on. (N = 3, *** = $p < 0.001$) C) F4/80 surface expression by flow cytometry. HDP-on were cultured with or without 40 nM 4-OHT or 1 μM ruxolitinib (Ruxo) and assayed for F4/80 expression at 2, 4 and 6 days. Neg = unlabeled cells, Iso = cells labeled with APC-labeled isotype control.

4.4 HDP-on-MΦ retain M1/M2 polarization responses and remain highly phagocytic

We determined if HDP-on MΦ retained typical MΦ behaviors and phenotypes using functional assays of phenotypic polarization and phagocytosis. One of the greatest potentials for MΦ-based therapies is to harness the plasticity of MΦ by polarization towards inflammatory (M1) or regenerative (M2) phenotypes. The broad spectrum of phenotypes demonstrate the potential applications of MΦ for a wide variety of conditions. It is important to note that the M1/M2 paradigm is not necessarily a binary distinction [37, 109], but rather describes a continuum of behaviors. However, there exist commonly accepted standards to describe M1-like and M2-like behaviors that can be elicited using specific polarization inducers. These methods were used to polarize and characterize HDP-on-MΦ. HDP-on MΦ treated with LPS, a M1 inducer, responded by upregulating known M1-associated genes, *IL12b*, *iNOS* and *TNF* (Figure 4-5A). Similarly, treatment with IL-4, a M2 inducer, upregulated the M2-associated genes, *Arg1*, *CD206* and *CCL17* (Figure 4-5A). This was not observed in HDP-on treated with LPS or IL-4 (Figure 4-3). Treatment of M1/M2 polarized HDP-on MΦ with the opposing polarization inducer also resulted in polarization to the opposing phenotype (Figure 4-4). Based on these results, it is clear HDP-on MΦ retain the plasticity that exists in conventionally derived MΦ.

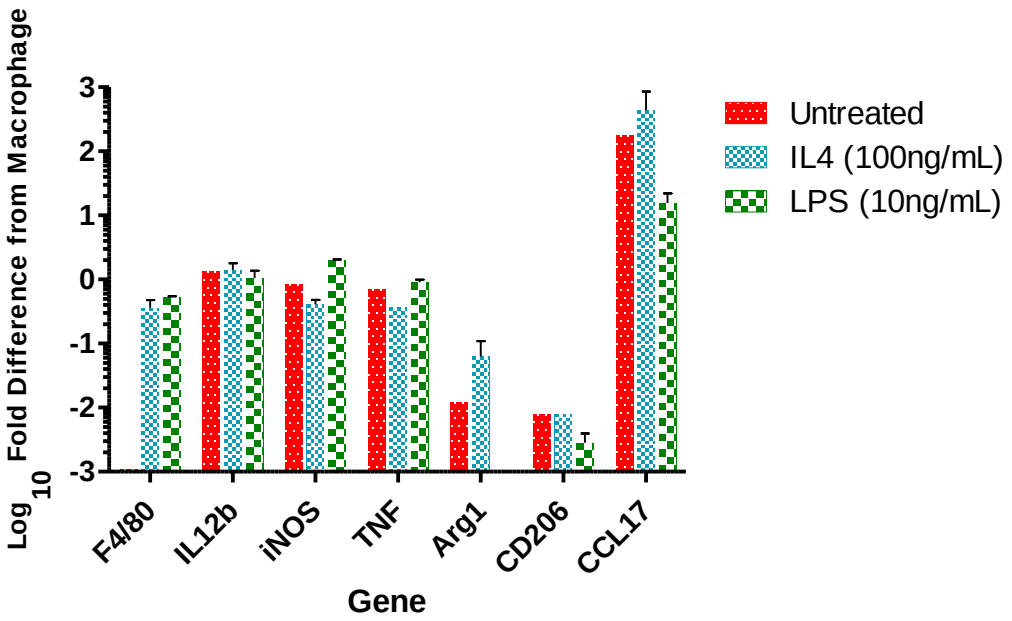

Figure 4-3: Gene expression of HDP-on treated with M1 and M2 inducers. HDP-on were treated overnight with 10 ng/mL LPS or 100 ng/mL IL-4 and gene expression of established M1 and M2 genes (M1: IL12b, iNOS, TNF; M2: Arg1, CD206, CCL17) was measured by qPCR. Fold enhancement is expressed relative to untreated HDP-on MΦs.

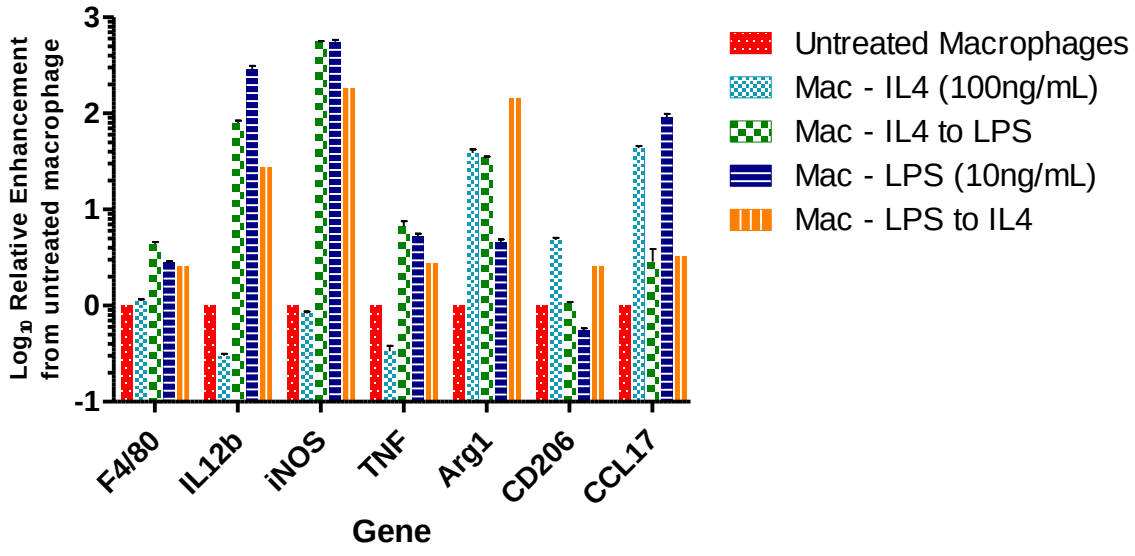

Figure 4-4: Relative gene expression of MΦ and M1/M2 markers of M1/M2 polarized HDP-on MΦ treated with opposing M1/M2 inducers. Cultures were treated for 24 h with 100 ng/mL IL-4 or 10 ng/mL LPS. For IL-4 to LPS or LPS to IL-4 cultures, cells were treated for 24 h with 100 ng/mL IL-4 or 10 ng/mL LPS before the media was swapped for the opposing treatment for another 24 h. MΦ were differentiated for 6 days in 40 nM 4-OHT and 1 µM ruxolitinib in tissue culture plastic flasks before $1x10^5$ cells were plated in a 12 well plate overnight before treatment. Relative expression is calculated by comparing expression levels between differentiated cells and HDP-on MΦ.

Another key function of MΦ is their ability to phagocytose other cells or materials. MΦ have also been proposed to act as drug carriers [141, 142, 145], so demonstrating this ability is key to enabling this form of MΦ cell therapy. HDP-on-MΦ were co-incubated with fluorescent DiD-labelled liposomes for 3 h in serum-free media and total lipid uptake was determined by measuring the total DiD fluorescence and comparing to a standard curve. RAW264, a MΦ cell line, was used as a positive control. Quantitative uptake studies demonstrated HDP-on-MΦ and RAW264 cells exhibited a similar ability to phagocytose negatively charged liposomes (Figure 4-5B). Fluorescent imaging of HDP-MΦ incubated with fluorescent HPTS-liposomes and TagBFP-expressing *E. coli* also shows HDP-on-MΦ are highly phagocytic for both liposomes and *E. coli* (Figure 4-5C).

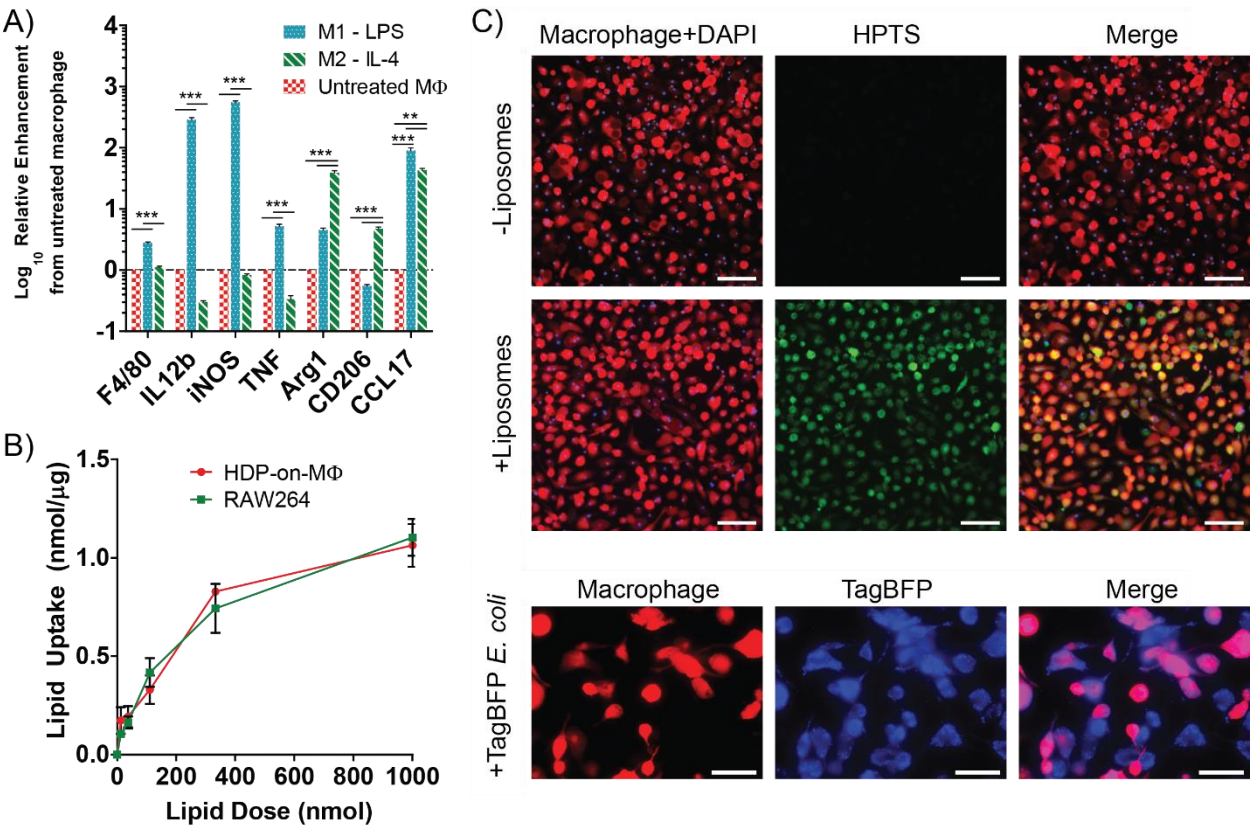

Figure 4-5: Functional analysis of HDP-on-MΦ for MΦ behaviors. A) HDP-on-MΦ respond to canonical M1 and M2 inducers, LPS and IL-4. MΦ were treated overnight with 10 ng/mL LPS or 100 ng/mL IL-4 and gene expression of established M1 and M2 genes (M1: *IL12b*, *iNOS*, *TNF*; M2: *Arg1*, *CD206*, *CCL17*) was measured by qPCR. Fold enhancement is expressed relative to untreated HDP-on-MΦ. (N = 3, *** = $p < 0.001$, ** = $p < 0.01$) B) HDP-on-MΦ phagocytose DiD-labeled liposomes at a similar rate as the MΦ cell line, RAW264. (N = 3 per condition) C) Fluorescent images of HDP-derived MΦ incubated with HPTS-fluorescent liposomes and TagBFP-expressing *E. coli*. (Scale bar: liposome uptake, 150 µm; *E. coli*. 100 µm)

4.5 HDP-on and MΦ survive at least 7 days in immunodeficient mice

We next determined the survival potential of HDP-on and MΦ injected into the immunodeficient NCG strain of mice which have lack B, T and NK cells to determine if

HDP-MΦ and HDP-on-MΦ survive in mice lacking an immune system. In some animals, live cells were detected in the peritoneal cavity and spleen (Figure 4-7). In the peritoneal cavity, HDP-on demonstrated significantly greater survival than HDP (151±4% vs 107±4% of the injected cells, or $7.55x10^6$ vs $5.35x10^6$ cells, $p < 0.01$). However, this trend was reversed in the spleen, where HDP-on survived significantly less than HDP (11% vs 2% of the injected cells, or $5x10^5$ vs $1x10^5$ cells, $p < 0.01$).

MΦ derived from either HDP or HDP-on had significantly reduced survival in the peritoneal cavity (4.4±0.3%, $2.2x10^5$ cells, or 19.4±3.3%, $9.7x10^5$ cells, respectively) when compared to the respective parental cell. Neither MΦ type was detected in the spleen. Other tissues were analyzed, including the liver, heart, bone marrow, lungs, brain, kidney and blood, but the combined percentage of injected cells detected across these tissues was below 1.5% in all conditions tested (Figure 4-6).

Furthermore, there was a differential in survival between the peritoneal cavity and spleen, with HDP-on having a greater number of cells in the peritoneal cavity than HDP. The opposite was true in the spleen (Figure 4-7). Overall, these experiments indicate that both HDP and MΦ with or without HDP-on modifications can survive at least 7 days in immunodeficient animals.

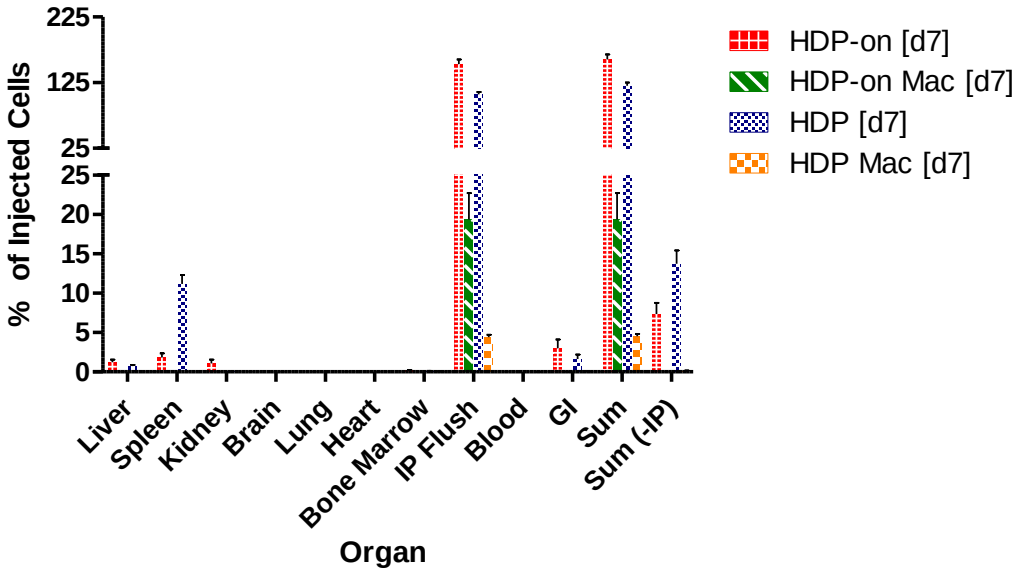

Figure 4-6: Biodistribution of HDP, HDP-on, HDP MΦs and HDP-on MΦs in immunodeficient NCG mice 7 days post injection. Mice were injected intraperitoneally with $5x10^6$ cells in 500 µL RPMI with a 28 gauge syringe, euthanized after 7 days and tissues were analyzed for luciferase activity. Statistics: N = 6 for HDP-on, N = 3 for other conditions.

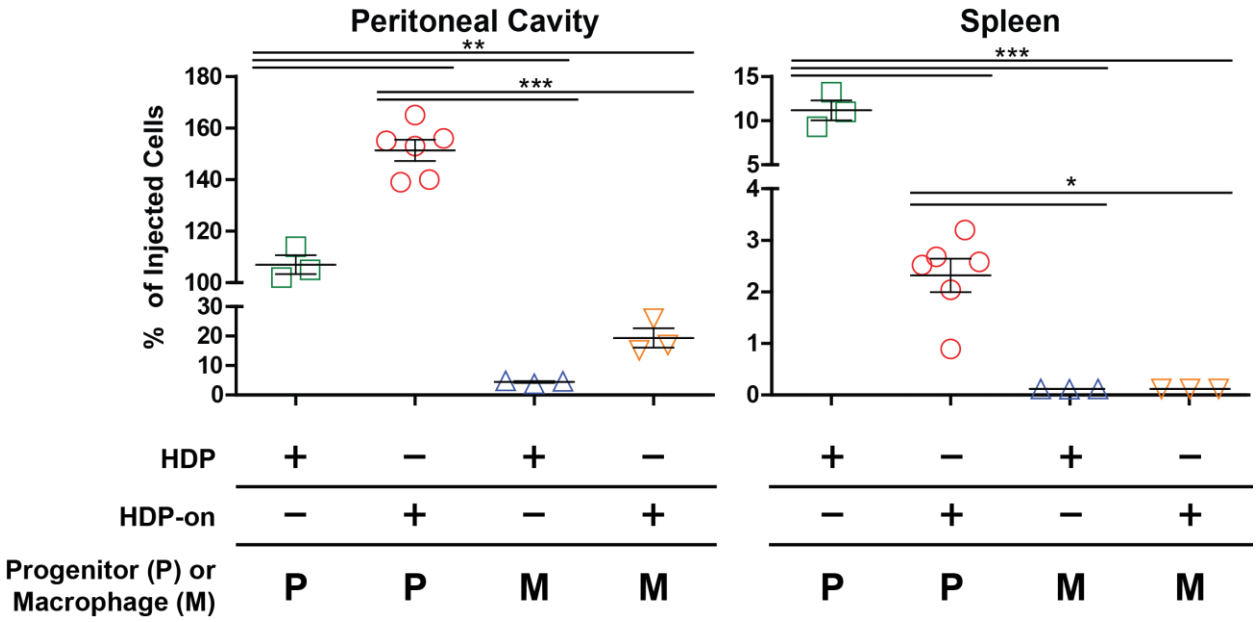

Figure 4-7: Biodistribution of HDP, HDP-on, HDP-MΦ and HDP-on-MΦ in immunodeficient NCG mice 7 days post injection. Peritoneal cavity and spleen are shown. Mice were injected IP with $5x10^6$ cells in 500 µL RPMI with a 28 gauge syringe, euthanized after 7 days and tissues were analyzed for luciferase activity. Statistics: N = 6 for HDP-on, N = 3 for other conditions, one-way ANOVA with Bonferroni post-analysis, *** = $p < 0.001$, ** = $p < 0.01$ and * = $p < 0.05$.

4.6 Clodronate pretreatment improves survival of HDP-on in immunocompetent mice

Due to the significantly higher survival of HDP and HDP-on when compared to the differentiated MΦ in immunodeficient NCG mice, we focused on determining the survival of HDP and HDP-on in healthy immunocompetent BALB/c mice (Figure 4-8). HDP were not detected in any tissues at 1 or 7 days post-transplantation. HDP-on had significantly higher survival in the peritoneal cavity 1 day post-transplantation compared to HDP (107±21% or $5.35x10^6$ cells, $p < 0.001$). However, survival of HDP-on in other tissues was limited; at 1 day post-transplantation, <1% was detected in the spleen or liver, and at 7 days post-transplantation, <0.5% was detected in the liver and no cells were detected in the peritoneal cavity or spleen. For other tissues, including, brain, lung, heart, bone marrow, liver, spleen, kidneys and blood, the total combined percentage of injected cells detected for either HDP or HDP-on was below 1% of the injected cells (Figure 4-9, Figure 4-10).

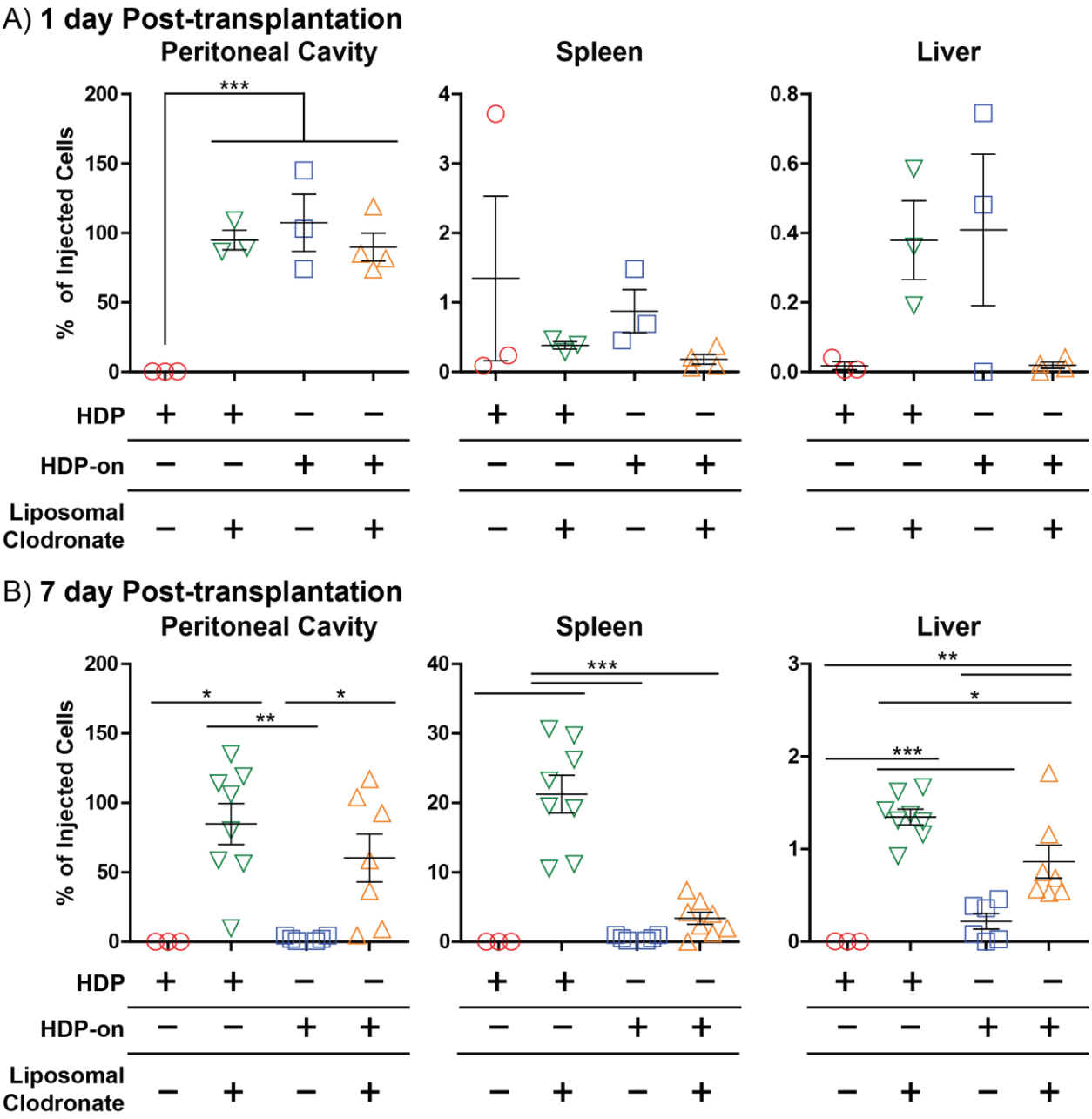

Figure 4-8: Biodistribution of HDP and HDP-on in mice pretreated with liposomal clodronate. Healthy BALB/c mice were IP injected with $5x10^6$ cells in 500 µL RPMI with a 28 gauge syringe, euthanized after A) 1 day or B) 7 days and tissues were analyzed for luciferase activity. Statistics: N = 3 for all conditions at 1 day post transplantation and HDP with no liposomal clodronate at 7 day post-transplantation point, N = 6 for all other 7 day

time points, one-way ANOVA with Bonferroni post-analysis, *** = $p < 0.001$, ** = $p < 0.01$ and * = $p < 0.05$.

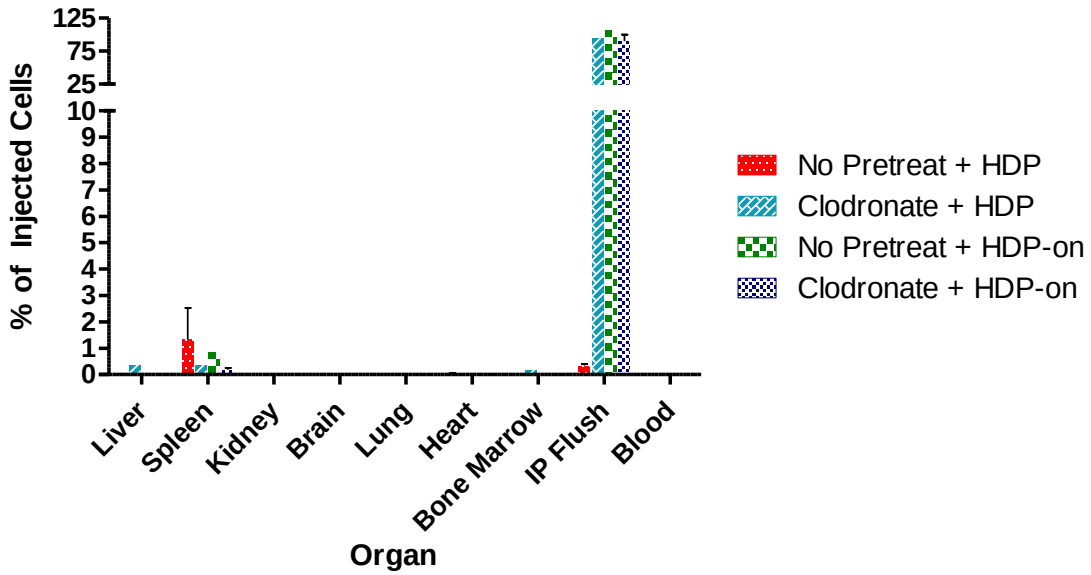

Figure 4-9: Biodistribution of HDP and HDP-on in mice pretreated with liposomal clodronate 1 day post-transplantation. For clodronate pretreatment, mice were injected IP with 100 µL liposomal clodronate (5mg/mL) 4 and 1 days before cell injection. Healthy BALB/c mice were injected intraperitoneally with $5x10^6$ cells in 500 µL RPMI with a 28 gauge syringe, euthanized after 1 days and tissues were analyzed for luciferase activity. Statistics: N = 3 per condition.

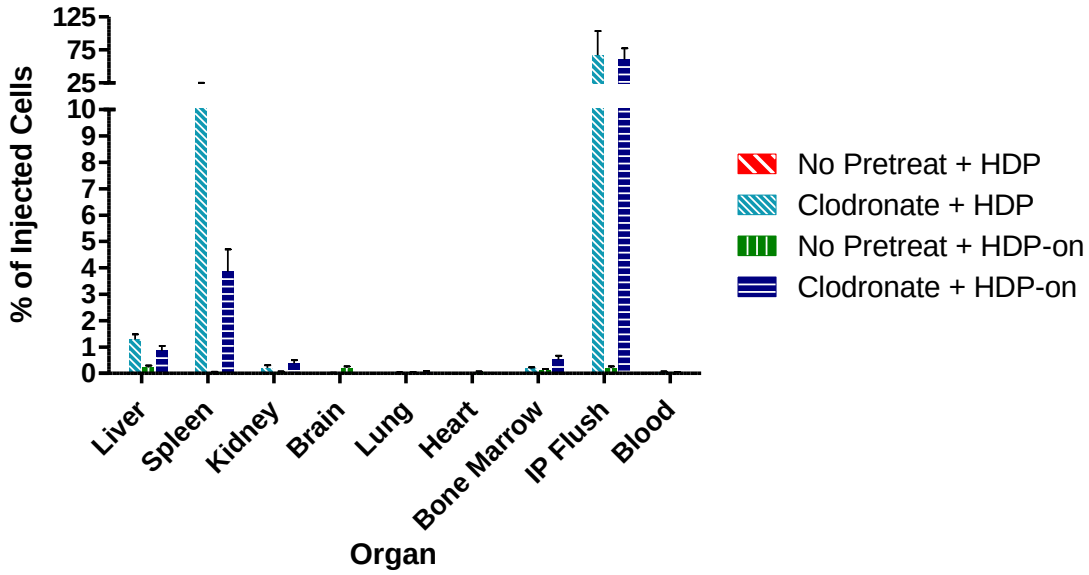

Figure 4-10: Biodistribution of HDP and HDP-on in mice pretreated with liposomal clodronate 7 days post-transplantation. For clodronate pretreatment, mice were injected IP with 100 µL liposomal clodronate (5mg/mL) 4 and 1 days before cell injection. Healthy BALB/c mice were injected intraperitoneally with $5x10^6$ cells in 500 µL RPMI with a 28 gauge syringe, euthanized after 7 days and tissues were analyzed for luciferase activity. Statistics: N = 3 for HDP with no liposomal clodronate, N = 6 for all other conditions

We sought to improve the survival of either HDP or HDP-on and hypothesized removal of endogenous MΦ may improve survival since improved survival of other cell types have been reported when animals are pretreated with MΦ-killing liposomal clodronate [250]. Endogenous MΦ are found in tissue niches that transplanted HDP might be able to occupy. Successful transplantation of MΦ have been reported in *Csf2rb*-knockout mice which have impaired MΦ activity and reduced numbers of MΦ [21, 22]. Additionally, $F4/80^+$ cells phagocytose stem cell-derived hematopoietic progenitor cells [250] and could be involved in removing HDP. Hence, removal of endogenous MΦ may be beneficial for HDP by creating a niche and interfering with active removal by endogenous

MΦ. Endogenous MΦ can be transiently removed from the peritoneal cavity, liver, spleen and blood with liposomal clodronate [194, 251-253]. We accomplished this by injecting 100 µL liposomal clodronate (5 mg/mL) IP 1 and 4 days prior to injection of cells.

At 1 day post-transplantation, liposomal clodronate pretreatment only increased survival in the peritoneal cavity for HDP, and no benefit was detected in other tissues. Compared to untreated mice, liposomal clodronate pretreatment significantly improved the survival of HDP in the peritoneal cavity (95±7.1% or $4.75x10^6$ cells versus undetectable, $p < 0.001$). This improvement was sustained at 7 days post-transplantation, with 85±15% ($4.25x10^6$ cells, $p < 0.001$) of the injected cells detected in the peritoneal cavity. HDP-on did not experience any significant improvement in the peritoneal cavity with liposomal clodronate pretreatment at 1 day post-transplantation when compared to untreated animals (90±10% or $4.5x10^6$ cells versus 107±20%, or $5.35x10^6$ cells). However, HDP-on experienced significant enhancement in survival at 7 days post-transplantation in the peritoneal cavity when compared to animals which did not undergo liposomal clodronate pretreatment (60±17% or $3x10^6$ cells versus undetectable, $p < 0.05$).

No improvements were seen in tissues other than the peritoneal cavity at 1 day post transplantation. At 7 days post transplantation, improvement in cell numbers was seen in the spleen and liver for both HDP and HDP-on. In the spleen, HDP increased from undetectable to 21.2±2.7% ($1.06x10^6$ cells, $p < 0.001$) and HDP-on increased from undetectable to 3.4±0.9% ($1.5x10^5$ cells, not significant). The enhancement was more modest in the liver, with HDP increasing from undetectable to 1.35±0.1% ($6.75x10^4$ cells, $p < 0.001$) and HDP-on increasing from 0.22±0.08% ($1.1x10^4$ cells) to 0.86±0.18%

($4.3x10^4$ cells, $p < 0.01$). In other tissues tested, there was no measurable benefit with respect to the cell number found in the tissue (Figure 4-9, Figure 4-10).

To summarize, in immunocompetent BALB/c mice, the HDP-on modifications significantly improved the number of HDP which survive in the peritoneal cavity 1 day post transplantation via the IP route of administration. This benefit is not maintained because no cells were detected at 7 days. Liposomal clodronate pretreatment to remove endogenous MΦ increased peritoneal cavity survival at 1 day post transplantation of HDP to similar levels as HDP-on. Liposomal clodronate pretreatment improved survival of HDP and HDP-on at 7 days post-transplantation in the peritoneal cavity, spleen and liver. MΦ differentiated from HDP and HDP-on did not show increased survival in any tissue in the liposomal clodronate treated animals (Figure 4-11).

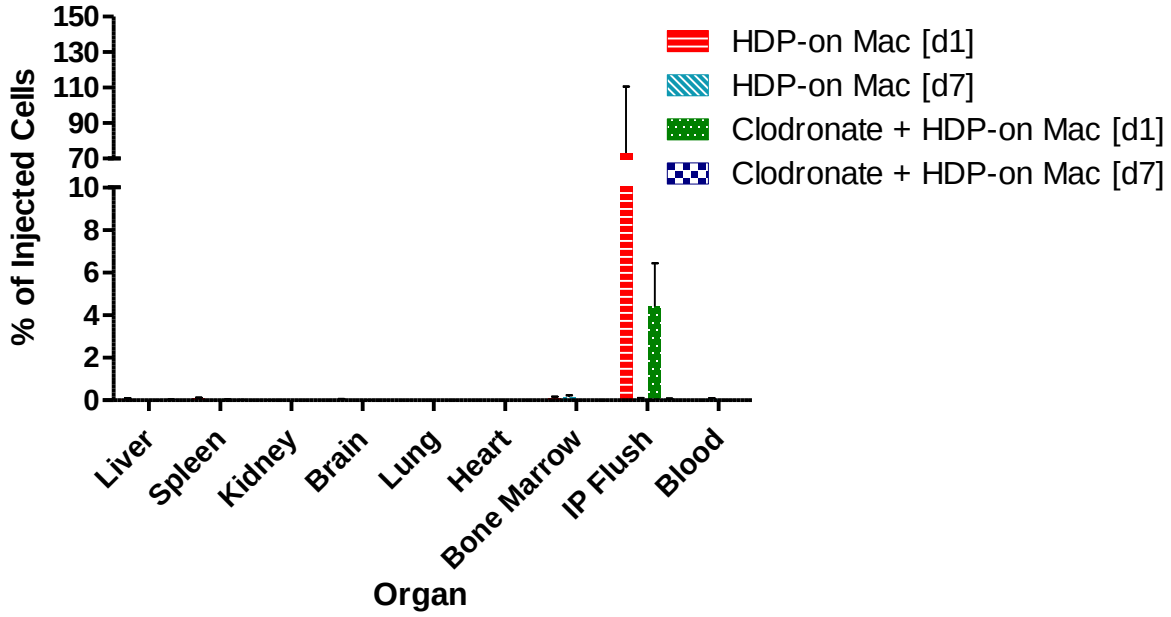

Figure 4-11: Biodistribution of macrophages derived from HDP and HDP-on in mice pretreated with liposomal clodronate 1 and 7 days post-transplantation. Healthy BALB/c mice were injected intraperitoneally with $5x10^6$ cells in 500 µL RPMI with a 28 gauge

syringe, euthanized after 1 or 7 days and tissues were analyzed for luciferase activity. Statistics: N = 3 for all conditions

4.7 Liposomal clodronate pretreatment does not enhance post-transplantation cell survival in immunocompetent mice beyond 7 days

We determined if liposomal clodronate pretreatment enabled long term survival of HDP-on beyond 7 days. HDP-on were injected IP into NCG mice not treated with liposomal clodronate and in liposomal clodronate pretreated BALB/c mice. Liposomal clodronate was not used in NCG mice due to unacceptably high mortality even at reduced doses of 15 mg/kg. To determine the kinetics of *in vivo* survival post transplantation for liposomal clodronate pretreated BALB/c mice, mice were euthanized at multiple time points and combined with data from the previous section to determine the biodistribution at 1, 3, 7 and 14 days post-transplantation. Similarly, biodistribution was also performed in NCG mice at 7 and 14 days post-transplantation.

Long-term survival of HDP-on was limited in liposomal clodronate treated BALB/c mice (Figure 4-12, Figure 4-13). In these mice, the number of live cells detected in the peritoneal cavity decreased steadily 1 day post-transplantation and were undetectable at 14 days. In the liver, spleen, kidney and bone marrow, the number of HDP-on increased from 1 day to 7 days post-transplantation. The total percentage of injected cells detected in these tissues at 7 days ranged from a low of 0.4% in the kidney to a high of 4% in the spleen. However, similar to the peritoneal cavity, 14 days post-transplantation, no cells were detected in these tissues. At no point were HDP-on detected in the brain, heart, lung or blood in BALB/c mice (Figure 4-12).

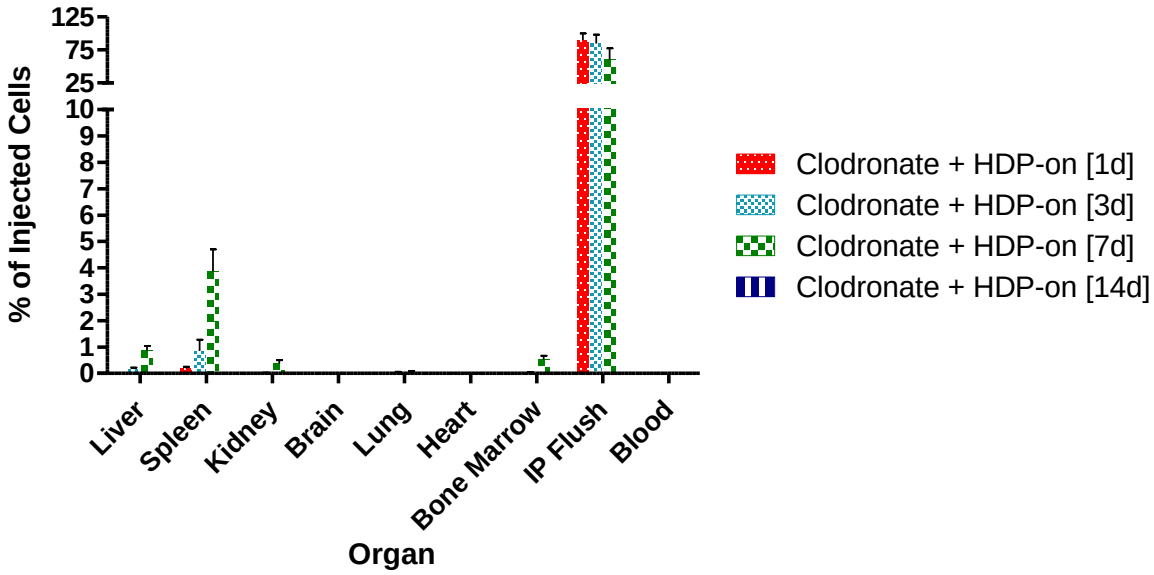

Figure 4-12: Biodistribution of HDP-on in clodronate-pretreated BALB/c mice at 1, 3, 7 and 14 days post-transplantation. Mice were injected IP with 100 µL liposomal clodronate (5mg/mL) 4 and 1 days before cell injection. BALB/c mice were injected intraperitoneally with $5x10^6$ cells in 500 µL RPMI with a 28 gauge syringe, euthanized after 14 days and tissues were analyzed for luciferase activity. Statistics: N = 3 per time point.

In NCG mice, the number of live HDP-on cells increased across all tissues between 7 day and 14 days post-transplantation. In the peritoneal cavity, the total percentage of injected cells detected increased from 151±4% ($7.55x10^6$ cells) at 7 days to 718±208% ($35.9x10^6$ cells) at 14 days post-transplantation, representing a 4.75-fold enhancement. The relative increase between 7 and 14 days was also high in the other organs, with 75, 4, 26 and 29-fold enhancement, in the liver, spleen, kidney and bone marrow, respectively. HDP-on were detected at 14 days in other tissues (brain, blood, and lungs) which typically did not show live cells in any conditions we have tested (Figure

4-14). Furthermore, at 14 days, NCG mice displayed significant morbidity and mortality and were euthanized in accordance with UCSF IACUC protocols.

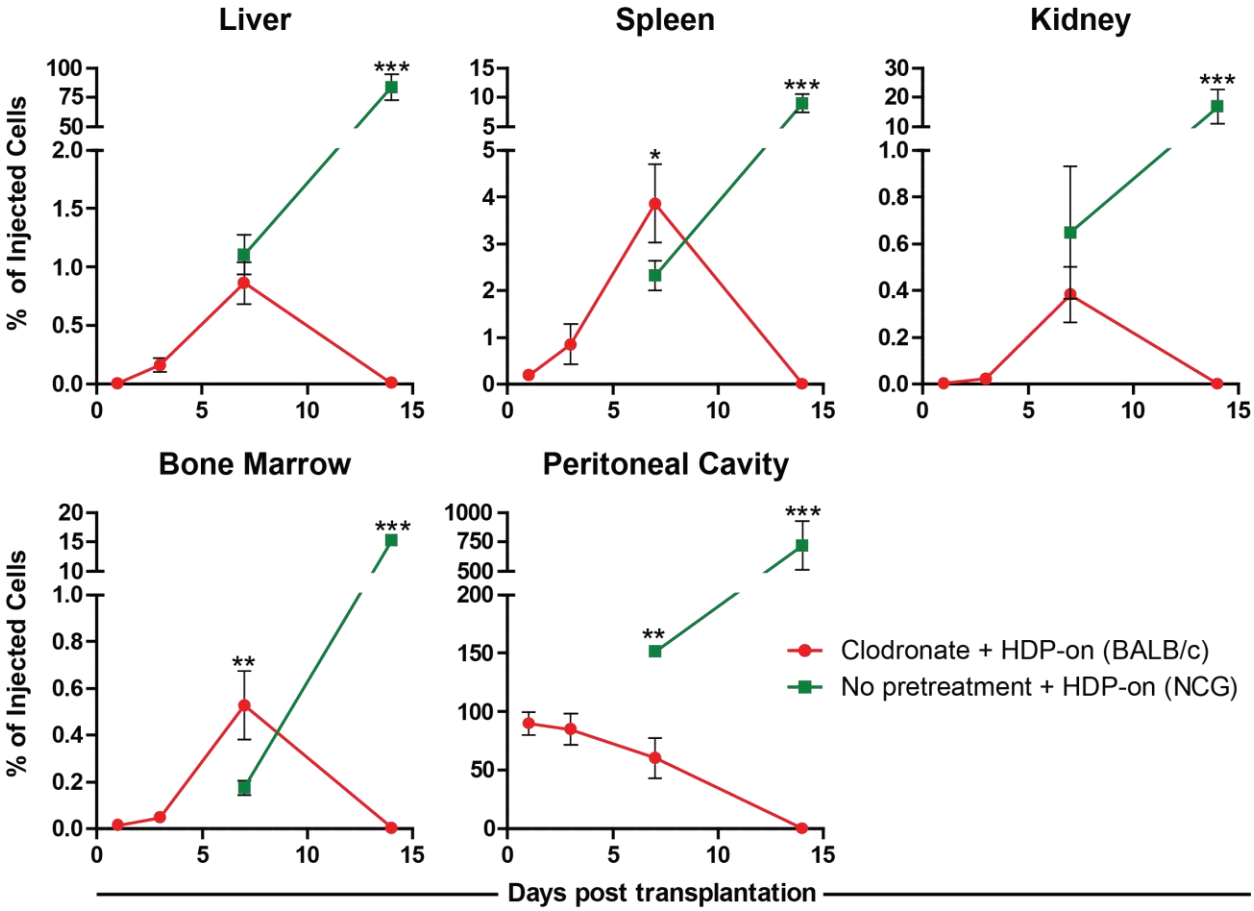

Figure 4-13: Pharmacokinetics of HDP-on in NCG mice and liposomal clodronate treated BALB/c mice. Biodistribution was determined by luciferase activity in tissue lysates up to 14 days post-injection. Mice were IP injected with $5x10^6$ cells and euthanized at 1, 3, 7 or 14 days. N ≥ 3 for each condition, statistical comparisons were made within the same time points, *** = $p < 0.001$, ** = $p < 0.01$ and * = $p < 0.05$.

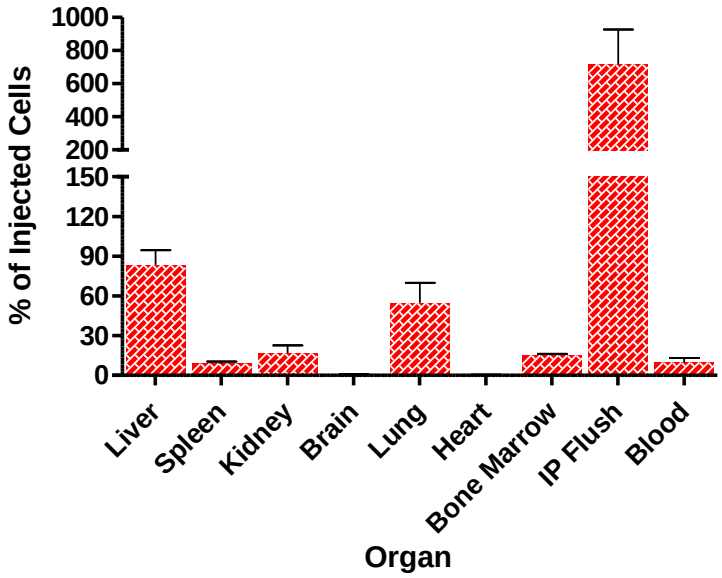

Figure 4-14: Biodistribution of HDP-on in immunodeficient NCG mice 14 days post-transplantation. NCG mice were injected intraperitoneally with $5x10^6$ cells in 500 µL RPMI with a 28 gauge syringe, euthanized after 14 days and tissues were analyzed for luciferase activity. Statistics: N = 3

4.8 Conclusions

In this study, we demonstrate 1) Hoxb8 dependent myeloid progenitors (HDP) modified with a constructively active GMCSFR and IRF8-ERT (HDP-on) can self-renew without cytokine and rapidly differentiate into MΦ, 2) HDP-on MΦ retain MΦ-like behaviors, including phagocytosis and M1/M2 polarization, 3) HDP-on and MΦ persist in immunodeficient NCG mice for at least 7 days using a quantitative luciferase-based assay and 4) liposomal clodronate pretreatment enhances survival of transplanted HDP-on in healthy BALB/c mice for at least 7 days.

We modified a method developed by Wang et al. [33, 34] to hold myeloid progenitors in a self-renewal state by inserting a constitutively expressed Hoxb8 construct flanked by loxP sites. Removal of Hoxb8 was performed by a tamoxifen-induced Cre recombinase

and induced differentiation of the progenitor into a MΦ. Addition of HDP-on modifications produced progenitors capable of self-renewal without GMCSF. F4/80 surface expression by flow cytometry demonstrated HDP-on differentiate into MΦ in 6 days when treated with 40 nM 4-OHT and 1 μM ruxolitinib. These HDP-on MΦ responded to M1/M2 polarization signals and were phagocytic for fluorescent liposomes.

Previous reports using MΦ for cell-based therapies [244] have used bone marrow derived MΦ [21, 22] or immortalized RAW264 cell lines [138, 147], which are either limited in number or highly transformed. Using HDP, we were able to easily genetically engineer HDP using retrovirus to tailor the cell for various applications, generate large numbers of HDP and differentiate these cells into functional MΦ. The ability to generate large numbers of cells is especially important. Other cell-based therapies, including T-cell and stem cell therapies rely on self-renewing cell types to generate therapeutic doses of the cell for animal and clinical studies [55, 81, 245]. Primary MΦ do not normally proliferate *in vitro*, so the methods described here reduce barriers for the evaluation of MΦ cell-based therapies. Having these cells enabled us to study the biodistribution of HDP and MΦ in immunocompromised NCG and healthy BALB/c mice.

There has been relative paucity in quantitative approaches to determine the biodistribution of MΦ-based therapies [244]. Most studies have relied on qualitative measures such as a biological functional response, histology or flow cytometry. While these methods may determine the presence of the transplanted cell, a quantitative approach is needed to measure biodistribution, dose response and cell survival to better assess and develop cell-based therapies. We used a luciferase-based system as it

provided a quantitative method to count only live cells due to poor-serum stability of luciferase when a cell dies.

Endogenous MΦ may serve as barriers to the post-transplantation survival of HDP-on and HDP-on MΦ. This may be due to the highly phagocytic nature of MΦ, or the lack of a tissue niche for transplanted cells to survive. Phagocytic endogenous MΦ are responsible for the low post-transplantation survival of embryonic stem cell-derived hematopoietic progenitors in the highly immunodeficient NOD/SCID mouse model [250]. Long term post-transplantation survival of wildtype bone marrow derived MΦ have been observed in a *Csf2rb* knockout mouse, which possess small numbers of dysfunctional MΦ [21, 22]. In this model, the lack of functional MΦ may have allowed the functional MΦ to engraft and survive. Much like how immunoablation by chemoablation or sublethal radiation is used to prepare hosts for transplantation of T-cells or hematopoietic stem cells [55], removal of endogenous MΦ may generate tissue niches for transplanted HDP-on and HDP-on MΦ to enable long term survival. Administration of liposomal clodronate has been shown to temporarily eliminate endogenous MΦ [194], and we observed that pretreating mice with liposomal clodronate increases the post-transplantation survival of HDP-on but not HDP-on MΦ.

We conducted biodistribution studies by injecting HDP, HDP-on, HDP-MΦ and HDP-on-MΦ IP in immunodeficient NCG and immunocompetent BALB/c mice. In NCG mice, HDP survived significantly better than MΦ, with HDP-on having a higher number of injected cells than HDP in the peritoneal cavity (120% vs 100%) 7 days post transplantation. In BALB/c mice, HDP were undetectable across all tissues 1 and 7 days post transplantation. Addition of the HDP-on modifications enabled detection of HDP in

the peritoneal cavity up to 1 day post transplantation. Pretreatment of animals with liposomal clodronate improved the survival of both HDP and HDP-on; with cells detected in multiple tissues, including the peritoneal cavity, liver and spleen up to 7 days post transplantation. Substantial proliferation of HDP-on in NCG mice was detected across most tissues while no cells were detected in the liposomal clodronate treated BALB/c mice 14 days post transplantation.

The robust survival in NCG mice indicated HDP can survive without additional cytokines *in vivo*. Detecting greater than 100% of the injected cells is very significant, as it also indicates cells are proliferating *in vivo*. The substantial reduction in surviving MΦ in both NCG and BALB/c may be indicative of the transplantation process being more deleterious on MΦ, or the peritoneal cavity may lack the survival factors required to support the survival of the $5x10^6$ MΦ that were transplanted. We initially believed that because NCG mice possess endogenous MΦ, niches may not have been available for transplanted MΦ. However, MΦ transplanted into BALB/c mice pretreated with liposomal clodronate to remove endogenous MΦ did not survive either. Improving the survival of transplanted MΦ is an obvious and important unachieved goal.

Administration of liposomal clodronate via the peritoneal cavity temporarily removes MΦ from the peritoneal cavity, spleen, liver and blood [194]. Thus removal of endogenous MΦ may be responsible for the improved HDP survival in liposomal clodronate treated BALB/c mice in the peritoneal cavity (60-85% of total injected cells at 7 days), liver (0.9-1.3%), spleen (3-21%), kidney (<1%) and bone marrow (<1%). In support of this observation, MΦ are primarily responsible for removing embryonic stem cell-derived hematopoietic progenitors [250]. We ascribe the enhanced HDP survival after

liposomal clodronate treatment is probably due to the removal of endogenous MΦ. The endogenous MΦ may phagocytose transplanted HDP or occupy tissue niches required by HDP for longer term survival [1].

In BALB/c mice pretreated with liposomal clodronate, the number of HDP-on steadily increased in the spleen, liver, kidneys and bone marrow site over 7 days, indicating migration from the peritoneal cavity to other tissues. However, no HDP-on were detected at 14 days in any tissues. We believe loss of HDP-on between 7 and 14 days is possibly related to the return of endogenous tissue MΦ. After liposomal clodronate treatment, MΦ repopulate in the mouse spleen and rat liver within 7-14 days [256, 257]. The returning endogenous MΦ may phagocytose the transplanted HDP-on and/or reoccupy the niche. To improve long term survival of HDP-on, repeated clodronate treatment may be required post-transplantation. Liposomal clodronate pretreatment did not improve MΦ survival, though this may be due to residual liposomal clodronate killing transplanted MΦ. Liposomal clodronate injected IV is not detectable in the blood 3 h post-injection [258], but IP administration may extend the overall clearance time. This may be addressed by a different injection schedule to allow for the clearance of liposomal clodronate before transplantation of MΦ.

Long term survival (at least 9 months) of transplanted bone marrow derived MΦ have been demonstrated in the lungs of *Csf2rb*$^{-}$ mice [21, 22]. These mice have a significantly reduced number of endogenous lung MΦ, which could result in niches for the transplanted MΦ to occupy. Furthermore, *Csf2rb* encodes for the GMCSF receptor, which provides both survival and proliferation signals to MΦ in the presence of GMCSF. Thus the wildtype MΦ had a survival and proliferative advantage over the endogenous *Csf2rb*$^{-}$ MΦ, and

over time, were able to outcompete the endogenous MΦ for the remaining niches. The addition of HDP-on modifications to HDP possibly provide a proliferative/survival advantage did not appear to mimic the effect observed in these studies. However, our studies used a different route of administration in healthy mice. Long-term survival of transplanted MΦ may be more successful in appropriate disease models with impaired MΦ.

Based upon the survival of HDP in NCG mice beyond 7 days, it is clear that the immunodeficiencies of NCG mice have an impact on the survival of HDP. Immunodeficient NCG mice possess MΦ, yet HDP-on survive beyond 7 days. This would imply B, T or NK cell activity may also be responsible for the loss of transplanted HDP in BALB/c mice. Syngeneic cells were injected into BALB/c mice, but the HDP were extensively modified to express foreign proteins, including fluorescent proteins, antibiotic resistance markers and luciferase. These types of foreign proteins can be immunogenic and lead to the rejection of transplanted cells [259-261]. To address this issue, we have designed new constructs which minimize the number of foreign components in HDP-on.

Rejection of GFP-expressing cells has been strongly associated with T-cells [259] and NK cells target stem cell derived hematopoietic progenitors [262]. Swijnenburg and colleagues performed studies with human embryonic stem cells xenografts into mice and dissected the immune response to identify $CD4^+$ T-cells and the adaptive immunity response to be responsible for the loss of transplanted cells [263, 264]. Using histology and flow cytometry on tissue digests, they identified significant immune cell (T, B, MΦ and neutrophil) infiltration in the injection site [264]. Furthermore, when immunocompetent mice received a second injection of stem cells, no cells were detected at 3 days post-injection

[263]. Similarly, in BALB/c mice which received an additional round of liposomal clodronate and injection of HDP-on (liposomal clodronate on day -4 and day -1, HDP-on injection on day 0, second round of liposomal clodronate on day 7 and 11, and second HDP-on injection on day 12; Figure 4-15), no cells were detected in any tissue 3 days after the second dose. Additionally, in mice which received the xenograft, splenocytes secreted more IL-4 than lFNγ, which respectively correspond to Th2 (humoral immunity) and Th1 (cellular immunity) responses. IgM levels were also significantly higher after transplantation. Swijnenburg and colleagues performed xenograft survival studies in Nude, $CD4^-$ and $CD8^-$ mice to determine $CD4^+$ T-cells as mediators for removing the xenograft. Finally, they identified a pretreatment strategy of a combination of Tacrolinus (calceinurin inhibitor) and rapamycin enabled the xenograft to survive for at least 28 days [263].

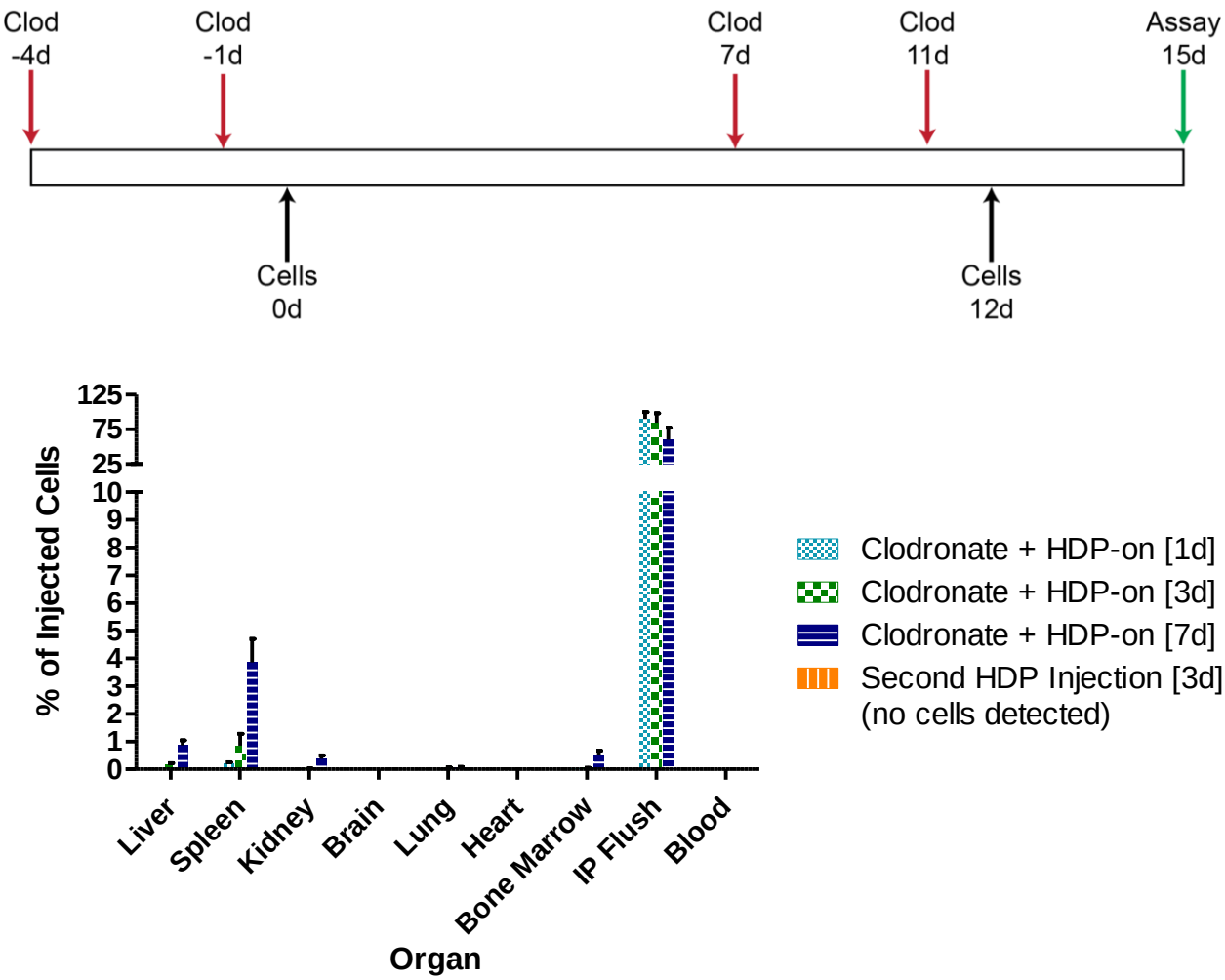

Figure 4-15: Biodistribution of HDP-on in clodronate-pretreated BALB/c mice which received a second injection of HDP-on. (Top): Treatment scheme of mice which received second injection. (Bottom): Biodistribution of mice which received second injection, presented with data from mice which receive only a single injection of HDP-on. Mice were injected IP with 100 µL liposomal clodronate (5mg/mL) 4 and 1 days before cell injection. BALB/c mice were injected intraperitoneally with $5x10^6$ cells in 500 µL RPMI with a 28 gauge syringe, euthanized after 14 days and tissues were analyzed for luciferase activity. Statistics: N = 3 per time point

We believe the combination of humoral and cellular immune responses they observed may also be applicable to HDP-on in syngeneic animals. Further experiments, using an array of immunodeficient mice or B/T/NK-cell depletion strategies are required to isolate the cell type(s) responsible for the rejection of HDP-on. A similar drug treatment approach, targeting T-cell activity, may also enhance the survival of HDP [265]. Other methods, such as blockade of co-stimulatory molecules (anti-LFA1, anti-CD40L or anti-CD80), genetically engineering cells to reduce MHCI or increase immunosuppressive cytokine production may also be explored to increase survival [266].

To summarize, we describe a modified Hoxb8-dependent myeloid progenitor (HDP) system to generate large numbers of fully functional MΦ and use these cells to perform quantitative biodistribution studies. We find liposomal clodronate pretreatment increases the *in vivo* survival of transplanted HDP-on from 1 to 7 days. Experiments in NCG mice demonstrated survival and expansion of HDP-on to at least 14 days, demonstrating the role of B, T and/or NK cells on preventing longer term survival. Our proposed model for this behavior is HDP-on are removed by two overlapping mechanisms (Figure 4-16). The first, is mediated by endogenous MΦ which act within 7 days to remove transplanted cells. The second, is mediated by B, T and/or NK cells, and removes transplanted cells beyond 7 days. Therefore, while liposomal clodronate and genetic modifications may enhance the acute survival of HDP, further efforts must be made to reduce the impact of the humoral and cellular mediated immune responses to increase long term survival of transplanted HDP.

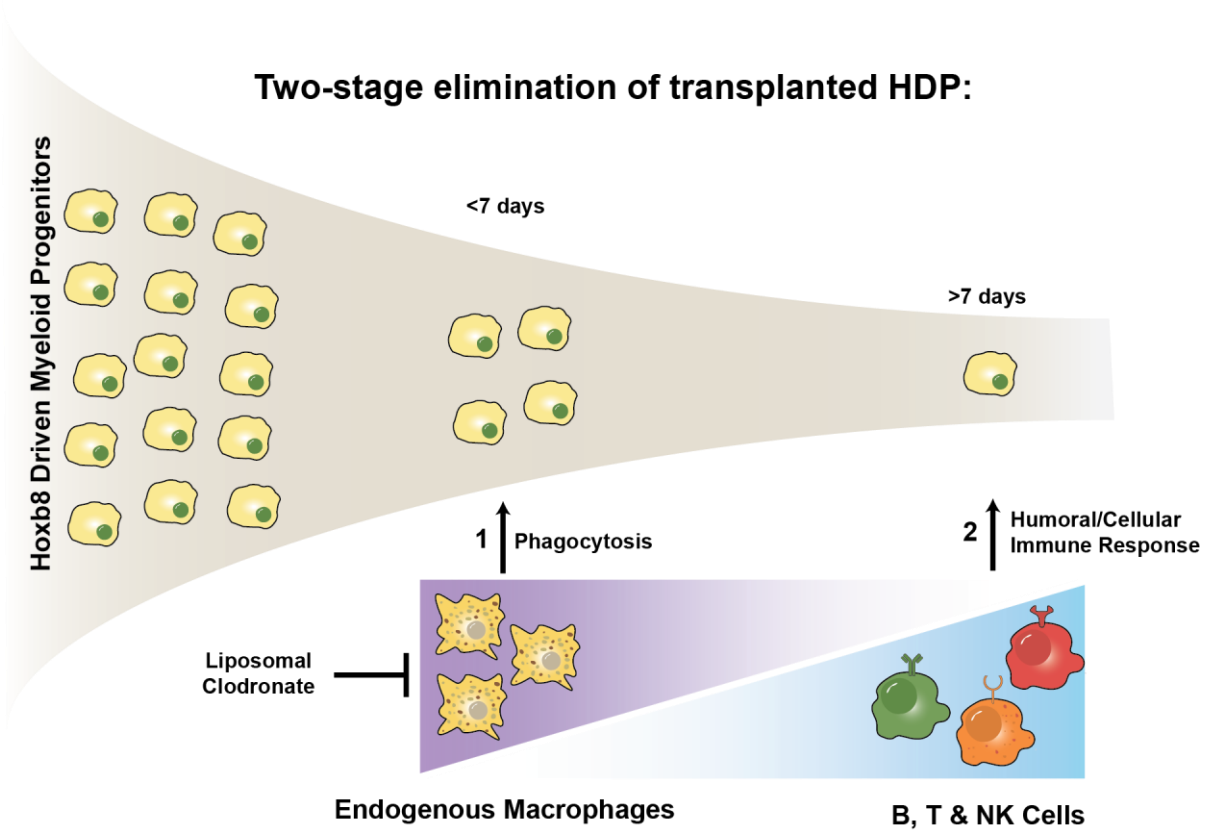

Figure 4-16: Model of two-stage immune rejection of HDP. Removal of endogenous MΦ by liposomal clodronate increases acute survival, but a humoral and cellular immune response from B, T and/or NK cells prevents long lasting engraftment.

4.9 Materials and Methods

4.9.1 Cell culture

Reagents were acquired from the University of California, San Francisco (UCSF) Cell Culture Facility (UCSF CCF) unless otherwise indicated. HDP were cultured in RPMI-1640 (50 mM HEPES, 1% PenStrep/Amphotericin B antibiotic/antimycotic, 1% Glutamax (Gibco), 10% heat inactivated fetal calf serum (Hyclone), 0.55 mM 2-mercaptoethanol (Life Technologies), 1% GMCSF supplement (appendix), using tissue culture treated flasks from GrenierBioOne (product # 658170) in a humidified incubator maintained at 37°C and 5% CO_2. Cells expressing the constitutively active GMCSFR were cultured

without the GMCSF supplement. Cell counts were determined using a hemocytometer and live cells enumerated using trypan blue staining.

HDP and HDP-on were differentiated into MΦ using different protocols. MΦ derived from HDP were differentiated by culturing cells in 200 nM 4-hydroxytamoxifen (4-OHT) (Enzo) for 10 days. Differentiation was started with a cell density of 2-4x10^5 cells/mL and the media was changed every 2 days for the first 6 days. Thereafter, no media changes were performed until MΦ were collected on day 10. MΦ differentiated from HDP-on were differentiated using 40 nM 4-OHT and 1 μM ruxolitinib (Selleckchem) for 6 days. Differentiation was started with a cell density of 2-4x10^5 cells/mL and the media was changed only on day 3.

4.9.2 Plasmid Construction

Plasmids for lentivirus and retrovirus production were cloned using standard techniques, including restriction cloning and Gibson assembly, depending on the applicability of each technique to the desired product. For production of plasmids containing Hoxb8 (GeneID 15416), GMCSFR (12983) and IRF8 (15900), murine cDNAs were acquired from GE Dharmacon and cloned into pLVX or pMSCV vectors for lentivirus or retrovirus production, respectively as described in the following section. Expression constructs also encoded antibiotic selection markers (blasticidin (bsd), puromycin (puro), zeocin (zeo) and neomycin (neo)). To engineer the constitutive activity of GMCSFR, a Quikchange Lightning Kit (Agilent) was used to modify the leucine in position 452 to glutamic acid (L452E), as adapted from Perugini et al [248]. Vectors for plasmid construction were obtained from Addgene or commercially available from Clontech. Constructs were sequence verified before use.

4.9.3 Lin$^-$ bone marrow culture and generating Hoxb8 dependent progenitors

Lineage negative (lin$^-$) cells were collected from the bone marrow of healthy female BALB/c mice by purifying the cells using a lineage depletion kit (Miltenyi Biotec #: 130-090-858) as per manufacturer protocols (appendix). Following collection, the lin$^-$ cells were cultured overnight in 100 ng/mL stem cell factor (SCF) (#250-03), 10 ng/mL IL-3 (#213-13) and 20 ng/mL IL-6 (#216-16) (all cytokines were murine and obtained from Peprotech) before they were transduced by lentivirus encoding the Hoxb8 construct. Following transduction with the Hoxb8 lentivirus, the cells were cultured in 30 ng/mL GMCSF (Peprotech, 315-03).

4.9.4 Lentivirus and retrovirus production

A second generation lentivirus was used, requiring three plasmids: pCMV-dR8.91 (Delta 8.9) (containing gag, pol and rev genes, Addgene #: 12263), VSV-G (envelope, Addgene #: 8454) and expression construct (pLVX-insert, Clontech #: 632187). For murine stem cell retrovirus, two plasmids are required, the packaging vector (pCL-Eco, Addgene #: 12371) and expression construct (pMSCV, Clontech #: 634401). To produce either retroviral or lentiviral vectors, HEK293T cells were transfected using Lipofectamine 2000 (Life Technologies) with the required plasmids and the media was collected and replaced every day for 3 days (appendix). The media containing the virus vector was concentrated by mixing 1:3 (v/v) with Lenti-X or Retro-X concentrator (Clontech) overnight and centrifugation for at 3000 rpm for 30 min in a 50 mL conical tube. The concentrated virus vector was resuspended in 200 µL RPMI and was used without further purification for viral vector transduction.

4.9.5 Lentiviral and retroviral transduction

Cells were transduced with retrovirus or lentivirus vectors using the spinfection method, as described in the appendix [254]. Briefly, $2x10^4$ cells were added to a retronectin (Clontech #: T100B) treated 48 well plate along with 50 µL of retrovirus or lentivirus vector. The plate was centrifuged for 90 mins at 4000 rpm and 30°C. The culture was then allowed to recover overnight in a humidified 5% CO_2 32°C incubator. The following day, the culture was returned to a humidified 5% CO_2 37°C incubator. After 3-5 days, the culture was expanded and tested for integration of the desired modifications. For antibiotic selection, 6 µg/mL blasticidin, 0.2 µg/mL puromycin, 30 µg/mL zeocin, or 1 mg/mL neomycin (Life Technologies) was added to the media.

4.9.6 MΦ M1/M2 polarization

MΦ were prepared as described previously. To polarize MΦ, the media was changed for the appropriate polarization media: 10 ng/mL LPS (Sigma), or 100 ng/mL IL-4 (Peprotech) for M1 or M2, respectively. Following an overnight treatment, MΦ were washed with D-PBS and RNA was collected using the RNeasy Mini Kit (Qiagen) following the manufacturer protocols. The expression of M1/M2 genes was then measured by qPCR.

4.9.7 qPCR

RNA was collected from cell samples as previously described. DNA for quantitative real time PCR (qPCR) was produced using the SuperScript VILO cDNA synthesis kit (ThermoFisher). qPCR was performed using SsoFast EvaGreen Supermix (BioRad) following manufacturer protocols using a BioRad CFX96 thermocycler. Each readout was

normalized against an internal mouse actin expression value and then compared to matched genes in other samples to determine fold change. For each sample and each gene, three replicates were performed and the fold enhancement averaged to yield a single value. To generate multiple values for statistical analysis, multiple experimental samples as indicated in the figure were subjected to the described method. For primer sequences, please refer to the appendix.

4.9.8 Flow cytometry

Flow cytometry was conducted at the UCSF Flow Cytometry core on a BD Fortessa instrument (appendix). The isotype antibody control used was APC-labelled Rat IgG2a, κ (Biolegend, Clone RTK2758). Fc-receptor blocking was performed using rat anti-mouse CD16/CD32 (BD Pharmingen, Clone 2.4G2). Cells were labelled with Allophycocyanin (APC)-labelled rat anti-F4/80 (Biolegend, Clone BM8, Rat IgG2a, κ) according to manufacturer instructions and the data was analyzed using FlowJo (FlowJo, LLC). Before analysis, dead cells and doublets were removed using FSC and SSC gating.

4.9.9 MΦ phagocytosis

Fluorescent liposomes were prepared with a 3:1:2 mole ratio of HSPC:DSPG:Cholesterol, (HSPC: L-α-phosphatidylcholine, hydrogenated (Soy), DSPG: 1,2-distearoyl-sn-glycero-3-phospho-(1'-rac-glycerol) (Avanti)) with 1% 8-Hydroxypyrene-1,3,6-trisulfonic acid (HPTS) (Sigma). The mixture of lipids in chloroform were placed in a round bottom flask and the chloroform was removed using a rotary evaporator. The resulting lipid film was dried under high vacuum overnight at room temperature. The film was reconstituted with HBS (140 mM NaCl, 10 mM HEPES) and sonicated under argon at room temperature for 40 min to form liposomes. The liposomes

were then dialyzed for 24 h in 2 L of HBS in a 10000 MW dialysis cassette (ThermoScientific) to remove unencapsulated HPTS and sterile filtered through a 0.45 µm filter (Millipore). For quantitative studies, liposomes were prepared in a similar fashion, using a 1:3:2 mole ratio of DSPG/DSPC/Cholesterol (DSPC: 1,2-distearoyl-sn-glycero-3-phosphocholine) with 0.01% DiD (Biotium). Lipid films were prepared as described and sonicated with D-PBS under argon at 45°C for 20 mins. DiD-labelled liposomes were extruded through a 100 nm polycarbonate membrane before sterile filtering through a 0.45 µm filter. The size and charge of the liposomes was determined using a Zetasizer (HPTS: diameter 76 nm, PDI 0.76, charge -57 mV, DiD: diameter 116 nm, PDI 0.216, charge -27.3 mV). Fluorescent bacteria were generated by transforming a BL21 *E. coli* strain with a pGEX-TagBFP plasmid.

Uptake experiments were performed on MΦ differentiated from HDP treated with 200 nM 4-OHT for 10 days or HDP-on treated with 40 nM 4-OHT and 1 µM ruxolitinib for 6 days. MΦ were removed from T-75 tissue culture plates using 5 mL of Hyqtase (GE) for 10 mins and $1x10^5$ MΦ were plated overnight in 1 mL media in a 12 well plate prior to incubation with liposomes or bacteria. For fluorescent imaging, MΦ were incubated with 1 mL of 500 µM HPTS-liposome solution or 1 mL 10% live TagBFP-*E. coli* culture (OD_{600} = 0.5) in serum free media for 3 h or 30 min, respectively, in a humidified 5% CO2 37°C incubator. Following the incubations, wells were rinsed three times with 1 mL D-PBS. Cultures treated with bacteria were imaged without any further treatment, while liposome-treated cultures were stained with DAPI prior to imaging on a fluorescent microscope. For quantitative liposomal uptake studies, $1x10^5$ MΦ were plated overnight in 1 mL media in a 12 well plate prior to incubation with liposomes. The next day, MΦ were incubated with

DiD-liposomes at varying concentrations in serum-free media for 6 h in a humidified 5% CO2 37°C incubator. The MΦ cell line, RAW264, was used as a comparative phagocytosis positive control cell line. The wells were washed with D-PBS three times and then the cells were lysed with 1 mL of radio immunoprecipitation assay (RIPA) buffer (150 mM NaCl (Sigma), 1% Triton -100 (Sigma), 10% Glycerol (molecular grade, Roche) and 50 mM Tris (Fisher)) was added. Total fluorescence was measured using a spectrofluorometer (Fluorlog, Horiba) (excitation 644, emission 665). The amount of liposomes taken up by the cells were determined from a standard curve of DiD-liposomes in RIPA buffer. To normalize the fluorescence signal to the number of MΦ in the well, total protein was measured using a BCA protein assay (ThermoFisher).

4.9.10 Animals

All mice used in this study were purchased from Charles River Laboratories (Wilmington, MA) and maintained under pathogen-free conditions at the University of California, San Francisco (UCSF). All mouse procedures were approved by the UCSF Institutional Animal Care and Use Committee (IACUC). Two mouse strains were used in this study: BALB/c (strain #028) and NCG (NOD-Prkdc^{em26Cd52}Il2rg^{em26Cd22}/NjuCrl; strain #572). Due to their immunodeficient status, NCG mice were housed in ultraclean barrier facilities.

4.9.11 Cell transplantation

Adherent MΦ were removed from T-75 tissue culture flasks by treatment with 5 mL Hyqtase (GE) for 10 mins and gentle tapping of the flask. After removal from the flask, the cells were treated identically to suspension cells. Suspension HDP were washed twice with plain RPMI, counted and the required dose was resuspended in 500 µL for

intraperitoneal (IP) injection. For each biodistribution experiment, the luciferase activity per cell was determined to calculate the total luciferase units injected into the mouse.

All animal work was conducted under the explicit approval of UCSF IACUC. For mice treated with liposomal clodronate (ClodLip BV), mice were dosed twice (4 days and 1 day prior to cell injection) with 100 µL liposomal clodronate (5 mg/mL) via IP injection. For IP injections, mice were scruffed and the ventral side was exposed. The head was tilted down slightly and the bottom right quadrant of the abdomen was wiped with an alcohol wipe. A 28 gauge insulin syringe containing up to 500 µL of solution was inserted bevel side up and slowly injected into the cleaned area. After the injection, the mouse was placed in a cage and observed for 10 min to ensure no adverse effects. No adverse effects were ever observed during this observation period. However, as reported by other groups, there was a 20-25% mortality within 5 days of liposomal clodronate treatment [255]. All animals were female and 8-10 weeks old at time of injection.

4.9.12 Biodistribution

Animals were euthanized by an IP injection of sodium pentobarbital (200 mg/kg) and cervical dislocation, as approved by UCSF IACUC. Organs were collected, weighed and placed on ice. Each organ was lysed with RIPA buffer (~200 mg tissue/mL of RIPA) using a glass dounce grinder with a tight fitting pestle and a lysate was formed by using the pestle until no tissue was visible. The organ lysates were centrifuged at 3000 rpm for 5 min and the supernatant was used for further analysis. Blood samples (~50-200 µL) were collected into a tube containing 10 µL 1 mg/mL heparin in D-PBS (Alfa Aeser) and were not processed further. Flushes of the peritoneal cavity were collected by injecting 5 mL of plain RPMI into the peritoneal cavity of a euthanized mouse. The mouse abdomen

was massaged slightly to ensure proper mixing in the peritoneal cavity before a cut was made into the abdomen to drain the fluid with suspended cells into a collection dish. This suspension was transferred to a 15 mL tube and stored on ice until ready for measurement. Immediately prior to the luciferase activity measurement of samples from the peritoneal cavity, the cell suspension was mixed thoroughly by inverting the tube several times.

Luciferase activity was determined using SteadyGLO (Promega) as per manufacturer protocols. Clarified organ lysate (100 µL) was mixed with 100 µL SteadyGLO in a glass tube. Total luminescence was measured using a luminometer (MGM Instruments) over a 10 second period. The luciferase activity from the measured sample was multiplied with an appropriate correction factor to determine the total luciferase activity in each organ. The percentage of injected cells in each organ was calculated by dividing the total luciferase activity in each organ by the total luciferase activity of the injected cells. In control experiments, the presence of organ lysate did not reduce the luciferase activity of a known number of cells by more than 10% when compared to cells in RIPA alone.

4.9.13 Statistics

Statistics was performed using GraphPad Prism 5. To determine significance between data sets, one way ANOVA was performed, followed by a Bonferroni post test. For comparison of pharmacokinetic data, a one-sided T-test was used to compare within the same time point. Significance was reported as follows: * = $p < 0.05$, ** = $p < 0.01$ or *** $p < 0.001$. Error bars are expressed as standard error.

5 Chapter 5: MΦ gene therapy for Hurlers Syndrome

5.1 Hurlers Syndrome

Mucopolysaccharidosis Type I, also known as Hurlers Syndrome (HS), is characterized by a deficiency of iduoronidase (IDUA), an enzyme critical in the degradation of glycosaminoglycans (GAG). The resulting systemic over accumulation of GAG manifests in significant developmental problems, particularly in the neural, skeletal and cardiovascular systems [267]. Untreated, individuals with HS rarely survive beyond ten years of age [267]. Current treatments include: enzyme replacement therapy (ERT) or hematopoietic stem cell transplantation (HSCT). Neither treatment is ideal. While HSCT is the current gold standard in treatment of HS, the inherent risks of HSCT, difficulty of finding matching donors and incomplete restoration of IDUA mean many patients are untreatable using this method [268]. ERT relies on the cross-corrective ability of recombinant IDUA (Aldurazyme, FDA approved 2003), which endogenously contains a mannose-6-phosphate (M6P) domain, allowing for extracellular IDUA to be taken up by other cells via the M6P-receptor pathway [269]. Patients are treated once a week with an infusion of Aldurazyme, representing a significant challenge for maintaining compliance. Furthermore, IDUA cannot cross the blood brain barrier, and thus ERT is unable to treat the neural component of HS.

We believe an innovative hybrid approach, using autologous MΦ genetically engineered to express IDUA, can address the challenges facing HSCT and ERT for the treatment of HS (Figure 5-1).

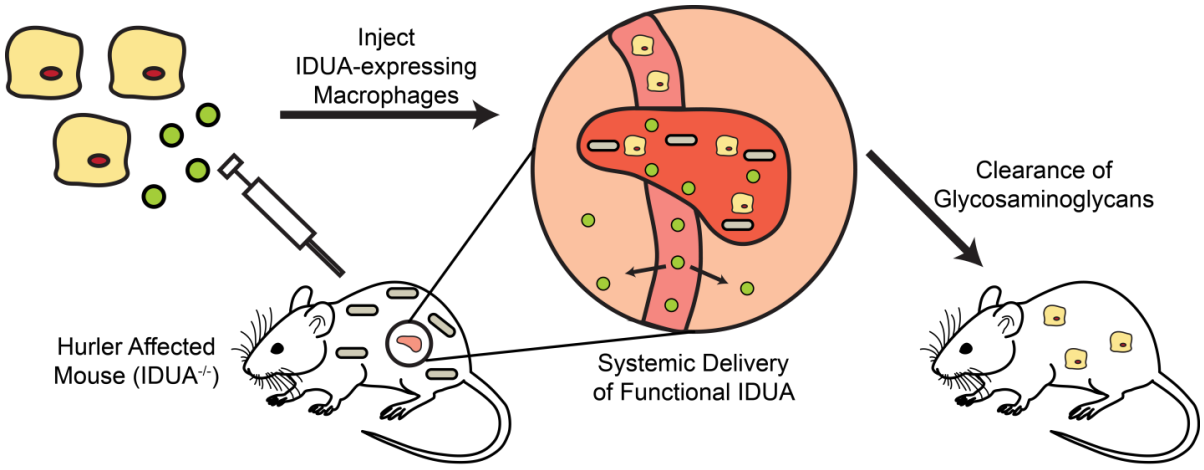

Figure 5-1: Overview of autologous genetically engineered MΦ expressing IDUA (IDUA-MΦ) to treat a mouse model of Hurlers syndrome. Engraftment of IDUA-MΦ results in systemic delivery of IDUA to alleviate over accumulation of glycosaminoglycans seen in Hurlers syndrome.

MΦ (MΦ) are highly plastic and adaptable cells found in every tissue, including the systems most deeply affected by HS [198, 270]. As one of the first lines in the innate immune system, MΦ are also innately recruited towards inflammatory sites, such as those developed when over accumulation of GAG results in tissue damage, and have also been observed to be recruited into the inflamed brain in models of Parkinson's [147]. Additionally, clinical trials in the 1990s demonstrated a strong safety profile of using autologous MΦ, whereupon infusion of 10^9 MΦ resulted in minimal side effects [94].

5.2 *In vitro* expression of IDUA in Cos-7 cells

To confirm IDUA could be secreted from modified cells, we transfected Cos-7 cells with plasmids encoding IDUA with a hemagglutinin (HA)-tag at either the N or C-terminus (Figure 5-2). An HA-tag was added to IDUA to aid the detection of the protein using western blot in subsequent experiments. Two days after transfection, the media and cells were collected to determine IDUA activity. The media of all transfected cultures contained

active IDUA (Figure 5-3). The addition of the HA tag to either the N or C terminus of IDUA reduced the activity, but there was no difference between the N or C terminus modifications. An anti-HA western blot was performed on the cell lysate and media to determine if the HA tag was preserved after expression and secretion. Only C-terminal IDUA-HA was detectable in the cell lysate and media. This suggests a post-translation modification results in cleavage or disruption of the N-terminus of IDUA. Therefore, any modifications to IDUA (i.e. attachment of the Fc or Ig-binding peptide to increase circulation time) should be made to the C-terminus.

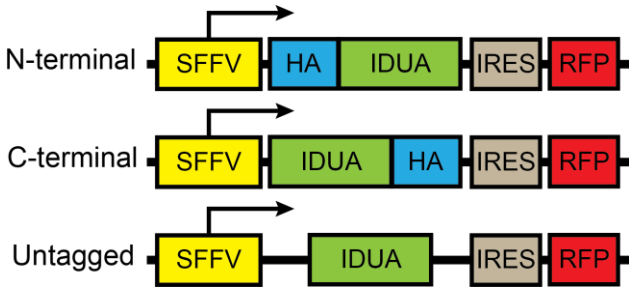

Figure 5-2: IDUA expression constructs. HA-tag was added to the N or C terminus to be used for tracking by western blot.

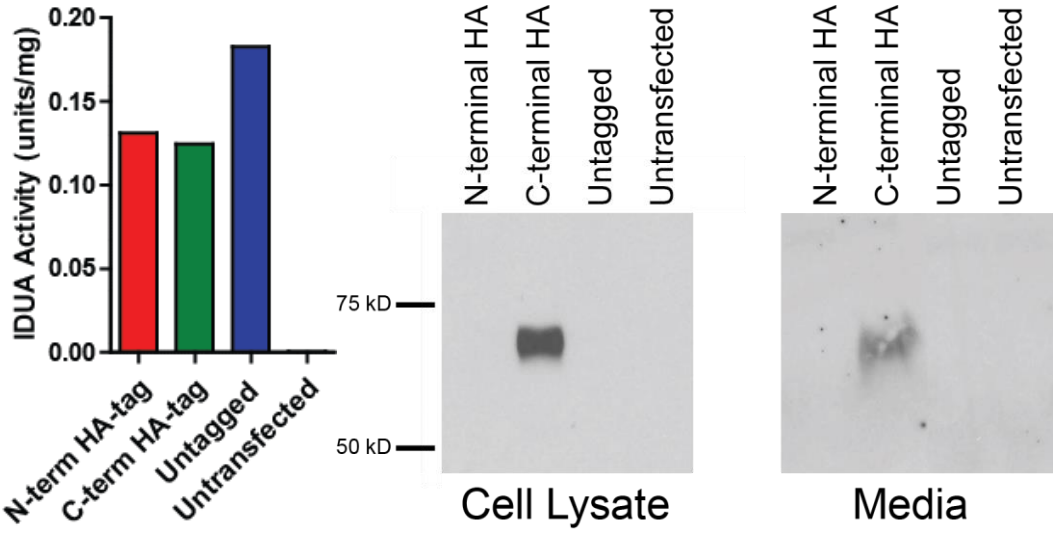

Figure 5-3: Activity and expression of modified IDUA in Cos-7 cells. IDUA activity of cell media, normalized by total protein from cell lysates, following transfection of Cos-7 cells by plasmids containing IDUA with a hemagglutinin (HA)-tag at either the N or C-terminus. Anti-HA western blot of cell lysates and media of transfected Cos-7 cells reveals C-terminal HA-tag is maintained during IDUA expression. N = 1 transfected culture per condition

5.3 IDUA expression in HDP and HDP-MΦ

Retrovirus was produced and used to transduce BL/6 HDP using the methods described in Chapter 2. The IDUA-HA construct was successfully integrated into HDP, as shown by colony PCR using primers specific for the IDUA construct (Figure 5-4A). Furthermore, IDUA-HDP differentiated into MΦ (IDUA-HDP-MΦ) in 10 days when treated with 200 nM 4-OHT. IDUA-HDP and IDUA-HDP-MΦ respectively secreted 10 or 80 times more IDUA than unmodified HDP or HDP-MΦ into the media (Figure 5-4B). Further modifications to the expression construct itself, such as using different promoters may increase the expression of IDUA. This can be done in combination with modifications to the protein, such as enhancing the circulation half-life modifying IDUA with IgG binding

peptides [271]. IDUA-HDP-MΦ secrete ~10 times more IDUA than IDUA-HDP. Enhanced survival of transplanted MΦ could enable HS therapy using either genetically modified HDP or HDP-MΦ. Further enhancement of long term cell survival would be necessary for a long term therapy to be realized.

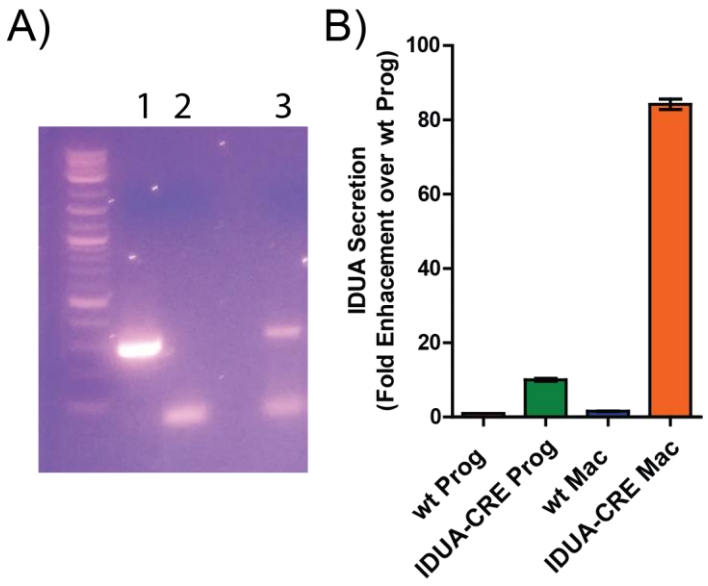

Figure 5-4: Transduction of HDP with IDUA retrovirus. A) Genotyping PCR of HDP infected with IDUA-retrovirus. 1: Positive control – retroviral vector alone, 2: Negative control – uninfected cells, 3: IDUA-retrovirus infected cells. B) IDUA secretion of IDUA-HDP and IDUA-HDP-MΦ.

5.4 Pharmacokinetic considerations

To determine the enzyme secretion rate per cell, we must consider that cells are proliferating during the 48h the assay takes place.

Define:

n_{cells} = number of cells at time t

n_0 = number of cells at the start of the culture

t = time elapsed in culture

$k = \frac{1}{t_{1/2}}$; $t_{1/2}$ = cell doubling time

SR = enzyme secretion rate

$$n_{cells} = n_0 2^{kt} \quad [1]$$

$$\text{Total Enzyme} = \int_0^t n_{cells} SR \, dt \quad [2]$$

Combine [1] and [2] to generate [3], solve the integral for [4] and rearrange for [5]:

$$\text{Total Enzyme} = \int_0^t n_0 2^{kt} SR \, dt \quad [3]$$

$$\text{Total Enzyme} = \frac{n_0 SR}{kln2}(2^{kt} - 1) \quad [4]$$

$$SR = \frac{kln2(\text{Total Enzyme})}{n_0(2^{kt} - 1)} \quad [5]$$

Note that [4] assumes:

a) Enzyme is stable in media after secretion

b) Secretion rate is constant and is unaffected by any changes in culture conditions

Based on an *in vitro* assay over 48h, 1x10^5 IDUA-HDP cultured in 1 mL of media secreted 30 units of IDUA in total (1 unit = 1 nmol/h), we can calculate the secretion rate per cell by using [5]. As per earlier experiments, the doubling time is 12 h.

$$SR = \frac{(\frac{1}{12\text{ h}})ln2(30\text{ units})}{(1\text{x}10^5\text{cells})(2^{\frac{1}{12\text{ h}}(48\text{ h})} - 1)} \quad [6]$$

$$SR = 1.155\text{x}10^{-6}\ \frac{\text{units}}{\text{cell·h}} \quad [7]$$

Assuming the secretion rate remains the same *in vivo*, we can use pharmacokinetic equations and known pharmacokinetic parameters of Aldurazyme to determine the feasibility of IDUA-HDP as an IDUA delivery method. For this calculation,

it is assumed that HDP-secreted IDUA is pharmacokinetically equivalent to Aldurazyme. Due to the short half-life of Aldurazyme, to determine equivalency, we will calculate the total exposure (i.e. AUC) of a standard course of Aldurazyme, which is administered once a week as a 6000 units/kg IV infusion over 4 hours.

To determine AUC, consider two separate segments of the drug concentration curve over 7 days: A) During the infusion where drug concentration rises and peaks at 4 h when the infusion stops and B) Post infusion where the drug concentration declines. We first calculate AUC for segment A:

$$AUC_A = \frac{k_0}{CL}\int_0^{240\text{ min}} (1 - e^{-k_e t})dt \quad [8]$$

$$k_0 = \frac{\text{6000 units/kg}}{\text{4h}} = 4\ \frac{\text{units}}{\text{kg·min}} \quad [9]$$

$$CL = 2.2\frac{\text{mL}}{\text{kg·min}}\ , V_d = 420\frac{\text{L}}{\text{kg}} \quad [10]$$

$$k_e = \frac{CL}{V_d} = \frac{2.2\frac{\text{mL}}{\text{kg·min}}}{420\frac{\text{L}}{\text{kg}}} = 5.24\text{x}10^{-3}\ \text{min}^{-1} \quad [11]$$

Solve the integral from [8]:

$$AUC_A = \frac{k_0}{CL}\left[\frac{e^{-k_e t}}{k_e} + t\right]_0^{240\text{ min}} \quad [12]$$

$$AUC_A = 85.45\frac{\text{units·min}}{\text{mL}} \quad [13]$$

To calculate the AUC for segment B for 7 days:

$$AUC_B = C_0\int_0^{10080\text{ min}} e^{-k_e t}dt \quad [14]$$

$$AUC_B = C_0 \left[\frac{e^{-k_e t}}{k_e}\right]_0^{10080\ \text{min}} \quad [15]$$

C_0 is the concentration at the end of the 4 hour infusion of segment A/beginning of segment B and is determined by:

$$C_0 = \frac{k_0}{CL}(1 - e^{-k_e t}) \quad [16]$$

$$C_0 = 1.818 \frac{\text{units}}{\text{mL}} \quad [17]$$

$$AUC_B = 346.9 \frac{\text{units·min}}{\text{mL}} \quad [18]$$

Total AUC of a standard dose of Aldurazyme can be determined by adding [13] and [18]:

$$AUC_{Drug} = 432.4 \frac{\text{units·min}}{\text{mL}} \quad [19]$$

To determine the AUC for transplanted IDUA-HDP, treat secretion of IDUA similar to a constant infusion over 7 days:

$$AUC_{IDUA-HDP} = \frac{k_0}{CL} t \quad [20]$$

$$k_0 = 1.155\text{x}10^{-6} \frac{\text{units}}{\text{cell·h}}\, n_{cells} = 1.925x10^{-8} \frac{\text{units}}{\text{cell·h}}\, n_{cells} \quad [21]$$

$$AUC_{IDUA-HDP} = 8.82\text{x}10^{-5} \frac{\text{units·min·kg}}{\text{mL·cell}} (n_{cells}) \quad [22]$$

Comparing the AUC, we can determine the number of cells required for the AUC of IDUA-HDP to match Aldurazyme:

$$\frac{AUC_{IDUA-HDP}}{AUC_{Drug}} = 1 = 2.04\text{x}10^{-7} \frac{\text{kg}}{\text{cell}} (n_{cells}) \quad [23]$$

$$n_{cells} = 4.88\text{x}10^{6} \frac{\text{cell}}{\text{kg}} \quad [24]$$

Based on these calculations, for a 25 g mouse, $1.22x10^5$ cells would be able to match the AUC of Aldurazyme. For a 50 kg human, $2.44x10^8$ cells would be required. As demonstrated in Chapter 4, in mice pretreated with liposomal clodronate, 50-60% ($2.5x10^6$) of injected HDP survived for at least 7 days. Assuming this is true for transplanted IDUA-HDP, treatment of HS may be viable using this method.

5.5 Conclusion

While MΦ are terminally differentiated cells and lack proliferative capacities, we have adapted and developed methods to generate highly proliferative monocyte progenitors from murine bone marrow by overexpressing the transcription factor Hoxb8 [34], as described in the previous chapters. As monocyte progenitors, genetic modifications can be made using retrovirus. Due to the rapid proliferation of the monocyte progenitors, we are able to rapidly generate large numbers of MΦ. Using this method, we have developed MΦ which overexpress and secrete approximately 80 times more IDUA than unmodified wild type MΦ. Owing to the cross-corrective ability of IDUA, we believe engraftment of these gene-corrected MΦ can result in long-term and systemic delivery of IDUA, without the dangers of HSCT and compliance concerns of ERT. Pharmacokinetic calculations, combined with the results from Chapter 4, demonstrate transplanted IDUA-HDP, may be a viable replacement for Aldurazyme. The expression constructs can be modified to further increase IDUA secretion rate or IDUA circulatory half-life. Improvement of long term post-transplantation survival is also necessary for long term treatment. We envision that this technology can be used as a platform for generating autologous gene-corrected MΦ to treat a variety of diseases, ranging from lysosomal storage diseases, to

other conditions with significant inflammatory and MΦ components, including cancer, arthritis, chronic infections and obesity/diabetes [238, 272].

5.6 Methods

5.6.1 Transfection

One hundred thousand Cos-7 cells were plated in a 12 well plate with 1 mL of media overnight prior to transfection. Transfection was performed using Lipofectamine 2000 (Invitrogen) using the manufacturer protocols. IDUA was subcloned from murine IDUA cDNA (GeneID: 15932, GE Dharmacon) into the retroviral vector, pMSCV-Hygro (Clontech) and sequence verified before use.

5.6.2 IDUA Activity

IDUA-HDP cells were made by transducing BL/6 HDP with a retroviral construct encoding IDUA and selecting transduced cells with hygromycin (see Chapter 2 for methods). IDUA activity was measured from cell lysate or conditioned growth media. Growth media was collected from transfected Cos-7, IDUA-HDP or IDUA-HDP-MΦ cells 2 days after plating $1x10^5$ cells in 1 mL of growth media (see Chapter 2) in a 12 well plate. Media was clarified by centrifugation and the supernatant was used for subsequent measurements. Cell lysates were formed by adding 1 mL RIPA buffer to the 12 well plate after growth media was collected. Cell debris was removed from lysates by centrifugation prior to IDUA activity measurement. IDUA activity was measured using 4-methylumbelliferyl (4MU)-α-L-idopyranosiduronic acid sodium salt (Toronto Research Chemicals) as a substrate for IDUA. In the presence of IDUA, 4MU is cleaved from the substrate. Addition of glycine buffer (high pH) increases the fluorescence of free 4MU (but not the uncleaved substrate). Comparison of the emission (ex 355, em 460) to a standard

curve of known concentrations of 4MU allows for determination of the amount of 4MU generated. By normalizing the activity against total protein in the test sample (media, lysate, tissue), the overall activity can be determined. A full extended protocol can be found in the appendix.

5.6.3 Western blot

The western blot was performed on cell lysate or media using standard techniques (appendix). Cell lysate or media was loaded on a 12% SDS-PAGE Gel (BioRad) and transferred onto a blotting membrane (BioRad). The blotting membrane was blocked with milk and the primary antibody (1:2000 Rat Anti-HA high affinity (Roche)) was added to the membrane to incubate overnight at 4°C. The next day, the membrane was thoroughly washed before addition of the secondary antibody (1:10000 anti-rat HRP (Jackson)). Following a 1 h incubation, the membrane was thoroughly washed before addition of Pierce ECL Western Blotting Substrate (Thermo). The membrane was then imaged using a film development cassette (GE).

6 Chapter 6: Summary, conclusions and future work

This chapter will summarize the findings presented in this dissertation, provide options for future directions and provide a prospective on the future of MΦ cell-based therapies.

6.1 Summary of Findings

In Chapter 2, we modified the method described by Wang et al [34] to generate the cells used throughout this dissertation. Instead of transducing lineage negative cells with an inducible Hoxb8 to retain the self-renewing phenotype, we instead used a constitutively expressed Hoxb8 flanked by loxP sites. To remove the Hoxb8 construct, we also transduced the cells with a construct containing Cre recombinase fused with an estrogen receptor (Cre-ERT) and luciferase. Induction of Cre activity by addition of tamoxifen (4-OHT) removed the Hoxb8 construct and resulted in the differentiation of the cell into a MΦ. The luciferase served as a reporter for live cells that would be used for biodistribution studies. We termed these cells Hoxb8 dependent myeloid progenitor cells (HDP). We showed HDP proliferated in suspension, with a rapid doubling time of 12 h, satisfying our need to generate the numbers of cells we required for further study. Additionally, MΦ derived from HDP (HDP MΦ) retained all MΦ behaviors we tested, including M1/M2 polarization potential, phagocytosis of bacteria and liposomes and chemoattraction towards 4T1 conditioned media. Based upon this characterization data, we were satisfied HDP and HDP MΦ were a good model for further development as a MΦ cell therapy.

In Chapter 3, we determined the biodistribution of HDP and HDP MΦ in BALB/c mice using multiple routes of administration and animal/cell pretreatment methods. We

empirically identified non-lethal doses for the IV and IP injection routes and determined luciferase activity, rather than DiD labeling, was a robust method of quantifying the number of live cells in a tissue sample. To reduce the number of cells entrapped in the lungs immediately post-injection, we determined 1 M mannitol, a hyperosmotic solution, could be used as an injection fluid with no adverse effects on the injected cells or mice.

We then proceeded to test the engraftment and survival of HDP, HDP treated with tamoxifen for 4 days (4DDP) and HDP MΦ administered via the IV, lung and IP routes. In the IV route, the total percentage of injected HDP or HDP MΦ recovered 24 h post-transplantation was <1% ($2x10^4$ cells) across all tissues analyzed (lung, liver, spleen and blood). We used a variety of approaches to increase cell survival, including: PEGylation of the cells to evade the RES, culturing cells in syngeneic BALB/c serum to prevent a foreign immune rejection response, dosing animals with thrombin inhibitors to reduce thrombosis and modifying cells to express complement inhibitors to reduce complement activation. None of the treatments improved survival beyond 10% of the injected number of cells across all measured tissues (liver, spleen, lung, brain, heart, kidney and blood) at 2 h post-transplantation. At 24 h post-transplantation, <1% of the injected cells were detected. Administration via the lung also did not significantly improve survival.

For the IP route, we took advantage of the space in the peritoneal cavity by co-injecting 4DDP with matrigel. This method allowed for significant recovery (20-100% of injected cells) up to 7 days post transplantation. However, cells were only found in the peritoneal cavity. To increase migration to other tissues, we implanted 4T1 tumors in mice, polarized cells with M1 or M2 inducers and overexpressed CCR2 (a receptor for a CCL2, a chemoattractant ligand secreted by 4T1 tumor cells). With these methods, we

were unable to observe migration of cells from the matrigel to other tissues. Nonetheless, we were encouraged that the matrigel was able to support the survival of the transplanted cells. We hypothesized enhancing cell survival and providing a niche for the transplanted cells would encourage further survival.

In Chapter 4, we continued our efforts to identify means to improve the post-transplantation survival of HDP and HDP MΦ. We modified HDP to express a constitutively active GMCSFR, which resulted in cytokine-free proliferation. A second modification added IRF8 fused with an estrogen receptor (IRF8-ERT) to increase the rate of differentiation. Together, these modifications formed what we designated HDP-on cells.

We determined HDP-on proliferated at the same rate as HDP without the need for GMCSF and also differentiated into MΦ at an accelerated rate (6 days vs 10 days). HDP-on MΦ also demonstrated established MΦ phenotypes, including M1/M2 polarization and phagocytosis. The biodistribution of HDP, HDP-on and MΦ from both cell lines was determined in immunocompromised NCG mice, which lack B, T and NK cells. A week after IP transplantation of the cells, we were able to recover 100-120% of the injected HDP and HDP-on, and 10-20% of the injected MΦ. We then repeated the experiment in immunocompetent mice. HDP were undetectable after 1 day, while HDP-on survived for at least 1 day, but was undetectable 7 days post-transplantation. Pretreatment of mice with liposomal clodronate improved the survival of HDP and HDP-on at 7 days to 50-80% of the injected number of cells in the peritoneal cavity, with cells also found in the spleen and liver. At 14 days post-transplantation in mice pretreated with liposomal clodronate, no HDP-on cells were detected in any of the examined tissues. In NCG mice injected with HDP-on, the number of cells detected in the examined tissues expanded over 14 days,

demonstrating that B, T and NK cells were likely involved in the rejection of HDP-on in BALB/c mice.

In Chapter 5, we demonstrate the possibility of using HDP and HDP MΦ to treat Hurler's Syndrome, or MPS I, a lysosomal storage disease caused by the loss of functional iduronidase (IDUA). We were able to transduce HDP with a retrovirus encoding IDUA and differentiated these IDUA-HDP into IDUA-HDP MΦ. Lastly, we demonstrated *in vitro* cultures of IDUA-HDP and IDUA-HDP MΦ secrete and produce IDUA detectable using a biochemical IDUA assay. Pharmacokinetic calculations demonstrated that based on the survival data from Chapter 4, IDUA-HDP may be a viable strategy for delivering IDUA. This method for treating Hurler's Syndrome may be significantly enhanced by development of new strategies to enable long term post-transplantation survival.

The results of this dissertation open opportunities to multiple pathways dissecting the mechanisms by which HDP and HDP-MΦ are removed post-transplantation. The next section will detail possible research directions to identify more methods to improve post-transplantation cell survival.

6.2 Future work

This dissertation describes methods for improving the survival of Hoxb8 driven myeloid progenitor cells by pretreating animals with liposomal clodronate and genetically modifying HDP to express a constitutively active GMCSFR Survival experiments conducted with NCG mice demonstrated the number of HDP continually increased up to at least 14 days, suggesting a characteristic of the NCG mouse is enabling HDP to survive for an extended period. NCG mice lack B, T and NK cells, but are also deficient in complement, among other immunological deficiencies [273].

My studies do not dissect which missing components are responsible for the low survival we observe in immunocompetent BALB/c mice. Further studies, using other immunodeficient models (Table 6-1) could dissect which components of the immune system have the greatest effect on the short and long term survival of transplanted HDP. The approach used by Swijnenburg and colleagues to study immune rejection of human stem cell xenografts in mice is a model for future analysis [263]. They performed experiments looking at immune cell infiltration, cytokine levels and antibody titer, in combination with immunodeficient animals to identify the probable cell types which were responsible for the immune rejection. By performing studies used by Swijnenburg and colleagues with HDP transplantation, new pretreatment protocols or HDP genetic modifications may be used to bolster survival in immunocompetent animals.

Table 6-1: Other immunodeficient animal models

Model	T-cell	B-cell	NK-cell	Complement
NCG/NSG	N	N	N	N
NOD/SCID	N	N	Partial	N
Nude	N	Y	Y	Y
NOD or C3 KO	Y	Y	Y	N
Anti-CD20	Y	N	Y	Y

An unbiased method could also be used to identify new factors to improve survival. This can be done using a genome wide (or a targeted) screen using CRISPR/Cas9 to knockout, upregulate or downregulate genes, depending on the type of Cas9 and accessory RNAs used [274]. HDP can be transduced with Cas9 to generate a Cas9-HDP line prior to further transduction with a barcoded retroviral library of different gRNAs. Following selection of gRNA+ cells, the gRNA-Cas9-HDP can be transplanted into mice. After a defined period of time, the DNA can be collected from the various organs for deep sequencing to identify the gRNAs responsible to enhanced survival. By separating organ-

to-organ data, migration effectors may also be identified. The genes identified in this method can then be validated by forming cell lines with the specific modifications. It would also be interesting to apply this method to MΦ. More broadly, the gene targets identified in this screen may also be applicable to other cell-therapies to improve survival.

One other approach that was briefly mentioned in Chapter 4 was to remove as many foreign components in the HDP as possible, including fluorescent proteins, resistance markers and luciferase. These foreign components are immunogenic and may be responsible for targeting of the HDP used in this thesis by the immune system [259, 260]. Most of the additional components in HDP can be removed. Due to the survival advantage provided by constitutively active GMCSFR or Hoxb8, these constructs do not require a selection marker and can be selected by culturing the cells for an extended period of time. Fluorescent proteins which were used to aid tracking of the cells by flow cytometry or fluorescent imaging can be eliminated. Rather than using luciferase for a quantitative measurement of biodistribution, it can be replaced with a DNA barcode that can be counted from organ lysates using droplet digital PCR, which is best suited to perform absolute quantification from low amounts of target DNA. Cre is a required component for differentiating HDP into MΦ, but it is possible to flank the Cre construct with lox sites (orthogonal to loxP to prevent cross pairing with Hoxb8) such that activation of Cre can cleave out both Cre and Hoxb8. Alternatively, the HDP can be transplanted into a mouse strain which endogenously expressed Cre and would have limited immunogenicity against Cre. The approaches outlined here may improve long term survival by reducing the immunogenicity of HDP.

6.3 Conclusions and Outlook

Since the first clinical use of MΦ as a cell-based therapy over 40 years ago, there have been significant developments in understanding the importance of MΦ in disease and homeostasis [2, 7, 239, 244]. The ubiquity of MΦ in tissues throughout the body and vast array of specialized functions performed by MΦ is obscured by the general designation "MΦ" to describe these cells. Rather than a discrete cell type, "MΦ" are better thought of as a highly plastic cell that can adopt numerous phenotypes depending on a confluence of environment factors, including tissue type, disease state and cell origin. Thus they present an opportunity to devise specialized organ specific treatments. From the broad M1/M2 paradigm to all the various tissue-specific MΦ, the signals that dictate the generation, behavior and phenotype of these MΦ have been increasingly better understood [7, 239]. In conjunction with developments in genetic engineering techniques, the possibilities of engineering MΦ for specific functions, with specific tissue homing capacities and perhaps even endowing non-MΦ functions such as production of therapeutic proteins are incredibly exciting [244].

An inherent difficulty of understanding and developing MΦ cell therapies is the broad applicability acts as a double edged sword; MΦ are incredibly complex and difficult to control. While the roles of MΦ in tumorigenesis are increasingly better understood, mechanisms are not distilled to single factors [7, 28, 107, 239, 275] and most behaviors are not easily perturbed. Thus, to modify MΦ behavior, multiple genes will need to be simultaneously altered. The advent of CRIPSR/Cas9 may be one way to accomplish this. This multi-factor approach is significantly more difficult than a relatively simpler CAR-T

therapy, which required decades to develop and followed discoveries in understanding T-cell biology.

Perhaps the most attainable MΦ cell therapy is gene therapy. Long term engraftment of engineered MΦ expressing a therapeutic protein, as shown in Chapter 5, and capable of low levels of proliferation/renewal may be an effective delivery strategy that circumvents the expense and low compliance of frequent treatment using recombinant proteins or the risk of bone marrow transplantation. The ubiquity of MΦ in most tissues suggests it may be possible for engineered MΦ to engraft systemically or be tailored for specific tissues for improved protein delivery.

This dissertation explored some of the practical limits of using MΦ for cell based therapies, including 1) the limited-proliferative nature of MΦ, 2) cytokine requirements for survival and 3) generating a niche in the tissue for transplanted MΦ to engraft. We were able to modify an established method of generating *ex vivo* MΦ that enabled the production of millions of functional MΦ without the need for using animals. Transplantation experiments demonstrated HDP survived in immunodeficient NCG mice but not in BALB/c mice, suggesting the immune system may play a role in rejecting HDP.

The results of this dissertation and a survey of the stem cell therapy field highlight a fundamental concern with cell-based therapeutics: post-transplantation survival of cells of all types is limited. In order to accomplish the ambitious goal of MΦ cell therapy, a greater understanding of HDP (and HDP MΦ) rejection will need to be made. Research strategies employed for developing stem cell therapies can be used to accelerate these studies. The factors that contribute to cell depletion is incomplete and strategies to improve cell survival remain inadequate [276, 277]. Transplanted cell depletion occurs even

when cytotoxic drugs or radiation are given to suppress the immune system or create a niche in which the transplanted cells can grow subsequent to the transplant [278]. CAR-T, the most successful cell-based therapy, also suffers from this, but immunoablation and co-treatment with IL-2 to boost *in vivo* proliferation lessened the impact of poor post-transplantation survival. Nonetheless, low CAR-T cell survival is correlated with poorer outcomes in CAR-T trials [279]. Methodologies such as the CRISPR/Cas9 screen presented in the previous section may identify new targets for increasing post-transplantation survival, increasing the potential of all cell-based therapeutics.

Understanding of MΦ and their importance in disease and homeostasis will continue to grow. In conjunction with ongoing advances in enhancing post-transplantation cell survival and the development of new tools to study and modify MΦ, I am hopeful that MΦ will evolve into a cell-based therapy for a variety of diseases.

7 References

1. Wynn, TA, Chawla, A, and Pollard, JW (2013). Macrophage biology in development, homeostasis and disease. *Nature* 496: 445-455.

2. Franken, L, Schiwon, M, and Kurts, C (2016). Macrophages: sentinels and regulators of the immune system. *Cellular microbiology*.

3. Martin, CJ, Peters, KN, and Behar, SM (2014). Macrophages clean up: efferocytosis and microbial control. *Current opinion in microbiology* 17: 17-23.

4. Soroosh, P, Doherty, TA, Duan, W, Mehta, AK, Choi, H, Adams, YF*, et al.* (2013). Lung-resident tissue macrophages generate Foxp3+ regulatory T cells and promote airway tolerance. *The Journal of experimental medicine* 210: 775-788.

5. Mantovani, A, Sica, A, Allavena, P, Garlanda, C, and Locati, M (2009). Tumor-associated macrophages and the related myeloid-derived suppressor cells as a paradigm of the diversity of macrophage activation. *Human immunology* 70: 325-330.

6. van Furth, R, and Cohn, ZA (1968). The origin and kinetics of mononuclear phagocytes. *The Journal of experimental medicine* 128: 415-435.

7. Varol, C, Mildner, A, and Jung, S (2015). Macrophages: development and tissue specialization. *Annual review of immunology* 33: 643-675.

8. Ginhoux, F, Greter, M, Leboeuf, M, Nandi, S, See, P, Gokhan, S*, et al.* (2010). Fate mapping analysis reveals that adult microglia derive from primitive macrophages. *Science* 330: 841-845.

9. Guilliams, M, De Kleer, I, Henri, S, Post, S, Vanhoutte, L, De Prijck, S*, et al.* (2013). Alveolar macrophages develop from fetal monocytes that differentiate into long-lived cells in the first week of life via GMCSF. *The Journal of experimental medicine* 210: 1977-1992.

10. Hoeffel, G, and Ginhoux, F (2015). Ontogeny of Tissue-Resident Macrophages. *Frontiers in immunology* 6: 486.

11. Kawakami, T, Lichtnekert, J, Thompson, LJ, Karna, P, Bouabe, H, Hohl, TM*, et al.* (2013). Resident renal mononuclear phagocytes comprise five discrete populations with distinct phenotypes and functions. *J Immunol* 191: 3358-3372.

12. Sheng, J, Ruedl, C, and Karjalainen, K (2015). Most Tissue-Resident Macrophages Except Microglia Are Derived from Fetal Hematopoietic Stem Cells. *Immunity* 43: 382-393.

13. Yona, S, Kim, KW, Wolf, Y, Mildner, A, Varol, D, Breker, M*, et al.* (2013). Fate mapping reveals origins and dynamics of monocytes and tissue macrophages under homeostasis. *Immunity* 38: 79-91.

14. Soucie, EL, Weng, Z, Geirsdottir, L, Molawi, K, Maurizio, J, Fenouil, R*, et al.* (2016). Lineage-specific enhancers activate self-renewal genes in macrophages and embryonic stem cells. *Science* 351: aad5510.

15. Jenkins, SJ, Ruckerl, D, Cook, PC, Jones, LH, Finkelman, FD, van Rooijen, N*, et al.* (2011). Local macrophage proliferation, rather than recruitment from the blood, is a signature of TH2 inflammation. *Science* 332: 1284-1288.

16. Bain, CC, Bravo-Blas, A, Scott, CL, Gomez Perdiguero, E, Geissmann, F, Henri, S*, et al.* (2014). Constant replenishment from circulating monocytes maintains the macrophage pool in the intestine of adult mice. *Nature immunology* 15: 929-937.

17. Molawi, K, Wolf, Y, Kandalla, PK, Favret, J, Hagemeyer, N, Frenzel, K*, et al.* (2014). Progressive replacement of embryo-derived cardiac macrophages with age. *The Journal of experimental medicine* 211: 2151-2158.

18. Tamoutounour, S, Guilliams, M, Montanana Sanchis, F, Liu, H, Terhorst, D, Malosse, C*, et al.* (2013). Origins and functional specialization of macrophages and of conventional and monocyte-derived dendritic cells in mouse skin. *Immunity* 39: 925-938.

19. Franklin, RA, Liao, W, Sarkar, A, Kim, MV, Bivona, MR, Liu, K*, et al.* (2014). The cellular and molecular origin of tumor-associated macrophages. *Science* 344: 921-925.

20. Epelman, S, Lavine, KJ, Beaudin, AE, Sojka, DK, Carrero, JA, Calderon, B*, et al.* (2014). Embryonic and adult-derived resident cardiac macrophages are maintained through distinct mechanisms at steady state and during inflammation. *Immunity* 40: 91-104.

21. Happle, C, Lachmann, N, Skuljec, J, Wetzke, M, Ackermann, M, Brennig, S*, et al.* (2014). Pulmonary transplantation of macrophage progenitors as effective and long-lasting therapy for hereditary pulmonary alveolar proteinosis. *Science translational medicine* 6: 250ra113.

22. Suzuki, T, Arumugam, P, Sakagami, T, Lachmann, N, Chalk, C, Sallese, A*, et al.* (2014). Pulmonary macrophage transplantation therapy. *Nature* 514: 450-454.

23. Haldar, M, Kohyama, M, So, AY, Kc, W, Wu, X, Briseno, CG*, et al.* (2014). Heme-mediated SPI-C induction promotes monocyte differentiation into iron-recycling macrophages. *Cell* 156: 1223-1234.

24. Okabe, Y, and Medzhitov, R (2014). Tissue-specific signals control reversible program of localization and functional polarization of macrophages. *Cell* 157: 832-844.

25. Schneider, C, Nobs, SP, Kurrer, M, Rehrauer, H, Thiele, C, and Kopf, M (2014). Induction of the nuclear receptor PPAR-gamma by the cytokine GMCSF is critical for the differentiation of fetal monocytes into alveolar macrophages. *Nature immunology* 15: 1026-1037.

26. Glass, CK (2015). Genetic and genomic approaches to understanding macrophage identity and function. *Arteriosclerosis, thrombosis, and vascular biology* 35: 755-762.

27. Lavin, Y, Winter, D, Blecher-Gonen, R, David, E, Keren-Shaul, H, Merad, M*, et al.* (2014). Tissue-resident macrophage enhancer landscapes are shaped by the local microenvironment. *Cell* 159: 1312-1326.

28. Martinez, FO, and Gordon, S (2015). The evolution of our understanding of macrophages and translation of findings toward the clinic. *Expert review of clinical immunology* 11: 5-13.

29. Zhang, X, Goncalves, R, and Mosser, DM (2008). The isolation and characterization of murine macrophages. *Current protocols in immunology / edited by John E Coligan [et al]* Chapter 14: Unit 14 11.

30. Mosser, DM, and Zhang, X (2008). Activation of murine macrophages. *Current protocols in immunology / edited by John E Coligan [et al]* Chapter 14: Unit 14 12.

31. Chitu, V, Yeung, YG, Yu, W, Nandi, S, and Stanley, ER (2011). Measurement of macrophage growth and differentiation. *Current protocols in immunology / edited by John E Coligan [et al]* Chapter 14: Unit 14 20 11-26.

32. Francke, A, Herold, J, Weinert, S, Strasser, RH, and Braun-Dullaeus, RC (2011). Generation of mature murine monocytes from heterogeneous bone marrow and description of their properties. *The journal of histochemistry and cytochemistry : official journal of the Histochemistry Society* 59: 813-825.

33. Redecke, V, Wu, R, Zhou, J, Finkelstein, D, Chaturvedi, V, High, AA*, et al.* (2013). Hematopoietic progenitor cell lines with myeloid and lymphoid potential. *Nature methods* 10: 795-803.

34. Wang, GG, Calvo, KR, Pasillas, MP, Sykes, DB, Hacker, H, and Kamps, MP (2006). Quantitative production of macrophages or neutrophils ex vivo using conditional Hoxb8. *Nature methods* 3: 287-293.

35. Gautier, EL, Shay, T, Miller, J, Greter, M, Jakubzick, C, Ivanov, S*, et al.* (2012). Gene-expression profiles and transcriptional regulatory pathways that underlie the identity and diversity of mouse tissue macrophages. *Nature immunology* 13: 1118-1128.

36. Mills, CD, Kincaid, K, Alt, JM, Heilman, MJ, and Hill, AM (2000). M-1/M-2 macrophages and the Th1/Th2 paradigm. *J Immunol* 164: 6166-6173.

37. Murray, PJ, Allen, JE, Biswas, SK, Fisher, EA, Gilroy, DW, Goerdt, S*, et al.* (2014). Macrophage activation and polarization: nomenclature and experimental guidelines. *Immunity* 41: 14-20.

38. Lawrence, T, and Natoli, G (2011). Transcriptional regulation of macrophage polarization: enabling diversity with identity. *Nature reviews Immunology* 11: 750-761.

39. Takaoka, A, Yanai, H, Kondo, S, Duncan, G, Negishi, H, Mizutani, T*, et al.* (2005). Integral role of IRF-5 in the gene induction programme activated by Toll-like receptors. *Nature* 434: 243-249.

40. Takeda, K, Tanaka, T, Shi, W, Matsumoto, M, Minami, M, Kashiwamura, S*, et al.* (1996). Essential role of Stat6 in IL-4 signalling. *Nature* 380: 627-630.

41. Krausgruber, T, Blazek, K, Smallie, T, Alzabin, S, Lockstone, H, Sahgal, N*, et al.* (2011). IRF5 promotes inflammatory macrophage polarization and TH1-TH17 responses. *Nature immunology* 12: 231-238.

42. Ohmori, Y, and Hamilton, TA (1998). STAT6 is required for the anti-inflammatory activity of interleukin-4 in mouse peritoneal macrophages. *The Journal of biological chemistry* 273: 29202-29209.

43. Ankrum, J, and Karp, JM (2010). Mesenchymal stem cell therapy: Two steps forward, one step back. *Trends in molecular medicine* 16: 203-209.

44. Horwitz, EM, Prockop, DJ, Fitzpatrick, LA, Koo, WW, Gordon, PL, Neel, M*, et al.* (1999). Transplantability and therapeutic effects of bone marrow-derived mesenchymal cells in children with osteogenesis imperfecta. *Nature medicine* 5: 309-313.

45. Koc, ON, Day, J, Nieder, M, Gerson, SL, Lazarus, HM, and Krivit, W (2002). Allogeneic mesenchymal stem cell infusion for treatment of metachromatic leukodystrophy (MLD) and Hurler syndrome (MPS-IH). *Bone marrow transplantation* 30: 215-222.

46. Otsuru, S, Gordon, PL, Shimono, K, Jethva, R, Marino, R, Phillips, CL*, et al.* (2012). Transplanted bone marrow mononuclear cells and MSCs impart clinical benefit to children with osteogenesis imperfecta through different mechanisms. *Blood* 120: 1933-1941.

47. Horwitz, EM, Prockop, DJ, Gordon, PL, Koo, WW, Fitzpatrick, LA, Neel, MD*, et al.* (2001). Clinical responses to bone marrow transplantation in children with severe osteogenesis imperfecta. *Blood* 97: 1227-1231.

48. Kim, SU (2014). Lysosomal storage diseases: Stem cell-based cell- and gene-therapy. *Cell transplantation*.

49. Orozco, L, Munar, A, Soler, R, Alberca, M, Soler, F, Huguet, M*, et al.* (2013). Treatment of knee osteoarthritis with autologous mesenchymal stem cells: a pilot study. *Transplantation* 95: 1535-1541.

50. Orozco, L, Soler, R, Morera, C, Alberca, M, Sanchez, A, and Garcia-Sancho, J (2011). Intervertebral disc repair by autologous mesenchymal bone marrow cells: a pilot study. *Transplantation* 92: 822-828.

51. Segers, VF, and Lee, RT (2008). Stem-cell therapy for cardiac disease. *Nature* 451: 937-942.

52. Garbern, JC, and Lee, RT (2013). Cardiac stem cell therapy and the promise of heart regeneration. *Cell stem cell* 12: 689-698.

53. Lee, RH, Pulin, AA, Seo, MJ, Kota, DJ, Ylostalo, J, Larson, BL*, et al.* (2009). Intravenous hMSCs improve myocardial infarction in mice because cells embolized in lung are activated to secrete the anti-inflammatory protein TSG-6. *Cell stem cell* 5: 54-63.

54. Clifford, DM, Fisher, SA, Brunskill, SJ, Doree, C, Mathur, A, Watt, S*, et al.* (2012). Stem cell treatment for acute myocardial infarction. *The Cochrane database of systematic reviews*: CD006536.

55. Trounson, A, and McDonald, C (2015). Stem Cell Therapies in Clinical Trials: Progress and Challenges. *Cell stem cell* 17: 11-22.

56. Trounson, A, and DeWitt, ND (2016). Pluripotent stem cells progressing to the clinic. *Nature reviews Molecular cell biology* 17: 194-200.

57. Rosenberg, SA, Restifo, NP, Yang, JC, Morgan, RA, and Dudley, ME (2008). Adoptive cell transfer: a clinical path to effective cancer immunotherapy. *Nature reviews Cancer* 8: 299-308.

58. Rosenberg, SA, and Dudley, ME (2009). Adoptive cell therapy for the treatment of patients with metastatic melanoma. *Current opinion in immunology* 21: 233-240.

59. Bonini, C, and Mondino, A (2015). Adoptive T-cell therapy for cancer: The era of engineered T cells. *European journal of immunology* 45: 2457-2469.

60. Zhang, L, Conejo-Garcia, JR, Katsaros, D, Gimotty, PA, Massobrio, M, Regnani, G*, et al.* (2003). Intratumoral T cells, recurrence, and survival in epithelial ovarian cancer. *The New England journal of medicine* 348: 203-213.

61. Clemente, CG, Mihm, MC, Jr., Bufalino, R, Zurrida, S, Collini, P, and Cascinelli, N (1996). Prognostic value of tumor infiltrating lymphocytes in the vertical growth phase of primary cutaneous melanoma. *Cancer* 77: 1303-1310.

62. Rosenberg, SA, Spiess, P, and Lafreniere, R (1986). A new approach to the adoptive immunotherapy of cancer with tumor-infiltrating lymphocytes. *Science* 233: 1318-1321.

63. Rosenberg, SA, Yannelli, JR, Yang, JC, Topalian, SL, Schwartzentruber, DJ, Weber, JS*, et al.* (1994). Treatment of patients with metastatic melanoma with autologous tumor-infiltrating lymphocytes and interleukin 2. *Journal of the National Cancer Institute* 86: 1159-1166.

64. Geukes Foppen, MH, Donia, M, Svane, IM, and Haanen, JB (2015). Tumor-infiltrating lymphocytes for the treatment of metastatic cancer. *Molecular oncology* 9: 1918-1935.

65. Khammari, A, Knol, AC, Nguyen, JM, Bossard, C, Denis, MG, Pandolfino, MC*, et al.* (2014). Adoptive TIL transfer in the adjuvant setting for melanoma: long-term patient survival. *Journal of immunology research* 2014: 186212.

66. Weber, JS (2014). At the bedside: adoptive cell therapy for melanoma-clinical development. *Journal of leukocyte biology* 95: 875-882.

67. Wu, R, Forget, MA, Chacon, J, Bernatchez, C, Haymaker, C, Chen, JQ*, et al.* (2012). Adoptive T-cell therapy using autologous tumor-infiltrating lymphocytes for metastatic melanoma: current status and future outlook. *Cancer J* 18: 160-175.

68. Lee, S, and Margolin, K (2012). Tumor-infiltrating lymphocytes in melanoma. *Current oncology reports* 14: 468-474.

69. Dudley, ME, Yang, JC, Sherry, R, Hughes, MS, Royal, R, Kammula, U*, et al.* (2008). Adoptive cell therapy for patients with metastatic melanoma: evaluation of intensive myeloablative chemoradiation preparative regimens. *Journal of clinical oncology : official journal of the American Society of Clinical Oncology* 26: 5233-5239.

70. Dudley, ME, Wunderlich, JR, Robbins, PF, Yang, JC, Hwu, P, Schwartzentruber, DJ*, et al.* (2002). Cancer regression and autoimmunity in patients after clonal repopulation with antitumor lymphocytes. *Science* 298: 850-854.

71. Fesnak, AD, June, CH, and Levine, BL (2016). Engineered T cells: the promise and challenges of cancer immunotherapy. *Nature reviews Cancer* 16: 566-581.

72. Jackson, HJ, Rafiq, S, and Brentjens, RJ (2016). Driving CAR T-cells forward. *Nature reviews Clinical oncology* 13: 370-383.

73. Maude, SL, Frey, N, Shaw, PA, Aplenc, R, Barrett, DM, Bunin, NJ*, et al.* (2014). Chimeric antigen receptor T cells for sustained remissions in leukemia. *The New England journal of medicine* 371: 1507-1517.

74. Grupp, SA, Kalos, M, Barrett, D, Aplenc, R, Porter, DL, Rheingold, SR*, et al.* (2013). Chimeric antigen receptor-modified T cells for acute lymphoid leukemia. *The New England journal of medicine* 368: 1509-1518.

75. Brentjens, RJ, Davila, ML, Riviere, I, Park, J, Wang, X, Cowell, LG*, et al.* (2013). CD19-targeted T cells rapidly induce molecular remissions in adults with chemotherapy-refractory acute lymphoblastic leukemia. *Science translational medicine* 5: 177ra138.

76. Turtle, CJ, Hanafi, LA, Berger, C, Hudecek, M, Pender, B, Robinson, E*, et al.* (2016). Immunotherapy of non-Hodgkin's lymphoma with a defined ratio of CD8+ and CD4+ CD19-specific chimeric antigen receptor-modified T cells. *Science translational medicine* 8: 355ra116.

77. Kochenderfer, JN, Dudley, ME, Kassim, SH, Somerville, RP, Carpenter, RO, Stetler-Stevenson, M*, et al.* (2015). Chemotherapy-refractory diffuse large B-cell lymphoma and indolent B-cell malignancies can be effectively treated with autologous T cells expressing an anti-CD19 chimeric antigen receptor. *Journal of clinical oncology : official journal of the American Society of Clinical Oncology* 33: 540-549.

78. Davila, ML, Riviere, I, Wang, X, Bartido, S, Park, J, Curran, K*, et al.* (2014). Efficacy and toxicity management of 19-28z CAR T cell therapy in B cell acute lymphoblastic leukemia. *Science translational medicine* 6: 224ra225.

79. Scholler, J, Brady, TL, Binder-Scholl, G, Hwang, WT, Plesa, G, Hege, KM*, et al.* (2012). Decade-long safety and function of retroviral-modified chimeric antigen receptor T cells. *Science translational medicine* 4: 132ra153.

80. Adams, B (2016). Rivals Kite and Novartis post new CAR-T data as both plot FDA approval http://www.fiercebiotech.com/biotech/rivals-kite-and-novartis-post-new-car-t-data-as-both-plot-fda-approval.

81. Norelli, M, Casucci, M, Bonini, C, and Bondanza, A (2016). Clinical pharmacology of CAR-T cells: Linking cellular pharmacodynamics to pharmacokinetics and antitumor effects. *Biochimica et biophysica acta* 1865: 90-100.

82. Caruana, I, Savoldo, B, Hoyos, V, Weber, G, Liu, H, Kim, ES*, et al.* (2015). Heparanase promotes tumor infiltration and antitumor activity of CAR-redirected T lymphocytes. *Nature medicine* 21: 524-529.

83. Moon, EK, Wang, LC, Dolfi, DV, Wilson, CB, Ranganathan, R, Sun, J*, et al.* (2014). Multifactorial T-cell hypofunction that is reversible can limit the efficacy of chimeric antigen receptor-transduced human T cells in solid tumors. *Clinical cancer research : an official journal of the American Association for Cancer Research* 20: 4262-4273.

84. Ahmed, N, Brawley, VS, Hegde, M, Robertson, C, Ghazi, A, Gerken, C*, et al.* (2015). Human Epidermal Growth Factor Receptor 2 (HER2) -Specific Chimeric Antigen Receptor-Modified T Cells for the Immunotherapy of HER2-Positive Sarcoma. *Journal of clinical oncology : official journal of the American Society of Clinical Oncology* 33: 1688-1696.

85. John, LB, Devaud, C, Duong, CP, Yong, CS, Beavis, PA, Haynes, NM*, et al.* (2013). Anti-PD-1 antibody therapy potently enhances the eradication of established tumors by gene-modified T cells. *Clinical cancer research : an official journal of the American Association for Cancer Research* 19: 5636-5646.

86. Chinnasamy, D, Yu, Z, Kerkar, SP, Zhang, L, Morgan, RA, Restifo, NP*, et al.* (2012). Local delivery of interleukin-12 using T cells targeting VEGF receptor-2 eradicates multiple vascularized tumors in mice. *Clinical cancer research : an official journal of the American Association for Cancer Research* 18: 1672-1683.

87. Kershaw, MH, Westwood, JA, Parker, LL, Wang, G, Eshhar, Z, Mavroukakis, SA*, et al.* (2006). A phase I study on adoptive immunotherapy using gene-modified T cells for ovarian cancer. *Clinical cancer research : an official journal of the American Association for Cancer Research* 12: 6106-6115.

88. Chinnasamy, D, Yu, Z, Theoret, MR, Zhao, Y, Shrimali, RK, Morgan, RA*, et al.* (2010). Gene therapy using genetically modified lymphocytes targeting VEGFR-2 inhibits the growth of vascularized syngenic tumors in mice. *The Journal of clinical investigation* 120: 3953-3968.

89. Fidler, IJ (1974). Inhibition of pulmonary metastasis by intravenous injection of specifically activated macrophages. *Cancer Res* 34: 1074-1078.

90. Fidler, IJ, and Poste, G (1982). Macrophage-mediated destruction of malignant tumor cells and new strategies for the therapy of metastatic disease. *Springer seminars in immunopathology* 5: 161-174.

91. Fidler, IJ, Barnes, Z, Fogler, WE, Kirsh, R, Bugelski, P, and Poste, G (1982). Involvement of macrophages in the eradication of established metastases following intravenous injection of liposomes containing macrophage activators. *Cancer Res* 42: 496-501.

92. Andreesen, R, Hennemann, B, and Krause, SW (1998). Adoptive immunotherapy of cancer using monocyte-derived macrophages: rationale, current status, and perspectives. *Journal of leukocyte biology* 64: 419-426.

93. Faradji, A, Bohbot, A, Schmitt-Goguel, M, Siffert, JC, Dumont, S, Wiesel, ML*, et al.* (1994). Large scale isolation of human blood monocytes by continuous flow centrifugation leukapheresis and counterflow centrifugation elutriation for adoptive cellular immunotherapy in cancer patients. *Journal of immunological methods* 174: 297-309.

94. Andreesen, R, Scheibenbogen, C, Brugger, W, Krause, S, Meerpohl, HG, Leser, HG*, et al.* (1990). Adoptive transfer of tumor cytotoxic macrophages generated in vitro from circulating blood monocytes: a new approach to cancer immunotherapy. *Cancer Res* 50: 7450-7456.

95. Tey, SK (2014). Adoptive T-cell therapy: adverse events and safety switches. *Clinical & translational immunology* 3: e17.

96. Stevenson, HC, Keenan, AM, Woodhouse, C, Ottow, RT, Miller, P, Steller, EP*, et al.* (1987). Fate of gamma-interferon-activated killer blood monocytes adoptively transferred into the abdominal cavity of patients with peritoneal carcinomatosis. *Cancer Res* 47: 6100-6103.

97. Quillien, V, Moisan, A, Lesimple, T, Leberre, C, and Toujas, L (2001). Biodistribution of 111indium-labeled macrophages infused intravenously in patients with renal carcinoma. *Cancer immunology, immunotherapy : CII* 50: 477-482.

98. Eggenhofer, E, Benseler, V, Kroemer, A, Popp, FC, Geissler, EK, Schlitt, HJ*, et al.* (2012). Mesenchymal stem cells are short-lived and do not migrate beyond the lungs after intravenous infusion. *Frontiers in immunology* 3: 297.

99. Karp, JM, and Leng Teo, GS (2009). Mesenchymal stem cell homing: the devil is in the details. *Cell stem cell* 4: 206-216.

100. Faradji, A, Bohbot, A, Schmitt-Goguel, M, Roeslin, N, Dumont, S, Wiesel, ML*, et al.* (1991). Phase I trial of intravenous infusion of ex-vivo-activated autologous blood-derived macrophages in patients with non-small-cell lung cancer: toxicity and immunomodulatory effects. *Cancer immunology, immunotherapy : CII* 33: 319-326.

101. Hennemann, B, Scheibenbogen, C, Schiimichen, C, and Andreesen, R (1995). Intrahepatic Adoptive Immunotherapy with Autologous Tumorcytotoxic Macrophages in Patients with Cancer. *Journal of Immunotherapy* 18: 19-27.

102. Faradji, A, Bohbot, A, Frost, H, Schmitt-Goguel, M, Siffert, JC, Dufour, P*, et al.* (1991). Phase I study of liposomal MTP-PE-activated autologous monocytes administered intraperitoneally to patients with peritoneal carcinomatosis. *Journal of clinical oncology : official journal of the American Society of Clinical Oncology* 9: 1251-1260.

103. Ritchie, D, Mileshkin, L, Wall, D, Bartholeyns, J, Thompson, M, Coverdale, J*, et al.* (2007). In vivo tracking of macrophage activated killer cells to sites of metastatic ovarian carcinoma. *Cancer immunology, immunotherapy : CII* 56: 155-163.

104. Burger, M, Thiounn, N, Denzinger, S, Kondas, J, Benoit, G, Chapado, MS*, et al.* (2010). The application of adjuvant autologous antravesical macrophage cell therapy vs.

BCG in non-muscle invasive bladder cancer: a multicenter, randomized trial. *Journal of translational medicine* 8: 54.

105. Dumont, S, Hartmann, D, Poindron, P, Oberling, F, Faradji, A, and Bartholeyns, J (1988). Control of the antitumoral activity of human macrophages produced in large amounts in view of adoptive transfer. *European Journal of Cancer and Clinical Oncology* 24: 1691-1698.

106. Okabe, Y, and Medzhitov, R (2015). Tissue biology perspective on macrophages. *Nature immunology* 17: 9-17.

107. Ruffell, B, Affara, NI, and Coussens, LM (2012). Differential macrophage programming in the tumor microenvironment. *Trends in immunology* 33: 119-126.

108. Squadrito, ML, and De Palma, M (2011). Macrophage regulation of tumor angiogenesis: implications for cancer therapy. *Molecular aspects of medicine* 32: 123-145.

109. Mosser, DM, and Edwards, JP (2008). Exploring the full spectrum of macrophage activation. *Nature reviews Immunology* 8: 958-969.

110. Bartel, RL, Cramer, C, Ledford, K, Longcore, A, Parrish, C, Stern, T*, et al.* (2012). The Aastrom experience. *Stem cell research & therapy* 3: 26.

111. Ledford, KJ, Zeigler, F, and Bartel, RL (2013). Ixmyelocel-T, an expanded multicellular therapy, contains a unique population of M2-like macrophages. *Stem cell research & therapy* 4: 134.

112. Henry, TD, Traverse, JH, Hammon, BL, East, CA, Bruckner, B, Remmers, AE*, et al.* (2014). Safety and efficacy of ixmyelocel-T: an expanded, autologous multi-cellular therapy, in dilated cardiomyopathy. *Circulation research* 115: 730-737.

113. Powell, RJ, Marston, WA, Berceli, SA, Guzman, R, Henry, TD, Longcore, AT*, et al.* (2012). Cellular therapy with Ixmyelocel-T to treat critical limb ischemia: the randomized, double-blind, placebo-controlled RESTORE-CLI trial. *Molecular therapy : the journal of the American Society of Gene Therapy* 20: 1280-1286.

114. Eymard, JC, Lopez, M, Cattan, A, Bouché, O, Adjizian, JC, and Bernard, J (1996). Phase I/II trial of autologous activated macrophages in advanced colorectal cancer. *European Journal of Cancer* 32: 1905-1911.

115. Hennemann, B, Beckmann, G, Eichelmann, A, Rehm, A, and Andreesen, R (1998). Phase I trial of adoptive immunotherapy of cancer patients using monocyte-derived macrophages activated with interferon gamma and lipopolysaccharide. *Cancer immunology, immunotherapy : CII* 45: 250-256.

116. Lesimple, T, Moisan, A, Guille, F, Leberre, C, Audran, R, Drenou, B*, et al.* (2000). Treatment of metastatic renal cell carcinoma with activated autologous macrophages and granulocyte--macrophage colony-stimulating factor. *J Immunother* 23: 675-679.

117. Baron-Bodo, V, Doceur, P, Lefebvre, ML, Labroquere, K, Defaye, C, Cambouris, C*, et al.* (2005). Anti-tumor properties of human-activated macrophages produced in large scale for clinical application. *Immunobiology* 210: 267-277.

118. Cao, Q, Wang, Y, Zheng, D, Sun, Y, Wang, C, Wang, XM*, et al.* (2014). Failed renoprotection by alternatively activated bone marrow macrophages is due to a proliferation-dependent phenotype switch in vivo. *Kidney international* 85: 794-806.

119. Wang, Y, Wang, YP, Zheng, G, Lee, VW, Ouyang, L, Chang, DH*, et al.* (2007). Ex vivo programmed macrophages ameliorate experimental chronic inflammatory renal disease. *Kidney international* 72: 290-299.

120. Sindrilaru, A, Peters, T, Wieschalka, S, Baican, C, Baican, A, Peter, H*, et al.* (2011). An unrestrained proinflammatory M1 macrophage population induced by iron impairs wound healing in humans and mice. *The Journal of clinical investigation* 121: 985-997.

121. Leovsky, C, Fabian, C, Naaldijk, Y, Jager, C, Jang, HJ, Bohme, J*, et al.* (2015). Biodistribution of in vitro-derived microglia applied intranasally and intravenously to mice: effects of aging. *Cytotherapy* 17: 1617-1626.

122. Hanke, ML, Heim, CE, Angle, A, Sanderson, SD, and Kielian, T (2013). Targeting macrophage activation for the prevention and treatment of Staphylococcus aureus biofilm infections. *J Immunol* 190: 2159-2168.

123. Ilium, L, Davis, SS, Wilson, CG, Thomas, NW, Frier, M, and Hardy, JG (1982). Blood clearance and organ deposition of intravenously administered colloidal particles. The effects of particle size, nature and shape. *International journal of pharmaceutics* 12: 135-146.

124. Patel, HM, and Moghimi, SM (1998). Serum-mediated recognition of liposomes by phagocytic cells of the reticuloendothelial system - The concept of tissue specificity. *Advanced drug delivery reviews* 32: 45-60.

125. Moghimi, SM, Hunter, AC, and Murray, JC (2001). Long-circulating and target-specific nanoparticles: theory to practice. *Pharmacological reviews* 53: 283-318.

126. Petros, RA, and DeSimone, JM (2010). Strategies in the design of nanoparticles for therapeutic applications. *Nature reviews Drug discovery* 9: 615-627.

127. Patel, SK, and Janjic, JM (2015). Macrophage targeted theranostics as personalized nanomedicine strategies for inflammatory diseases. *Theranostics* 5: 150-172.

128. Ahsan, F, Rivas, IP, Khan, MA, and Torres Suarez, AI (2002). Targeting to macrophages: role of physicochemical properties of particulate carriers--liposomes and microspheres--on the phagocytosis by macrophages. *Journal of controlled release : official journal of the Controlled Release Society* 79: 29-40.

129. Champion, JA, Katare, YK, and Mitragotri, S (2007). Particle shape: a new design parameter for micro- and nanoscale drug delivery carriers. *Journal of controlled release : official journal of the Controlled Release Society* 121: 3-9.

130. He, C, Hu, Y, Yin, L, Tang, C, and Yin, C (2010). Effects of particle size and surface charge on cellular uptake and biodistribution of polymeric nanoparticles. *Biomaterials* 31: 3657-3666.

131. Lee, WH, Loo, CY, Traini, D, and Young, PM (2015). Nano- and micro-based inhaled drug delivery systems for targeting alveolar macrophages. *Expert opinion on drug delivery* 12: 1009-1026.

132. Anselmo, AC, and Mitragotri, S (2016). Impact of particle elasticity on particle-based drug delivery systems. *Advanced drug delivery reviews*.

133. Otto, DP, Otto, A, and de Villiers, MM (2015). Differences in physicochemical properties to consider in the design, evaluation and choice between microparticles and nanoparticles for drug delivery. *Expert opinion on drug delivery* 12: 763-777.

134. Bareford, LM, and Swaan, PW (2007). Endocytic mechanisms for targeted drug delivery. *Advanced drug delivery reviews* 59: 748-758.

135. Khalil, IA, Kogure, K, Akita, H, and Harashima, H (2006). Uptake pathways and subsequent intracellular trafficking in nonviral gene delivery. *Pharmacological reviews* 58: 32-45.

136. Rajendran, L, Knolker, HJ, and Simons, K (2010). Subcellular targeting strategies for drug design and delivery. *Nature reviews Drug discovery* 9: 29-42.

137. Batrakova, EV, Gendelman, HE, and Kabanov, AV (2011). Cell-mediated drug delivery. *Expert opinion on drug delivery* 8: 415-433.

138. Haney, MJ, Zhao, Y, Harrison, EB, Mahajan, V, Ahmed, S, He, Z*, et al.* (2013). Specific transfection of inflamed brain by macrophages: a new therapeutic strategy for neurodegenerative diseases. *Plos One* 8: e61852.

139. Zhao, Y, Haney, MJ, Mahajan, V, Reiner, BC, Dunaevsky, A, Mosley, RL*, et al.* (2011). Active Targeted Macrophage-mediated Delivery of Catalase to Affected Brain Regions in Models of Parkinson's Disease. *Journal of nanomedicine & nanotechnology* S4.

140. Brynskikh, AM, Zhao, Y, Mosley, RL, Li, S, Boska, MD, Klyachko, NL*, et al.* (2010). Macrophage delivery of therapeutic nanozymes in a murine model of Parkinson's disease. *Nanomedicine (Lond)* 5: 379-396.

141. Nowacek, AS, Miller, RL, McMillan, J, Kanmogne, G, Kanmogne, M, Mosley, RL*, et al.* (2009). NanoART synthesis, characterization, uptake, release and toxicology for human monocyte-macrophage drug delivery. *Nanomedicine (Lond)* 4: 903-917.

142. Dou, H, Grotepas, CB, McMillan, JM, Destache, CJ, Chaubal, M, Werling, J*, et al.* (2009). Macrophage delivery of nanoformulated antiretroviral drug to the brain in a murine model of neuroAIDS. *J Immunol* 183: 661-669.

143. Batrakova, EV, Li, S, Reynolds, AD, Mosley, RL, Bronich, TK, Kabanov, AV*, et al.* (2007). A macrophage-nanozyme delivery system for Parkinson's disease. *Bioconjugate chemistry* 18: 1498-1506.

144. Dou, H, Destache, CJ, Morehead, JR, Mosley, RL, Boska, MD, Kingsley, J*, et al.* (2006). Development of a macrophage-based nanoparticle platform for antiretroviral drug delivery. *Blood* 108: 2827-2835.

145. Bressani, RF, Nowacek, AS, Singh, S, Balkundi, S, Rabinow, B, McMillan, J*, et al.* (2011). Pharmacotoxicology of monocyte-macrophage nanoformulated antiretroviral drug uptake and carriage. *Nanotoxicology* 5: 592-605.

146. Choi, J, Kim, HY, Ju, EJ, Jung, J, Park, J, Chung, HK*, et al.* (2012). Use of macrophages to deliver therapeutic and imaging contrast agents to tumors. *Biomaterials* 33: 4195-4203.

147. Zhao, Y, Haney, MJ, Gupta, R, Bohnsack, JP, He, Z, Kabanov, AV*, et al.* (2014). GDNF-transfected macrophages produce potent neuroprotective effects in Parkinson's disease mouse model. *Plos One* 9: e106867.

148. Raposo, G, and Stoorvogel, W (2013). Extracellular vesicles: exosomes, microvesicles, and friends. *The Journal of cell biology* 200: 373-383.

149. Haney, MJ, Klyachko, NL, Zhao, Y, Gupta, R, Plotnikova, EG, He, Z*, et al.* (2015). Exosomes as drug delivery vehicles for Parkinson's disease therapy. *Journal of controlled release : official journal of the Controlled Release Society* 207: 18-30.

150. Yang, TD, Choi, W, Yoon, TH, Lee, KJ, Lee, JS, Joo, JH*, et al.* (2016). In vivo photothermal treatment by the peritumoral injection of macrophages loaded with gold nanoshells. *Biomedical optics express* 7: 185-193.

151. Madsen, SJ, Baek, SK, Makkouk, AR, Krasieva, T, and Hirschberg, H (2012). Macrophages as cell-based delivery systems for nanoshells in photothermal therapy. *Annals of biomedical engineering* 40: 507-515.

152. Choi, MR, Bardhan, R, Stanton-Maxey, KJ, Badve, S, Nakshatri, H, Stantz, KM*, et al.* (2012). Delivery of nanoparticles to brain metastases of breast cancer using a cellular Trojan horse. *Cancer nanotechnology* 3: 47-54.

153. Burke, B, Sumner, S, Maitland, N, and Lewis, CE (2002). Macrophages in gene therapy: cellular delivery vehicles and in vivo targets. *Journal of leukocyte biology* 72: 417-428.

154. Jablonska, J, Leschner, S, Westphal, K, Lienenklaus, S, and Weiss, S (2010). Neutrophils responsive to endogenous IFN-beta regulate tumor angiogenesis and growth in a mouse tumor model. *The Journal of clinical investigation* 120: 1151-1164.

155. Thomas, KE, Galligan, CL, Newman, RD, Fish, EN, and Vogel, SN (2006). Contribution of interferon-beta to the murine macrophage response to the toll-like receptor 4 agonist, lipopolysaccharide. *The Journal of biological chemistry* 281: 31119-31130.

156. Koba, C, Haruta, M, Matsunaga, Y, Matsumura, K, Haga, E, Sasaki, Y*, et al.* (2013). Therapeutic effect of human iPS-cell-derived myeloid cells expressing IFN-beta against peritoneally disseminated cancer in xenograft models. *Plos One* 8: e67567.

157. Escobar, G, Moi, D, Ranghetti, A, Ozkal-Baydin, P, Squadrito, ML, Kajaste-Rudnitski, A*, et al.* (2014). Genetic engineering of hematopoiesis for targeted IFN-alpha delivery inhibits breast cancer progression. *Science translational medicine* 6: 217ra213.

158. Wang, BX, Rahbar, R, and Fish, EN (2011). Interferon: current status and future prospects in cancer therapy. *Journal of interferon & cytokine research : the official journal of the International Society for Interferon and Cytokine Research* 31: 545-552.

159. Anguille, S, Lion, E, Willemen, Y, Van Tendeloo, VF, Berneman, ZN, and Smits, EL (2011). Interferon-alpha in acute myeloid leukemia: an old drug revisited. *Leukemia : official journal of the Leukemia Society of America, Leukemia Research Fund, UK* 25: 739-748.

160. Kan, O, Day, D, Iqball, S, Burke, F, Grimshaw, MJ, Naylor, S*, et al.* (2011). Genetically modified macrophages expressing hypoxia regulated cytochrome P450 and P450 reductase for the treatment of cancer. *International journal of molecular medicine* 27: 173-180.

161. Herold, J, Pipp, F, Fernandez, B, Xing, Z, Heil, M, Tillmanns, H*, et al.* (2004). Transplantation of monocytes: a novel strategy for in vivo augmentation of collateral vessel growth. *Human gene therapy* 15: 1-12.

162. Basel, MT, Balivada, S, Shrestha, TB, Seo, GM, Pyle, MM, Tamura, M*, et al.* (2012). A cell-delivered and cell-activated SN38-dextran prodrug increases survival in a murine disseminated pancreatic cancer model. *Small* 8: 913-920.

163. Buschmann, IR, Hoefer, IE, van Royen, N, Katzer, E, Braun-Dulleaus, R, Heil, M*, et al.* (2001). GMCSF: a strong arteriogenic factor acting by amplification of monocyte function. *Atherosclerosis* 159: 343-356.

164. Rosas, M, Davies, LC, Giles, PJ, Liao, CT, Kharfan, B, Stone, TC*, et al.* (2014). The transcription factor Gata6 links tissue macrophage phenotype and proliferative renewal. *Science* 344: 645-648.

165. Kohyama, M, Ise, W, Edelson, BT, Wilker, PR, Hildner, K, Mejia, C*, et al.* (2009). Role for Spi-C in the development of red pulp macrophages and splenic iron homeostasis. *Nature* 457: 318-321.

166. Hagemann, T, Biswas, SK, Lawrence, T, Sica, A, and Lewis, CE (2009). Regulation of macrophage function in tumors: the multifaceted role of NF-kappaB. *Blood* 113: 3139-3146.

167. Hagemann, T, Lawrence, T, McNeish, I, Charles, KA, Kulbe, H, Thompson, RG*, et al.* (2008). "Re-educating" tumor-associated macrophages by targeting NF-kappaB. *The Journal of experimental medicine* 205: 1261-1268.

168. Li, Y, Zhao, L, Shi, B, Ma, S, Xu, Z, Ge, Y*, et al.* (2015). Functions of miR-146a and miR-222 in Tumor-associated Macrophages in Breast Cancer. *Scientific reports* 5: 18648.

169. Dang, W, Tang, H, Cao, H, Wang, L, Zhang, X, Tian, W*, et al.* (2015). Strategy of STAT3beta cell-specific expression in macrophages exhibits antitumor effects on mouse breast cancer. *Gene therapy* 22: 977-983.

170. Sieweke, MH, and Allen, JE (2013). Beyond stem cells: self-renewal of differentiated macrophages. *Science* 342: 1242974.

171. Aziz, A, Soucie, E, Sarrazin, S, and Sieweke, MH (2009). MafB/c-Maf deficiency enables self-renewal of differentiated functional macrophages. *Science* 326: 867-871.

172. Eggenhofer, E, Luk, F, Dahlke, MH, and Hoogduijn, MJ (2014). The life and fate of mesenchymal stem cells. *Frontiers in immunology* 5: 148.

173. Fischer, UM, Harting, MT, Jimenez, F, Monzon-Posadas, WO, Xue, H, Savitz, SI*, et al.* (2009). Pulmonary passage is a major obstacle for intravenous stem cell delivery: the pulmonary first-pass effect. *Stem cells and development* 18: 683-692.

174. Barbash, IM, Chouraqui, P, Baron, J, Feinberg, MS, Etzion, S, Tessone, A*, et al.* (2003). Systemic delivery of bone marrow-derived mesenchymal stem cells to the

infarcted myocardium: feasibility, cell migration, and body distribution. *Circulation* 108: 863-868.

175. Dubey, P (2012). Reporter gene imaging of immune responses to cancer: progress and challenges. *Theranostics* 2: 355-362.

176. Pajarinen, J, Lin, TH, Sato, T, Loi, F, Yao, Z, Konttinen, YT*, et al.* (2015). Establishment of Green Fluorescent Protein and Firefly Luciferase Expressing Mouse Primary Macrophages for In Vivo Bioluminescence Imaging. *Plos One* 10: e0142736.

177. Wang, X, Rosol, M, Ge, S, Peterson, D, McNamara, G, Pollack, H*, et al.* (2003). Dynamic tracking of human hematopoietic stem cell engraftment using in vivo bioluminescence imaging. *Blood* 102: 3478-3482.

178. Park, JS, Suryaprakash, S, Lao, YH, and Leong, KW (2015). Engineering mesenchymal stem cells for regenerative medicine and drug delivery. *Methods* 84: 3-16.

179. Corradetti, B, and Ferrari, M (2015). Nanotechnology for mesenchymal stem cell therapies. *Journal of controlled release : official journal of the Controlled Release Society*.

180. Assis, AC, Carvalho, JL, Jacoby, BA, Ferreira, RL, Castanheira, P, Diniz, SO*, et al.* (2010). Time-dependent migration of systemically delivered bone marrow mesenchymal stem cells to the infarcted heart. *Cell transplantation* 19: 219-230.

181. Ge, J, Guo, L, Wang, S, Zhang, Y, Cai, T, Zhao, RC*, et al.* (2014). The size of mesenchymal stem cells is a significant cause of vascular obstructions and stroke. *Stem cell reviews* 10: 295-303.

182. Guilak, F, Erickson, GR, and Ting-Beall, HP (2002). The effects of osmotic stress on the viscoelastic and physical properties of articular chondrocytes. *Biophysical journal* 82: 720-727.

183. Kiehl, TR, Shen, D, Khattak, SF, Jian Li, Z, and Sharfstein, ST (2011). Observations of cell size dynamics under osmotic stress. *Cytometry Part A : the journal of the International Society for Analytical Cytology* 79: 560-569.

184. Elmoazzen, HY, Chan, CC, Acker, JP, Elliott, JA, and McGann, LE (2005). The effect of cell size distribution on predicted osmotic responses of cells. *Cryo letters* 26: 147-158.

185. Burke, AM, Quest, DO, Chien, S, and Cerri, C (1981). The effects of mannitol on blood viscosity. *Journal of neurosurgery* 55: 550-553.

186. Janowski, M, Lyczek, A, Engels, C, Xu, J, Lukomska, B, Bulte, JW*, et al.* (2013). Cell size and velocity of injection are major determinants of the safety of intracarotid stem cell transplantation. *Journal of cerebral blood flow and metabolism : official journal of the International Society of Cerebral Blood Flow and Metabolism* 33: 921-927.

187. Aguado, BA, Mulyasasmita, W, Su, J, Lampe, KJ, and Heilshorn, SC (2012). Improving viability of stem cells during syringe needle flow through the design of hydrogel cell carriers. *Tissue engineering Part A* 18: 806-815.

188. Wong Po Foo, CT, Lee, JS, Mulyasasmita, W, Parisi-Amon, A, and Heilshorn, SC (2009). Two-component protein-engineered physical hydrogels for cell encapsulation. *Proceedings of the National Academy of Sciences of the United States of America* 106: 22067-22072.

189. Parisi-Amon, A, Mulyasasmita, W, Chung, C, and Heilshorn, SC (2013). Protein-engineered injectable hydrogel to improve retention of transplanted adipose-derived stem cells. *Advanced healthcare materials* 2: 428-432.

190. Mulyasasmita, W, Cai, L, Dewi, RE, Jha, A, Ullmann, SD, Luong, RH*, et al.* (2014). Avidity-controlled hydrogels for injectable co-delivery of induced pluripotent stem cell-derived endothelial cells and growth factors. *Journal of controlled release : official journal of the Controlled Release Society* 191: 71-81.

191. Laflamme, MA, Chen, KY, Naumova, AV, Muskheli, V, Fugate, JA, Dupras, SK*, et al.* (2007). Cardiomyocytes derived from human embryonic stem cells in pro-survival factors enhance function of infarcted rat hearts. *Nature biotechnology* 25: 1015-1024.

192. Covarrubias, AJ, Aksoylar, HI, Yu, J, Snyder, NW, Worth, AJ, Iyer, SS*, et al.* (2016). Akt-mTORC1 signaling regulates Acly to integrate metabolic input to control of macrophage activation. *eLife* 5.

193. Schrepfer, S, Deuse, T, Reichenspurner, H, Fischbein, MP, Robbins, RC, and Pelletier, MP (2007). Stem cell transplantation: the lung barrier. *Transplantation proceedings* 39: 573-576.

194. van Rooijen, N, and Hendrikx, E (2010). Liposomes for specific depletion of macrophages from organs and tissues. *Methods Mol Biol* 605: 189-203.

195. Forraz, N, Pettengell, R, and McGuckin, CP (2004). Characterization of a lineage-negative stem-progenitor cell population optimized for ex vivo expansion and enriched for LTC-IC. *Stem Cells* 22: 100-108.

196. Spencer, JA, Ferraro, F, Roussakis, E, Klein, A, Wu, J, Runnels, JM*, et al.* (2014). Direct measurement of local oxygen concentration in the bone marrow of live animals. *Nature* 508: 269-273.

197. Mantovani, A, Sozzani, S, Locati, M, Allavena, P, and Sica, A (2002). Macrophage polarization: tumor-associated macrophages as a paradigm for polarized M2 mononuclear phagocytes. *Trends in immunology* 23: 549-555.

198. Gordon, S, and Taylor, PR (2005). Monocyte and macrophage heterogeneity. *Nature reviews Immunology* 5: 953-964.

199. Shi, C, and Pamer, EG (2011). Monocyte recruitment during infection and inflammation. *Nature reviews Immunology* 11: 762-774.

200. Murdoch, C, Giannoudis, A, and Lewis, CE (2004). Mechanisms regulating the recruitment of macrophages into hypoxic areas of tumors and other ischemic tissues. *Blood* 104: 2224-2234.

201. Lee, HW, Choi, HJ, Ha, SJ, Lee, KT, and Kwon, YG (2013). Recruitment of monocytes/macrophages in different tumor microenvironments. *Biochimica et biophysica acta* 1835: 170-179.

202. Heinrich, MC, Kuhlmann, MK, Grgic, A, Heckmann, M, Kramann, B, and Uder, M (2005). Cytotoxic effects of ionic high-osmolar, nonionic monomeric, and nonionic iso-osmolar dimeric iodinated contrast media on renal tubular cells in vitro. *Radiology* 235: 843-849.

203. Boone, MD, Oren-Grinberg, A, Robinson, TM, Chen, CC, and Kasper, EM (2015). Mannitol or hypertonic saline in the setting of traumatic brain injury: What have we learned? *Surgical neurology international* 6: 177.

204. Miura, S, Teramura, Y, and Iwata, H (2006). Encapsulation of islets with ultra-thin polyion complex membrane through poly(ethylene glycol)-phospholipids anchored to cell membrane. *Biomaterials* 27: 5828-5835.

205. Teramura, Y, and Iwata, H (2009). Islet encapsulation with living cells for improvement of biocompatibility. *Biomaterials* 30: 2270-2275.

206. Itagaki, T, Arima, Y, Kuwabara, R, Kitamura, N, and Iwata, H (2015). Interaction between cells and poly(ethylene glycol)-lipid conjugates. *Colloids and surfaces B, Biointerfaces* 135: 765-773.

207. Teramura, Y, and Iwata, H (2011). Improvement of graft survival by surface modification with poly(ethylene glycol)-lipid and urokinase in intraportal islet transplantation. *Transplantation* 91: 271-278.

208. Escolar, G, Bozzo, J, and Maragall, S (2006). Argatroban: a direct thrombin inhibitor with reliable and predictable anticoagulant actions. *Drugs Today (Barc)* 42: 223-236.

209. Eto, N, Kojima, I, Uesugi, N, Inagi, R, Miyata, T, Fujita, T*, et al.* (2005). Protection of endothelial cells by dextran sulfate in rats with thrombotic microangiopathy. *Journal of the American Society of Nephrology : JASN* 16: 2997-3005.

210. Desai, BJ, Boothello, RS, Mehta, AY, Scarsdale, JN, Wright, HT, and Desai, UR (2011). Interaction of thrombin with sucrose octasulfate. *Biochemistry* 50: 6973-6982.

211. Looney, MR, Nguyen, JX, Hu, Y, Van Ziffle, JA, Lowell, CA, and Matthay, MA (2009). Platelet depletion and aspirin treatment protect mice in a two-event model of transfusion-related acute lung injury. *The Journal of clinical investigation* 119: 3450-3461.

212. Undas, A, Brummel-Ziedins, KE, and Mann, KG (2007). Antithrombotic properties of aspirin and resistance to aspirin: beyond strictly antiplatelet actions. *Blood* 109: 2285-2292.

213. Zeerleder, S, Mauron, T, Lammle, B, and Wuillemin, WA (2002). Effect of low-molecular weight dextran sulfate on coagulation and platelet function tests. *Thrombosis research* 105: 441-446.

214. Chen, H, Teramura, Y, and Iwata, H (2011). Immobilization of anticoagulant-loaded liposomes on cell surfaces by DNA hybridization. *Biomaterials* 32: 7971-7977.

215. Renner, B, Coleman, K, Goldberg, R, Amura, C, Holland-Neidermyer, A, Pierce, K*, et al.* (2010). The complement inhibitors Crry and factor H are critical for preventing autologous complement activation on renal tubular epithelial cells. *J Immunol* 185: 3086-3094.

216. Huang, RY, Wong, MK, Tan, TZ, Kuay, KT, Ng, AH, Chung, VY*, et al.* (2013). An EMT spectrum defines an anoikis-resistant and spheroidogenic intermediate mesenchymal state that is sensitive to e-cadherin restoration by a src-kinase inhibitor, saracatinib (AZD0530). *Cell death & disease* 4: e915.

217. Kurt, RA, Baher, A, Wisner, KP, Tackitt, S, and Urba, WJ (2001). Chemokine receptor desensitization in tumor-bearing mice. *Cellular immunology* 207: 81-88.

218. Wurdinger, T, Badr, C, Pike, L, de Kleine, R, Weissleder, R, Breakefield, XO*, et al.* (2008). A secreted luciferase for ex vivo monitoring of in vivo processes. *Nature methods* 5: 171-173.

219. Jokerst, JV, Lobovkina, T, Zare, RN, and Gambhir, SS (2011). Nanoparticle PEGylation for imaging and therapy. *Nanomedicine (Lond)* 6: 715-728.

220. Kieler-Ferguson, HM, Chan, D, Sockolosky, J, Finney, L, Maxey, E, Vogt, S*, et al.* (2017). Encapsulation, controlled release, and antitumor efficacy of cisplatin delivered in liposomes composed of sterol-modified phospholipids. *European journal of pharmaceutical sciences : official journal of the European Federation for Pharmaceutical Sciences*.

221. Kierstead, PH, Okochi, H, Venditto, VJ, Chuong, TC, Kivimae, S, Frechet, JM*, et al.* (2015). The effect of polymer backbone chemistry on the induction of the accelerated blood clearance in polymer modified liposomes. *Journal of controlled release : official journal of the Controlled Release Society* 213: 1-9.

222. Riviere, K, Huang, Z, Jerger, K, Macaraeg, N, and Szoka, FC, Jr. (2011). Antitumor effect of folate-targeted liposomal doxorubicin in KB tumor-bearing mice after intravenous administration. *Journal of drug targeting* 19: 14-24.

223. Li, W, Huang, Z, MacKay, JA, Grube, S, and Szoka, FC, Jr. (2005). Low-pH-sensitive poly(ethylene glycol) (PEG)-stabilized plasmid nanolipoparticles: effects of PEG

chain length, lipid composition and assembly conditions on gene delivery. *The journal of gene medicine* 7: 67-79.

224. Nilsson, B, Ekdahl, KN, and Korsgren, O (2011). Control of instant blood-mediated inflammatory reaction to improve islets of Langerhans engraftment. *Current opinion in organ transplantation* 16: 620-626.

225. Jin, K, Mao, X, Xie, L, Galvan, V, Lai, B, Wang, Y*, et al.* (2010). Transplantation of human neural precursor cells in Matrigel scaffolding improves outcome from focal cerebral ischemia after delayed postischemic treatment in rats. *Journal of cerebral blood flow and metabolism : official journal of the International Society of Cerebral Blood Flow and Metabolism* 30: 534-544.

226. Tsuchiya, H, Sakata, N, Yoshimatsu, G, Fukase, M, Aoki, T, Ishida, M*, et al.* (2015). Extracellular Matrix and Growth Factors Improve the Efficacy of Intramuscular Islet Transplantation. *Plos One* 10: e0140910.

227. Vanacker, J, Luyckx, V, Dolmans, MM, Des Rieux, A, Jaeger, J, Van Langendonckt, A*, et al.* (2012). Transplantation of an alginate-matrigel matrix containing isolated ovarian cells: first step in developing a biodegradable scaffold to transplant isolated preantral follicles and ovarian cells. *Biomaterials* 33: 6079-6085.

228. Zschenker, O, Streichert, T, Hehlgans, S, and Cordes, N (2012). Genome-wide gene expression analysis in cancer cells reveals 3D growth to affect ECM and processes associated with cell adhesion but not DNA repair. *Plos One* 7: e34279.

229. Page, JL, Johnson, MC, Olsavsky, KM, Strom, SC, Zarbl, H, and Omiecinski, CJ (2007). Gene expression profiling of extracellular matrix as an effector of human

hepatocyte phenotype in primary cell culture. *Toxicological sciences : an official journal of the Society of Toxicology* 97: 384-397.

230. Chen, GY, and Nunez, G (2010). Sterile inflammation: sensing and reacting to damage. *Nature reviews Immunology* 10: 826-837.

231. Rider, P, Carmi, Y, Guttman, O, Braiman, A, Cohen, I, Voronov, E*, et al.* (2011). IL-1alpha and IL-1beta recruit different myeloid cells and promote different stages of sterile inflammation. *J Immunol* 187: 4835-4843.

232. Haverkamp, JM, Crist, SA, Elzey, BD, Cimen, C, and Ratliff, TL (2011). In vivo suppressive function of myeloid-derived suppressor cells is limited to the inflammatory site. *European journal of immunology* 41: 749-759.

233. Pulaski, BA, and Ostrand-Rosenberg, S (2001). Mouse 4T1 breast tumor model. *Current protocols in immunology / edited by John E Coligan [et al]* Chapter 20: Unit 20 22.

234. Lee, HS, Ha, AW, and Kim, WK (2012). Effect of resveratrol on the metastasis of 4T1 mouse breast cancer cells in vitro and in vivo. *Nutrition research and practice* 6: 294-300.

235. Jha, AK, Tharp, KM, Ye, J, Santiago-Ortiz, JL, Jackson, WM, Stahl, A*, et al.* (2015). Enhanced survival and engraftment of transplanted stem cells using growth factor sequestering hydrogels. *Biomaterials* 47: 1-12.

236. Chang, CY, Chan, AT, Armstrong, PA, Luo, HC, Higuchi, T, Strehin, IA*, et al.* (2012). Hyaluronic acid-human blood hydrogels for stem cell transplantation. *Biomaterials* 33: 8026-8033.

237. Rigo, A, Gottardi, M, Zamo, A, Mauri, P, Bonifacio, M, Krampera, M*, et al.* (2010). Macrophages may promote cancer growth via a GMCSF/HB-EGF paracrine loop that is enhanced by CXCL12. *Molecular cancer* 9: 273.

238. Condeelis, J, and Pollard, JW (2006). Macrophages: obligate partners for tumor cell migration, invasion, and metastasis. *Cell* 124: 263-266.

239. Mass, E, Ballesteros, I, Farlik, M, Halbritter, F, Günther, P, Crozet, L*, et al.* (2016). Specification of tissue-resident macrophages during organogenesis. *Science*.

240. Zhou, P, Shaffer, DR, Alvarez Arias, DA, Nakazaki, Y, Pos, W, Torres, AJ*, et al.* (2014). In vivo discovery of immunotherapy targets in the tumour microenvironment. *Nature* 506: 52-57.

241. Martinez, FO, Gordon, S, Locati, M, and Mantovani, A (2006). Transcriptional profiling of the human monocyte-to-macrophage differentiation and polarization: new molecules and patterns of gene expression. *J Immunol* 177: 7303-7311.

242. Sato, K (2015). Effects of Microglia on Neurogenesis. *Glia* 63: 1394-1405.

243. Burke, B (2003). Macrophages as novel cellular vehicles for gene therapy. *Expert opinion on biological therapy* 3: 919-924.

244. Lee, S, Kivimae, S, Dolor, A, and Szoka, FC (2016). Macrophage-based cell therapies: The long and winding road. *Journal of controlled release : official journal of the Controlled Release Society* 240: 527-540.

245. Staal, FJ, Baum, C, Cowan, C, Dzierzak, E, Hacein-Bey-Abina, S, Karlsson, S*, et al.* (2011). Stem cell self-renewal: lessons from bone marrow, gut and iPS toward clinical applications. *Leukemia : official journal of the Leukemia Society of America, Leukemia Research Fund, UK* 25: 1095-1102.

246. Stevenson, HC, Foon, KA, and Sugarbaker, PH (1986). Ex vivo activated monocytes and adoptive immunotherapy trials in colon cancer patients. *Progress in clinical and biological research* 211: 75-82.

247. Rosas, M, Osorio, F, Robinson, MJ, Davies, LC, Dierkes, N, Jones, SA*, et al.* (2011). Hoxb8 conditionally immortalised macrophage lines model inflammatory monocytic cells with important similarity to dendritic cells. *European journal of immunology* 41: 356-365.

248. Perugini, M, Brown, AL, Salerno, DG, Booker, GW, Stojkoski, C, Hercus, TR*, et al.* (2010). Alternative modes of GMCSF receptor activation revealed using activated mutants of the common beta-subunit. *Blood* 115: 3346-3353.

249. Rosenbauer, F, and Tenen, DG (2007). Transcription factors in myeloid development: balancing differentiation with transformation. *Nature reviews Immunology* 7: 105-117.

250. Thompson, HL, van Rooijen, N, McLelland, BT, and Manilay, JO (2016). F4/80+ Host Macrophages Are a Barrier to Murine Embryonic Stem Cell-Derived Hematopoietic Progenitor Engraftment In Vivo. *Journal of immunology research* 2016: 2414906.

251. van Rooijen, N, and Hendrikx, E (2010). Liposomes for Specific Depletion of Macrophages from Organs and Tissues. In: Weissig, V (ed). *Liposomes: Methods and Protocols, Volume 1: Pharmaceutical Nanocarriers*. Humana Press: Totowa, NJ. pp 189-203.

252. Robbins, CS, Hilgendorf, I, Weber, GF, Theurl, I, Iwamoto, Y, Figueiredo, JL*, et al.* (2013). Local proliferation dominates lesional macrophage accumulation in atherosclerosis. *Nature medicine*.

253. Boulter, L, Govaere, O, Bird, TG, Radulescu, S, Ramachandran, P, Pellicoro, A*, et al.* (2012). Macrophage-derived Wnt opposes Notch signaling to specify hepatic progenitor cell fate in chronic liver disease. *Nature medicine* 18: 572-579.

254. Berggren, WT, Lutz, M, and Modesto, V (2008). General Spinfection Protocol. *StemBook*: Cambridge (MA).

255. Li, Z, Xu, X, Feng, X, and Murphy, PM (2016). The Macrophage-depleting Agent Clodronate Promotes Durable Hematopoietic Chimerism and Donor-specific Skin Allograft Tolerance in Mice. *Scientific reports* 6: 22143.

256. van Rooijen, N, Kors, N, and Kraal, G (1989). Macrophage subset repopulation in the spleen: differential kinetics after liposome-mediated elimination. *Journal of leukocyte biology* 45: 97-104.

257. Van Rooijen, N, Kors, N, vd Ende, M, and Dijkstra, CD (1990). Depletion and repopulation of macrophages in spleen and liver of rat after intravenous treatment with liposome-encapsulated dichloromethylene diphosphonate. *Cell Tissue Res* 260: 215-222.

258. Buiting, AM, Zhou, F, Bakker, JA, van Rooijen, N, and Huang, L (1996). Biodistribution of clodronate and liposomes used in the liposome mediated macrophage 'suicide' approach. *Journal of immunological methods* 192: 55-62.

259. Ansari, AM, Ahmed, AK, Matsangos, AE, Lay, F, Born, LJ, Marti, G*, et al.* (2016). Cellular GFP Toxicity and Immunogenicity: Potential Confounders in in Vivo Cell Tracking Experiments. *Stem cell reviews* 12: 553-559.

260. Stripecke, R, Carmen Villacres, M, Skelton, D, Satake, N, Halene, S, and Kohn, D (1999). Immune response to green fluorescent protein: implications for gene therapy. *Gene therapy* 6: 1305-1312.

261. Riddell, SR, Elliott, M, Lewinsohn, DA, Gilbert, MJ, Wilson, L, Manley, SA*, et al.* (1996). T-cell mediated rejection of gene-modified HIV-specific cytotoxic T lymphocytes in HIV-infected patients. *Nature medicine* 2: 216-223.

262. Tabayoyong, WB, Salas, JG, Bonde, S, and Zavazava, N (2009). HOXB4-transduced embryonic stem cell-derived Lin-c-kit+ and Lin-Sca-1+ hematopoietic progenitors express H60 and are targeted by NK cells. *J Immunol* 183: 5449-5457.

263. Swijnenburg, RJ, Schrepfer, S, Govaert, JA, Cao, F, Ransohoff, K, Sheikh, AY*, et al.* (2008). Immunosuppressive therapy mitigates immunological rejection of human

embryonic stem cell xenografts. *Proceedings of the National Academy of Sciences of the United States of America* 105: 12991-12996.

264. Swijnenburg, RJ, Schrepfer, S, Cao, F, Pearl, JI, Xie, X, Connolly, AJ*, et al.* (2008). In vivo imaging of embryonic stem cells reveals patterns of survival and immune rejection following transplantation. *Stem cells and development* 17: 1023-1029.

265. Huber, BC, Ransohoff, JD, Ransohoff, KJ, Riegler, J, Ebert, A, Kodo, K*, et al.* (2013). Costimulation-adhesion blockade is superior to cyclosporine A and prednisone immunosuppressive therapy for preventing rejection of differentiated human embryonic stem cells following transplantation. *Stem Cells* 31: 2354-2363.

266. Pearl, JI, Kean, LS, Davis, MM, and Wu, JC (2012). Pluripotent stem cells: immune to the immune system? *Science translational medicine* 4: 164ps125.

267. Clarke, LA, and Heppner, J (1993). Mucopolysaccharidosis Type I. In: Pagon, RA*, et al.* (eds). *GeneReviews(R)*: Seattle (WA).

268. Peters, C, and Steward, CG (2003). Hematopoietic cell transplantation for inherited metabolic diseases: an overview of outcomes and practice guidelines. *Bone marrow transplantation* 31: 229-239.

269. Wraith, JE, Beck, M, Lane, R, van der Ploeg, A, Shapiro, E, Xue, Y*, et al.* (2007). Enzyme replacement therapy in patients who have mucopolysaccharidosis I and are younger than 5 years: results of a multinational study of recombinant human alpha-L-iduronidase (laronidase). *Pediatrics* 120: e37-46.

270. Davies, LC, and Taylor, PR (2015). Tissue-resident macrophages: then and now. *Immunology* 144: 541-548.

271. Sockolosky, JT, Kivimae, S, and Szoka, FC (2014). Fusion of a short peptide that binds immunoglobulin G to a recombinant protein substantially increases its plasma half-life in mice. *Plos One* 9: e102566.

272. Chawla, A, Nguyen, KD, and Goh, YP (2011). Macrophage-mediated inflammation in metabolic disease. *Nature reviews Immunology* 11: 738-749.

273. Laboratories, CR (2017). NCG Mouse.

274. Qi, LS, Larson, MH, Gilbert, LA, Doudna, JA, Weissman, JS, Arkin, AP*, et al.* (2013). Repurposing CRISPR as an RNA-guided platform for sequence-specific control of gene expression. *Cell* 152: 1173-1183.

275. Hume, DA (2015). The Many Alternative Faces of Macrophage Activation. *Frontiers in immunology* 6: 370.

276. Ezquer, FE, Ezquer, ME, Vicencio, JM, and Calligaris, SD (2017). Two complementary strategies to improve cell engraftment in mesenchymal stem cell-based therapy: Increasing transplanted cell resistance and increasing tissue receptivity. *Cell adhesion & migration* 11: 110-119.

277. Matta, BM, Reichenbach, DK, Blazar, BR, and Turnquist, HR (2017). Alarmins and Their Receptors as Modulators and Indicators of Alloimmune Responses. *American journal of transplantation : official journal of the American Society of Transplantation and the American Society of Transplant Surgeons* 17: 320-327.

278. Kenderian, SS, Porter, DL, and Gill, S (2017). Chimeric Antigen Receptor T Cells and Hematopoietic Cell Transplantation: How Not to Put the CART Before the Horse. *Biology of blood and marrow transplantation : journal of the American Society for Blood and Marrow Transplantation* 23: 235-246.

279. Mueller, KT, Chakraborty, A, Wood, PA, Awasthi, R, Quintas-Cardam, A, Han, X*, et al.* (2016). Cellular Kinetics of Chimeric Antigen Receptor T Cells (CTL019) in Patients with Relapsed/Refractory CD19+ Leukemia. *58th ASH Meeting*, vol. Oral and Poster Abstract 220 Session: 614.: San Diego, California.

8 Appendix

8.1.1 Lentivirus and Retrovirus Production

Preparation:

1. Make sure you have enough DNA for transfecting HEK293T cells (~30 µg total). Make midi-preps of plasmids that are required.
2. Culture HEK293T cells for at least 2 passages (~5 days) prior to transfection
3. Note: HEK293T cells have very poor adherency, especially during the virus production phase. Take great care in gently changing media, and use 1% gelatin treated flasks.

Method:

1. One day prior to transfection, passage HEK293T into a T75 treated with 1% gelatin solution (apply solution for ~10 min, wash 2x with PBS) such that it will be 70-80% confluency on the day of transfection.
2. Prepare lipofectamine and DNA solution:
    a. 1.875 mL Opti-Mem + 75 µL Lipofectamine 2000 (Invitrogen)
    b. 1.875 mL Opti-Mem + 30 µg DNA (Lentivirus: 14 µg pLVX-insert, 6 µg VSV, 10 µg dR8.2; retrovirus: 15 µg pCL-Eco, 15 µg pMSCV-insert)
3. Allow solutions to incubate individually for 5 min, then mix together, incubating the mixed solution for 20 min.
4. Remove media from flask and add lipo/DNA solution (dilute to 10 mL Opti-MEM)
5. After 6 h, replace with fresh DMEM media.
6. Collect and change media every 24 h, up to 4 days, storing at 4°C.

a. Check after 24 h for fluorescence of HEK293T cells if insertion construct has a fluorescent marker
b. Be very careful, as the culture gets older, the cells become less adherent. Pipette gently and handle the flask with care to prevent the cells from sloughing off the surface
c. *All materials from this point on should be treated with bleach solution*

7. Filter the collected media through a 0.45 µm filter.
8. Add Lenti-X-Concentrator or Retro-X-Concentrator (Clontech) (~13 mL to 40 mL of media), and incubate overnight at 4C
9. Spin at max speed (~4000 rpm) for 45 min at 4C, and resuspend pellet in 400 µL of PBS.
10. Aliquot into 50 or 100 µL vials and freeze at -80°C until ready for use.

8.1.2 Lentivirus and Retrovirus Transduction

Cells were transduced with retrovirus or lentivirus using the spinfection method. Briefly, $2x10^4$ cells were added to a retronectin treated 48 well plate along with 50 µL of retrovirus or lentivirus. The plate was centrifuged for 90 min at 4000 rpm then allowed to recover overnight in a humidified 5% CO_2 32°C incubator. The following day, the culture was returned to a humidified 5% CO_2 37°C incubator. After 3-5 days, the culture was expanded and tested for successful integration of the desired modifications.

1. Coat infection wells (48 well plate) day before with 5-10 µg/mL retronectin (Clontech) in PBS overnight at 4°C.
2. Next day rinse coated wells 1x with PBS
3. Block non-specific binding with PBS+0.5% BSA for 30 min at room temperature.

4. Rinse blocked wells 2x with cell media
5. Mix in coated wells 20,000 cells in 200 µL growth media + 50 µL virus + 0.1% Lipofectamine 2000
6. Spin plate for 90 min at 4000 rpm at 30°C.
7. After spin add 300 µl growth media
8. Place cells overnight to 32°C cell culture incubator
9. Transfer next day to 37°C
10. Expand and assay for integration 5 days after infection. Split before if too dense after 3-4 days.

8.1.3 Lin$^-$ bone marrow culture and infection

Lin$^-$ cells were collected from the bone marrow of healthy female BALB/c and C57BL/6 mice by purifying the cells using a magnetic bead mixture and associated column. Following collection, the lin$^-$ cells were grown in tissue culture plates overnight before they were transduced by lentivirus encoding the Hoxb8 construct.

(Adapted from the Lanier Lab at UCSF)

Preparation:

Progenitor outgrowth media:

RPMI + 10% FBS + 50 µM 2-mercaptoethanol + 100 ng/mL SCF + 10 ng/mL IL-3 + 20 ng/mL IL-6 (all cytokines from Peprotech)

Maintenance media:

RPMI1640 + 10% FBS +50 µM 2-mercaptoethanol + cytokine (30 ng/mL GMCSF)

Method:

1. CO_2 euthanize one mouse and collect the leg bones: femur, tibia and fibula. Remove as much of the tissue as possible and rinse in PBS.
2. Crush bones in PBS/0.5%BSA+2% mouse serum 2x(1 wet crush + 1 dry crush), collect into 50 mL Falcon tube
3. Triturate cell clumps by pipetting up and down with 5 mL tissue culture pipet
4. Filter cells/bone fragments through 40 µm strainer into another 50 ml Falcon tube
5. Spin 5 min at 1500 rpm
6. Resuspend in 4 mL PBS/0.5%BSA
7. Load on 3 mL Ficoll-Paque gradient
8. Spin 10 min at 2000 rpm
9. Collect all cells except bottom pellet
10. Dilute in 43 mL PBS/0.5%BSA
11. Spin 5 min at 2000 rpm
12. Resuspend in 3 mL PBS/0.5%BSA
13. Count cells
14. Spin 5 min at 1500 rpm
15. Resuspend at 40 µL/10^7 cells in PBS/0.5%BSA
16. Add 10 µL of biotinylated antibody cocktail/ 10^7 cells (Miltenyi Lineage Depletion Kit)
17. Mix, incubate 20 min at 4°C in cold room (mix gently second time at 10 min)
18. Add 30µl of PBS/0.5%BSA per 10^7 cells
19. Add 20µl of magnetic beads/ 10^7 cells (Miltenyi Lineage Depletion Kit)
20. Mix, incubate 15min at 4°C (mix gently second time at 7 min)

21. Add 1 mL PBS/0.5%BSA
22. Spin 10 min at 300g
23. Equilibrate Miltenyi MS column on magnet with 500 µL PBS/0.5%BSA while cells are spinning
24. Resuspend cells in 500 µL PBS/0.5%BSA per 10^8 cells
25. Apply cells to column
26. Collect flowthrough – **this contains the lin$^-$ cells** (approximately 1x10^5-5x10^5 cells depending on strain and age)
27. Wash column 2x with 750 µL PBS/0.5%BSA
28. Collect and pool washes with flowthrough (total 2 mL)
29. Count cells
30. Spin 5 min at 1500rpm
31. Resuspend at 10^6 cells/ml in *progenitor outgrowth* media in 48 or 24 well (will grow/differentiate faster when more dense)
32. Incubate cells 24-48 h at 37°C
33. Count cells
34. Infect 2 x 10^5 cells/ml by spinoculation on retronectin coated 48 well plate in 0.3 mL at 3000rpm for 90min (*maintenance* media + conc. virus + 0.1% Lipofectamine2000)
35. Add 0.3 mL media after spin
36. Incubate overnight at 32°C in tissue culture incubator
37. Change ½ media next day
38. Passage non-adherent cells to new well with new media every 1-3 days

8.1.4 qPCR

*Note that all pipette tips used in these protocols should be filter tipped to prevent cross contamination

Reverse transcription to generate first-strand cDNA

1. Mix the following components:
    a. 4 µL Superscript VILO Mastermix (Invitrogen)
    b. 500 ng RNA
    c. X µL DEPC-treated water to 20 µL final volume
2. In a thermocycler, using the following program:
    a. 25°C for 10 min
    b. 42°C for 60 min
    c. 85°C for 5 min
3. Dilute the 20 µL solution into 380 µL water and store at -20°C until ready for use

Quantitative PCR (qPCR)

1. For each single run, prepare the following mixture. A mastermix can be made without the cDNA and pipetted into the wells of the plate (96 well thin walled hard shell PCR plates HSP9655 (Bio-Rad)). cDNA should be added individually to each well (scale as appropriate):
    a. 10 µL SsoFast Evogreen MM (Bio-Rad)
    b. 1 µL cDNA
    c. 0.8 µL Forward Primer (10 µM)
    d. 0.8 µL Reverse Primer (10 µM)
    e. 7.4 µL Water

2. Prepare triplicates for each gene per each cDNA sample.

3. Seal the plate with B seals (MSB1001, Bio-Rad)

4. In a Bio-Rad CFX96 thermocycler, set the following program:

Cycling Step	Temperature (°C)	Time (s)	# of Cycles
Enzyme Activation	95	30	1
Denaturation	95	15	40
Annealing	59	20	
Extension	72	40	
Melt Curve	65-95 (0.5 inc)	5/step	1

5. For each sample, calculate the ΔC_t values between actin and the gene of interest.

   To determine fold change from an untreated sample, use the following equation:

$$Fold\ Change = 2^{-(\Delta C_{t-sample} - \Delta C_{t-control})}$$

qPCR Primers

Gene	Sequence	PrimerBank ID*
Actin F	GGCTGTATTCCCCTCCATCG	6671509a1
Actin R	CCAGTTGGTAACAATGCCATGT	
Elane F	AGCAGTCCATTGTGTGAACGG	7657060a1
Elane R	CACAGCCTCCTCGGATGAAG	
Prtn3 F	ATGGCTGGAAGCTACCCATC	31981542a1
Prtn3 R	TGCCCACCTACAATCTTGGAG	
Ms4a3 F	GTGGTTCTGTTTATCAGCCCTT	18875420a1
Ms4a3 R	ACAGTGGGTAGCCTGTGTAGA	
Plac8 F	GCTCAGGCACCAACAGTTATC	21105853a1
Plac8 R	GCTGCCACTTGACATCCAAGA	
Emr1 (F4/80) F	TGACTCACCTTGTGGTCCTAA	2078508a1
Emr1 (F4/80) R	CTTCCCAGAATCCAGTCTTTCC	
IL12b F	TGGTTTGCCATCGTTTTGCTG	6680397a1
IL12b R	ACAGGTGAGGTTCACTGTTTCT	
iNOS (Nos 2) F	GTTCTCAGCCCAACAATACAAGA	6754872a1
iNOS R	GTGGACGGGTCGATGTCAC	
TNF F	CCCTCACACTCAGATCATCTTCT	7305585a1
TNF R	GCTACGACGTGGGCTACAG	
Arg1 F	CTCCAAGCCAAAGTCCTTAGAG	7106255a1
Arg1 R	AGGAGCTGTCATTAGGGACATC	
CD206 (Mrc1) F	CTCTGTTCAGCTATTGGACGC	6678932a1
CD206 R	CGGAATTTCTGGGATTCAGCTTC	
CCL17 F	TACCATGAGGTCACTTCAGATGC	225735578c1

CCL17 R	GCACTCTCGGCCTACATTGG	
*Each pair is identified with one PrimerBankID, taken from PrimerBank https://pga.mgh.harvard.edu/primerbank/)		

8.1.5 Flow Cytometry

Cell Surface Labeling

1. Spin down 500,000+ cells, 400 g 4 min
2. Resuspend cells in PBS+0.5% FBS
3. Spin cells down again
4. Resuspend cells in PBS+0.5% FBS at 10^6 cells per 100µl
5. Mix 100 µL of cells with 1 µg of unlabeled anti-CD16/32 (FcBlock)
6. Incubate RT, 10min
7. Add labeling antibody (0.1-1µg) (directly conjugated or biotinylated). For F4/80, use rat IgG2b κ isotype, anti-mouse F4/80 (0.2 µg per 10^6 cells in 100 µL), labelled with APC (Biolegend). Isotype used for control was unlabeled rat IgG2b κ isotype (Biolegend)
8. Incubate on ice 30-60 min
9. Add 200 ng labeled streptavidin if labeling antibody was biotinylated for 10min
10. Add 900 µl PBS+0.5% FBS
11. Spin down cells, 400 g 4 min
12. Resuspend labeled cells in 500 µL PBS+0.5% FBS
13. Read out on FACS (BD Fortessa at Parnassus Flow Cytometry Core, UCSF)

Have neg controls (no Ab, isotype specific non-specific Ab, no-expression-of-target cells)

Fluorescent Protein Cell Analysis

For cells that are fluorescently labeled, cells can be centrifuged and resuspended in D-PBS and analyzed on FACS without any further treatment.

DRAQ7 Staining for Dead Cells

Staining for live/dead cells was done using DRAQ7 (Abcam), which labels dead and apoptotic cells for flow cytometry, using the manufacturer protocols.

8.1.6 Plasmid Construction

Gibson Assembly

1. Assemble desired product *in silico*, making note of areas were separate segments will be joined. Design primers with sufficient homology on each side of the segments, aiming for a T_M of 60-70°C. Extend each of the primers to also include the homology of the adjacent segment, creating a primer that is 30-40 nt long. The overlap region between the complementary primers on adjoining segments should be 15-20 nt. There should be two primers for each segment to be joined
2. Perform PCR and gel purify the PCR products using standard methods and confirm segments are the correct size
3. Measure concentration of gel purified products using a Nanodrop spectrometer
4. Assemble the reaction in a PCR tube:

    5 µL NEB Gibson Assembly Master Mix

    0.100 pmol of each segment

    X µL Water to 10 µL final volume
5. In a thermocycler, heat the reaction mixture for 1 h at 50°C

6. Take 1-2 µL of the reaction mix and transform into competent bacteria using the manufacturer's protocol

Grow bacteria on an appropriate selection agar plate and select colonies for sequencing

8.1.7 IDUA Activity

Buffers:

0.4M Sodium Formate Buffer: 0.27204g Sodium Formate (Fisher) in 10mL of MilliQ Water, Adjust pH to 3.2

0.1M Glycine Buffer: 0.37535g Glycine (Fisher) in 50mL of MilliQ Water, Adjust pH to 10.2

5mM 4-MU: 0.0098g 4-MU Sodium Salt (Sigma) in 10 mL of MilliQ Water

2.5mM (4MU)-α-L-idopyranosiduronic acid: 1mg (4MU)-α-L-idopyranosiduronic acid (Toronto Research Chemicals) in 1.07 mL of 0.4M Sodium Formate Buffer

Activity Assay:

1. Make aliquots of 2.5mM (4MU)-α-L-idopyranosiduronic acid in 0.4M Sodium Formate Buffer.
2. Mix 10 µL of sample with 25 µL substrate in a 96 well plate.
3. Incubate at 37C for 1hr.
4. Add 65uL 0.1M glycine buffer to stop reaction.
5. Measure emission (ex 355/em460)
6. For standards, make serial dilutions of 4-MU, starting with 150 µM (150, 75, 37.5, 18.75, 9.375, 4.6875, 2.34375, 0). Add 50 µL to well and add 50 µL glycine buffer. Measure emission

8.1.8 Western blot

Buffers

Lysis Buffer	*SDS-PAGE Loading Buffer*	*Transfer Buffer*	*Blocking Buffer*	*Wash Buffer*
RIPA: 500 mL 150 mM sodium chloride 1.0% Triton X-100 0.5% sodium deoxycholate 50 mM Tris, pH 8.0	**Laemmli 2X buffer:** 1mL 4% SDS 10% 2-mercaptoehtanol 20% glycerol 0.004% bromophenol blue 0.125 M Tris HCl, pH 6.8	1L 25 mM Tris base 190 mM glycine 20% MeOH pH 8.3	200 mL 5% milk in TBST (5 g per 100 mL) .05% Sodium Azide 1% PMSF	**TBST:** 1L 100 mL TBS 10x 900mL MilliQ water 1mL Tween (.1%) **TBS 10x** (concentrated TBS) =: 1L 24g Tris HCl 5.6g Tris Base 88 g NaCl Mix in 800 ml ultra pure water. pH to 7.6 with pure HCl. Top up to 1 L.
-Add protease inhibitor tablet before use	-Stock available that makes 1mL following addition of mercaptoethanol	-10X stock is commercially available. Add 200mL MeOH + 100mL 10x and fill to 1 L	-Allow milk time to dissolve in water prior to adding other ingredients (add TBS 10x)	

<u>Preparation of lysate from cell culture</u>

Everything should be kept cold beyond this point

1. Save media (concentrate as necessary with centricon filters)
2. Wash cells with 37 °C PBS (w/ Ca/Mg). If cells are non-adherent, pellet the cells with each wash. Wash 3x.
3. Drain the PBS, then add ice-cold RIPA lysis buffer (1 mL per 10^7 cells/100 mm dish/150 cm^2 flask; 0.5 mL per $5x10^6$ cells/60 mm dish/75 cm^2 flask, 250 µL for 24 well).

4. Leave on ice for 10-15 min to allow for cell lysis.
5. Centrifuge in a microcentrifuge at 4 °C [~12000 rpm for 20 min]
6. Remove the tubes from the centrifuge and place on ice, remove desired amount of supernatant and discard the pellet.

Running SDS-Page

1. Mix protein supernatant sample 1:1 with loading buffer (Lamelli Buffer with B-ME). 50 µL of each is plenty
2. Denature sample by heating at 70 °C for 10 min or 95 °C for 10 min (Twice as long if frozen)
3. Load sample into gel and run at 170 V (constant voltage)
4. Run until dye front leaves the gel
5. Extract gel from case and wash thoroughly with MilliQ water

Transferring Protein

1. Cut a sheet of transfer membrane 7.5 cm x 10 cm
2. Fill three boxes: Fill 2 with transfer buffer and one with millipure water
3. Soak mesh in transfer buffer, soak transfer membrane in millipure water
4. Remove gel

   a. Use tool to gently crack box on four sides to reveal gel (allow it to stick to one end)

   b. Using a razor to cut off top portion of gel (about space found between markers)

   c. Cut off bottom portion of gel at edge

d. Gently transfer the gel from the bottom using a razor and place in transfer buffer

5. Add paper to same transfer buffer as gel. From bottom of gel gently slide paper underneath
6. Place gel cage with black side down. Assemble sandwich in this manner

   Assembly order: Mesh, Paper, Gel, Membrane, Paper

   a. Place one mesh down

   b. Place paper and gel combination on top

   c. Place transfer membrane down (ensure no air bubbles)

   d. Soak another sheet of paper in transfer buffer then place on top of membrane

   e. Add final mesh on top

   f. Roll a pipette over to sure there are not any air bubbles
7. Seal the sandwich and place in box
8. Add **cold** transfer buffer such that sandwich is completely covered. Run at constant mAmp for 1 h [160 mAmp/gel]

<u>Blocking & Primary Antibody</u>

1. Gently disassemble sandwich and cut border off membrane with a razor that wasn't in contact with the gel. (*The membrane can be dried at this point prior to blocking if necessary – place the membrane between paper towels and leave on the bench* When restarting, the dry membrane is very fragile, and wet in TBST before blocking in milk) Place membrane in washing box.
2. At this point, never let the membrane dry, otherwise there will be very high background.

3. Add sufficient blocking buffer to cover the membrane
4. Incubate for 1 h at RT under agitation (use horizontal shaker)
5. Rinse for 5 s in TBST after the incubation
6. Dilute primary antibody in necessary volume of blocking buffer to cover gel (1:2000 for Rat Anti-HA high affinity (Roche) – make 15 mL)
7. Incubate overnight at 4 °C under agitation

Washing & Secondary Antibody

1. Remove primary antibody –blocking buffer solution and store (can be used multiple times) – wash container immediately
2. Wash 6X for at least 5 minutes each in ~100 mL TBST at room temperature
3. Dilute secondary antibody in necessary volume of TBST to cover gel (1:10000 for anti-rat HRP)
4. Add secondary antibody solution and run 1 hours at room temperature with agitation (don't save secondary)
5. Wash again 6X for at least 5 min each in TBST at room temperature

Development

1. Mix HRP solutions 1:1 to a volume large enough to cover gel membrane
2. Add to blot and run for 5 min with agitation at RT

   TIME SENSITIVE
3. Place blot on napkins to remove any residual solution
4. Place face down in clear wrap and begin to seal

   Leave one side open then gently roll pipette over to remove air bubbles
5. Tape into film cassette and close

6. Take cassette into dark room
7. Add film over blot and repeat for various times: 5 s, 2 min, 5 min, 30 min (do not exceed) -Be sure film does not move—secure to edge of cassette and gently place down.

Publishing Agreement

It is the policy of the University to encourage the distribution of all theses, dissertations, and manuscripts. Copies of all UCSF theses, dissertations, and manuscripts will be routed to the library via the Graduate Division. The library will make all theses, dissertations, and manuscripts accessible to the public and will preserve these to the best of their abilities, in perpetuity.

I hereby grant permission to the Graduate Division of the University of California, San Francisco to release copies of my thesis, dissertation, or manuscript to the Campus Library to provide access and preservation, in whole or in part, in perpetuity.

Author Signature 

Date: Jun 7, 2017